Manganese, Iron and Cobalt Catalyzed Reductive Hydrogenation and Cross-Coupling Reactions

Dissertation

zur Erlangung des Doktorgrades der Naturwissenschaften

Dr. rer. nat.

an der Fakultät für Chemie und Pharmazie der Universität Regensburg

vorgelegt von

Efrain Reyes-Rodriguez

Regensburg 2018

Für meine Mutter

The experimental part of this work was carried out between January 2015 and March 2018 at the University of Regensburg, Institute of Organic Chemistry under the supervision of Prof. Dr. Axel Jacobi von Wangelin.

The thesis was submitted on: 19.12.2018
Date of the defense: 25.01.2019

Board of examiners:
Prof. Dr. Rainer Müller (chairman)
Prof. Dr. Axel Jacobi von Wangelin (1st referee)
Jun.-Prof. Dr. Ivana Fleischer (2nd referee)
Prof. Dr. Frank-Michael Matysik (examiner)

Contents

Introduction

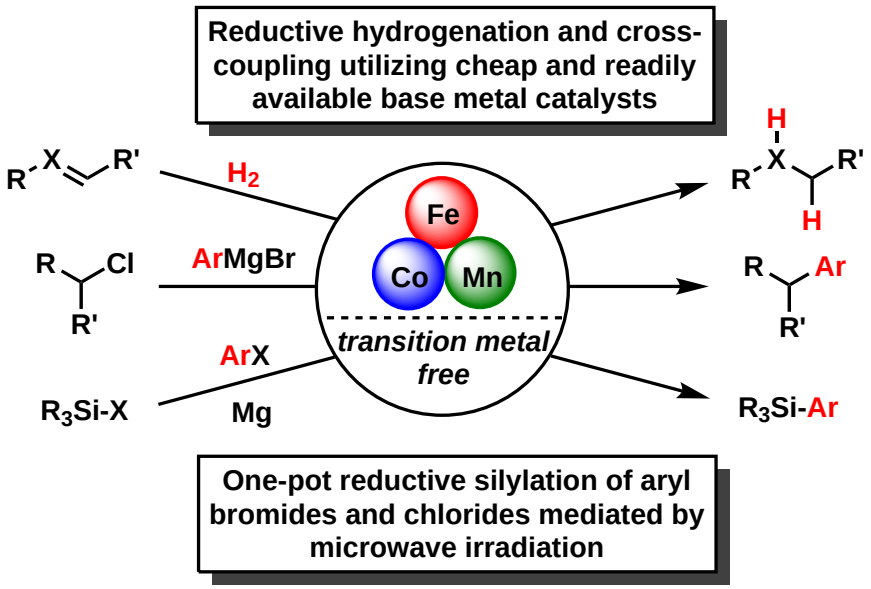

Abstract: The need for sustainable chemical transformations has been steadily increasing in recent years due to the rising prices of noble metals and new ecological policies to reduce atmospheric pollution and hazardous waste. This introductory chapter strives to describe the basic principles necessary to attain "green" and sustainable chemistry in our modern industrial age as well as going into more detail on the importance of base metal catalysis. Lastly, an overview of the subsequent chapters is given.

1.1 Environmental Aspects of Chemical Transformations

The biosphere of our planet has enabled the proliferation of aerobic organisms and the accumulation of oxidized matter on the earth's surface (water, CO_2, oxides, carbohydrates). On the other hand, reduced chemical compounds are valuable sources of energy found only in deeper layers or isolated reservoirs (hydrogen, methane, petroleum, natural gas, coal, solid metals). Many oxidation events proceed spontaneously or are highly thermodynamically favored, while reduction reactions often require an external driving force through the supply of energy or high-energy reagents. The scarcity of high-energy resources makes the reductive transformation of available oxidized raw materials (biomass, water, atmosphere) into energy sources (H_2, methanol) and intermediates (NH_3, synthesis gas, platform chemicals) one of the greatest challenges of modern industrial societies.[1]

The emerging field of Green Chemistry aims to overcome these challenges in an environmentally sustainable way. Its main goals are summarized by the *Twelve Principles of Green Chemistry* which were postulated by Paul Anastas and John Warner in 1998.[2] In general, Green Chemistry strives to minimize the use of hazardous chemicals and waste production as well as maximizing the efficiency of chemical reactions while relying mostly on renewable feedstocks. A lot of different methods have been developed to reduce energy consumption (e.g. by using microwave irradiation instead of conventional heating methods),[3] waste generation (e.g. recycling of catalyst material[4] or the use of flow reactors[5]) and the use of hazardous chemicals (e.g. substitution of solvents for water[6] or ionic liquids[7]).

The use of catalysts represent a cornerstone in the abovementioned principles of Green Chemistry and is generally seen as a very important aspect for the economical generation of chemical compounds in industry. Catalytic processes are a vital tool in the development of new synthetic routes for the functionalization of molecules. It is estimated that 75% of the existing industrial chemical transformations and 90% of newly developed processes include the use of catalysts.[8] The established catalyst systems are based predominantly on second- and third-row transition metals, i.e. ruthenium, rhodium, palladium and iridium[9] as well as on nickel and copper.[10] Despite their high efficiency and broad application, the development of novel synthetic routes and catalytic systems is in full swing. This is not least owed to the increasing prices of noble metals, the toxicity of nickel and the new ecological policies to reduce atmospheric pollution and to eliminate hazardous waste. In this regard, first-row transition metals, like Mn, Co and Fe constitute a viable alternative to the existing catalyst metals.

The selected examples in Figure 1.1 show the advantages of first-row transition metals in comparison to the most-used noble metals - they are abundant, very cheap and pose small threat to the environment and to human health. A direct comparison shows a difference of multiple orders of magnitude between the selected 3d transition

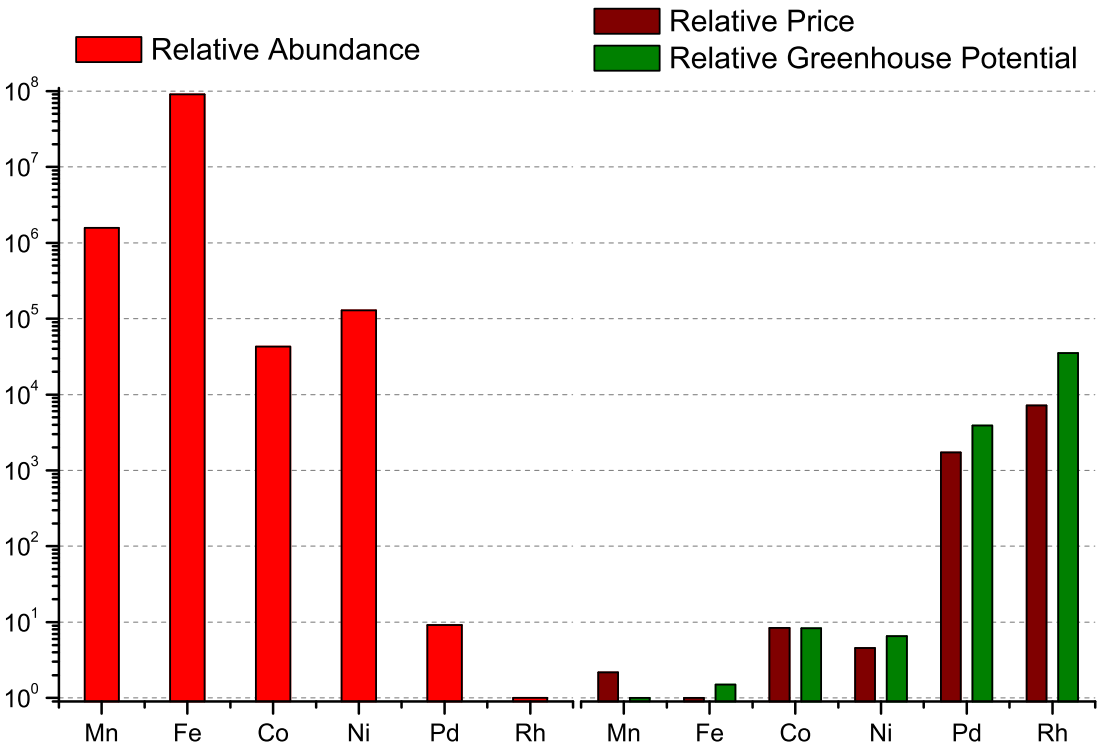

Figure 1.1: Comparison of abundance, price, and greenhouse potential for highly-used catalyst metals. A logarithmic scale was used as ordinate.[11,12]

metals and the noble metals in terms of availability and cost. As a viable alternative for industrial applications, however, base metals have to meet multiple criteria from low catalyst loadings to high selectivities - the hallmark of noble metal catalysis. Great successes have been achieved in recent years with the developement of competent ligand systems and composite materials which enable competitive reactivities and selectivities and which makes them viable for use in industrial synthesis.

1.2 Current State of 3d Transition Metal Catalysis

Platinum group metals have received significant attention in the field of organometallic chemistry. The continuous advances in this field have led to a variety of novel carbon-carbon bond forming reactions since the mid-1960s. Most notably, the Nobel Price in chemistry in 2010 was awarded to Richard F. Heck, Ei-ichi Negishi and Akira Suzuki for palladium-catalyzed cross-couplings in organic synthesis. Besides the use of palladium in cross-coupling reactions,[13] noble metal catalysts still dominate important chemical transformations ranging from iridium- and rhodium-catalyzed C–H activations[14] to ruthenium-catalyzed alkene metathesis.[15]

As discussed in the previous chapter, the change to base metal catalysis is the logical next step on the way to a sustainable chemical industry. Unfortunately, the weak

ligand field of first-row metals often lead to paramagnetic high-spin complexes. This fact complicates NMR analysis, hinders the ability to understand the coordination environment of the metal complex as well as mechanistic details which are important factors for the rational design of novel catalysts. Other differences of 3d transition metals complexes in comparison to their heavier congeners include their lower M-L bond energy, field splitting and affinity towards unpolar double bonds and their propensity to undergo single electron transfer processes which can lead to unselective reaction pathways.[16,17]

Only in recent years, mechanistical studies and DFT calculations have shown ways for first-row transition metals to sidestep these restrictions. One method is to use low-spin complexes requiring strong field ligands (e.g. CO and CN) which can be employed to emulate the predictable two-electron chemistry seen in organic chemistry and with most noble metal complexes (for selected examples, see scheme 1.1a). They enable the classical elementary steps of the catalytic cycle (e.g. oxidative addition, reductive elimination) but are rarely used in catalysis due to their strong ligand coordination and saturated electronic configurations.[18] Cooperative ligand effects represent a different approach, as the ligand backbone can be used to store/transfer electrons. These so-called redox-active or non-innocent ligands have received significant attention in recent literature together with the appearence of pincer ligands which made significant advances in the activity of homogeneous catalytic systems.[19] An example of a cooperative ligand effect in the hydrogenation of ketones using an iron pincer complex is shown in scheme 1.1b. In this case, the catalyst operates via heterolytic bond cleavage of the hydrogen molecule. This process is aided by the strong-field CO ligand increasing the energy gap between the d-orbitals and – more to the point – the ability of the pyridyl backbone to switch between the aromatic and non-aromatic state. At the same time iron complexes bearing pyridyldiimine scaffolds are known which can be reduced by two successive SET processes that don't change the oxidation state of the metal but lead to a stable diradical.[20] Other advantages of this ligand design are the ease of modulation of the electronic and steric properties by changing the side-arms and the high structural rigidity and thermal stability of the resulting complexes.

Spin acceleration permits the third way of enabling access to two-electron transfer processes. By spin flipping, a low-spin state can be achieved temporarily since 3d metals often display multiple spin states with similar energies. For example, the β-hydride elimination (BHE) involves the two electron hydride transfer to the first-row transition metal which can only take place if empty d-orbitals are available. Usually, a high spin 3d-metal complex with five or more d-electrons is BHE-resistant but in the right ligand sphere the change into a different spin state while obtaining a free d-orbital is possible. For this to work, the potential energy surfaces of the two spin states have to intersect during the reaction step (see scheme 1.1c).[17]

Moreover, it is notable that the orbital configuration is dependent on the geometry of the complex. The distortion of the complex geometry in between the reaction steps

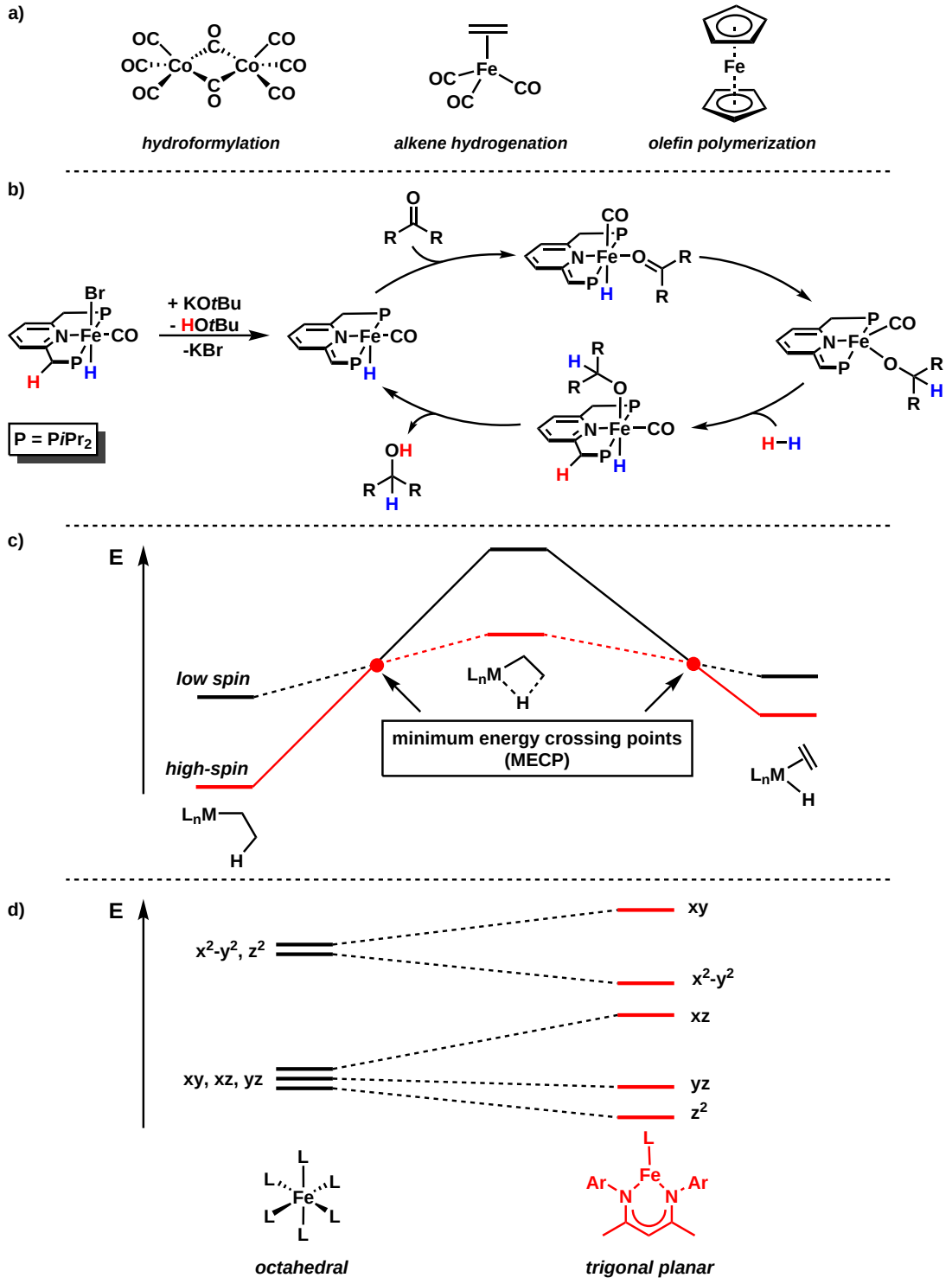

Scheme 1.1: a) Examples of high ligand field transition metal complexes and their corresponding applications;[17,18] b) Example of a cooperative ligand effect in the hydrogenation of ketones using an iron pincer complex;[21] c) Energy diagram of a metal catalyzed β-hydride elimination. Crossing of spin-states indicated by red dots;[17] d) Loss in degeneracy of the d-orbital energies going from octahedral to trigonal planar geometry.[22]

can lead to changes in orbital energies which can alter the spin state. This explaines why rigid ligand systems generally lead to BHE-resistant complexes whereas the use of a flexible scaffold may allow transient conformational changes which lead to a change in the electronic state of the complex. In case of iron, the octahedral geometry is most common but low-coordinate iron complexes are easily accessible. The use of a β-ketimine ligand bearing sufficientyl bulky substituents, as seen in scheme 1.1d, can occupy almost the whole ligand sphere and therefore lead to tri-coordinate iron complexes which removes the orbital degeneracy.[22,23]

Going from mono- to multimetallic catalyst species, the outcome is reliant on the character of the metals involved. Multiple connected metallic centers of the same element can more easily distribute the available electron density by virtue of a wider range of possible oxidation states whereas the combination of two or more metals with different electron affinities can facilitate heterolytic bond cleavage. Metal-metal cooperative effects can be seen in use throughout nature. A prominent example is the nitrogenase enzyme as it is able to catalyze the proton-coupled multi-electron reduction of dinitrogen to ammonia as shown in eq. 1.1.

$$N_2 + 8e^- + 16\text{ATP} + 8H^+ \rightarrow 2\text{N}H_3 + H_2 + 16\text{ADP} + 16P_i \tag{1.1}$$

The dinitrogen coordinates to the iron-molybdenum cofactor (MoFe-co), a cluster containing seven iron and one molybdenum atom, which in turn gets the electron necessary for the reduction from the [Fe_4-S_4] iron-sulfur cluster (P-cluster) via forward electron transfer.[22,24] Understanding the way nature handles the difficult task of activating strong and unreactive bonds can help aid the development of finely-tuned catalyst systems that account not only for the effect of metal and ligand on the substrate but incorporates cooperative effects between metals and ligands. The use of metal clusters in organic synthesis has been demonstrated for a sizable range of transformations.[25]

Small metal clusters are only an intermediate step in going from soluable metal complexes to bulk catalyst materials which entail a different set of challenges. On a heterogeneous metal catalyst only the top layer of atoms is able to interact with the substrate directly. As a result the amount of catalytically active sites is strongly dependent on the ratio of atoms on the surface to those inside the solid. Secondary, the adsorption rate of the catalyst relies mostly on diffusion of the reactants to the metal surface. To mitigate these problems, the synthesis of small, stable and easily dispersable metal nanoparticles has been an important research goal for multiple decades. From figure 1.2 it is easy to see that nanoparticles can combine the beneficial properties of homogeneous and heterogeneous catalysis. Due to their small size (1-100 nm), the surface area contains a significant amount of the available atoms (in some cases more than 50%). At the same time recovering the catalyst after reaction can be achieved by filtration or magnetic separation.[26]

Synthesis of metal nanoparticles is achieved in a myriad of different ways from either a) a top-down approach, starting with bulk metal, ores or minerals and using thermal

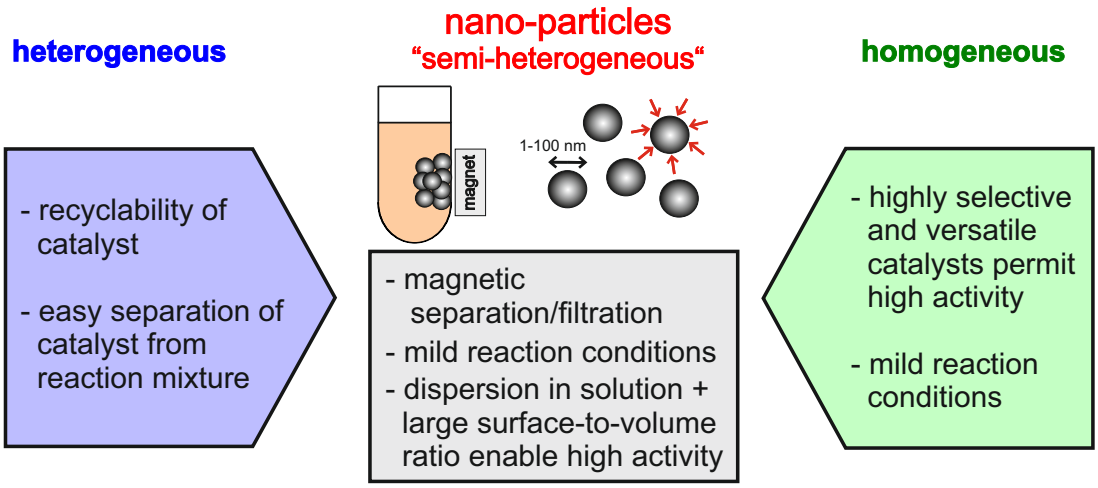

Figure 1.2: Comparison between the properties of homo- and heterogeneous catalysts as well as nano-particles for catalytic applications.

decomposition, mechanical abrasion (ball mill) or laser ablation to reduce the particle size or b) a bottom-up approach, starting from molecular precursors or by chemical vapor deposition.[26,27] In this context the manufacture of base metal nanoparticles has received far less attention than less reducing metals (e.g. Pd, Pt, Ag, Au). Due to their high reactivity, base metal nanoparticles are difficult to synthesize in a controlled manner and with a specified size distribution. Reoxidation and agglomeration of the particles are significant challenges in the synthesis of high-quality nanoparticles. Feldmann *et al.* have recently published the preparation of a range of base metal nanoparticles by reduction of their chloride salts in etheral solutions. The use of a strong reducing agent (sodium naphthalenide) enabled control of nucleation and growth of the particle formation which produced small-sized monodisperse nanoparticles.[28]

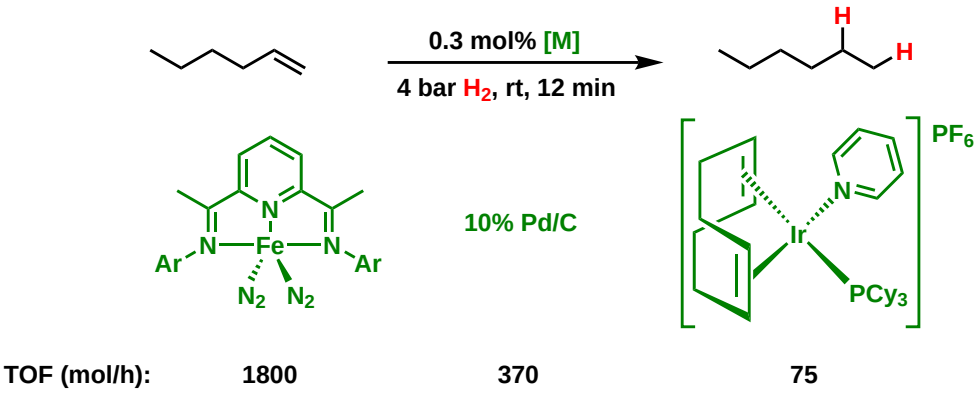

Scheme 1.2: Catalytic activity of selected metal catalysts in the hydrogenation of 1-hexene.

For a wide variety of chemical transformations highly active base metal catalysts already exist. In 2004, Chirik *et al.* did a comparison study between a highly active iron(0) dinitrogen complex bearing a 2,6-pyridyl-diimine backbone to well known noble metal catalysts, e.g. palladium on activated charcoal and Crabtree's catalyst, in the hydrogenation of 1-hexene (scheme 1.2).[29] In terms of stability, however, an iron(0) catalyst with labile dinitrogen ligands cannot be competitive to the bench-stable palladium and iridium reagents which reduces its viability in industrial applications. The same goes for selectivity, since only diminished activity was observed for the sole heteroatom-bearing substrate reported (dimethyl itaconate).

In summary, the trend going over from very successful and well investigated but harmful and rare noble metal catalysts to environmental friendly and low cost 3d transition metals is a contemporary but still challenging task for the realization of efficient organometallic reactions. In order to establish such effective catalyst systems the main challenges of 3d base metal complexes have to be addressed. These invole a) a weak ligand field resulting in high-spin complexes b) the propensity of such complexes to undergo single electron transfer reactions and c) their paramagnetism oftentimes exacerbating reaction analysis. A lot of work has been done to develop appropriate ligand systems which act as electron reservoirs and enable classical 2-electron redox chemistry. Multi-metallic cluster design allows for efficient distribution of the electron density while metal nanoparticles offer high reactivity and easy separation from the product. The prevalence of noble metal catalysts is due to a massive research effort which in turn led to a 30 year hiatus in the development of base metal catalysis. Although it is known for over a century, first-row transition metal catalysis has only recently received enough traction to tackle the important challenges for a sustainable chemical industry.

1.3 Scope of the Thesis

This thesis is divided in 5 chapters. The main goals of this thesis were the development of viable synthetic methods for the use of iron, cobalt and manganese as catalyst metals in hydrogenation reactions, the research on an operationally easy cross-coupling protocol using simple iron salts, the mechanistic investigation into three-coordinate β-diketiminato(phenyl)iron complexes as cross-coupling catalysts, and the design of a microwave-mediated and transition metal free silylation protocol.

Chapter 2: This chapter deals with the synthesis of finely dispersed cobalt nanoparticles (Co-NP) and their application in the hydrogenation of over 60 different alkenes, alkynes, imines and heteroaromatics. The protocol presented was able to hydrogenate demanding substrates (e.g. trisubstituted olefins, quinolines) under moderate reaction conditions (5 mol% Co-NP, 10-20 bar H_2, 60-80 °C, 3-24 h) while tolerating ester, ether, fluoride, chloride, amine, amide and sulfone moieties. The small, uniform diameter of the particles (< 4 nm) was shown by high-resolution transmission

electron microscopy (HRTEM) and highangle annular dark-field scanning transmission electron microscopy (HAADF-STEM) and was confirmed for particles in THF suspension using dynamic light scattering (DLS). The high purity of the sample was determined via X-ray powder diffraction (XRD). The heterogeneous nature of the catalyst was furthermore studied by kinetic poisoning experiments showing complete reaction inhibition after amalgamation with mercury or the addition of substoichiometric amounts of PMe_3. Recyclability of the Co-NP was studied due to their magnetic properties. The activity of the catalyst was shown to be stable over multiple weeks and did not degrade after ten consecutive hydrogenation reactions. In the process, a commercial neodymium magnet was used to seperate and wash the catalyst particles in between batches. Additionally, inductively coupled plasma mass spectrometry and optical emission spectrometry (ICP-MS and -OES) showed minimal leaching of the catalyst into the organic phase. Only traces could be detected in the product phase after workup.

This chapter was published in the journal Catalysis, Science & Technology: E. Reyes-Rodriguez, P. Büschelberger, C. Schöttle, C. Feldmann, R. Wolf, A. Jacobi von Wangelin; Recyclable Cobalt(0) Nanoparticle Catalysts for Hydrogenations. *Catal. Sci. Technol.* **2018**, 8, 2648-2653. DOI: 10.1039/C8CY00595H. P. Büschelberger and the author of this thesis did all the synthetic work (isolation and characterization of the hydrogenation products, recycling experiments, poisoning experiments). P. Büschelberger wrote the manuscript and the author of this thesis most of the supporting information. The characterization of the nanoparticles was done by C. Schöttle.

Chapter 3: Herein we report the formation of a novel heteroleptic Mn_6 nanocluster with an unprecedented flat-chair topology and its application in the hydrogenation of alkenes, alkynes and imines. A simple ligand-exchange procedure between the metal amide precursor $Mn[N(SiMe_3)_2]_3$ and the commercial hydride source diisobutylaluminium hydride (Dibal-H) yielded a low-valent manganese nanosheet which was shown to be a molecular precursor to catalytically active nanoparticles exhibiting previously unreported catalytical activity. After synthesis and isolation, the Mn_6 hydrido cluster was identified via single crystal X-ray analysis. Further insight into the properties of the cluster was furnished using superconducting quantum interference device (SQUID) measurements. It indicates strong antiferromagnetic interactions between the manganese atoms and a diamagnetic ground state. The interactions may also explain the low measured effective magnetic moment (μ_{eff}) in comparison to six uncoupled $S = 5/2$ spins. The presence of at least five active hydride ligands was determined in stoichoimetric reduction experiments while the addition of Dibal-H led to the formation of a black solution, presumably owing to degradation of the complex to soluble Mn nanoparticles. The Mn cluster also showed reactivity towards alkynes, exhibiting the first Mn-catalyzed cyclotrimerization. When employing equimolar amounts of Dibal-H to the Mn nanocluster, the first efficient hydrogenation of unpolar olefins, such as alkenes and alkynes as well as the hydrogenation of imines using Mn catalysis could be demonstrated. Besides the hydrogenation of mono- and disubstituted alkenes as well as alkynes at room temperature (5 mol% Mn, 2 bar H_2, 3

h) it was possible to selectively hydrogenate the polar C=N bonds in α,β-unsaturated imines. In total the substrate scope was extended to over 40 different compounds.

This chapter was published in the journal Angewandte Chemie: U. Chakraborty, E. Reyes-Rodriguez, S. Demeshko, F. Meyer, A. Jacobi von Wangelin; A Manganese Nanosheet: New Cluster Topology and Catalysis. *Angew. Chem. Int. Ed.* **2018**, *57*, 4970-4975. DOI: 10.1002/anie.201800079. U. Chakraborty wrote the manuscript and performed the mechanistic studies and most of the alkene and alkyne hydrogenation experiments. The author of this thesis was involved in the isolation of the imine and chinoline hydrogenation products and their characterization as well as the radical clock experiments. The magnetic susceptibility measurements were done by S. Demeshko.

Chapter 4: This chapter gives an overview on the catalytic activity of different alkene/arene metalates (M=Co, Fe) in olefin hydrogenation as well as mechanistic insight into the catalyst activation and ligand exchange reactions. Potassium bis(η^4-anthracene)metalates have been shown to be competent hydrogenation catalysts and can easily be synthesized by a simple reduction of metal bromides with potassium in the presence of anthracene. As part of the mechanistic investigation, a series of homo- and heteroleptic alkene/arene cobaltates and ferrates were synthesized and characterized by single crystal X-ray diffraction. These precatalysts were then subjected to hydrogen pressure in presence of simple alkenes to evaluate their catalytic activities. As a result it could be shown that ligand exchange with the substrate seems to be an important step in the catalytic cycle since strongly binding π-hydrocarbon ligands led to a reduction or even inhibition of the reaction. Kinetic NMR spectroscopy studies support the notion of ligand exchange prior to alkene hydrogenation and didn't show the formation of metal hydride species. Reaction progress monitoring showed the absence of an induction period and sigmoidal curvature which supports the homogeneous reaction pathway. This could furthermore be corroborated by catalyst poisoning experiments in presence of typical metal scavengers (Hg, PMe_3, and dibenzo[*a*,*e*]cyclooctatetraene (dct)) or through filtration tests. Lastly, the formation of the active intermediate through ligand exchange could be supported via negative-ion mode ESI mass spectrometry, e.g. showing the dissociation of the anthracene ligand in bis(η^4-anthracene)cobaltate and its substitution by two equivalents of styrene. Extending the different precatalysts to ketone and imine hydrogenation, good catalytic activity was only observed for potassium bis(anthracene)cobaltate at elevated reaction conditions (10 bar H_2, 60 °C). Possible deactivation pathways were demonstrated in the pinacol coupling of acetophenone possibly resulting from an two-electron transfer from the metallate as well as in the ring-opening reaction of α-cyclopropylstyrene showing the radical character of cyclooctadiene-bearing catalysts.

This chapter was published in the journal Chemistry - A European Journal: P. Büschelberger, D. Gärtner, E. Reyes-Rodriguez, F. Kreyenschmidt, K. Koszinowski, A. Jacobi von Wangelin, R. Wolf; Alkene Metalates as Hydrogenation Catalysts. *Chem.*

Eur. J. **2017**, *23*, 3139-3151. DOI: 10.1002/chem.201605222. P. Büschelberger synthesized and characterized the precatalysts, was involved in the mechanistic hydrogenation reactions and NMR studies and wrote the manuscript. D. Gärtner was involved in the alkene and ketone hydrogenations as well as product isolation. The author of this thesis was involved in the imine hydrogenations as well as the pinacol coupling and ring opening reactions. The ESI-MS analysis was done by F. Kreyenschmidt.

Chapter 5: This chapter deals with the iron-catalyzed cross-coupling reaction between aryl Grignard reagents and secondary alkyl chlorides. Initially, the optimization of the reaction conditions led to the development of a general protocol, utilizing *N*,*N*,*N*′,*N*′-tetramethylethylenediamine (TMEDA) and iron(III) chloride together with lithium chloride to furnish a selection of functionalized arenes with mild reaction conditions (5 mol% $FeCl_3$, 10 °C, 4 h) in moderate to excellent yields. The reaction conditions employed effectively reduced the formation of the biaryl side-product. In addition, using a wide variety of structurally different *N*-donor ligands, the effect of the coordination environment on catalyst reactivity was studied. For mechanistic investigations, the diimine ligand $dipp_2$nacnacH was selected for its high *N*-donor strength and effectiveness in cross-coupling reactions. Therefore, several three-coordinate β-diketiminato(aryl)iron complexes were synthesized and fully characterized as they represented possible active intermediates. Several mechanistic studies (NMR and UV/Vis reaction progress analyses, radical clock reactions) indicated a reaction mechanism initiated by a single electron transfer to the organic electrophile.

E. Reyes-Rodriguez, D. Schaarschmidt, S. Grupe, C. Rödl, B. Rezai Rad, R. Wolf, A. Jacobi von Wangelin; Iron-Catalyzed Cross-Coupling of Secondary Alkyl Chlorides. *in preparation*. S. Grupe developed the original reaction reaction protocol, and together with the author of this thesis shared the reaction optimization, diamine ligand screening, synthetic work and characterization of the products. The first syntheses and characterizations of the β-diketiminato iron complexes as well as part of the reaction optimization for the cross-coupling of alkyl bromides and chlorids were done by C. Rödl and B. Rezai Rad. Further mechanistic studies (UV/Vis, NMR, cyclic voltammetry, competition reactions) as well as the optimized synthetic protocol for the synthesis of the β-diketiminato iron complexes were performed by D. Schaarschmidt. The author of this thesis was furthermore involved in the development of the ligand-free reaction conditions as well as mechanistic investigations (catalyst poisoning experiments, radical clock reactions).

Chapter 6: In the last chapter, a transition-metal free, one-pot reductive silylation protocol for the synthesis of di-, tri- and tetraorganosilanes was presented using silyl chlorides and aryl bromides. The *in-situ* formation of the Grignard reagent is accelerated by the addition of lithium chloride and furnishes a wide variety of aryl and heteroaryl silanes under mild reation conditions near room temperature (40 °C, 3 h; 30 examples). Hydrosilanes as well as tetraethyl orthosilicate were shown to have similar reactivity under standard reaction conditions. Using dielectric microwave heating, the reaction was able to be extended to aryl chlorides and silyl ethers while

drastically reducing reaction time (as low as 5 min @ 120 °C). Due to the high thermal energy neccessary to activate aryl chlorides the sequential diarylation of dichlorosilanes using an aryl bromide and chloride in one pot was achieved by only increasing the reaction temperature for the second half of the reaction. Expanding the scope of this method should give an operationally simple method for the synthesis of unsymmetric diarylsilanes.

E. Reyes-Rodriguez, S. Gülak, D. Gärtner, A. Jacobi von Wangelin; Transition Metal-Free Reductive Silylation of (Het)Aryl Bromides. *in preparation*. S. Gülak developed the original reaction protocol, and together with the author of this thesis shared the reaction optimization, synthetic work and characterization of the products. The author of this thesis developed the microwave assisted silyl coupling.

1.4 References

[1] (a) Demibras, A.; Sahin-Demibras, A.; Demibras, A. H. Global Energy Sources, Energy Usage, and Future Developments. *Energ. Sources* **2004**, *26*, 191–204; (b) Owen, N. A.; Inderwildi, O. R.; King, D. A. The status of conventional world oil reserves—Hype or cause for concern? *Energ. Policy* **2010**, *38*, 4743–4749; (c) Olah, G. A.; Goeppert, A.; Prakash, G. K. S. *Beyond Oil and Gas: The Methanol Economy*; Wiley-VCH, **2011**.

[2] Anastas, P.; Warner, J. *Green Chemistry: Theory and Practice*; Oxford University Press, **1998**.

[3] (a) Dallinger, D.; Kappe, C. O. Microwave-Assisted Synthesis in Water as Solvent. *Chem. Rev.* **2007**, *107*, 2563–2591; (b) Larhed, M.; Moberg, C.; Hallberg, A. Microwave-Accelerated Homogeneous Catalysis in Organic Chemistry. *Acc. Chem. Res.* **2002**, *35*, 717–727; (c) de la Hoz, A.; Díaz-Ortiz, A.; Prieto, P. *Green Chemistry Series*; Royal Society of Chemistry, **2016**; Chapter 1. Microwave-Assisted Green Organic Synthesis, pp. 1–33.

[4] Polshettiwar, V.; Luque, R.; Fihri, A.; Zhu, H.; Bouhrara, M.; Basset, J.-M. Magnetically Recoverable Nanocatalysts. *Chem. Rev.* **2011**, *111*, 3036–3075.

[5] (a) Blacker, A. J.; Breen, J. R.; Bourne, R. A.; Hone, C. A. In *Green and Sustainable Medicinal Chemistry: Methods, Tools and Strategies for the 21st Century Pharmaceutical Industry*; Summerton, L., Sneddon, H. F., Eds.; Royal Society of Chemistry, **2016**; Chapter 12. The Growing Impact of Continuous Flow Methods on the Twelve Principles of Green Chemistry, pp. 140–155; (b) Vaccaro, L., Ed. *Sustainable Flow Chemistry*; Wiley-VCH Verlag GmbH & Co. KGaA, **2017**.

[6] Chanda, A.; Fokin, V. V. Organic Synthesis "On Water". *Chem. Rev.* **2009**, *109*, 725–748.

[7] (a) Jain, N.; Kumar, A.; Chauhan, S.; Chauhan, S. Chemical and biochemical transformations in ionic liquids. *Tetrahedron* **2005**, *61*, 1015–1060; (b) Hallett, J. P.; Welton, T. Room-Temperature Ionic Liquids: Solvents for Synthesis and Catalysis. 2. *Chem. Rev.* **2011**, *111*, 3508–3576.

[8] Nicolaou, K. C.; Bulger, P. G.; Sarlah, D. Metathesis Reactions in Total Synthesis. *Angew. Chem. Int. Ed.* **2005**, *44*, 4490–4527.

[9] (a) Cornils, B.; Herrmann, W. A. Concepts in homogeneous catalysis: the industrial view. *J. Catal.* **2003**, *216*, 23–31; (b) Bhaduri, S.; Mukesh, D. *Homogeneous Catalysis: Mechanisms and Industrial Applications*; Wiley, **2014**.

[10] (a) Yorimitsu, H.; Oshima, K. Recent Progress in Asymmetric Allylic Substitutions Catalyzed by Chiral Copper Complexes. *Angew. Chem. Int. Ed.* **2005**, *44*, 4435–4439; (b) Tasker, S. Z.; Standley, E. A.; Jamison, T. F. Recent advances in homogeneous nickel catalysis. *Nature* **2014**, *509*, 299–309.

[11] (a) Nuss, P.; Eckelman, M. J. Life Cycle Assessment of Metals: A Scientific Synthesis. *PLoS ONE* **2014**, *9*, e101298; (b) Cox, P. A. *The Elements: Their Origin, Abundance, and Distribution*; OXFORD UNIV PR, **1989**.

[12] To compare the value of the selected metals, prices for available metal powders with similar purity (>99%) and pore sizes (60-100 mesh) were obtained from the chemical supplier Strem Chemicals; www.strem.com, accessed on 05/2018.

[13] (a) Johansson Seechurn, C. C. C.; Kitching, M. O.; Colacot, T. J.; Snieckus, V. Palladium-Catalyzed Cross-Coupling: A Historical Contextual Perspective to the 2010 Nobel Prize. *Angew. Chem. Int. Ed.* **2012**, *51*, 5062–5085; (b) Roy, D.; Uozumi, Y. Recent Advances in Palladium-Catalyzed Cross-Coupling Reactions at ppm to ppb Molar Catalyst Loadings. *Adv. Synth. Catal.* **2018**, *360*, 602–625.

[14] (a) Kim, J. G.; Shin, K.; Chang, S. In *C-H Bond Activation and Catalytic Functionalization I*; Dixneuf, P., Doucet, H., Eds.; Springer International Publishing, **2015**; Chapter Rh(III)- and Ir(III)-Catalyzed Direct C–H Bond Transformations to Carbon–Heteroatom Bonds, pp. 29–51; (b) Gensch, T.; James, M. J.; Dalton, T.; Glorius, F. Increasing Catalyst Efficiency in C-H Activation Catalysis. *Angew. Chem. Int. Ed.* **2018**, *57*, 2296–2306.

[15] (a) Trnka, T. M.; Grubbs, R. H. The Development of L2X2RuCHR Olefin Metathesis Catalysts: An Organometallic Success Story. *Acc. Chem. Res.* **2001**, *34*, 18–29; (b) Ogba, O. M.; Warner, N. C.; O'Leary, D. J.; Grubbs, R. H. Recent advances in ruthenium-based olefin metathesis. *Chem. Soc. Rev.* **2018**, *47*, 4510–4544.

[16] Crabtree, R. H. *The Organometallic Chemistry of the Transition Metals*; John Wiley & Sons Inc., **2014**.

[17] Holland, P. L. Distinctive Reaction Pathways at Base Metals in High-Spin Organometallic Catalysts. *Acc. Chem. Res.* **2015**, *48*, 1696–1702.

[18] Chirik, P. J. Iron- and Cobalt-Catalyzed Alkene Hydrogenation: Catalysis with Both Redox-Active and Strong Field Ligands. *Acc. Chem. Res.* **2015**, *48*, 1687–1695.

[19] Lyaskovskyy, V.; de Bruin, B. Redox Non-Innocent Ligands: Versatile New Tools to Control Catalytic Reactions. *ACS Catal.* **2012**, *2*, 270–279.

[20] Bart, S. C.; Chłopek, K.; Bill, E.; Bouwkamp, M. W.; Lobkovsky, E.; Neese, F.; Wieghardt, K.; Chirik, P. J. Electronic Structure of Bis(imino)pyridine Iron Dichloride, Monochloride, and Neutral Ligand Complexes: A Combined Structural, Spectroscopic, and Computational Study. *J. Am. Chem. Soc.* **2006**, *128*, 13901–13912.

[21] Zell, T.; Milstein, D. Hydrogenation and Dehydrogenation Iron Pincer Catalysts Capable of Metal–Ligand Cooperation by Aromatization/Dearomatization. *Acc. Chem. Res.* **2015**, *48*, 1979–1994.

[22] Fürstner, A. Iron Catalysis in Organic Synthesis: A Critical Assessment of What It Takes To Make This Base Metal a Multitasking Champion. *ACS Cent. Sci.* **2016**, *2*, 778–789.

[23] Holland, P. L. Electronic Structure and Reactivity of Three-Coordinate Iron Complexes. *Acc. Chem. Res.* **2008**, *41*, 905–914.

[24] Hoffman, B. M.; Lukoyanov, D.; Yang, Z.-Y.; Dean, D. R.; Seefeldt, L. C. Mechanism of Nitrogen Fixation by Nitrogenase: The Next Stage. *Chem. Rev.* **2014**, *114*, 4041–4062.

[25] (a) Braunstein, P., Oro, L. A., Raithby, P. R., Eds. *Metal Clusters in Chemistry*; Wiley-VCH Verlag GmbH, **1999**; (b) Buchwalter, P.; Rosé, J.; Braunstein, P. Multimetallic Catalysis Based on Heterometallic Complexes and Clusters. *Chem. Rev.* **2014**, *115*, 28–126.

[26] Aliofkhazraei, M., Ed. *Handbook of Nanoparticles*; Springer International Publishing, **2016**.

[27] Lu, A.-H.; Salabas, E.; Schüth, F. Magnetic Nanoparticles: Synthesis, Protection, Functionalization, and Application. *Angew. Chem. Int. Ed.* **2007**, *46*, 1222–1244.

[28] Schöttle, C.; Bockstaller, P.; Popescu, R.; Gerthsen, D.; Feldmann, C. Sodium-Naphthalenide-Driven Synthesis of Base-Metal Nanoparticles and Follow-up Reactions. *Angew. Chem. Int. Ed.* **2015**, *54*, 9866–9870.

[29] Bart, S. C.; Lobkovsky, E.; Chirik, P. J. Preparation and Molecular and Electronic Structures of Iron(0) Dinitrogen and Silane Complexes and Their Application to Catalytic Hydrogenation and Hydrosilation. *J. Am. Chem. Soc.* **2004**, *126*, 13794–13807.

Recyclable Cobalt(0) Nanoparticle Catalysts for Hydrogenations

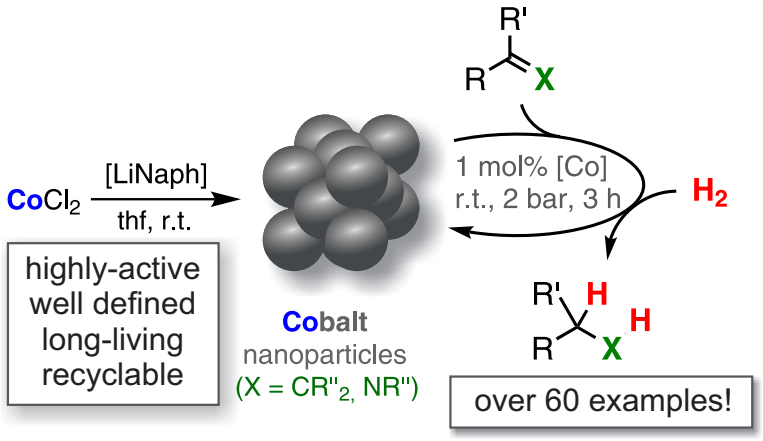

Abstract: The search for new hydrogenation catalysts to replace commonly used noble metals is largely driven by sustainability concerns and the distinct mechanistic features of 3d transition metals. Several combinations of cobalt precursors and special ligands in the presence of reductants or under high-thermal conditions were reported to provide active hydrogenation catalysts. This study reports a new method for the preparation of small, monodisperse Co(0) nanoparticles (3-4 nm) from the reduction of commercial $CoCl_2$ in the absence of ligands or surfactants. High catalytic activity was observed in hydrogenations of alkenes, alkynes, imines, and heteroarenes (1-20 bar H_2). The magnetic properties enabled catalyst separation and multiple recyclings.

2.1 Introduction

The recent advent of powerful synthetic and spectroscopic techniques for the preparation and analysis of sensitive metallic compounds has prompted a rapidly increasing interest in colloidal and nanoparticulate base metal(0) catalysts.[1] The characteristics of metallic nanoparticles as hybrids between homogeneous and heterogeneous species address the key criteria for catalytic applications: high dispersion, large surface area, good separability, rich surface coordination chemistry, and high reactivity.[2] Molecular cobalt catalysts have recently been intensively studied toward their application to hydrogenation reactions (Scheme 2.1, top).[3,4] The liquid-phase synthesis of base cobalt nanoparticles is often limited by their sensitivity towards moisture and air, the rapid ageing of the particles, and the availability of convenient precursor molecules. Low-valent organometallic precursors (e.g. carbonyl, alkyl, aryl complexes) can be volatile and toxic or require multi-step syntheses, special conditions, and elaborate handling procedures (Scheme 2.1, center).[5] Typically, tailor-made surfactants (e.g. amines, thiols, polydentate ligands, ionic liquids) are needed to control particle size and growth and prevent agglomeration.[6]

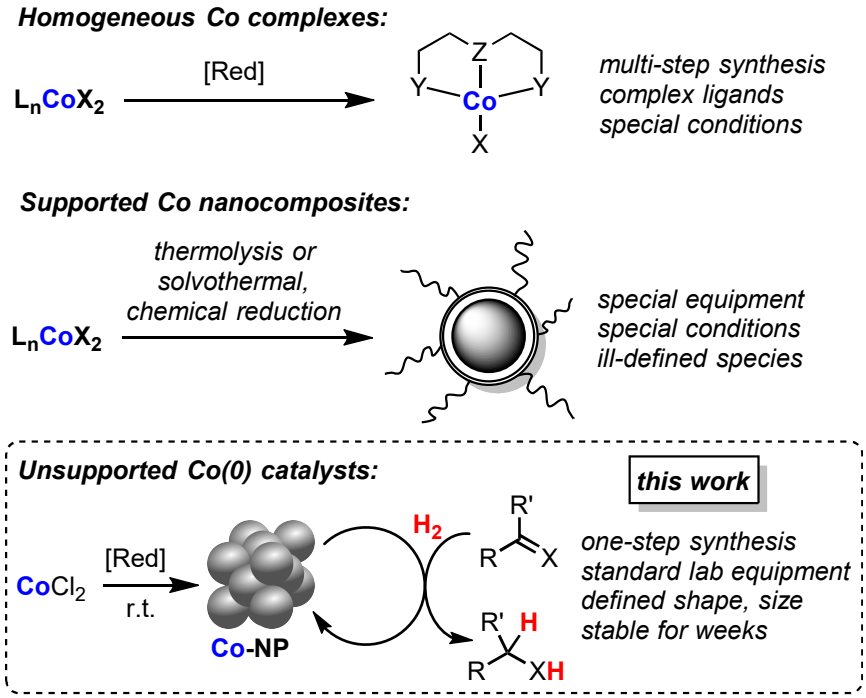

Scheme 2.1: Molecular and heterogeneous cobalt catalysts for hydrogenations.

Several heterogeneous hydrogenation catalysts were prepared by the reduction of 3d transition metal precursors with organometallic or hydride reagents and by thermal decomposition of transition metal-ligand complexes, often in the presence of

stable support materials.[7] Beller and co-workers successfully applied cobalt oxide nanoparticles supported on Al_2O_3 to catalytic hydrogenations of heteroarenes, nitriles, and ketones.[8] The same group recently reported graphitic shell encapsulated Co nanoparticles for the synthesis of amines by reductive amination,[9] while Yuan reported nanocomposite Co/CoO on graphene for catalytic nitroarene hydrogenations.[10] Reusable Co nanoparticle catalysts on silicon carbon nitride were prepared by Kempe and co-workers.[11] Zhang *et al.* developed *Z*-selective semihydrogenations of alkynes with an ill-defined Co/B catalyst formed from cobalt(II) acetate and $NaBH_4$.[12] Similar chemoselectivity was reported for Co@*N*-graphite nanoparticles.[13]

Here, we present a complementary synthesis of a Co nanoparticle catalyst that avoids complex ligands, high-temperature conditions, and special support materials. Very small and monodisperse Co(0) nanoparticles are accessible by the precise control of the reducing conditions in the presence of an alkali metal/arene couple (Scheme 2.1, bottom). The resultant Co(0) catalysts present tangible advances over the current state-of-the-art in that they are easily accessible from commercial reagents, exhibit long-term stability and activity, exhibit a wide substrate scope in hydrogenation reactions, and allow facile separation and catalyst recycling. The complementary properties of such Co nanoparticles and related molecular catalysts prepared under similar conditions demonstrate the close conceptual relationship between homogeneous and heterogeneous catalysts.[4,14]

2.2 Results and Discussion

Highly pure M(0) nanoparticles (M = Ti, Mo, W, Re, Fe, Zn) with diameters of ≤ 10 nm were prepared by the reduction of metal halides with alkaline metal naphthalenides.[15] However, the related quasi-naked Co(0) nanoparticles were still elusive due to their strong superparamagnetism and the resulting agglomeration. A modified procedure has now enabled the facile preparation of small and uniform nanoparticles in quantitative yield by reduction of $CoCl_2$ with lithium naphthalenide ([LiNaph]) at 20 °C and centrifugation (Co-NP) or magnetic separation (mCo-NP, Figure 2.1a). Alkaline metal naphthalenides were also used to obtain so-called activated Rieke metals,[15] which, however, are barely characterized and typically represent bulk metals. Nanoparticles made via the Rieke approach often show significant agglomeration and oxide impurities.[15] The here shown Co nanoparticles nevertheless may also support understanding of mechanism of activated Rieke metals.

Here, Co(0) formation was apparent from the immediate color change to black (Figure 2.1b). The use of an excessively strong reductant (E^0([NaNaph]) = –3.1 V vs. Fc/Fc^+, *cf.* $E^0(Co^{2+}/Co^0)$ = –0.28 V vs. NHE)[16] ensured high oversaturation and thus enabled excellent control of nucleation and particle growth (LaMer model).[17] The precipitates were separated by centrifugation (20,000 rpm) to obtain powderous

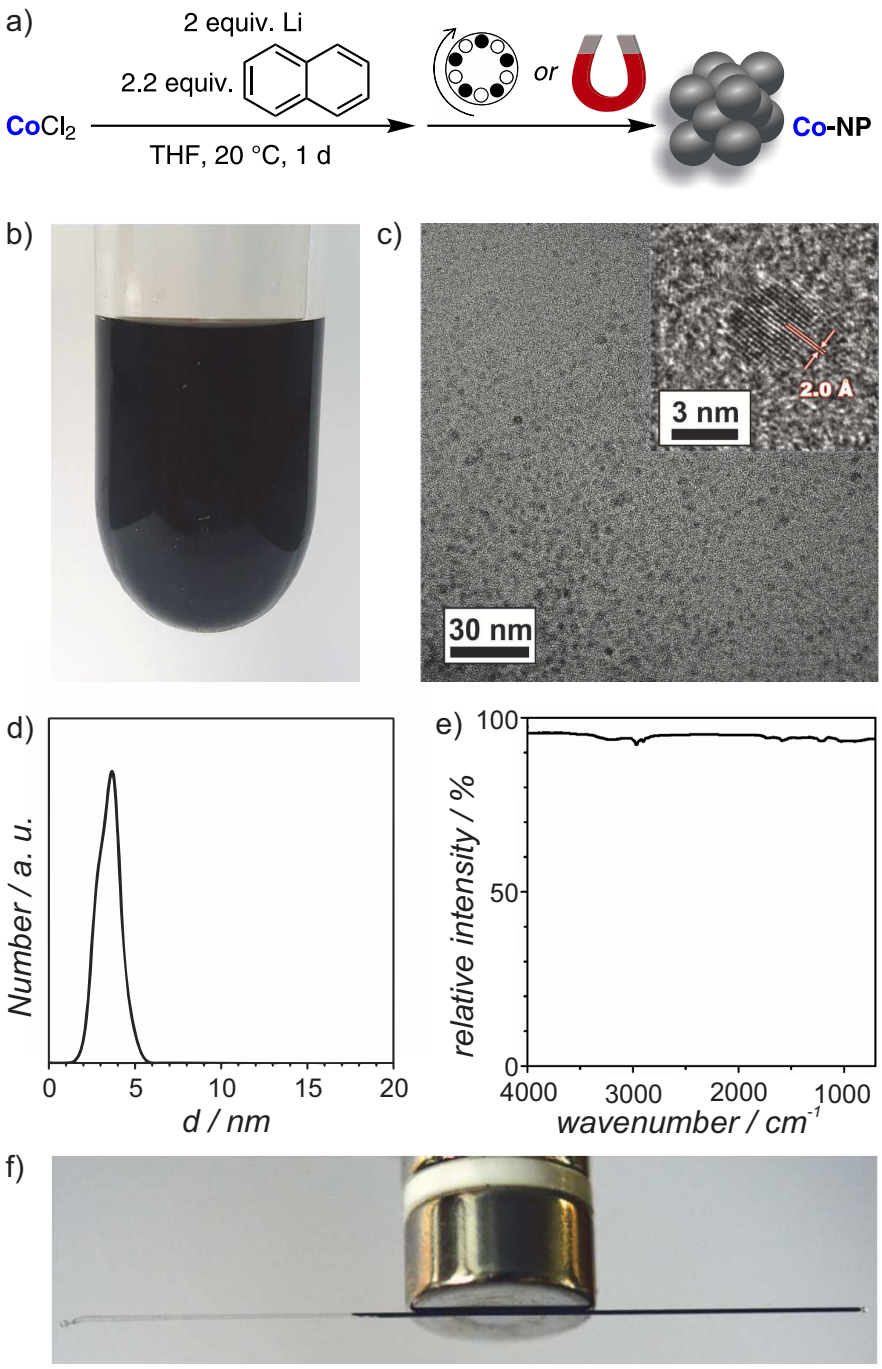

Figure 2.1: a) Synthesis of defined Co(0) nanoparticles (Co-NP) by reduction of $CoCl_2$ with LiNaph and subsequent centrifugation or magnetic separation; b) Co-NP suspension in THF; c) HRTEM overview and HAADF-STEM images (with lattice fringes and lattice distance); d) Particle size distribution from DLS; e) FT-IR spectrum with weak vibrations; f) Magnetic Co-NP powder in 0.3 mm glass capillary.

Co(0) samples with quasi-naked surfaces. The nanoparticles could be redispersed in THF or toluene. High-resolution transmission electron microscopy (HRTEM) and high-angle annular dark-field scanning transmission electron microscopy (HAADF-STEM) displayed uniform, non-agglomerated nanoparticles of 3.4 ± 0.4 nm diameter (Figure 2.1c and inset).

HAADF STEM images showed highly ordered lattice fringes that indicate the presence and crystallinity of the Co(0) nanoparticles. The lattice distance (2.0 Å) matches that of cubic bulk-Co^0 (d(111) = 2.0 Å). Dynamic light scattering (DLS) documented the size distribution of the as-prepared Co-NPs in THF suspension with a mean hydrodynamic diameter of 3.6 ± 0.9 nm (Figure 2.1d). Fourier transform infrared spectroscopy (FT-IR) gave very weak absorption related to surface-adhered molecules (mostly THF, Figure 2.1e), which documented the presence of quasi-naked nanoparticles.[15]

X-ray powder diffraction (XRD) confirmed the presence and purity of metallic Co.[1] Glass capillaries containing the powderous Co-NPs were strongly attracted to a permanent magnet (Figure 2.1f). The latter property was exploited in the development of a highly practical and operationally simple procedure for preparation and work-up. The 'naked' Co-NPs were successfully isolated from the suspension by magnetic immobilization (cylindrical neodymium magnet, 10 x 20 mm, N45, 15 min, 4 mmol Co in 20 ml THF) instead of the centrifugation.[18]

We have evaluated the catalytic activity of the freshly prepared Co(0) nanoparticles in hydrogenations of unsaturated substrates that lie outside the well-explored scope of highly polar carbonyl, nitro, and cyano compounds. There are much fewer reports of Co-catalyzed hydrogenations of non-polar or less polar substrates such as alkenes, alkynes, and imines.[19] Highly reproducible catalyst activities, facile handling, and dosing were achieved by ultrasonication of the catalyst suspension for 1 h prior to use. Mono- and di-substituted alkenes as well as terminal and internal alkynes were cleanly hydrogenated under very mild conditions (1 mol% Co-NP or mCo-NP, 2 bar H_2, 20 °C, 3 h). Sterically demanding, functionalized, and tetra-substituted alkenes required slightly harsher conditions. Good chemoselectivities were observed for bifunctional molecules such as limonene and 2-vinylpyridine. Functional group tolerance tests showed that cyano, nitro, and carbonyl functions were detrimental to the reaction, while esters, ethers, amines, fluoro and chloro groups were tolerated.[2]

The catalytic protocol was further simplified by preparing nanoparticles *in situ* via the standard protocol but without laborious work-up and isolation procedures. Control experiments showed the identical catalytic activity and long-term stability of *in situ* prepared and isolated Co-NPs (Table 2.1). Magnetic separation also afforded active Co(0) nanoparticles (mCo-NP) with identical catalytic activity that could be

[1] See subsection 2.4.10 on p. 64 for further information.

[2] For an overview on all additives used in the functional group tests as well as their respective yields and conversions see subsection 2.4.7 on p. 62.

easily recycled over multiple runs (Figure 2.3).[3] The decoration of nanoparticles with organic surfactants is a versatile method for alteration of the surface properties and introduction of functionalities.[6,20] The addition of oleylamine (1.5 equiv. per Co) to the freshly prepared nanoparticles resulted in the formation of a very stable, highly dispersed nanoparticle suspension (aCo-NP) that could not be magnetically separated by a standard magnet. The oleylamine-supported aCo-NP were catalytically less active and less stable than the amine-free Co-NPs so that there is no benefit of surfactant addition to Co-NP catalysis under these conditions (Table 2.1).

Table 2.1: Comparison of different Co-NP catalysts and ageing periods.

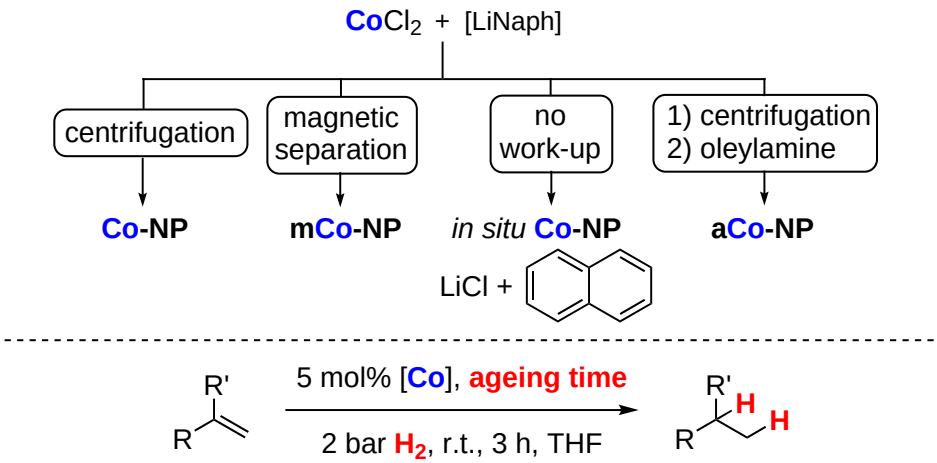

Substrate	[Co]	Yield [%] after 1 week	Yield [%] after 6-35 weeks
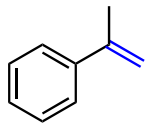	Co-NP	>99	>99 [a]
	mCo-NP	>99	98 [b]
	in situ Co-NP	>99	97 [c]
	aCo-NP	66 (69)	3 (8) [a]
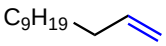	Co-NP	96	98 [a]
	mCo-NP	>99	96 [b]
	in situ Co-NP	>99	96 [c]
	aCo-NP	>99	91 [a]

Conditions: 0.5 mmol substrate, 2 ml THF, yields were determined by quantitative GC-FID vs. internal *n*-pentadecane. Conversion in parentheses if not >95%. [a] 35 weeks. [b] 9 weeks. [c] 6 weeks.

[3] For a reaction progress analysis comparing the isolated Co-NP, *in situ* Co-NP, and mCo-NP see subsection 2.4.8 on p. 63.

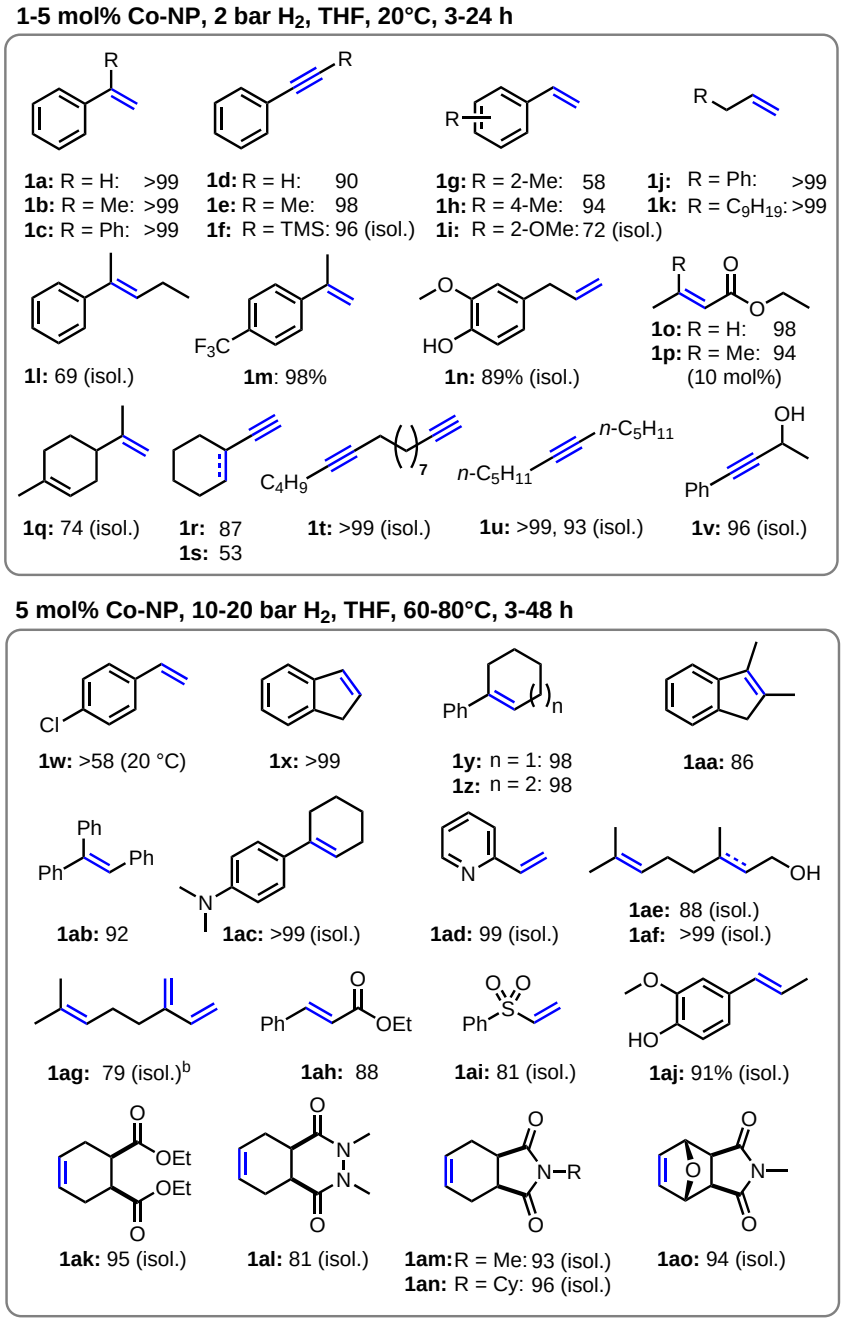

Figure 2.2: Co-catalyzed hydrogenation of alkenes and alkynes. Blue bonds indicate the sites of π-bond hydrogenation. Standard conditions: 0.25 mmol substrate, 1 ml in THF, 1 mol% Co-NP, 2 bar H_2, 20 °C, 3 h. If not otherwise noted, yields were determined by GC-FID vs. internal *n*-pentadecane.

The standard reaction conditions enabled effective catalyst recycling after each reaction run by an external magnet without loss of catalyst material and activity (Figure 2.3). More than 99.6% of the particles were removed from the organic phase by

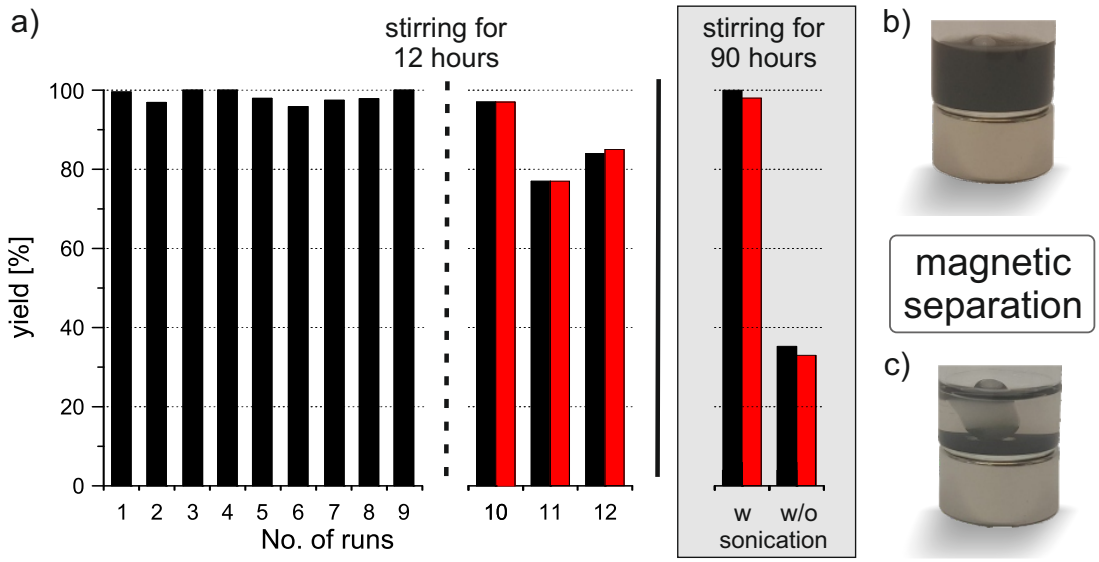

Figure 2.3: a) Consecutive hydrogenation runs of styrene (0.5 mmol) using the same catalyst particles (5 mol%) and regeneration of catalyst activity by ultrasonication (box). Yields (black), conversions (red); b) Suspension of the hydrogenation reaction of styrene with 5 mol% Co-NP; c) Catalyst separation by an external magnet (after 1 min).

a commercial Nd magnet (10x20 mm, N45) and decantation (Figure 2.3b,c). ICP-OES studies documented minimal leaching (< 0.4% Co, < 0.02 mol%) into the liquid phase after the first run. After filtering the decanted reaction solution over silica, an insignificant amount of cobalt (0.68 ppm per Co supplied) remained in the organic phase.

TEM images showed only marginal differences of particle topology between the Co catalysts (Co-NPs and *in situ* Co-NPs) before and after the hydrogenations.[4] Multiple sequential reactions were performed with the same catalyst portion. Importantly, ultrasonication of the catalyst suspension resulted in a healing of catalytic activity after multiple recycling operations (> 10) and when the catalyst aged during storage for extended periods (several days).

Proof of the heterogeneous nature of the catalyst was also derived from kinetic poisoning experiments (Figure 2.4).[14] Addition of the selective homotopic poison dibenzo[*a*,*e*]cyclooctatetraene (dct)[14,21] at 40% conversion of a model hydrogenation did not change the reaction rate. Consistently, complete inhibition resulted from the addition of mercury (300 equiv. per Co). This quantitative amalgamation was accompanied by decolorization and formation of a metallic mercury drop with silvery luster at the bottom of the reaction.[22] An identical reaction ceased immediately after addition of a 0.1 equiv. PMe_3 per Co. Lower amounts of PMe_3 (0.025 equiv.)

[4]See Figures 2.9-2.12 on pp. 65-66

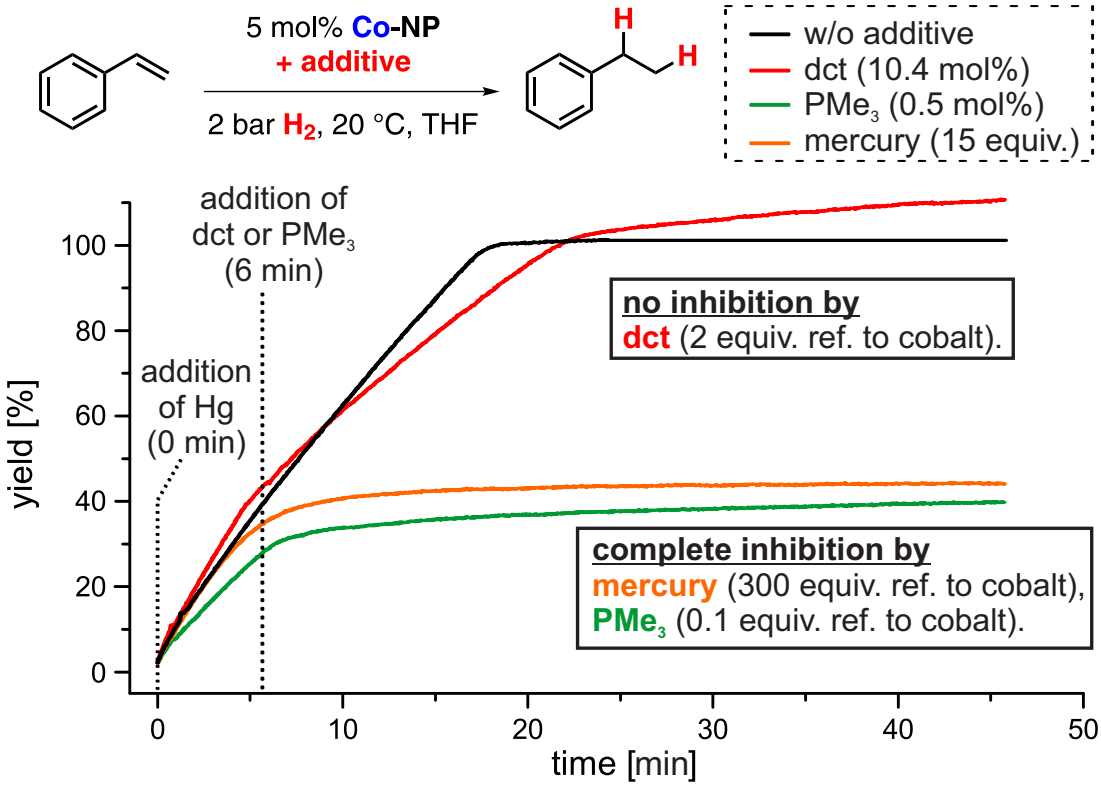

Figure 2.4: Catalyst poisoning with dct (2 equiv. per Co), PMe_3 (0.1 equiv. per Co), Hg (300 equiv. per Co). Yields were determined from the H_2 consumption.

resulted in partial catalyst poisoning. These studies provide strong indications of a heterotopic mechanism in full accord with literature reports.[14]

Finally, we extended the substrate scope of our nanoparticles beyond alkene hydrogenations to imines and heteroaromatic quinolines. Homogeneous and heterogeneous 3d metals that catalyze imine and quinoline hydrogenation are still relatively scarce even though such hydrogenations are an attractive, atom-economic route to amines. Moreover, compounds with a 1,2,3,4-tetrahydroquinoline scaffold are found in natural products and bioactive compounds.[23] Gratifyingly, our Co-NP catalysts were active in the clean hydrogenation of small and bulky aldimines, ketimines, and various quinolines (Figure 2.5). Chloro, ester, hydroxyl, benzyl, furan, and pyridine functions were tolerated. Besides the hydrogenation of the imine moiety, the furanyl and pyridyl imines **2d**-**2f** underwent partial hydrogenation of the heterocycle. Interestingly, only for the 2-, 3- or 4-substituted quinolines **2t**-**2v** unselective hydrogenation towards the 1,2,3,4- and 5,6,7,8-tetrahydroquinoline products was observed.[5]

[5]For a detailed list of the reaction conditions for each substrate see subsection 2.4.4.1 on p. 30.

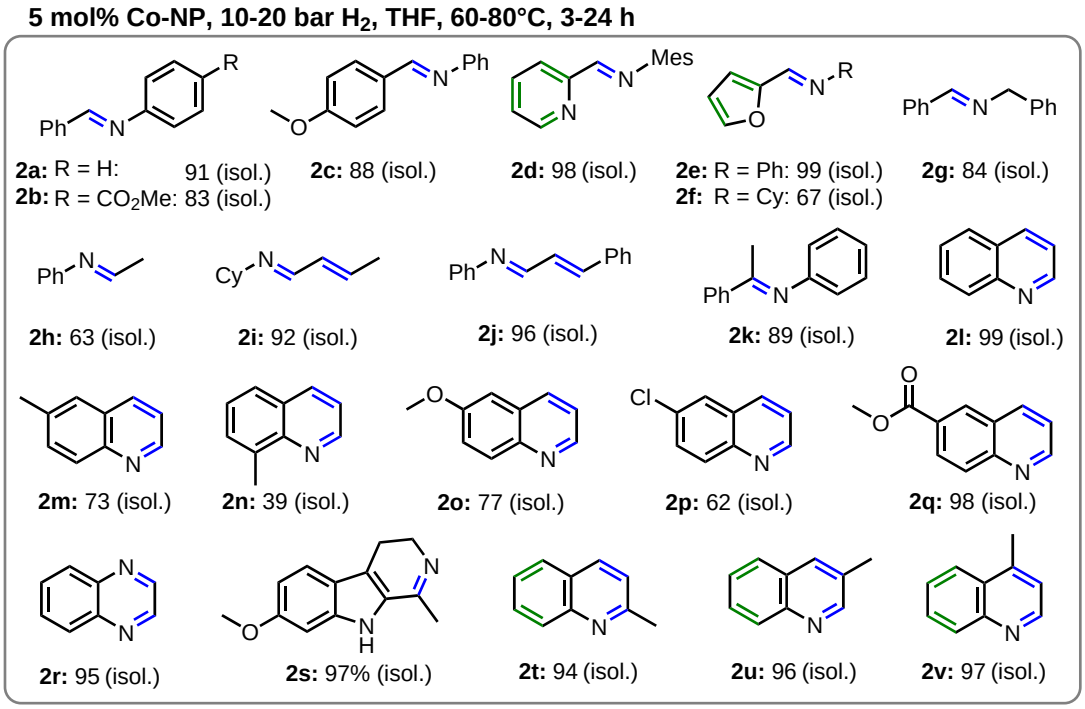

Figure 2.5: Co-catalyzed hydrogenation of imines and quinolines. Blue bonds are sites of hydrogenation. Green bonds indicate traces of over-hydrogenation. Standard conditions: 0.5 mmol substrate, 2 ml THF, 5 mol% Co-NP, 10 bar H_2, 60 °C, 24 h. If not otherwise noted, yields were determined by GC-FID vs. *n*-pentadecane.

2.3 Conclusion

In summary, we have established a straightforward and operationally simple synthesis of stable Co(0) nanoparticles from commercial reagents. Detailed analytical studies (TEM, XRD, DLS, poisoning) documented the heterogeneous nature of the small and uniform nanoparticles of 3.4 ± 0.4 nm. Applications to catalytic hydrogenations enabled the clean conversion of alkenes, alkynes, imines, and quinolines under mild conditions (2 - 20 bar H_2, 20 - 80 °C). The catalysts could be easily mechanically separated and recycled for multiple hydrogenation runs without loss of activity. The ease of synthetic preparation in the absence of complex ligands, their wide catalytic applicability, the facile catalyst recycling and long-term stability constitute prime advantages of such cobalt catalysts that should stimulate further use in the realm of organic synthesis.

2.4 Experimental Section

2.4.1 General information

Analytical Thin-Layer Chromatography: Thin layer chromatography was carried out using aluminium plates with silica gel and fluorescent indicator (Merck, TLC Silica gel 60 F_{254}). Thin layer chromatography plates were visualized by exposure to ultraviolet light (366 or 254 nm) or by immersion in a staining solution of molybdatophosphoric acid in ethanol or potassium permanganate in water.

Chemicals and Solvents: Commercially available alkenes and alkynes were distilled under reduced pressure prior to use. Solvents (THF, Et_2O, *n*-hexane, toluene) were distilled over sodium and benzophenone and stored over molecular sieves (4 Å). Oleylamine was stored over molecular sieve (4 Å) for 30 days and degassed in vacuum. Cobalt(II)chloride (99.999%, ABCR), lithium (99%, Alfa Aesar) and naphthalene (99%, Alfa Aesar) were used as received.

Column Chromatography: Flash column chromatography with silica gel 60 from KMF (0.040-0.063 mm). Mixtures of solvents used are noted in brackets.

High Pressure Reactor: Hydrogenation reactions were carried out in 160 and 300 ml high pressure reactors (ParrTM) in 4 ml glass vials. The reactors were loaded under argon, purged with H_2 (1 min), then three times with 2 bar H_2, sealed and the internal pressure was adjusted. Hydrogen (99.9992%) was purchased from Linde.

^{1}H- und ^{13}C-NMR-Spectroscopy: Nuclear magnetic resonance spectra were recorded on a Bruker Avance 300 (300 MHz) and Bruker Avance 400 (400 MHz). ^{1}H-NMR: The following abbreviations are used to indicate multiplicities: s = singlet; d = doublet; t = triplet, q = quartet; m = multiplet, dd = doublet of doublet, dt = doublet of triplet, dq = doublet of quartet, ddt = doublet of doublet of quartet. Chemical shift δ is given in ppm to tetramethylsilane.

Fourier-Transformations-Infrared-Spectroscopy (FT-IR): Spectra were recorded on an Agilent Cary 630 FTIR with ATR-device. All spectra were recorded at room temperature. Wave number is given in cm^{-1}. Bands are marked as s = strong, m = medium, w = weak and b = broad.

Gas Chromatography Flame Ionization Detector (GC-FID): Measurements were carried out on a HP6890 GC-System with injector 7683B and Agilent 7820A System. Column: HP-5, 19091J-413 (30 m × 0.32 mm × 0.25 μm), carrier gas: N_2. GC-FID was used for reaction control and catalyst screening (Calibration with internal standard *n*-pentadecane and analytically pure samples).

Gas Chromatography with Mass-Selective Detector (GC-MS): Measurements were performed on an Agilent 6890N Network GC-System, mass detector 5975 MS. Column: HP-5MS (30 m × 0.25 mm × 0.25 μm, 5% phenylmethylsiloxane, carrier gas: H_2. Standard heating procedure: 50 °C (2 min), 25 °C/min -> 300 °C (5 min).

High Resolution Mass Spectrometry (HRMS): The spectra were recorded by the Central Analytics Lab at the Department of Chemistry, University of Regensburg, on a MAT SSQ 710 A from Finnigan.

Inductively Coupled Plasma Optical Emission Spectrometry (ICP-OES): Spectro Analytical Instruments Spectroflame (Type: FSMEA85C) was used for measurements.

Inductively Coupled Plasma Mass Spectrometry (ICP-MS): Measurements were carried out on a Perkin Elmer Elan 9000.

Gas-Uptake Reaction Monitoring: Gas-uptake was monitored with a Man On the Moon X201 kinetic system to maintain a constant reaction pressure. The system was purged with hydrogen prior to use. Reservoir pressure was set to about 9 bar H_2. Calibration of the reservoir pressure drop in relation to H_2 consumption was performed by quantitative hydrogenation of various amounts of α-methylstyrene with a Pd/C catalyst in 1 ml of THF.

Transmission Electron Microscopy (TEM): (HR)TEM, and high-angle annular dark-field scanning transmission electron microscopy (HAADF-STEM) were conducted with an aberration-corrected FEI Titan3 80-300 microscope operating at 300 and 80 kV, a FEI Osiris microscope at 200 kV, and a Philips CM 200 FEG/ST microscope at 200 kV. TEM samples were prepared by evaporating DME, THF or *n*-heptane suspensions on amorphous carbon (lacey-)film suspended on copper grids. The deposition of the samples on the carbon (lacey-)film copper grids was performed under argon atmosphere in a glovebox. The grids were thereafter transferred with a suitable vacuum/inert gas transfer module into the transmission electron microscope without any contact to air. Average particle diameters were calculated by statistical evaluation of at least 150 particles (ImageJ 1.47v software).

X-Ray Powder Diffraction (XRD): X-ray powder diffraction was carried out with a Stoe STADI-P diffractometer operating with Ge-monochromatized Cu-Kα radiation. Co^0 powder samples sintered at 800 °C for 7 h in vacuum for crystallization of the metal and eventual oxide impurities. The powder samples were measured on a Stoe IPDS II image plate diffractometer using Mo-Kα radiation (graphite monochromator). Samples were diluted with glass spheres (9-13 μm, Sigma-Aldrich) to reduce the X-ray absorption of the metal nanoparticles and prepared in glass capillaries under argon. Since the scattering power of the small-sized metal nanoparticles (diameter $\leq$ 10 nm) is low, certain non-specific background is observed for all nanoparticles. This non-specific scattering was fitted by background correction.

2.4.2 General Procedures

Synthesis of Co Nanoparticles

Cobalt(II)chloride (519 mg, 4.0 mmol), lithium (56 mg, 8.0 mmol) and naphthalene (1.20 g, 9.4 mmol) were stirred in 20 ml THF for 24 h. The resultant nanoparticles were separated by centrifugation (20,000 rpm) and purified by redispersion and

centrifugation (320 ml THF). Subsequently, the solids were dried in vacuum (for storage as powder) or redispersed in 40 ml THF (Co-NPs, for catalytic applications). The preparation of amine-stabilized nanoparticles (aCo-NPs) was effected by treatment of the dried solids with 38 ml THF and 2 ml oleylamine (aCo-NP). As an alternative to the separation by centrifugation, the particles can be separated by an external commercial neodymium magnet (mCo-NPs). The preparation of related nanoparticles followed the same reduction protocol but without the washing procedures (*in situ* Co-NPs). The primary THF solutions (containing the by-products LiCl, naphthalene) were directly employed in catalytic reactions. The removal of the magnetic stir bar appeared to be important to ensure long-term catalyst stability. After extended periods of storage of the catalysts suspensions, ultrasonification for 15-60 min effected complete redispersion and secured highest reproducibility.

General Procedure for Hydrogenation

Under an atmosphere of argon, a 5 ml screw cap vial with a PTFE septum and magnetic stir bar was charged with the substrate (0.25 mmol) and THF (875 μL). The catalyst suspension (125 μL; 0.0125 mmol Co) was added and the septum punctured with a short needle (Braun). The vial was placed into a high-pressure reactor (Parr Instr.), which was sealed, removed from the glove box, placed on a magnetic stirrer plate, and purged with H_2. After 3 h at r.t. under an atmosphere of H_2 (2 bar), the pressure was released, the vial retrieved, and the reaction quenched with saturated aqueous NH_4Cl (1 ml). For quantitative GC-FID analyses, *n*-pentadecane was added as internal standard. The mixture was extracted with ethyl acetate and the combined organic layers were dried (Na_2SO_4). For isolation of the products, the reaction mixture was filtered through a Pasteur pipette filled with SiO_2. The pipette was washed with *n*-pentane (3 x 1 ml) and the solvents evaporated. Amines were isolated as the corresponding ammonium salts after addition of $HCl{\cdot}Et_2O$.

General Method for Kinetic Examination in Catalytic Hydrogenation

A flame-dried 10 ml two-neck flask was connected to a Man on the Moon X201 gas-uptake system. After purging with H_2, the system was set to a reaction pressure of 1.9 bar. The catalyst mixture in THF (2 ml) was added using a Teflon septum. Monitoring of the hydrogen uptake started with the addition of the substrate (0.5 mmol). The pressure was recorded every two seconds until the pressure in the reaction vessel remained stationary.

2.4.3 Synthesis of Starting Materials

General Procedure for the Synthesis of Imines

Silica (6 g) was weighed into a 100 ml round-bottom flask and suspended in ethanol (35 ml). After addition of the aldehyde (20 mmol) and amine (20 mmol, 1 equiv.), the flask was put into an ultrasonic bath for 20 min at room temperature. The mixture was stirred overnight, filtered and the solvent removed. The crude product mixture was vacuum distilled (80 °C, 0.02 mbar) and the imines collected. Modified procedure according to K. P. Guzen, A. S. Guarezemini, A. T. Órfão, R. Cella, C. M. Pereira, H. A. Stefani, Tetrahedron Lett. 2007, 48, 1845.

N-(2-Furanylmethylene)-benzenamine

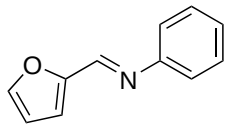

$C_{11}H_9NO$

171.20 g/mol

Pale yellow liquid

Yield 1.72 g, 10.0 mmol (50%)

^{1}H-NMR (300 MHz, MeOD) δ 8.37 (s, 1H), 7.77 (d, J = 1.8 Hz, 1H), 7.44 – 7.33 (m, 2H), 7.29 – 7.19 (m, 3H), 7.12 (dd, J = 3.5, 0.7 Hz, 1H), 6.64 (dd, J = 3.5, 1.8 Hz, 1H).

^{13}C-NMR (75 MHz, MeOD) δ 153.08, 151.98, 150.21, 147.68, 130.38, 127.63, 122.05, 118.77, 113.52.

GC-MS t_R = 8.044 min, (EI, 70 eV): m/z = 171 [M^+], 142, 115, 104, 93, 77, 66, 51.

Analytical data were in full agreement with H. Naka, D. Koseki, Y. Kondo, *Adv. Synth. Catal.* **2008**, *350*, 1901.

N-(2-Furanylmethylene)-cyclohexylamine

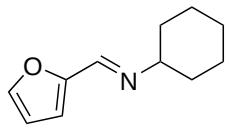

$C_{11}H_{15}NO$

177.25 g/mol

Yellow liquid

Yield 2.68 g, 15.1 mmol (76%)

^{1}H-NMR (300 MHz, MeOD) δ 8.16 (s, 1H), 7.67 (d, J = 1.8 Hz, 1H), 6.91 (dd, J = 3.6, 0.8 Hz, 1H), 6.56 (dd, J = 3.5, 1.8 Hz, 1H), 3.18 (tt, J = 10.8, 4.1 Hz, 1H), 1.88 – 1.78 (m, 1H), 1.78 – 1.66 (m, 2H), 1.62 – 1.46 (m, 2H), 1.46 – 1.15 (m, 3H).

^{13}C-NMR (75 MHz, MeOD) δ 152.56, 150.41, 146.59, 116.23, 112.95, 70.97, 35.25, 26.56, 25.89.

GC-MS t_R = 7.46 min, (EI, 70 eV): m/z = 177 [M^+], 162, 148, 134, 122, 107, 94, 81, 67, 53.

HRMS found 177.11437 (calculated: 177.11482)

(rac)-N-(2-Butenylidene)-cyclohexlyamine

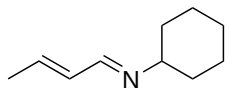

$C_{10}H_{17}N$

151.25g/mol

Yield 2.04 g, 13.5 mmol (68%)

^{1}H-NMR (300 MHz, MeOD) δ 7.93 – 7.87 (m, 1H), 7.76 (t, J = 2.8 Hz, 1H), 6.43 – 6.29 (m, 1H), 6.19 (ddq, J = 15.4, 8.8, 1.4 Hz, 1H), 3.67 – 3.56 (m, 1H), 3.08 – 2.95 (m, 2H), 1.89 (d, J = 6.7 Hz, 3H), 1.84 – 1.61 (m, 11H), 1.50 – 1.31 (m, 7H), 1.17 (d, J = 6.2 Hz, 3H).

^{13}C-NMR (75 MHz, MeOD) δ 164.2, 163.6, 163.6, 143.6, 143.5, 132.0, 75.8, 70.5, 70.0, 36.9, 35.4, 35.3, 35.3, 26.6, 26.3, 25.8, 25.8, 19.5, 18.6, 18.5.

GC-MS t_R = 6.26 min, (EI, 70 eV): m/z = 150 [M^+-H], 136, 122, 110, 94, 82, 68, 55.

Analytical data were in full agreement with A. Saoudi, A. Benguedach, H. Benhaoua, *Synth. Commun.* **1995**, *25*, 2349.

2.4.4 Hydrogenation Reactions

2.4.4.1 Catalyst and Substrate Screening

	Substrate	[Co]	[mol%]	[bar]	[°C]	[h]	Yield [%]	Comment
1a	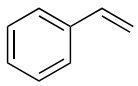	Co-NP	1			3	>99	-
		Co-NP	5			0.5	>99	-
		mCo-NP	5	2	20	0.5	98	-
		in situ NP	5			0.5	97	-
		aCo-NP	1			3	16 (26)	-
1b	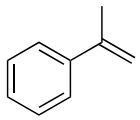	Co-NP	1			3	>99	-
		Co-NP	5			1	98	-
		mCo-NP	5	2	20	0.5	>99	-
		in situ NP	5			0.5	>99	-
		aCo-NP	1			3	16 (26)	-
1c	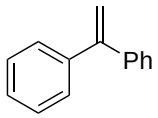	Co-NP	1	2	20	3	>99	-
		in situ NP	5				99	-
1d	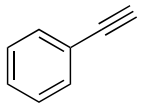	Co-NP	5			8	>99	-
		mCo-NP	1	2	20	24	88	-
		mCo-NP	5			3	90	-
1e	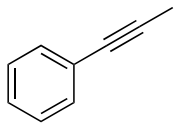	Co-NP	5	2	20	8	98	-
1f	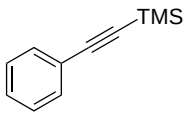	mCo-NP	5	2	20	3	96 (isol.)	-

	Substrate	[Co]	[mol%]	[bar]	[°C]	[h]	Yield [%]	Comment
1g	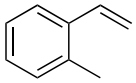	mCo-NP	1	2	20	3	58	-
1h	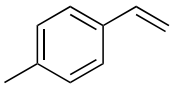	mCo-NP	1	2	20	3	94	-
1i	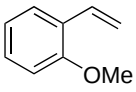	mCo-NP	1	2	20	3	72 (isol.)	100% according to ^{1}H-NMR of the mixture
1j	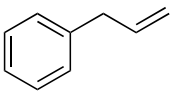	Co-NP	1	2	20	3	>99	-
		in situ Co-NP	5				97	-
1k	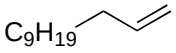	Co-NP	1	2	20	3	>96	-
		Co-NP	5			0.5	92	-
		mCo-NP	5			0.5	>99	-
		in situ NP	5			0.5	>99	-
1l	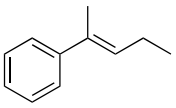	mCo-NP	5	2	20	24	69 (isol.)	-
1m	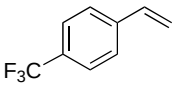	mCo-NP	5	2	20	3	98	-
1n	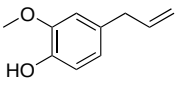	mCo-NP	5	2	20	3	89 (isol.)	-
1o	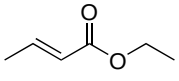	mCo-NP	5	2	20	3	98	-

	Substrate	[Co]	[mol%]	[bar]	[°C]	[h]	Yield [%]	Comment
1p	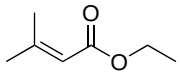	mCo-NP	5	2	20	3	42	-
		mCo-NP	10				94	-
1q	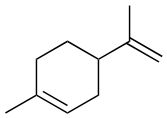	mCo-NP	5	2	20	24	74 (isol.)	residual solvent (*vide infra*)
1r	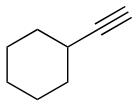	mCo-NP	5	2	20	3	87	yield of ethyl-cyclohexane (100% conv.).
1s	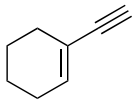	mCo-NP	5	2	20	3	53	See **1q**
1t	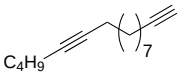	mCo-NP	5	2	20	8	99 (isol.)	-
1u	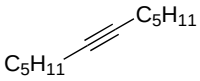	Co-NP	5	2	20	8	>99	-
		mCo-NP	5			24	93 (isol.)	-
1v	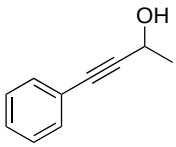	mCo-NP	5	2	20	3	96 (isol.)	-
1w	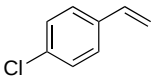	Co-NP	5	10	20	24	58	-
1x	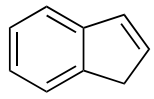	Co-NP	5	10	10	60	>99	-
		Co-NP	5	60	60	20	>99	-

	Substrate	[Co]	[mol%]	[bar]	[°C]	[h]	Yield [%]	Comment
1y	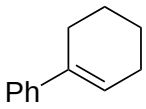	Co-NP	5	10	60	24	98	-
		aCo-NP	5				80	-
1z	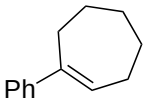	Co-NP	5	10	60	24	98	-
		aCo-NP	5				79	-
1aa	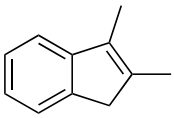	Co-NP	5	10	60	24	86	-
1ab	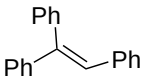	Co-NP	5	10	20	3	71	-
		Co-NP	5		60		92	-
1ac	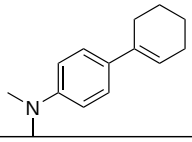	mCo-NP	5	10	60	24	99 (isol.)	-
1ad	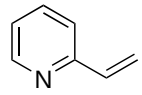	mCo-NP	5	2	20	3	99 (isol.)	-
1ae	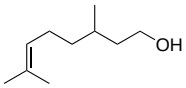	mCo-NP	5	20	80	24	88 (isol.)	-
1af	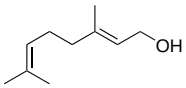	mCo-NP	5	10	60	24	99 (isol.)	-
1ag	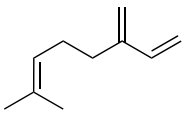	mCo-NP	5	20	80	24	79 (isol.)	-
1ah	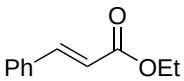	mCo-NP	5	2	20	3	49	-
		mCo-NP	5	10	60	24	88	-

	Substrate	[Co]	[mol%]	[bar]	[°C]	[h]	Yield [%]	Comment
1ai	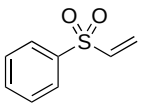	mCo-NP	5	10	60	24	81	Purity: *vide infra*
1aj	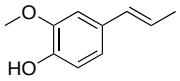	mCo-NP	5	10	60	24	91 (isol.)	-
1ak	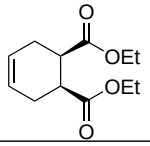	mCo-NP	5	10	60	24	95 (isol.)	-
1al	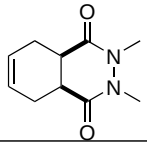	mCo-NP	5	20	80	24	81 (isol.)	-
1am	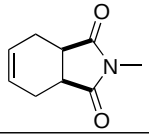	mCo-NP	5	10	60	24	93 (isol.)	-
1an	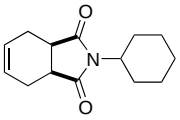	mCo-NP	5	10	60	24	96 (isol.)	-
1ao	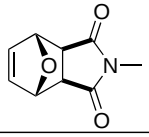	mCo-NP	5	10	60	24	94	-
2a	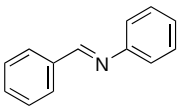	Co-NP	5	10	60	6	87	-
		Co-NP	5				>99	-
		mCo-NP	5			24	91 (isol.)	-
2b	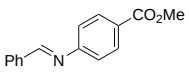	mCo-NP	5	10	60	24	83 (isol.)	-

	Substrate	[Co]	[mol%]	[bar]	[°C]	[h]	Yield [%]	Comment
2c	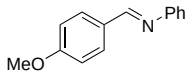	mCo-NP	5	10	60	24	88 (isol.)	-
2d	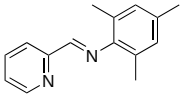	mCo-NP	5	10	60	24	98 (isol.)	mixture: *vide infra*
2e	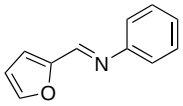	mCo-NP	5	10	60	24	99 (isol.)	mixture: *vide infra*
2f	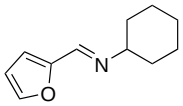	mCo-NP	5	10	60	24	67 (isol.)	mixture: *vide infra*
2g	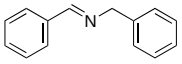	mCo-NP	5	10	60	24	84 (isol.)	-
2h	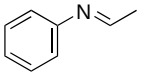	mCo-NP	5	10	60	24	63 (isol.)	-
2j	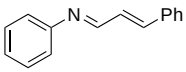	mCo-NP	5	10	60	24	96 (isol.)	-
2k	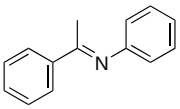	mCo-NP	5	20	80	48	89 (isol.)	Purity: *vide infra*
2l	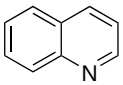	mCo-NP	5	10	100	24	99 (isol.)	-

	Substrate	[Co]	[mol%]	[bar]	[°C]	[h]	Yield [%]	Comment
2m	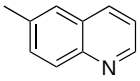	mCo-NP	5	20	80	48	75 (isol.)	-
2n	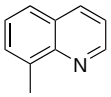	mCo-NP	5	20	80	24	39 (isol.)	-
2o	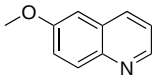	mCo-NP	5	20	80	24	77 (isol.)	-
2p	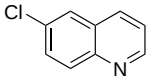	mCo-NP	5	20	80	48	62 (isol.)	-
2q	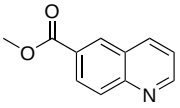	mCo-NP	5	20	80	24	98 (isol.)	-
2r	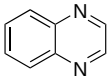	mCo-NP	5	20	80	24	95 (isol.)	-
2s	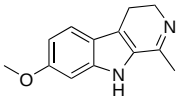	mCo-NP	5	10	60	24	97 (isol.)	-
2t	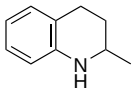	mCo-NP	5	20	80	24	49 (isol.)	-
2t′	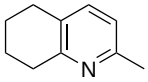	mCo-NP	5	20	80	24	45 (isol.)	-
2u	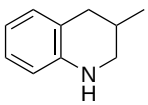	mCo-NP	5	20	80	48	46 (isol.)	-

	Substrate	[Co]	[mol%]	[bar]	[°C]	[h]	Yield [%]	Comment
2u′	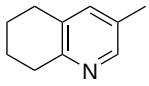	mCo-NP	5	20	80	48	50 (isol.)	-
2v	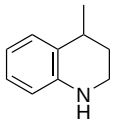	mCo-NP	5	20	80	48	31 (isol.)	-
2v′	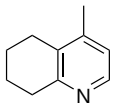	mCo-NP	5	20	80	48	66 (isol.)	-

2.4.4.2 Isolated Hydrogenation Reaction Products

Trimethyl(phenethyl)silane (1f)

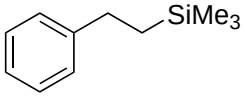

$C_{11}H_{18}Si$

178.35 g/mol

Yield	85.2 mg, 0.48 mmol (96%)
^{1}H-NMR	(300 MHz, $CDCl_3$) δ 7.30 – 7.10 (m, 5H), 2.66 – 2.56 (m, 2H), 0.91 – 0.80 (m, 2H), 0.00 (s, 9H).
^{13}C-NMR	(75 MHz, $CDCl_3$) δ 145.5, 128.4, 127.9, 125.6, 30.2, 18.8, -1.6.
GC-MS	t_R = 6.16 min, (EI, 70 eV): m/z = 178 [M^+], 163, 135, 104, 91, 73, 59, 51.

Analytical data were in full agreement with E. Negishi, D. R. Swanson, C. J. Rousset, *J. Org. Chem.* **1990**, *55*, 5406.

1-Ethyl-2-methoxybenzene (1i)

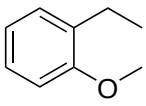

$C_9H_{12}O$

136.19 g/mol

Yield	52.2 mg, 0.38 mmol (72%)
^{1}H-NMR	(400 MHz, $CDCl_3$) δ 7.22 – 7.13 (m, 2H), 6.91 (td, J = 7.4, 1.1 Hz, 1H), 6.86 (dd, J = 8.0, 1.1 Hz, 1H), 3.84 (s, 3H), 2.66 (q, J = 7.5 Hz, 2H), 1.21 (t, J = 7.5 Hz, 3H).
^{13}C-NMR	(101 MHz, $CDCl_3$) δ 157.5, 132.7, 129.0, 126.9, 120.6, 110.3, 55.4, 23.4, 14.3.
GC-MS	t_R = 5.30 min, (EI, 70 eV): m/z = 136 [M^+], 121, 103, 91, 77, 65, 51.

Analytical data were in full agreement with M. Mirza-Aghayan, R. Boukherroub, M. Rahimifard, *J. Organomet. Chem.* **2008**, *693*, 3567.

2-Phenylpentane (1l)

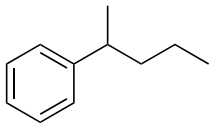

$C_{11}H_{16}$

148.25 g/mol

Yield	53.4 mg, 0.36 mmol (69%)
^{1}H-NMR	(300 MHz, $CDCl_3$) δ 7.33 – 7.26 (m, 2H), 7.22 – 7.14 (m, 3H), 2.70 (h, J = 7.0 Hz, 1H), 1.65 – 1.43 (m, 2H), 1.36 – 1.09 (m, 5H), 0.87 (t, J = 7.3 Hz, 3H).
^{13}C-NMR	(75 MHz, $CDCl_3$) δ 148.1, 128.4, 127.1, 125.9, 40.9, 39.8, 22.4, 21.0, 14.3.
GC-MS	t_R = 5.42 min, (EI, 70 eV): m/z = 148 [M^+], 105, 91, 77, 65, 51.

Analytical data were in full agreement with R. B. Bedford, P. B. Brenner, E. Carter, T. W. Carvell, P. M. Cogswell, T. Gallagher, J. N. Harvey, D. M. Murphy, E. C. Neeve, J. Nunn, D. R. Pye, *Chem. Eur. J.* **2014**, *20*, 7935.

2-Methoxy-4-propylphenol (1n/1aj)

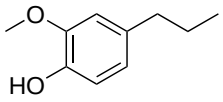

$C_{10}H_{14}O_2$

166.22 g/mol

Yield	from eugenol: 75.6 mg, 0.45 mmol (89%) from isoeugenol: 75.7 mg, 0.46 mmol (91%)
^{1}H-NMR	(300 MHz, $CDCl_3$) δ 6.86 – 6.81 (m, 1H), 6.71 – 6.65 (m, 2H), 5.48 (brs, 1H), 3.88 (s, 3H), 2.52 (t, J = 7.8 Hz, 2H), 1.69 – 1.55 (m, 2H), 0.94 (t, J = 7.3 Hz, 3H).
^{13}C-NMR	(75 MHz, $CDCl_3$) δ 146.4, 143.6, 134.8, 121.1, 114.2, 111.1, 56.0, 37.9, 25.0, 14.0.
GC-MS	t_R = 7.038 min, (EI, 70 eV): m/z = 166 [M^+], 137, 122, 107, 94, 77, 65, 51.

Analytical data were in full agreement with C. Smit, M. W. Fraaije, A. J. Minnaard, *J. Org. Chem.* **2008**, *73*, 9482.

4-Isopropyl-1-methylcyclohexene (1q)

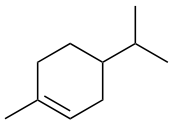

$C_{10}H_{18}$

138.25 g/mol

Yield	33.7 mg, 0.24 mmol (95%; 78% purity) Due to the volatile nature of the product, the solvents could not be removed completely. NMR-analysis showed 74% hydrogenation product, 14% THF, 7% *n*-pentane
^{1}H-NMR	(400 MHz, $CDCl_3$) δ 5.46 – 5.28 (m, 1H), 2.08 – 1.91 (m, 3H), 1.80 – 1.67 (m, 2H), 1.64 (s, 3H), 1.46 (dq, J = 13.1, 7.1, 6.5 Hz, 1H), 1.35 – 1.16 (m, 2H), 0.92 – 0.84 (m, 6H).
^{13}C-NMR	(101 MHz, $CDCl_3$) δ 134.1, 121.2, 40.2, 32.4, 31.0, 29.1, 26.6, 23.6, 20.2, 19.9.
GC-MS	t_R = 4.84 min, (EI, 70 eV): m/z = 138 [M^+], 123, 109, 95, 81, 67, 55.

Analytical data were in full agreement with G. Villa, G. Povie, P. Renaud, *J. Am. Chem. Soc.* **2011**, *133*, 5913.

4-Isopropyl-1-methylcyclohexene (1t)

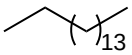

$C_{16}H_{34}$

226.45 g/mol

Yield	59.3 mg, 0.26 mmol (99%)
^{1}H-NMR	(300 MHz, $CDCl_3$) δ 1.26 (s, 28H), 0.94 – 0.82 (m, 6H).
^{13}C-NMR	(75 MHz, $CDCl_3$) δ 32.1, 29.9, 29.8, 29.6, 22.9, 14.3.
GC-MS	t_R = 8.185 min, (EI, 70 eV): m/z = 226 [M^+], 197, 183, 169, 155, 141, 127, 113, 99, 85, 71, 57.

Analytical data were in full agreement with T. Brenstrum, D. A. Gerristma, G. M. Adjabeng, C. S. Frampton, J. Britten, A. J. Robertson, J. McNulty, A. Capretta, *J. Org. Chem.* **2004**, *69*, 7635.

_n_-Dodecane (1u)

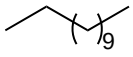

$C_{12}H_{26}$

170.34 g/mol

Yield	78.6 mg, 0.46 mmol (93%)
^{1}H-NMR	(400 MHz, $CDCl_3$) δ 1.26 (s, 20H), 0.94 – 0.84 (m, 6H).
^{13}C-NMR	(101 MHz, $CDCl_3$) δ 32.1, 29.9, 29.8, 29.5, 22.9, 14.3.
GC-MS	t_R = 6.01 min, (EI, 70 eV): m/z = 170 [M^+], 141, 127, 112, 98, 85, 71, 57.

Analytical data were in full agreement with X. Xu, D. Cheng, W. Pei, *J. Org. Chem.* **2006**, *71*, 6637.

4-Phenylbutan-2-ol (1v)

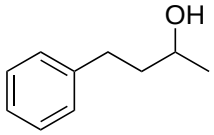

$C_{10}H_{14}O$

150.22 g/mol

Yield	73.9 mg, 0.49 mmol (96%) Purity: 93%; 7% semihydrogenation product
^{1}H-NMR	(300 MHz, $CDCl_3$) δ 7.26 – 7.31 (m, 2H), 7.17 – 7.24 (m, 3H), 3.84 (dq, 1H, J = 6.22, 12.10 Hz), 2.61 – 2.83 (m, 2H), 1.73 – 1.83 (m, 2H), 1.53 (br s, 1H), 1.24 (d, 3H, J = 6.17 Hz).
^{13}C-NMR	(75 MHz, $CDCl_3$) δ 142.2, 128.5, 125.9, 67.6, 41.0, 32.3, 23.8.
GC-MS	t_R = 6.51 min, (EI, 70 eV): m/z = 150 [M^+], 132, 117, 91, 77, 65, 51.

Analytical data were in full agreement with Z. E. Clarke, P. T. Maragh, T. P. Dasgupta, D. G. Gusev, A. J. Lough, K. Abdur-Rashid, *Organometallics* **2006**, *25*, 4113.

4-Cyclohexyl-*N*,*N*-dimethylaniline (1ac)

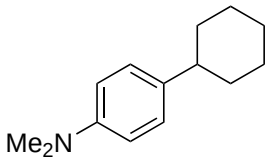

$C_{14}H_{21}N$

203.33 g/mol

Yield	100.7 mg, 0.50 mmol (99%)
^{1}H-NMR	(400 MHz, $CDCl_3$) δ 7.15 – 7.08 (m, 2H), 6.77 – 6.70 (m, 2H), 2.93 (s, 6H), 2.43 (tq, J = 9.0, 3.3 Hz, 1H), 1.92 – 1.81 (m, 4H), 1.75 (dtt, J = 12.6, 3.1, 1.4 Hz, 1H), 1.47 – 1.33 (m, 4H), 1.27 (ddt, J = 14.5, 9.0, 3.3 Hz, 1H).
^{13}C-NMR	(101 MHz, $CDCl_3$) δ 149.1, 136.8, 127.4, 113.1, 43.6, 41.1, 34.9, 27.2, 26.4.
GC-MS	t_R = 9.15 min, (EI, 70 eV): m/z = 203 [M^+], 160, 146, 134, 115, 103, 93, 77, 51.

Analytical data were in full agreement with W. M. Czaplik, M. Mayer, A. Jacobi von Wangelin, *Angew. Chem. Int. Ed.* **2009**, *48*, 607.

2-Ethylpyridine hydrochloride (1ad)

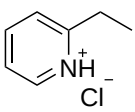

$C_7H_{10}OClN$

143.61 g/mol

Yield	36.1 mg, 0.25 mmol (99%)
^{1}H-NMR	(300 MHz, MeOD) δ 8.75 (dt, J = 4.8, 2.3 Hz, 1H), 8.65 – 8.53 (m, 1H), 8.04 (d, J = 8.1 Hz, 1H), 8.00 – 7.90 (m, 1H), 3.21 – 3.06 (m, 2H), 2.02 (s, 1H), 1.50 – 1.41 (m, 3H).
^{13}C-NMR	(75 MHz, MeOD) δ 160.0, 148.3, 142.1, 128.0, 126.0, 27.8, 13.3.
GC-MS (freebase)	t_R = 3.79 min, (EI, 70 eV): m/z = 106 [M^+], 92, 79, 65, 51.

3,7-Dimethyl-1-octanol (1ae: from citronellol; 1af: from geraniol)

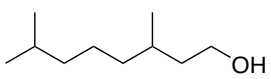

$C_{10}H_{22}O$

158.29 g/mol

Yield	from citronellol: 68.3 mg, 0.43 mmol (88%), from geraniol: 40.4 mg, 0.26 mmol (99%)

^{1}H-NMR	(300 MHz, $CDCl_3$) δ 3.76 – 3.57 (m, 2H), 1.67 – 1.46 (m, 3H), 1.43 – 1.32 (m, 2H), 1.32 – 1.21 (m, 3H), 1.19 – 1.06 (m, 3H), 0.87 (dd, J = 8.0, 6.5 Hz, 9H).
^{13}C-NMR	(75 MHz, $CDCl_3$) δ 61.4, 40.1, 39.4, 37.5, 29.6, 28.1, 24.8, 22.8, 22.7, 19.7.
GC-MS	t_R = 6.016 min, (EI, 70 eV): m/z = 140 [M^+-OH_2], 125, 112, 97, 83, 70, 55.
HRMS	Calcd. for $C_{10}H_{21}O$ 157.15869; found: 157.15836.
IR	3324 (b), 2955 (s), 2926 (s), 2870 (s), 1461 (m), 1379 (m), 1260 (m), 1051 (s), 805 (s) cm^{-1}.

2,6-Dimethyloctane (1ag)

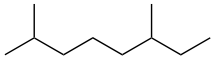

$C_{10}H_{22}$

142.29 g/mol

Yield	57.6 mg, 0.40 mmol (79%)
^{1}H-NMR	(300 MHz, $CDCl_3$) δ 1.52 (dp, J = 13.1, 6.6 Hz, 1H), 1.38 – 1.22 (m, 5H), 1.18 – 1.01 (m, 4H), 0.85 (t, J = 6.8 Hz, 12H).
^{13}C-NMR	(75 MHz, $CDCl_3$) δ 39.5, 37.0, 34.6, 29.7, 28.2, 25.0, 22.9, 22.8, 19.4, 11.6.
GC-MS	t_R = 4.03 min, (EI, 70 eV): m/z = 142 [M^+], 127, 113, 97, 85, 71, 57.

Analytical data were in full agreement with R. V. Ottenbacher, D. G. Samsonenko, E. P. Talsi, K. P. Bryliakov, *Org. Lett.* **2012**, *14*, 4310.

(Ethylsulfonyl)benzene (1ai)

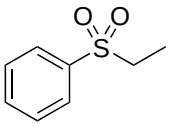

$C_8H_{10}O_2S$

170.23 g/mol

Yield	77.1 mg, 0.45 mmol (91%) Purity: 89%; 12% starting material
^{1}H-NMR	(300 MHz, $CDCl_3$) δ 7.93 – 7.86 (m, 2H), 7.72 – 7.59 (m, 1H), 7.60 – 7.53 (m, 2H), 3.11 (q, J = 7.4 Hz, 2H), 1.26 (t, J = 7.4 Hz, 3H).

^{13}C-NMR	(75 MHz, $CDCl_3$) δ 138.6, 133.8, 129.4, 128.3, 50.7, 7.6.
GC-MS	t_R = 9.00 min, (EI, 70 eV): m/z = 170 [M^+], 154, 141, 125, 105, 94, 77, 65, 51.

Analytical data were in full agreement with R. V. Kupwade, S. S. Khot, U. P. Lad, U. V. Desai, P. P. Wadgaonkar, *Res. Chem. Intermed.* **2017**, *43*, 6875.

Diethyl cis-1,2-cyclohexanedicarboxylate (1ak)

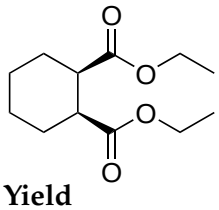

$C_{12}H_{20}O_4$

228.29 g/mol

Yield	107.8 mg, 0.47 mmol (95%)
^{1}H-NMR	(300 MHz, $CDCl_3$) δ 4.12 (q, J = 7.1 Hz, 4H), 2.85 – 2.74 (m, 2H), 2.10 – 1.89 (m, 2H), 1.83 – 1.66 (m, 2H), 1.58 – 1.30 (m, 4H), 1.23 (t, J = 7.2 Hz, 6H).
^{13}C-NMR	(75 MHz, $CDCl_3$) δ 173.8, 60.4, 42.8, 26.4, 23.9, 14.3.
GC-MS	t_R = 9.33 min, (EI, 70 eV): m/z = 228 [M^+], 183, 154, 140, 125, 108, 99, 81, 67, 55.

Analytical data were in full agreement with T. Volk, D. Bernicke, J. W. Bats, H.-G. Schmalz, *Eur. J. Inorg. Chem.* **1998**, 1883.

2,3-Dimethyloctahydrophthalazine-1,4-dione (1al)

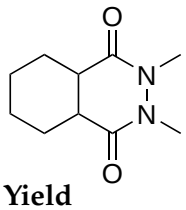

$C_{10}H_{16}N_2O_2$

196.25 g/mol

Yield	79.5 mg, 0.41 mmol (81%)
^{1}H-NMR	(300 MHz, $CDCl_3$) δ 3.24 (s, 6H), 2.79 – 2.62 (m, 2H), 1.97 – 1.49 (m, 6H), 1.49 – 1.29 (m, 2H).
^{13}C-NMR	(75 MHz, $CDCl_3$) δ 170.4, 32.7, 24.3.
GC-MS	t_R = 8.78 min, (EI, 70 eV): m/z = 196 [M^+], 180, 166, 153, 141, 125, 109, 96, 81, 67, 59.

(3a*R*,7a*S*)-2-Methylhexahydro-1*H*-isoindole-1,3(2H)-dione (1am)

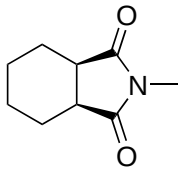

$C_9H_{13}NO_2$

167.21 g/mol

Yield 78.3 mg, 0.47 mmol (93%)

^{1}H-NMR (300 MHz, $CDCl_3$) δ 2.96 (s, 3H), 2.90 – 2.79 (m, 2H), 1.93 – 1.66 (m, 4H), 1.51 – 1.34 (m, 4H).

^{13}C-NMR (75 MHz, $CDCl_3$) δ 180.1, 39.9, 24.8, 23.8, 21.7.

GC-MS t_R = 7.46 min, (EI, 70 eV): m/z = 167 [M^+], 152. 138. 125. 113. 82. 67. 54.

Analytical data were in full agreement with T. N. Gieshoff, U. Chakraborty, M. Villa, A. Jacobi von Wangelin, *Angew. Chem. Int. Ed.* **2017**, *56*, 3585.

(3a*R*,7a*S*)-2-Cyclohexylhexahydro-1*H*-isoindole-1,3(2H)-dione (1an)

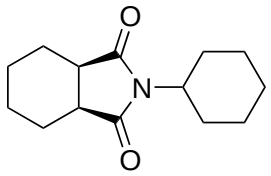

$C_{14}H_{21}NO_2$

235.33 g/mol

Yield 111.0 mg, 0.47 mmol (96%)

^{1}H-NMR (300 MHz, $CDCl_3$) δ 3.92 (tt, J = 12.3, 3.9 Hz, 1H), 2.77 (ddd, J = 6.4, 4.4, 2.1 Hz, 2H), 2.11 (qd, J = 12.3, 3.4 Hz, 2H), 1.89 – 1.76 (m, 4H), 1.75 – 1.51 (m, 5H), 1.49 – 1.34 (m, 4H), 1.34 – 1.15 (m, 3H).

^{13}C-NMR (75 MHz, $CDCl_3$) δ 180.0, 51.3, 39.7, 28.9, 26.0, 25.2, 24.0, 21.8.

GC-MS t_R = 9.83 min, (EI, 70 eV): m/z = 235 [M^+], 207, 192, 178, 164, 154, 136, 124, 108, 98, 81, 67, 55.

Analytical data were in full agreement with M. Ostendorf, R. Romagnoli, I. C. Pereiro, E. C. Roos, M. J. Moolenaar, W. Speckamp, H. Hiemstra, *Tetrahedron: Asymmetry* **1997**, *8*, 1773.

exo-3,6-Epoxy-_N_-methyl-hexahydrophthalimide (1ao)

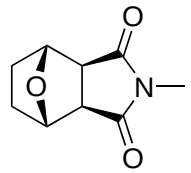

$C_9H_{11}NO_3$

181.19 g/mol

Yield	85.2 mg, 0.47 mmol (94%)
^{1}H-NMR	(300 MHz, $CDCl_3$) δ 4.86 (dd, J = 3.3, 2.1 Hz, 2H), 2.95 (s, 3H), 2.87 (s, 2H), 1.92 – 1.80 (m, 2H), 1.64 – 1.53 (m, 2H).
^{13}C-NMR	(75 MHz, $CDCl_3$) δ 177.4, 79.1, 50.1, 28.7, 25.2.
GC-MS	t_R = 9.65 min, (EI, 70 eV): m/z = 181 [M^+], 152, 140, 125, 108, 99, 81, 67, 55.

Analytical data were in full agreement with W. Sun, Z. Liu, Y. Zhang, *Int. J. Mol. Sci.* **2013**, *14*, 1.

_N_-Benzylaniline hydrochloride (2a)

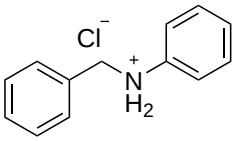

$C_{13}H_{14}ClN$

219.71 g/mol

Yield	99.4 mg, 0.45 mmol (91%)
^{1}H-NMR	(300 MHz, MeOD) δ 7.59 – 7.50 (m, 3H), 7.48 – 7.38 (m, 7H), 4.61 (s, 2H).
^{13}C-NMR	(75 MHz, MeOD) δ 136.2, 131.9, 131.5, 131.4, 131.0, 130.9, 130.2, 124.3, 57.0.
GC-MS (freebase)	t_R = 8.97 min, (EI, 70 eV): m/z = 183 [M^+], 154, 107, 91, 77, 65, 51.
Elemental Analysis	Calcd: 71.07% C, 6.42% H, 6.38% N; found: 70.57% C, 6.80% H, 6.27% N

Analytical data were in full agreement with T. Li, X. Cui, L. Sun, C. Li, *RSC Adv.* **2014**, *4*, 33599.

Methyl 4-(benzylamino)benzoate (2b)

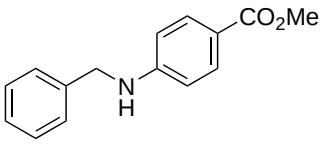

$C_{15}H_{15}NO_2$

241.29 g/mol

Yield	49.0 mg, 0.20 mmol (83%)
^{1}H-NMR	(300 MHz, $CDCl_3$) δ 7.87 (d, J = 8.8 Hz, 2H), 7.41 – 7.27 (m, 5H), 6.61 (d, J = 8.8 Hz, 2H), 4.81 (br s, 1H), 4.39 (s, 2H), 3.85 (s, 3H).
^{13}C-NMR	(75 MHz, $CDCl_3$) δ 167.4, 151.6, 138.3, 131.7, 128.9, 127.7, 127.6, 119.0, 112.0, 51.7, 48.0.
GC-MS	t_R = 11.24 min, (EI, 70 eV): m/z = 241 [M^+], 210, 180, 164, 151, 135, 119, 104, 91, 78, 65, 51.
Elemental Analysis	Calcd: 74.67% C, 6.27% H, 5.81% N; found: 73.82% C, 6.37% H, 5.63% N.

Analytical data were in full agreement with L. Fan, J. Jia, H. Hou, Q. Lefebvre, M. Rueping, *Chem. Eur. J.* **2016**, *22*, 16437.

***N*-(4-Methoxybenzyl)aniline hydrochloride (2c)**

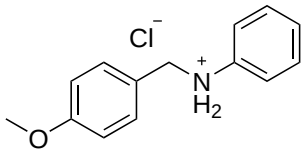

$C_{14}H_{16}ClNO$

249.74 g/mol

Yield	110.1 mg, 0.44 mmol (88%)
^{1}H-NMR	(300 MHz, $CDCl_3$) δ 7.59 – 7.48 (m, 3H), 7.45 – 7.36 (m, 2H), 7.35 – 7.30 (m, 2H), 6.97 – 6.92 (m, 2H), 4.54 (s, 2H), 3.80 (s, 3H).
^{13}C-NMR	(75 MHz, $CDCl_3$) δ 162.29, 136.10, 133.05, 131.34, 130.97, 124.34, 123.53, 115.41, 56.77, 55.82.
GC-MS (freebase)	t_R = 10.12 min, (EI, 70 eV): m/z = 213 [M^+], 196, 180, 168, 152, 142, 121, 106, 91, 77, 65, 51.
HRMS	Calcd. for $C_{14}H_{16}NO$: 214.1226; found: 214.1226.
IR	3060 (w), 2896 (m), 2840 (m), 2669 (s), 2550 (s), 2423 (s), 1595 (s), 1513 (s), 1305 (m), 1249 (s), 1033 (s), 815 (s), 795 (s) cm^{-1}.

N-(2,4,6-Trimethylphenyl)-2-pyridinemethanamine hydrochloride (2d)

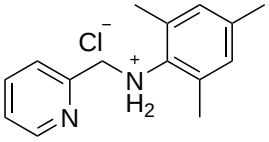

$C_{15}H_{19}ClN_2$

262.78 g/mol

Yield 128.2 mg, 0.49 mmol (98%)
23% pyridine hydrogenation

^{1}H-NMR (300 MHz, MeOD) δ 8.85 (ddd, J = 5.5, 1.6, 0.8 Hz, 1H), 8.37 (td, J = 7.9, 1.7 Hz, 1H), 7.93 (dd, J = 7.9, 1.1 Hz, 1H), 7.93 – 6.99 (m, 1H), 7.03 (s, 2H), 4.77 (s, 2H), 2.41 (s, 6H), 2.29 (s, 3H).

^{13}C-NMR (75 MHz, MeOD) δ 151.3, 146.4, 144.4, 139.8, 132.8, 131.8, 127.5, 127.3, 52.7, 20.8, 18.0.

GC-MS (freebase) t_R = 9.84 min, (EI, 70 eV): m/z = 226 [M^+], 211, 196, 181, 148, 134, 120, 107, 93, 79, 65, 51.

HRMS Calcd. for $C_{15}H_{19}N_2$ 227.1543; found: 227.1543;
Calcd. for $C_{15}H_{25}N_2$ 223.2012; found: 223.2011.

N-(2-Furanylmethyl)aniline (2e)

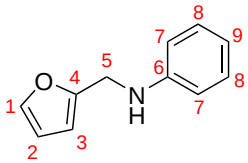

$C_{11}H_{11}NO$

173.22 g/mol

Yield 88.8 mg, 0.51 mmol (99%); Selectivity: 81%

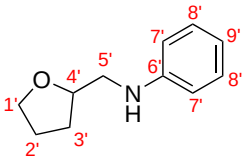

Only detectable side product:

^{1}H-NMR (400 MHz, $CDCl_3$) δ 7.38 (dd, J = 1.9, 0.8 Hz, 1H, 1), 7.20 (qd, J = 6.6, 6.1, 1.7 Hz, 3H, 8), 6.76 (t, J = 7.3 Hz, 1H, 9), 6.73 – 6.62 (m, 2H, 7), 6.34 (dd, J = 3.2, 1.9 Hz, 1H, 2), 6.25 (dd, J = 3.2, 0.9 Hz, 1H, 3), 4.33 (s, 2H, 5).
Side product (400 MHz, $CDCl_3$) δ 7.18 – 7.15 (m, 2H, 8′), 6.67 – 6.63 (m, 3H, 7′/9′), 4.15 (qd, J = 7.2, 3.8 Hz, 1H, 4′), 3.91 (dt, J = 8.3, 6.7 Hz, 1H, 1′), 3.80 (dt, J = 8.2, 6.8 Hz, 1H, 1′), 3.28 (dd, J = 12.3, 3.8 Hz, 1H, 5′), 3.10 (dd, J = 12.3, 7.5 Hz, 1H, 5′), 2.10 – 2.00 (m, 1H, 3′), 1.99 – 1.89 (m, 2H, 2′), 1.67 (ddt, J = 11.6, 8.3, 7.0 Hz, 1H, 3′).

^{13}C-NMR (101 MHz, $CDCl_3$) δ 152.9 (6), 147.8 (4), 142.0 (1), 129.4 (8), 118.1 (9), 113.3 (7), 110.5 (2), 107.1 (3), 41.6 (5).
Side product (101 MHz, $CDCl_3$) δ 148.5 (6′), 129.3 (8′), 117.6 (9′), 113.2 (7′), 77.7 (4′), 68.2 (1′), 48.3 (5′), 29.2 (3′), 25.9 (2′).

GC-MS t_R = 7.97 min, (EI, 70 eV): m/z = 173 [M^+], 144, 130, 115, 104, 91, 81, 65, 53.

Analytical data were in full agreement with M. L. Kantam, G. T. Venkanna, C. Sridhar, B. Sreedhar, B. M. Choudary, *J. Org. Chem.* **2006**, *71*, 9522.

N-(2-Furanylmethyl)cyclohexylamine (2f)

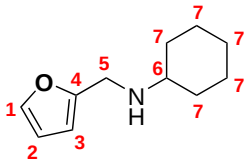

$C_{11}H_{17}NO$

179.26 g/mol

Yield 58.8 mg, 0.33 mmol (67%); Selectivity 53%

Only detectable side product:

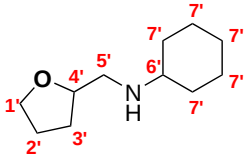

^{1}H-NMR (400 MHz, $CDCl_3$) δ 7.34 (dd, J = 1.9, 0.8 Hz, 1H, 1), 6.29 (dd, J = 3.2, 1.9 Hz, 1H, 2), 6.15 (d, J = 3.1 Hz, 1H, 3), 3.80 (s, 2H, 5), 2.44 (tt, J = 10.4, 3.8 Hz, 1H, 6), 1.91 – 1.83 (m, 5H, 7/7′), 1.72 (dt, J = 12.5, 3.6 Hz, 4H, 7/7′), 1.63 – 1.57 (m, 2H, 7/7′), 1.30 – 1.02 (m, 8H, 7/7′).
Side product (400 MHz, $CDCl_3$) δ 3.99 (ddt, J = 11.1, 7.4, 3.7 Hz, 1H, 4′), 3.84 (dt, J = 8.4, 6.7 Hz, 1H, 1′), 3.73 (dt, J = 8.2, 6.8 Hz, 1H, 1′), 2.74 (dd, J = 11.8, 3.7 Hz, 1H, 5′), 2.63 (dd, J = 11.8, 8.1 Hz, 1H, 5′), 2.44 (tt, J = 10.4, 3.8 Hz, 1H, 6′), 2.03 – 1.92 (m, 1H, 3′), 1.91 – 1.83 (m, 2H, 2′), 1.91 – 1.83 (m, 5H, 7/7′), 1.72 (dt, J = 12.5, 3.6 Hz, 4H, 7/7′), 1.63 – 1.57 (m, 2H, 7/7′), 1.57 – 1.47 (m, 1H, 3′), 1.30 – 1.02 (m, 8H, 7/7′).

^{13}C-NMR (101 MHz, $CDCl_3$) δ 154.4 (4), 141.8 (1), 110.2 (3), 106.7 (2), 55.9 (6), 43.5 (5), 33.5 (7/7′), 33.5 (7/7′), 33.4 (7/7′), 26.3 (7/7′), 25.2 (7/7′), 25.2 (7/7′), 25.1 (7/7′).
Side product (101 MHz, $CDCl_3$) δ 78.6 (4′), 68.0 (1′), 57.1 (6′), 51.6 (5′), 33.5 (7/7′), 33.5 (7/7′), 33.4 (7/7′), 29.6 (3′), 26.3 (7/7′), 25.9 (2′), 25.2 (7/7′), 25.2 (7/7′), 25.1 (7/7′).

GC-MS	t_R = 7.24 min, (EI, 70 eV): m/z = 179 [M^+], 150, 136, 122, 96, 81, 67, 53. Side product: t_R = 7.65 min, (EI, 70 eV): m/z = 183 [M^+], 140, 122, 112, 105, 96, 83, 68, 55.
HRMS	Calcd. for $C_{11}H_{18}NO$ 180.1383; found: 180.1386; Calcd. for $C_{11}H_{22}NO$ (side product) 184.1696; found: 184.1700.

***N,N*-Dibenzylamine hydrochloride (2g)**

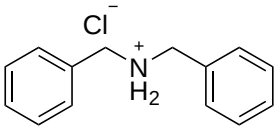

$C_{14}H_{16}ClN$

233.10 g/mol

Yield	49.0 mg, 0.21 mmol (84%)
^{1}H-NMR	(400 MHz, MeOD) δ 7.55 – 7.49 (m, 4H), 7.49 – 7.44 (m, 6H), 4.25 (s, 4H).
^{13}C-NMR	(101 MHz, MeOD) δ 132.4, 131.1, 130.7, 130.3, 52.0.
GC-MS (freebase)	t_R = 10.9 min, (EI, 70 eV): m/z = 196 [M-H^+], 179, 165, 152, 139, 120, 106, 91, 77, 65 ,51.

Analytical data were in full agreement with L. Xing, C. Cheng, R. Zhu, B. Zhang, X. Wang, Y. Hu, *Tetrahedron* **2008**, *64*, 11783.

***N*-Benzylmethylamine hydrochloride (2h)**

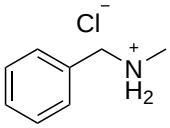

$C_8H_{12}ClN$

157.64 g/mol

Yield	52.7 mg, 0.33 mmol (63%)
^{1}H-NMR	(400 MHz, MeOD) δ 7.53 – 7.43 (m, 5H), 4.19 (s, 2H), 2.72 (s, 3H).
^{13}C-NMR	(101 MHz, MeOD) δ 132.56, 130.90, 130.72, 130.31, 53.61, 33.12.
GC-MS	t_R = 5.22 min, (EI, 70 eV): m/z = 120 [M^+], 104, 91, 78, 65, 51.

Analytical data were in full agreement with N. L. Lampland, M. Hovey, D. Mukherjee, A. D. Sadow, *ACS Catal.* **2015**, *5*, 4219.

N-Benzylmethylamine hydrochloride (2i)

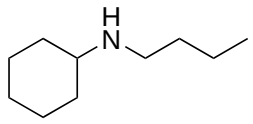

$C_{10}H_{21}N$

155.29 g/mol

Yield	72.0 mg, 0.46 mmol (92%)
^{1}H-NMR	(400 MHz, MeOD) δ 3.12 – 2.95 (m, 3H), 2.20 – 2.03 (m, 2H), 1.93 – 1.82 (m, 2H), 1.78 – 1.61 (m, 3H), 1.45 (dt, J = 15.1, 7.5 Hz, 2H), 1.42 – 1.31 (m, 4H), 1.31 – 1.15 (m, 1H), 0.99 (t, J = 7.4 Hz, 3H).
^{13}C-NMR	(101 MHz, MeOD) δ 58.39, 45.58, 30.35, 29.52, 26.12, 25.48, 20.90, 13.92.
GC-MS	t_R = 6.00 min, (EI, 70 eV): m/z = 155 [M^+], 126, 112, 98, 84, 70, 56.

Analytical data were in full agreement with R. Nacario, S. Kotakonda, D. M. D. Fouchard, L. M. V. Tillekeratne, R. A. Hudson, *Org. Lett.* **2005**, *7*, 471.

N-(3-Phenylpropyl)aniline hydrochloride (2j)

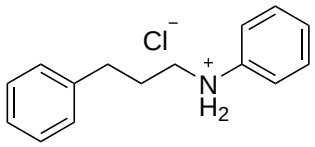

$C_{15}H_{18}ClN$

247.77 g/mol

Yield	58.2 mg, 0.23 mmol (96%)
^{1}H-NMR	(300 MHz, MeOD) δ 7.69 – 7.46 (m, 5H), 7.34 – 7.17 (m, 5H), 3.53 – 3.36 (m, 2H), 2.75 (t, J = 7.6 Hz, 2H), 2.14 – 1.98 (m, 2H).
^{13}C-NMR	(75 MHz, MeOD) δ 141.5, 136.7, 131.6, 131.1, 129.7, 129.4, 127.5, 123.8, 52.9, 33.4, 28.9.
GC-MS	t_R = 9.88 min, (EI, 70 eV): m/z = 211 [M^+], 118, 106, 91, 77, 65, 51.
HRMS	Calcd. for $C_{15}H_{18}N$ 212.1434; found: 212.1436.
IR	3370 (b), 3063 (w), 3026 (m), 2870 (m), 2646 (m), 2017 (m), 1603 (m), 1491 (m), 749 (s), 690 (s) cm^{-1}.

N-(1-Phenylethyl)aniline (2k)

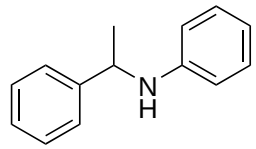

$C_{14}H_{15}N$

197.28 g/mol

Yield	87.5 mg, 0.44 mmol (89%) Starting material could not be separated (5%)
^{1}H-NMR	(400 MHz, $CDCl_3$) δ 7.41 – 7.37 (m, 2H), 7.38 – 7.29 (m, 2H), 7.28 – 7.22 (m, 1H), 7.11 (dd, J = 8.6, 7.3 Hz, 2H), 6.68 (tt, J = 7.3, 1.1 Hz, 1H), 6.57 – 6.52 (m, 2H), 4.51 (q, J = 6.7 Hz, 1H), 4.20 (brs, 1H), 1.54 (d, J = 6.7 Hz, 3H).
^{13}C-NMR	(101 MHz, $CDCl_3$) δ 147.2, 145.2, 129.2, 128.8, 127.0, 126.0, 117.5, 113.6, 53.7, 25.1.
GC-MS	t_R = 8.83 min, (EI, 70 eV): m/z = 197 [M^+], 182, 167, 152, 120, 105, 93, 77, 65, 51.

Analytical data were in full agreement with A. H. Vetter, A. Berkessel, *Synthesis* **1995**, 419.

1,2,3,4-Tetrahydroquinoline hydrochloride (2l)

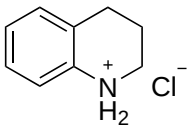

$C_9H_{12}ClN$

169.65 g/mol

Yield	43.8 mg, 0.26 mmol (99%)
^{1}H-NMR	(300 MHz, $CDCl_3$) δ 7.46 – 7.33 (m, 3H), 7.30 (dd, J = 8.2, 1.7 Hz, 1H), 3.56 – 3.50 (m, 2H), 2.97 (t, J = 6.5 Hz, 2H), 2.25 – 2.07 (m, 2H).
^{13}C-NMR	(75 MHz, $CDCl_3$) δ 132.9, 132.2, 131.3, 130.4, 128.7, 124.1, 43.8, 25.8, 20.7.
GC-MS (freebase)	t_R = 7.01 min, (EI, 70 eV): m/z = 132 [M^+-H], 118, 104, 91, 77, 65, 51.

Analytical data were in full agreement with M. Ortiz-Marciales, L. D. Rivera, M. de Jesús, S. Espinosa, J. A. Benjamin, O. E. Casanova, I. G. Figueroa, S. Rodríguez, W. Correa, *J. Org. Chem.* **2005**, *70*, 10132.

6-Methyl-1,2,3,4-tetrahydroquinoline (2m)

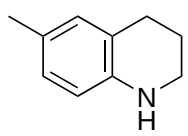

$C_{10}H_{13}N$

147.22 g/mol

Yield 53.2 mg, 0.36 mmol (73%)

^{1}H-NMR (400 MHz, $CDCl_3$) δ 6.82 – 6.77 (m, 2H), 6.43(d, J = 8.6 Hz, 1H), 3.48 (brs, 1H), 3.31 – 3.25 (m, 2H), 2.75 (t, J = 6.4 Hz, 2H), 2.22 (s, 3H), 2.00 – 1.89 (m, 2H).

^{13}C-NMR (101 MHz, $CDCl_3$) δ 142.4, 130.2, 127.4, 126.5, 121.8, 114.7, 42.3, 27.0, 22.5, 20.5.

GC-MS t_R = 7.53 min, (EI, 70 eV): m/z = 147 [M^+], 132, 117, 103, 91, 77, 65, 51.

Analytical data were in full agreement with R. Adam, J. R. Cabrero-Antonino, A. Spannenberg, K. Junge, R. Jackstell, M. Beller, *Angew. Chem. Int. Ed.* **2017**, *56*, 3216.

8-Methyl-1,2,3,4-tetrahydroquinoline (2n)

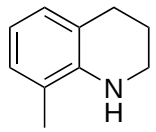

$C_{10}H_{13}N$

147.22 g/mol

Yield 28.4 mg, 0.19 mmol (39%)

^{1}H-NMR (300 MHz, $CDCl_3$) δ 6.92 – 6.82 (m, 2H), 6.57 (t, J = 7.4 Hz, 1H), 3.59 (brs, 1H), 3.41 – 3.35 (m, 2H), 2.80 (t, J = 6.4 Hz, 2H), 2.09 (s, 3H), 2.00 – 1.90 (m, 2H).

^{13}C-NMR (75 MHz, $CDCl_3$) δ 142.6, 128.0, 127.5, 121.5, 121.2, 116.7, 42.5, 27.4, 22.3, 17.3.

GC-MS t_R = 7.48 min, (EI, 70 eV): m/z = 147 [M^+], 132, 117, 103, 91, 77, 65, 51.

Analytical data were in full agreement with R. Adam, J. R. Cabrero-Antonino, A. Spannenberg, K. Junge, R. Jackstell, M. Beller, *Angew. Chem. Int. Ed.* **2017**, *56*, 3216.

6-Methoxy-1,2,3,4-tetrahydroquinoline (2o)

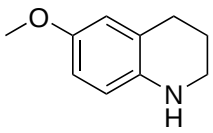

$C_{10}H_{13}NO$

163.22 g/mol

Yield 31.9 mg, 0.20 mmol (77%)

^{1}H-NMR (400 MHz, $CDCl_3$) δ 6.62 – 6.55 (m, 2H), 6.45 (d, J = 8.5 Hz, 1H), 3.73 (s, 3H), 3.44 (brs, 1H), 3.26 (t, J = 5.4 Hz, 2H), 2.76 (t, J = 6.5 Hz, 2H), 1.98 – 1.89 (m, 2H).

^{13}C-NMR (101 MHz, $CDCl_3$) δ 151.9, 139.0, 123.0, 115.7, 115.0, 113.0, 55.9, 42.5, 27.3, 22.6.

GC-MS t_R = 8.31 min, (EI, 70 eV): m/z = 163 [M^+], 148, 130, 118, 103, 91, 77, 65, 51.

Analytical data were in full agreement with R. Adam, J. R. Cabrero-Antonino, A. Spannenberg, K. Junge, R. Jackstell, M. Beller, *Angew. Chem. Int. Ed.* **2017**, *56*, 3216.

6-Chloro-1,2,3,4-tetrahydroquinoline (2p)

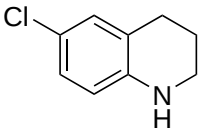

$C_9H_{10}ClN$

167.64 g/mol

Yield 51.7 mg, 0.31 mmol (62%)

^{1}H-NMR (400 MHz, $CDCl_3$) δ 6.94 – 6.84 (m, 2H), 6.38 (dd, J = 7.9, 0.9 Hz, 1H), 3.82 (brs, 1H), 3.28 (t, J = 5.5 Hz, 2H), 2.72 (t, J = 6.4 Hz, 2H), 1.97 – 1.84 (m, 2H).

^{13}C-NMR (101 MHz, $CDCl_3$) δ 143.4, 129.2, 126.6, 123.0, 121.3, 115.2, 42.0, 27.0, 21.9.

GC-MS t_R = 8.35 min, (EI, 70 eV): m/z = 167 [M^+], 152, 130, 117, 103, 89 ,77, 65, 51.

Analytical data were in full agreement with R. Adam, J. R. Cabrero-Antonino, A. Spannenberg, K. Junge, R. Jackstell, M. Beller, *Angew. Chem. Int. Ed.* **2017**, *56*, 3216.

Methyl 1,2,3,4-tetrahydroquinoline-6-carboxylate (2q)

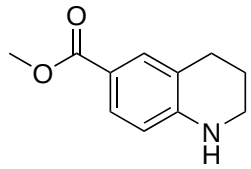

$C_{11}H_{13}NO_2$

191.23 g/mol

Yield	93.4 mg, 0.49 mmol (98%)
^{1}H-NMR	(300 MHz, $CDCl_3$) δ 7.66 – 7.61 (m, 2H), 6.41 – 6.37 (m, 1H), 4.35 (brs, 1H), 3.83 (s, 3H), 3.35 (t, J = 5.7 Hz, 2H), 2.76 (t, J = 6.3 Hz, 2H), 2.00 – 1.85 (m, 2H).
^{13}C-NMR	(75 MHz, $CDCl_3$) δ 167.6, 148.8, 131.4, 129.2, 120.0, 117.6, 112.8, 51.6, 41.8, 27.0, 21.5.
GC-MS	t_R = 9.68 min, (EI, 70 eV): m/z = 191 [M^+], 176, 160, 144, 132, 117, 104, 89, 77, 64, 51.

Analytical data were in full agreement with R. Adam, J. R. Cabrero-Antonino, A. Spannenberg, K. Junge, R. Jackstell, M. Beller, *Angew. Chem. Int. Ed.* **2017**, *56*, 3216.

1,2,3,4-Tetrahydroquinoxaline (2r)

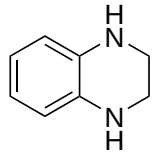

$C_8H_{10}N_2$

134.18 g/mol

Yield	64.2 mg, 0.48 mmol (95%)
^{1}H-NMR	(400 MHz, $CDCl_3$) δ 6.59 (dd, J = 5.8, 3.4 Hz, 2H), 6.50 (dd, J = 5.8, 3.4 Hz, 2H), 3.59 (brs, 2H), 3.42 (s, 4H).
^{13}C-NMR	(101 MHz, $CDCl_3$) δ 133.8, 118.9, 114.8, 41.5.
GC-MS	t_R = 7.94 min, (EI, 70 eV): m/z = 134 [M^+], 119, 104, 92, 77, 66, 51.

Analytical data were in full agreement with R. Adam, J. R. Cabrero-Antonino, A. Spannenberg, K. Junge, R. Jackstell, M. Beller, *Angew. Chem. Int. Ed.* **2017**, *56*, 3216.

Tetrahydroharmine (2s)

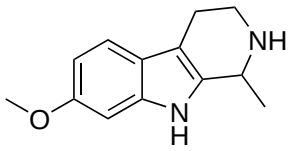

$C_{13}H_{16}N_2O$

216.28 g/mol

Yield	104.6 mg, 0.48 mmol (97%)
^{1}H-NMR	(300 MHz, $CDCl_3$) δ 8.06 (brs, 1H), 7.33 (d, J = 8.5 Hz, 1H), 6.83 (d, J = 2.2 Hz, 1H), 6.75 (dd, J = 8.6, 2.3 Hz, 1H), 4.14 (q, J = 6.6 Hz, 1H), 3.81 (s, 3H), 3.32 – 3.27 (m, 1H), 3.01 (ddd, J = 12.9, 8.6, 5.4 Hz, 1H), 2.80 – 2.66 (m, 2H), 2.52 (brs, 1H), 1.43 (d, J = 6.7 Hz, 3H).
^{13}C-NMR	(75 MHz, $CDCl_3$) δ 156.2, 136.5, 135.8, 122.0, 118.7, 108.9, 108.2, 95.2, 55.9, 48.3, 42.7, 22.7, 20.8.
GC-MS	t_R = 10.76 min, (EI, 70 eV): m/z = 216 [M^+], 201, 186, 172, 158, 144, 130, 115, 100, 89, 77, 63, 51.

Analytical data were in full agreement with J. Wu, D. Talwar, S. Johnston, M. Yan, J. Xiao, *Angew. Chem. Int. Ed.* **2013**, *52*, 6983.

2-Methyl-1,2,3,4-tetrahydroquinoline (2t)

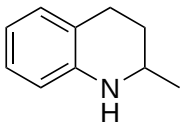

$C_{10}H_{13}N$

147.22 g/mol

Yield	37.7 mg, 0.26 mmol (49%)
^{1}H-NMR	(300 MHz, $CDCl_3$) δ 7.02 – 6.93 (m, 2H), 6.62 (td, J = 7.4, 1.2 Hz, 1H), 6.48 (dd, J = 8.3, 1.2 Hz, 1H), 3.70 (s, 1H), 3.41 (dqd, J = 10.0, 6.3, 2.9 Hz, 1H), 2.93 – 2.79 (m, 1H), 2.74 (ddd, J = 16.4, 5.5, 3.5 Hz, 1H), 1.94 (dddd, J = 12.9, 5.7, 3.5, 2.9 Hz, 1H), 1.60 (dddd, J = 12.8, 11.4, 9.9, 5.5 Hz, 1H), 1.22 (d, J = 6.2 Hz, 3H).
^{13}C-NMR	(75 MHz, $CDCl_3$) δ 267.5, 144.9, 129.4, 126.8, 121.2, 117.1, 114.1, 47.3, 30.3, 26.7, 22.8.
GC-MS	t_R = 6.59 min, (EI, 70 eV): m/z = 147 [M^+], 132, 119, 104, 91, 77, 65, 51.

Analytical data were in full agreement with R. Adam, J. R. Cabrero-Antonino, A. Spannenberg, K. Junge, R. Jackstell, M. Beller, *Angew. Chem. Int. Ed.* **2017**, *56*, 3216.

2-Methyl-5,6,7,8-tetrahydroquinoline (2t')

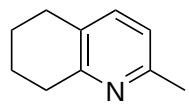

$C_{10}H_{13}N$

147.22 g/mol

Yield 34.0 mg, 0.23 mmol (45%)

^{1}H-NMR (300 MHz, $CDCl_3$) δ 7.22 (d, J = 7.7 Hz, 1H), 6.87 (d, J = 7.7 Hz, 1H), 2.87 (t, J = 6.4 Hz, 2H), 2.70 (t, J = 6.3 Hz, 2H), 2.47 (s, 3H), 1.95 – 1.70 (m, 4H).

^{13}C-NMR (75 MHz, $CDCl_3$) δ 156.5, 155.1, 137.2, 129.0, 120.6, 32.7, 28.5, 24.3, 23.3, 22.9.

GC-MS t_R = 7.00 min, (EI, 70 eV): m/z = 147 [M^+], 132, 117, 103, 91, 77, 65, 51.

Analytical data were in full agreement with J. E. Shaw, P. R. Stapp, *J. Heterocyclic Chem.* **1987**, *24*, 1477.

3-Methyl-1,2,3,4-tetrahydroquinoline (2u)

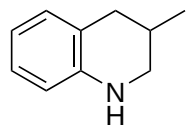

$C_{10}H_{13}N$

147.22 g/mol

Yield 34.1 mg, 0.23 mmol (46%)

^{1}H-NMR (400 MHz, $CDCl_3$) δ 7.03 – 6.92 (m, 2H), 6.62 (td, J = 7.4, 1.2 Hz, 1H), 6.51 (dd, J = 7.9, 1.1 Hz, 1H), 3.57 (s, 1H), 3.28 (ddd, J = 11.0, 3.7, 2.0 Hz, 1H), 2.91 (dd, J = 11.0, 9.6 Hz, 1H), 2.79 (ddd, J = 16.0, 5.0, 2.0 Hz, 1H), 2.44 (dd, J = 16.0, 10.3 Hz, 1H), 2.16 – 1.99 (m, 1H), 1.06 (d, J = 6.6 Hz, 3H).

^{13}C-NMR (101 MHz, $CDCl_3$) δ 144.2, 129.7, 126.8, 121.4, 117.2, 114.1, 49.0, 35.6, 27.3, 19.2.

GC-MS t_R = 7.04 min, (EI, 70 eV): m/z = 147 [M^+], 132, 119, 104, 91, 77, 65, 51.

Analytical data were in full agreement with R. Adam, J. R. Cabrero-Antonino, A. Spannenberg, K. Junge, R. Jackstell, M. Beller, *Angew. Chem. Int. Ed.* **2017**, *56*, 3216.

3-Methyl-5,6,7,8-tetrahydroquinoline (2u')

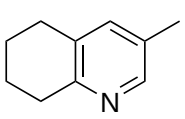

$C_{10}H_{13}N$

147.22 g/mol

Yield 37.0 mg, 0.25 mmol (50%)

^{1}H-NMR (400 MHz, $CDCl_3$) δ 8.17 (s, 1H), 7.16 (s, 1H), 2.87 (t, J = 6.4 Hz, 2H), 2.71 (t, J = 6.3 Hz, 2H), 2.25 (s, 3H), 1.91 – 1.83 (m, 2H), 1.78 (dtt, J = 9.2, 6.2, 2.7 Hz, 2H).

^{13}C-NMR (101 MHz, $CDCl_3$) δ 154.3, 147.1, 137.6, 131.8, 130.2, 32.1, 28.8, 23.3, 22.9, 18.1.

GC-MS t_R = 7.28 min, (EI, 70 eV): m/z = 147 [M^+], 132, 118, 104, 91, 77, 65, 51.

Analytical data were in full agreement with R. C. Boruah, S. Ahmed, U. Sharma, J. S. Sandhu, *J. Org. Chem.* **2000**, *65*, 922.

4-Methyl-1,2,3,4-tetrahydroquinoline (2v)

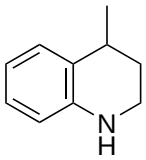

$C_{10}H_{13}N$

147.22 g/mol

Yield 23.0 mg, 0.16 mmol (31%)

^{1}H-NMR (400 MHz, $CDCl_3$) δ 7.07 (dt, J = 7.5, 1.1 Hz, 1H), 6.98 (dddd, J = 7.9, 7.2, 1.6, 0.6 Hz, 1H), 6.65 (td, J = 7.4, 1.2 Hz, 1H), 6.49 (dd, J = 8.0, 1.2 Hz, 1H), 3.56 (s, 1H), 3.40 – 3.21 (m, 2H), 2.93 (h, J = 6.6 Hz, 1H), 2.00 (ddt, J = 17.7, 5.4, 4.0 Hz, 1H), 1.69 (dtd, J = 13.0, 6.5, 3.6 Hz, 1H), 1.30 (d, J = 7.0 Hz, 3H).

^{13}C-NMR (101 MHz, $CDCl_3$) δ 144.3, 128.6, 126.8, 126.8, 117.1, 114.3, 39.1, 30.4, 30.0, 22.8.

GC-MS t_R = 7.17 min, (EI, 70 eV): m/z = 147 [M^+], 132, 119, 104, 91, 77, 65, 51.

Analytical data were in full agreement with R. Adam, J. R. Cabrero-Antonino, A. Spannenberg, K. Junge, R. Jackstell, M. Beller, *Angew. Chem. Int. Ed.* **2017**, *56*, 3216.

4-Methyl-5,6,7,8-tetrahydroquinoline (2v')

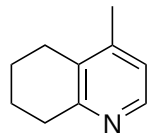

$C_{10}H_{13}N$

147.22 g/mol

Yield 49,2 mg, 0.33 mmol (66%)

^{1}H-NMR (400 MHz, $CDCl_3$) δ 8.21 (d, J = 4.9 Hz, 1H), 6.88 (d, J = 4.9 Hz, 1H), 2.94 – 2.86 (m, 2H), 2.63 (t, J = 5.8 Hz, 2H), 2.19 (s, 3H), 1.84 (qt, J = 4.4, 2.3 Hz, 4H).

^{13}C-NMR (101 MHz, $CDCl_3$) δ 156.7, 146.1, 146.0, 131.2, 122.7, 33.0, 25.9, 23.0, 22.9, 19.0.

GC-MS t_R = 7.32 min, (EI, 70 eV): m/z = 147 [M^+], 132, 117, 104, 91, 77, 65, 51.

Analytical data were in full agreement with J. E. Shaw, P. R. Stapp, *J. Heterocyclic Chem.* **1987**, *24*, 1477.

2.4.5 ICP-OES Measurement

The cobalt concentration in the organic layer after hydrogenation was determined by ICP-OES. Five stock solutions of $CoCl_2$ in 35% HNO_3 were prepared and a calibration curve was measured by integration of the emission signal of cobalt at 230.786 nm. Each data point corresponds to the mean value of three consecutive measurements correcting for the observed background signals.

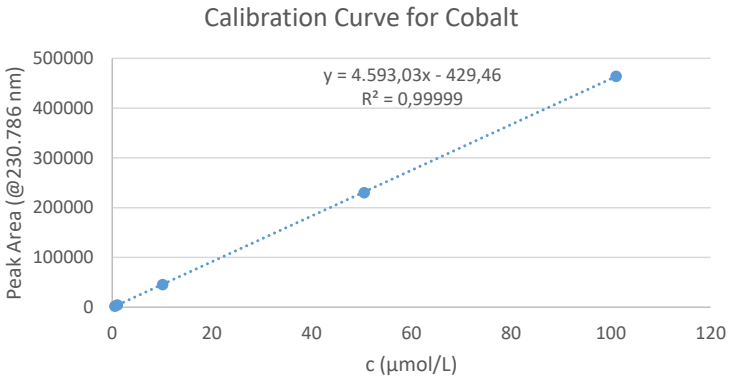

Figure 2.6: ICP-OES calibration curve for cobalt.

For the actual measurement, styrene (0.25 mmol) was hydrogenated using 5 mol% of the cobalt nanoparticles (12.5 mmol/L Co) under standard conditions (2 bar H_2, 3 h in 1 ml THF). After reaction, two reaction vials were placed on separate neodymium magnets and allowed to settle down for 2 and 24 h respectively. The organic phase was removed with a Pasteur Pipette, the solvent removed under vacuum and the residue dissolved in 5 ml dilute HNO_3.

Table 2.16: ICP-OES measurement of the cobalt concentration in the organic phase after magnetic particle separation.

PBcat135_2h	Peak Area	c (μmol/L)	PBcat135_24h	Peak Area	c (μmol/L)
Run 1	41231	9.07	Run 1	31624.5	6.98
Run 2	42226	9.29	Run 2	31439.7	6.94
Run 3	41338.2	9.09	Run 3	31299.3	6.91
Average	41598.4	9.15	Average	31454.5	6.94
StdDev	546.15	0.12	StdDev	163.10	0.04

This results in a cobalt concentration of 45.75±0.6 and 34.7±0.2 μmol/L in the organic

phase after 2 and 24 h settle time respectively, which corresponds to 0.37 and 0.28% of the cobalt concentration in the reaction vessel.

2.4.6 ICP-MS Measurement

In preparation for the measurement, half of the vials were charged with styrene (1 mmol) and 5 mol% of the cobalt nanoparticles (12.5 mmol/L Co), the other vials omitting the cobalt catalyst (blank reaction solution). All were hydrogenated under standard conditions (2 bar H_2, 3 h in 4 ml THF). After the reaction, each vial was put on a neodymium magnet and the organic phase was transferred to a new vial, leaving behind most of the cobalt metal. The vials were washed twice with an additional 1 ml of ethyl acetate. To the first set of vials (Co-reaction and blank) was then added 1 ml saturated ammonium chloride solution which was extracted three times with ethyl acetate, the second set was eluted through a short silica plug inside a Pasteur pipette using ethyl acetate. The solvent was subsequently removed from all vials under vacuum and the residue dissolved in 50 ml dilute HNO_3.

Table 2.17: ICP-MS measurement of the cobalt concentration in the organic phase after work-up.

Reactions	Peak Area	c (ng/ml)	nCo (nmol)
Extraction	838524.5	0.80	0.6780
Extraction (blank)	23595.3	0.02	0.01696
Silica	52582.7	0.05	0.0424
Silica (blank)	13541.0	0.01	0.00848

This results in a cobalt concentration of 165 nmol/L and 8.5 nmol/L in the organic phase after extraction and elution respectively, which corresponds to 13.2 and 0.68 ppm of the cobalt concentration in the reaction vessel.

2.4.7 Functional Group Tolerance Tests

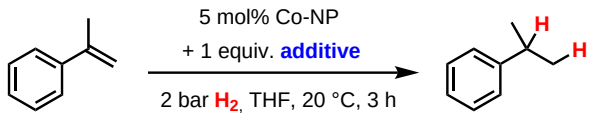

Additives and yield of cumene:

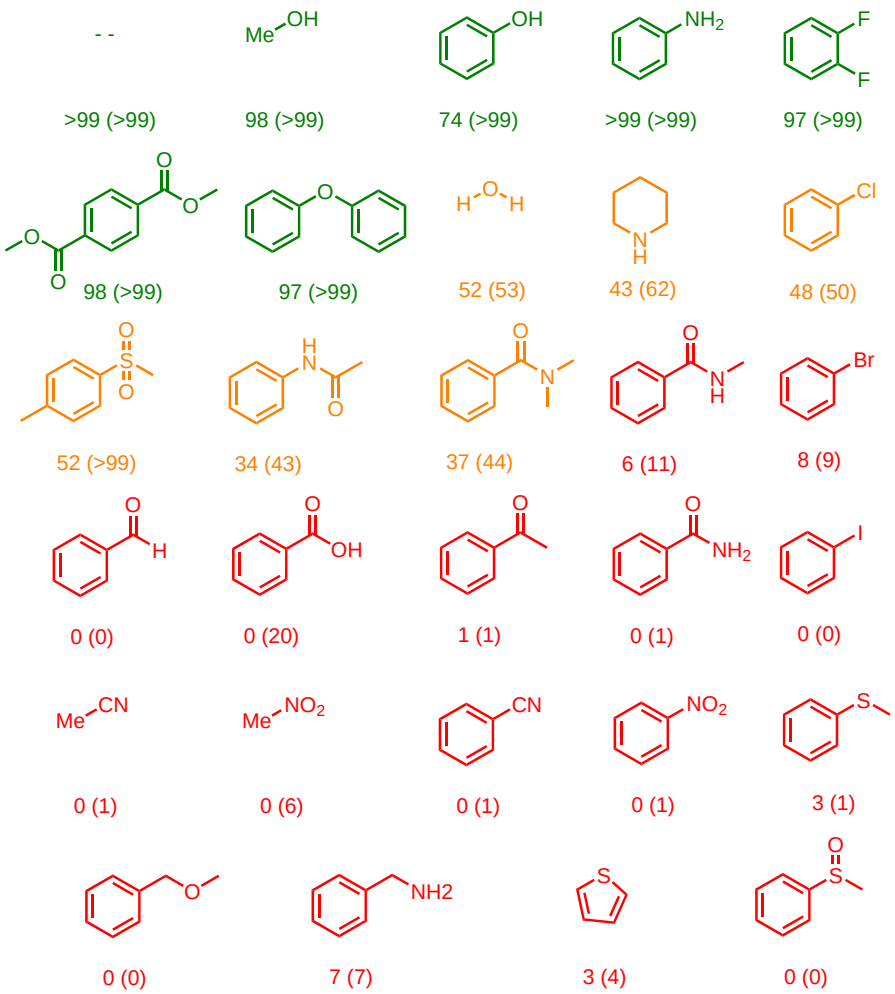

Scheme 2.2: Functional group tolerance of Co-NP catalyzed hydrogenation of α-methylstyrene in presence of 1 equiv. additive. Standard conditions: 0.25 mmol substrate in 1 ml THF; yields of hydrogenation product (cumene) determined by quantitative GC vs. internal reference *n*-pentadecane. Conversion of α-methylstyrene shown in parentheses.

2.4.8 Comparison of Different Co-Np Preparations

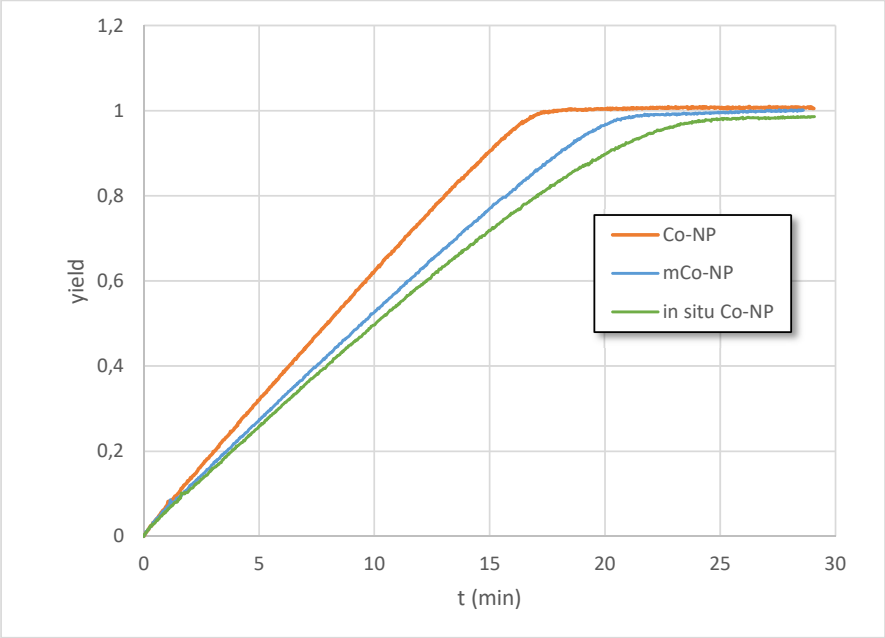

Figure 2.7: Hydrogenation of styrene using the nanoparticles isolated by centrifugation, separation by a magnet, and using the *in situ* protocol. The conditions were 1.9 bar H_2, 5 mol% [Co], r.t., THF. The reaction yield was determined by measuring the consumption of H_2.

Kinetic experiments were carried out to compare the catalytic activity of the different catalyst systems described previously. Figure 2.7 shows a similar catalytic activity of the various nanoparticles, yielding complete conversion after 17 to 24 minutes.

2.4.9 Recycling Experiments

The reactions were set up according to the general hydrogenation procedure with styrene (0.5 mmol) as substrate in 2 ml THF. The hydrogenations were carried out for 30 min each (2 bar H_2, r.t., 5 mol% Co-NP). After reaction, the autoclave was introduced into the glovebox and the reaction vial put on top of a neodymium magnet (cylindrical, 10 x 20 mm (height x diameter), N45) for 5 min. The solvent was removed using a Pasteur pipette and the particles washed once with 2 ml THF. New substrate and solvent were added, the vial was put back into the autoclave and a new hydrogenation reaction started. The organic phase was analyzed using quantitative GC-FID. After nine consecutive reactions, the particles were dissolved in 1 ml THF and stirred inside the glovebox overnight. The next day, three more runs were carried out. After these three reactions the particles were stirred again inside the glovebox for another 72 hours before a last hydrogenation reaction was started.

2.4.10 Particle Analyses

Purity and Crystallinity

The purity of the as-prepared Co(0) nanoparticles was proven by X-ray powder diffraction (XRD) after powder sintering (800 °C, Ar). This treatment ensured crystallization of all products including potentially amorphous residual components (e.g. oxides and hydroxides). Despite the resultant non-nanoparticulate state, the presence of pure cobalt (cubic modification as majority phase with traces of a hexagonal phase) and the absence of any cobalt oxide impurities was validated (Figure 2.8).

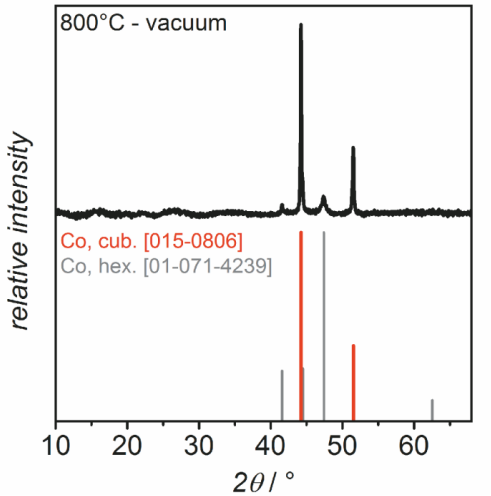

Figure 2.8: XRD Co(0) powder samples after annealing (800 °C, Ar).

Particle Size Distribution

Average particle diameters of the Co(0) nanoparticles before and after the hydrogenation reaction were calculated by statistical evaluation of >200 particles on TEM images using the ImageJ 1.47v software. Figure 2.9 shows the results for [NaNaph]-made Co(0) nanoparticles (Co-NPs) isolated by centrifugation. Figure 2.10 shows the results for *in situ*-generated cobalt nanoparticles (*in situ* Co-NPs). It should be noted that dynamic light scattering (DLS) as an alternative analytical tool gives less conclusive results due to the magnetic interaction of the nanoparticles.

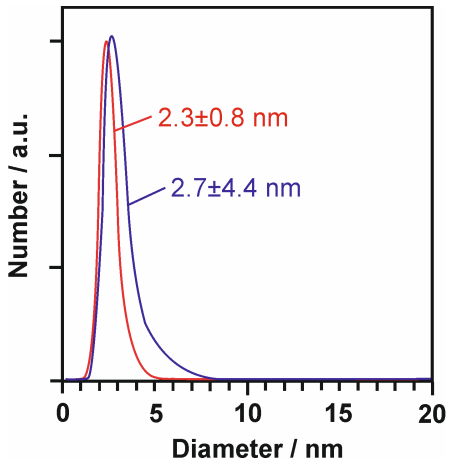

Figure 2.9: Particle size distribution according to statistical evaluation of TEM images (>200 particles) of cobalt nanoparticles (Co-NPs) before (red) and after (blue) hydrogenation reaction.

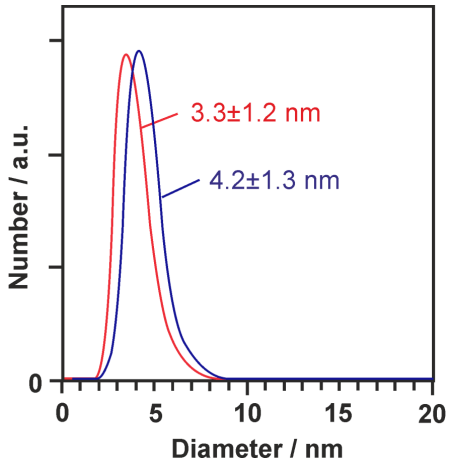

Figure 2.10: Particle size distribution according to statistical evaluation of TEM images (>200 particles) of *in situ* generated cobalt nanoparticles (*in situ* Co-NPs) before (red) and after (blue) hydrogenation reaction.

TEM Measurements

TEM images of Co(0) nanoparticles before and after the catalytical reaction are shown in Figure S5 and Figure S6 for *ex situ* and *in situ* generated nanoparticles.

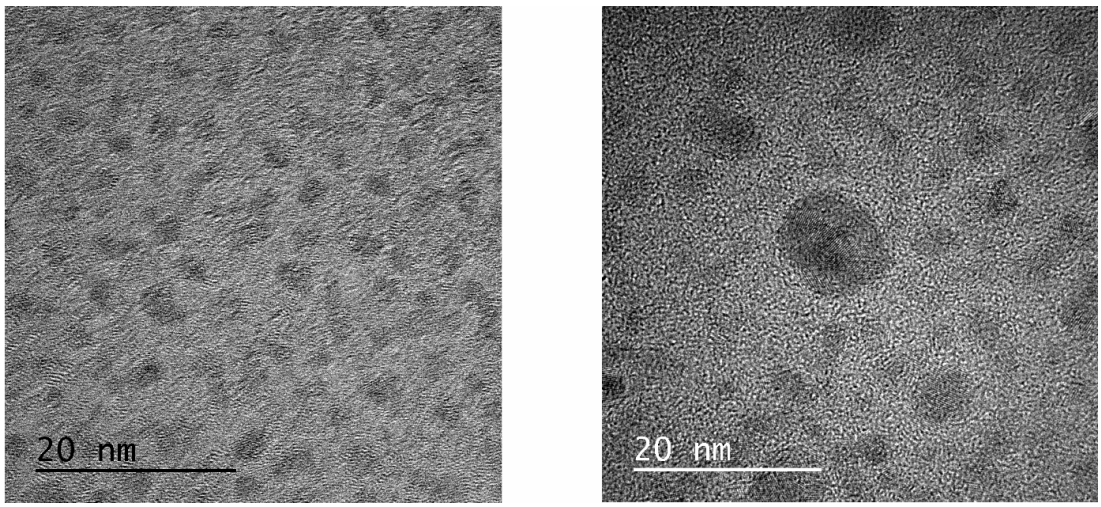

Figure 2.11: TEM measurement of cobalt nanoparticles (Co-NP) before (left) and after (right) hydrogenation reaction.

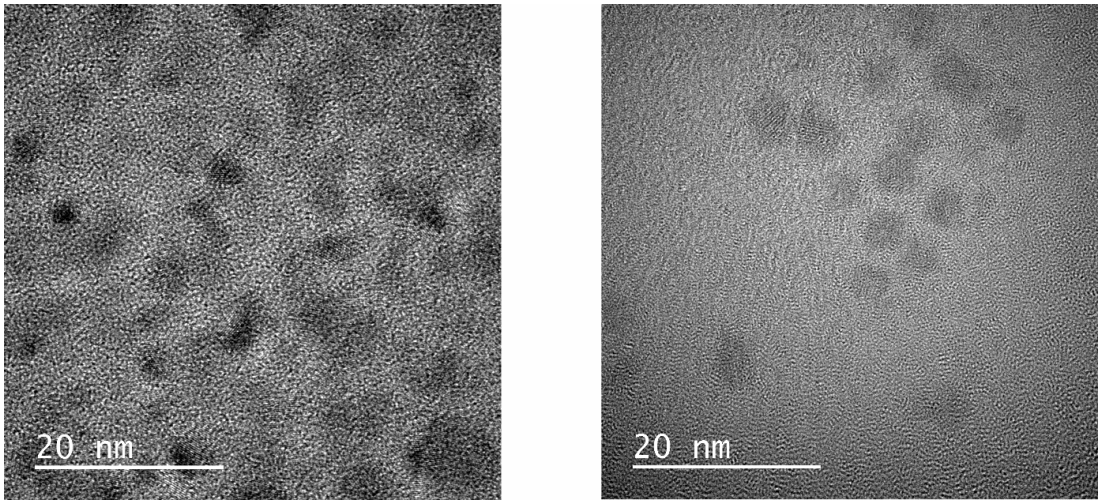

Figure 2.12: TEM measurement of *in situ* generated cobalt nanoparticles (*in situ* Co-NP) before (left) and after (right) hydrogenation reaction.

2.5 References

[1] (a) An, K.; Somorjai, G. A. Nanocatalysis I: Synthesis of Metal and Bimetallic Nanoparticles and Porous Oxides and Their Catalytic Reaction Studies. *Catal. Lett.* **2014**, *145*, 233–248; (b) Singh, A. K.; Xu, Q. Synergistic Catalysis over Bimetallic Alloy Nanoparticles. *ChemCatChem* **2013**, *5*, 652–676; (c) Sankar, M.; Dimitratos, N.; Miedziak, P. J.; Wells, P. P.; Kiely, C. J.; Hutchings, G. J. Designing bimetallic catalysts for a green and sustainable future. *Chem. Soc. Rev.* **2012**, *41*, 8099.

[2] (a) Taccardi, N.; Grabau, M.; Debuschewitz, J.; Distaso, M.; Brandl, M.; Hock, R.; Maier, F.; Papp, C.; Erhard, J.; Neiss, C.; Peukert, W.; Görling, A.; Steinrück, H.-P.; Wasserscheid, P. Gallium-rich Pd-Ga phases as supported liquid metal catalysts. *Nature Chem.* **2017**, *9*, 862–867; (b) Su, H.; Zhang, K.-X.; Zhang, B.; Wang, H.-H.; Yu, Q.-Y.; Li, X.-H.; Antonietti, M.; Chen, J.-S. Activating Cobalt Nanoparticles via the Mott-Schottky Effect in Nitrogen-Rich Carbon Shells for Base-Free Aerobic Oxidation of Alcohols to Esters. *J. Am. Chem. Soc.* **2017**, *139*, 811–818; (c) Jover, J.; García-Ratés, M.; López, N. The Interplay between Homogeneous and Heterogeneous Phases of PdAu Catalysts for the Oxidation of Alcohols. *ACS Catal.* **2016**, *6*, 4135–4143; (d) Yasukawa, T.; Suzuki, A.; Miyamura, H.; Nishino, K.; Kobayashi, S. Chiral Metal Nanoparticle Systems as Heterogeneous Catalysts beyond Homogeneous Metal Complex Catalysts for Asymmetric Addition of Arylboronic Acids to α,β-Unsaturated Carbonyl Compounds. *J. Am. Chem. Soc.* **2015**, *137*, 6616–6623; (e) Li, Z.-X.; Xue, W.; Guan, B.-T.; Shi, F.-B.; Shi, Z.-J.; Jiang, H.; Yan, C.-H. A conceptual translation of homogeneous catalysis into heterogeneous catalysis: homogeneous-like heterogeneous gold nanoparticle catalyst induced by ceria supporter. *Nanoscale* **2013**, *5*, 1213; (f) Gross, E.; Krier, J. M.; Heinke, L.; Somorjai, G. A. Building Bridges in Catalysis Science. Monodispersed Metallic Nanoparticles for Homogeneous Catalysis and Atomic Scale Characterization of Catalysts Under Reaction Conditions. *Top. Catal.* **2012**, *55*, 13–23; (g) Bayram, E.; Linehan, J. C.; Fulton, J. L.; Roberts, J. A. S.; Szymczak, N. K.; Smurthwaite, T. D.; Özkar, S.; Balasubramanian, M.; Finke, R. G. Is It Homogeneous or Heterogeneous Catalysis Derived from $[RhCpCl_2]_2$? In Operando XAFS, Kinetic, and Crucial Kinetic Poisoning Evidence for Subnanometer Rh_4 Cluster-Based Benzene Hydrogenation Catalysis. *J. Am. Chem. Soc.* **2011**, *133*, 18889–18902.

[3] (a) Knijnenburg, Q.; Horton, A. D.; van der Heijden, H.; Kooistra, T. M.; Hetterscheid, D. G.; Smits, J. M.; de Bruin, B.; Budzelaar, P. H.; Gal, A. W. Olefin hydrogenation using diimine pyridine complexes of Co and Rh. *J. Mol. Catal. A* **2005**, *232*, 151–159; (b) Zhang, G.; Vasudevan, K. V.; Scott, B. L.; Hanson, S. K. Understanding the Mechanisms of Cobalt-Catalyzed Hydrogenation and Dehydrogenation Reactions. *J. Am. Chem. Soc.* **2013**, *135*, 8668–8681; (c) Friedfeld, M. R.; Shevlin, M.; Hoyt, J. M.; Krska, S. W.; Tudge, M. T.; Chirik, P. J. Cobalt Precursors for High-Throughput Discovery of Base Metal Asymmetric Alkene Hy-

drogenation Catalysts. *Science* **2013**, *342*, 1076–1080; (d) Rösler, S.; Obenauf, J.; Kempe, R. A Highly Active and Easily Accessible Cobalt Catalyst for Selective Hydrogenation of C=O Bonds. *J. Am. Chem. Soc.* **2015**, *137*, 7998–8001; (e) Gorgas, N.; Stöger, B.; Veiros, L. F.; Kirchner, K. Highly Efficient and Selective Hydrogenation of Aldehydes: A Well-Defined Fe(II) Catalyst Exhibits Noble-Metal Activity. *ACS Catal.* **2016**, *6*, 2664–2672; (f) Tokmic, K.; Markus, C. R.; Zhu, L.; Fout, A. R. Well-Defined Cobalt(I) Dihydrogen Catalyst: Experimental Evidence for a Co(I)/Co(III) Redox Process in Olefin Hydrogenation. *J. Am. Chem. Soc.* **2016**, *138*, 11907–11913; (g) Cabrero-Antonino, J. R.; Adam, R.; Junge, K.; Jackstell, R.; Beller, M. Cobalt-catalysed transfer hydrogenation of quinolines and related heterocycles using formic acid under mild conditions. *Catal. Sci. Technol.* **2017**, *7*, 1981–1985.

[4] (a) Gärtner, D.; Welther, A.; Rad, B. R.; Wolf, R.; von Wangelin, A. J. Heteroatom-Free Arene-Cobalt and Arene-Iron Catalysts for Hydrogenations. *Angew. Chem. Int. Ed.* **2014**, *53*, 3722–3726; (b) Büschelberger, P.; Gärtner, D.; Reyes-Rodriguez, E.; Kreyenschmidt, F.; Koszinowski, K.; von Wangelin, A. J.; Wolf, R. Alkene Metalates as Hydrogenation Catalysts. *Chem. Eur. J.* **2017**, *23*, 3139–3151.

[5] (a) Buck, M. R.; Schaak, R. E. Emerging Strategies for the Total Synthesis of Inorganic Nanostructures. *Angew. Chem. Int. Ed.* **2013**, *52*, 6154–6178; (b) Lu, Y.; Chen, W. Sub-nanometre sized metal clusters: from synthetic challenges to the unique property discoveries. *Chem. Soc. Rev.* **2012**, *41*, 3594; (c) Lim, B.; Xia, Y. Metal Nanocrystals with Highly Branched Morphologies. *Angew. Chem. Int. Ed.* **2010**, *50*, 76–85; (d) Sau, T. K.; Rogach, A. L. Nonspherical Noble Metal Nanoparticles: Colloid-Chemical Synthesis and Morphology Control. *Adv. Mater.* **2010**, *22*, 1781–1804.

[6] (a) Mourdikoudis, S.; Liz-Marzán, L. M. Oleylamine in Nanoparticle Synthesis. *Chem. Mater.* **2013**, *25*, 1465–1476; (b) Vollmer, C.; Janiak, C. Naked metal nanoparticles from metal carbonyls in ionic liquids: Easy synthesis and stabilization. *Coord. Chem. Rev.* **2011**, *255*, 2039–2057.

[7] (a) Bönnemann, H.; Brijoux, W.; Brinkmann, R.; Joußen, T.; Korall, B.; Dinjus, E. Formation of Colloidal Transition Metals in Organic Phases and Their Application in Catalysis. *Angew. Chem. Int. Ed.* **1991**, *30*, 1312–1314; (b) Bönnemann, H.; Brijoux, W.; Brinkmann, R.; Matoussevitch, N.; Waldöfner, N.; Palina, N.; Modrow, H. A size-selective synthesis of air stable colloidal magnetic cobalt nanoparticles. *Inorg. Chim. Acta* **2003**, *350*, 617–624; (c) Xu, R.; Xie, T.; Zhao, Y.; Li, Y. Quasi-homogeneous catalytic hydrogenation over monodisperse nickel and cobalt nanoparticles. *Nanotechnology* **2007**, *18*, 055602; (d) Alonso, F.; Riente, P.; Yus, M. Nickel Nanoparticles in Hydrogen Transfer Reactions. *Acc. Chem. Res.* **2011**, *44*, 379–391; (e) Tejeda-Serrano, M.; Cabrero-Antonino, J. R.; Mainar-Ruiz, V.; López-Haro, M.; Hernández-Garrido, J. C.; Calvino, J. J.; Leyva-Pérez, A.; Corma, A. Synthesis of Supported Planar Iron Oxide Nanoparticles

and Their Chemo- and Stereoselectivity for Hydrogenation of Alkynes. *ACS Catal.* **2017**, *7*, 3721–3729.

[8] (a) Chen, F.; Surkus, A.-E.; He, L.; Pohl, M.-M.; Radnik, J.; Topf, C.; Junge, K.; Beller, M. Selective Catalytic Hydrogenation of Heteroarenes with N-Graphene-Modified Cobalt Nanoparticles (Co_3O_4-Co/NGr@α-Al_2O_3). *J. Am. Chem. Soc.* **2015**, *137*, 11718–11724; (b) Chen, F.; Topf, C.; Radnik, J.; Kreyenschulte, C.; Lund, H.; Schneider, M.; Surkus, A.-E.; He, L.; Junge, K.; Beller, M. Stable and Inert Cobalt Catalysts for Highly Selective and Practical Hydrogenation of C=N and C=O Bonds. *J. Am. Chem. Soc.* **2016**, *138*, 8781–8788.

[9] Jagadeesh, R. V.; Murugesan, K.; Alshammari, A. S.; Neumann, H.; Pohl, M.-M.; Radnik, J.; Beller, M. MOF-derived cobalt nanoparticles catalyze a general synthesis of amines. *Science* **2017**, *358*, 326–332.

[10] Chen, B.; Li, F.; Huang, Z.; Yuan, G. Recyclable and Selective Nitroarene Hydrogenation Catalysts Based on Carbon-Coated Cobalt Oxide Nanoparticles. *ChemCatChem* **2016**, *8*, 1132–1138.

[11] Schwob, T.; Kempe, R. A Reusable Co Catalyst for the Selective Hydrogenation of Functionalized Nitroarenes and the Direct Synthesis of Imines and Benzimidazoles from Nitroarenes and Aldehydes. *Angew. Chem. Int. Ed.* **2016**, *55*, 15175–15179.

[12] Chen, C.; Huang, Y.; Zhang, Z.; Dong, X.-Q.; Zhang, X. Cobalt-catalyzed (Z)-selective semihydrogenation of alkynes with molecular hydrogen. *Chem. Comm.* **2017**, *53*, 4612–4615.

[13] Chen, F.; Kreyenschulte, C.; Radnik, J.; Lund, H.; Surkus, A.-E.; Junge, K.; Beller, M. Selective Semihydrogenation of Alkynes with N-Graphitic-Modified Cobalt Nanoparticles Supported on Silica. *ACS Cat.* **2017**, *7*, 1526–1532.

[14] (a) Anton, D. R.; Crabtree, R. H. Dibenzo[*a*,*e*]cyclooctatetraene in a proposed test for heterogeneity in catalysts formed from soluble platinum-group metal complexes. *Organometallics* **1983**, *2*, 855–859; (b) Widegren, J. A.; Finke, R. G. A review of the problem of distinguishing true homogeneous catalysis from soluble or other metal-particle heterogeneous catalysis under reducing conditions. *J. Mol. Catal. A: Chem.* **2003**, *198*, 317–341; (c) Crabtree, R. H. Resolving Heterogeneity Problems and Impurity Artifacts in Operationally Homogeneous Transition Metal Catalysts. *Chem. Rev.* **2011**, *112*, 1536–1554; (d) Sonnenberg, J. F.; Morris, R. H. Distinguishing homogeneous from nanoparticle asymmetric iron catalysis. *Catal. Sci. Technol.* **2014**, *4*, 3426–3438.

[15] (a) Schöttle, C.; Bockstaller, P.; Popescu, R.; Gerthsen, D.; Feldmann, C. Sodium-Naphthalenide-Driven Synthesis of Base-Metal Nanoparticles and Follow-up Reactions. *Angew. Chem. Int. Ed.* **2015**, *54*, 9866–9870; (b) Schöttle, C.; Doronkin, D. E.; Popescu, R.; Gerthsen, D.; Grunwaldt, J.-D.; Feldmann, C. Ti^0

nanoparticles via lithium-naphthalenide-driven reduction. *Chem. Comm.* **2016**, *52*, 6316–6319; (c) Schöttle, C.; Rudel, S.; Popescu, R.; Gerthsen, D.; Kraus, F.; Feldmann, C. Nanosized Gadolinium and Uranium—Two Representatives of High-Reactivity Lanthanide and Actinide Metal Nanoparticles. *ACS Omega* **2017**, *2*, 9144–9149.

[16] Connelly, N. G.; Geiger, W. E. Chemical Redox Agents for Organometallic Chemistry. *Chem. Rev.* **1996**, *96*, 877–910.

[17] LaMer, V. K.; Dinegar, R. H. Theory, Production and Mechanism of Formation of Monodispersed Hydrosols. *J. Am. Chem. Soc.* **1950**, *72*, 4847–4854.

[18] Zhu, Y.; Stubbs, L. P.; Ho, F.; Liu, R.; Ship, C. P.; Maguire, J. A.; Hosmane, N. S. Magnetic Nanocomposites: A New Perspective in Catalysis. *ChemCatChem* **2010**, *2*, 365–374.

[19] (a) Zhang, G.; Scott, B. L.; Hanson, S. K. Mild and Homogeneous Cobalt-Catalyzed Hydrogenation of C=C, C=O, and C=N Bonds. *Angew. Chem. Int. Ed.* **2012**, *51*, 12102–12106; (b) Zhang, G.; Hanson, S. K. Cobalt-catalyzed transfer hydrogenation of C=O and C=N bonds. *Chem. Comm.* **2013**, *49*, 10151; (c) Friedfeld, M. R.; Margulieux, G. W.; Schaefer, B. A.; Chirik, P. J. Bis(phosphine)cobalt Dialkyl Complexes for Directed Catalytic Alkene Hydrogenation. *J. Am. Chem. Soc.* **2014**, *136*, 13178–13181; (d) Chirik, P. J. Iron- and Cobalt-Catalyzed Alkene Hydrogenation: Catalysis with Both Redox-Active and Strong Field Ligands. *Acc. Chem. Res.* **2015**, *48*, 1687–1695; (e) Zhao, T.-J.; Zhang, Y.-N.; Wang, K.-X.; Su, J.; Wei, X.; Li, X.-H. General transfer hydrogenation by activating ammonia-borane over cobalt nanoparticles. *RSC Adv.* **2015**, *5*, 102736–102740; (f) Zhang, G.; Yin, Z.; Tan, J. Cobalt(II)-catalysed transfer hydrogenation of olefins. *RSC Adv.* **2016**, *6*, 22419–22423; (g) Landge, V. G.; Pitchaimani, J.; Midya, S. P.; Subaramanian, M.; Madhu, V.; Balaraman, E. Phosphine-free cobalt pincer complex catalyzed Z-selective semi-hydrogenation of unbiased alkynes. *Catal. Sci. Technol.* **2018**, *8*, 428–433.

[20] Heinz, H.; Pramanik, C.; Heinz, O.; Ding, Y.; Mishra, R. K.; Marchon, D.; Flatt, R. J.; Estrela-Lopis, I.; Llop, J.; Moya, S.; Ziolo, R. F. Nanoparticle decoration with surfactants: Molecular interactions, assembly, and applications. *Surf. Sci. Rep.* **2017**, *72*, 1–58.

[21] (a) Wudl, F.; Chaffins, S.; Brettreich, M. An Efficient Synthesis of Dibenzocycloocta-4a,6a,-diene-5,11-diyne and its Precursors. *Synthesis* **2002**, *2002*; (b) Franck, G.; Brill, M.; Helmchen, G. Dibenzo[*a*,*e*]cyclooctene: Multigram Synthesis of a Bidentate Ligand. *Org. Synth.* **2012**, *89*, 55.

[22] Hirayama, C.; Galus, Z.; Guminski, C. In *Metals in Mercury (IUPAC Solubility Data Series)*; Oxford, P. P., Ed.; Pergamon, **1986**; Vol. 25.

[23] (a) Fish, R. H.; Thormodsen, A. D.; Cremer, G. A. Homogeneous catalytic hydrogenation. 1. Regiospecific reductions of polynuclear aromatic and polynuclear heteroaromatic nitrogen compounds catalyzed by transition metal carbonyl hydrides. *J. Am. Chem. Soc.* **1982**, *104*, 5234–5237; (b) Bommannavar, A.; Montano, P. In situ study of the hydrogenation of quinoline over a Ni-Mo supported catalyst. *Appl. Surf. Sci.* **1984**, *19*, 250–266; (c) Eijsbouts, S.; Beer, V. D.; Prins, R. Hydrodenitrogenation of quinoline over carbon-supported transition metal sulfides. *J. Catal.* **1991**, *127*, 619–630; (d) Kaneda, K.; Mikami, Y.; Mitsudome, T.; Mizugaki, T.; Jitsukawa, K. Reversible Dehydrogenation-Hydrogenation of Tetrahydroquinoline-Quinoline Using a Supported Cooper Nanoparticle Catalyst. *Heterocycles* **2010**, *82*, 1371; (e) Chakraborty, S.; Brennessel, W. W.; Jones, W. D. A Molecular Iron Catalyst for the Acceptorless Dehydrogenation and Hydrogenation of N-Heterocycles. *J. Am. Chem. Soc.* **2014**, *136*, 8564–8567; (f) Xu, R.; Chakraborty, S.; Yuan, H.; Jones, W. D. Acceptorless, Reversible Dehydrogenation and Hydrogenation of N-Heterocycles with a Cobalt Pincer Catalyst. *ACS Cat.* **2015**, *5*, 6350–6354; (g) Zuo, W.; Morris, R. H. Synthesis and use of an asymmetric transfer hydrogenation catalyst based on iron(II) for the synthesis of enantioenriched alcohols and amines. *Nat. Protoc.* **2015**, *10*, 241–257; (h) Wei, Z.; Chen, Y.; Wang, J.; Su, D.; Tang, M.; Mao, S.; Wang, Y. Cobalt Encapsulated in N-Doped Graphene Layers: An Efficient and Stable Catalyst for Hydrogenation of Quinoline Compounds. *ACS Cat.* **2016**, *6*, 5816–5822; (i) Chen, F.; Sahoo, B.; Kreyenschulte, C.; Lund, H.; Zeng, M.; He, L.; Junge, K.; Beller, M. Selective cobalt nanoparticles for catalytic transfer hydrogenation of N-heteroarenes. *Chem. Sci.* **2017**, *8*, 6239–6246; (j) Brenna, D.; Rossi, S.; Cozzi, F.; Benaglia, M. Iron catalyzed diastereoselective hydrogenation of chiral imines. *Org. Biomol. Chem.* **2017**, *15*, 5685–5688.

A Manganese Nanosheet: New Cluster Topology and Catalysis

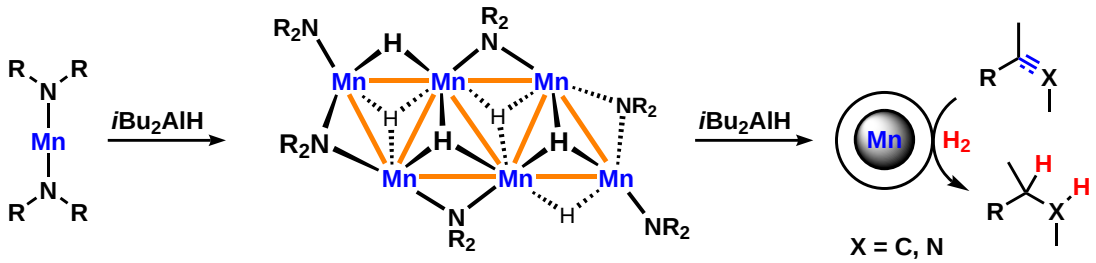

Abstract: While the coordination chemistry of monometallic complexes and the surface characteristics of larger metal particles are well understood, preparations of molecular metallic nanoclusters remain a great challenge. Discrete planar metal clusters constitute nanoscale snapshots of cluster growth but are especially rare owing to the strong preference for three-dimensional structures and rapid aggregation or decomposition. A simple ligand-exchange procedure has led to the formation of a novel heteroleptic Mn_6 nanocluster that crystallized in an unprecedented flat-chair topology and exhibited unique magnetic and catalytic properties. Magnetic susceptibility studies documented strong electronic communication between the manganese ions. Reductive activation of the molecular Mn_6 cluster enabled catalytic hydrogenations of alkenes, alkynes, and imines.

3.1 Introduction

Two-dimensional materials have gained a strong foothold in the rapidly developing field of nanoscience. Carbon nanosheets and monolayers of metals and other elements show profoundly different physical properties from the bulk systems.[1] Unlike graphene, transition-metal nanosheets are very challenging to prepare owing to the lack of convenient metal precursors, the preference for three-dimensional geometries, and the generally high reactivity of metal monolayers.[2] Consequently, only very few examples of small transition-metal nanosheets with planar or raft-like arrangements of the metal atoms have been reported. The vast majority of transition-metal clusters contain six or more metal atoms in three-dimensional cluster geometries.[3,4] From a conceptual viewpoint, 3D metal nanoclusters are models of the bulk material. Small 2D metal nanoclusters can be viewed as intermediate stages of the growth of soluble metals or metal ions towards metallic monolayers (Figure 3.1).[5]

Flat metal clusters exhibit unique magnetic properties and distinct catalytic activities owing to the electronic, magnetic, and steric communication between the neighboring metals in the plane. Polynuclear metal carbonyl species are by far the most studied class of 2D and 3D clusters; they exhibit strong coordination of the CO ligands to the metals, are coordinatively saturated, and thus provide not the best models for metal clusters and surfaces under other, CO-free conditions.[4] An example of a planar, CO-free cluster is the oligohydride Rh_7 wheel (type **A**, Figure 3.1), which contains a planar Rh core that mimics a M(111) monolayer.[3]

Recently, Ohki and co-workers and our group have shown that the reaction of easily available transition-metal amide precursor complexes $M\{N(SiMe_3)_2\}_2$ (M = Co,

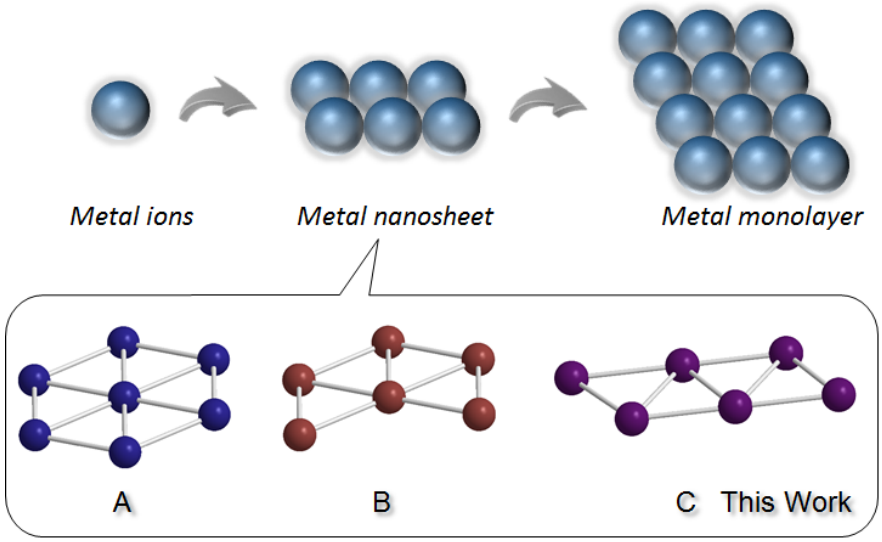

Figure 3.1: Growth of 2D and 3D transition-metal architectures.

Fe) with commercial hydride sources (diisobutylaluminium hydride, Dibal-H; pinacolborane, HBpin) is a convenient strategy to access new topologies of low-valent transition-metal nanoclusters in high yields. Planar Co_4, Co_7, Fe_4, Fe_6, and Fe_7 clusters have been isolated and characterized. Among the larger metal clusters with six or more metal atoms, the type **A** topology has been realized with Fe and Co, and the truncated wheel of type **B** with Fe.[3]

Given the synthetic ease of the formation of the precursors and clusters, the use of simple hydrides as initiators of cluster growth, and the high yields of the resultant nanoclusters, we set out to further explore the potential of such facile procedures for the preparation of carbonyl-ligand-free transition-metal nanoclusters with new topologies. Herein, we report the synthesis of a low-valent manganese nanosheet with a hitherto unknown arrangement of six Mn atoms in a nearly planar ladder-type architecture (**C**). Magnetic susceptibility measurements support the notion of strong antiferromagnetic interactions between the Mn ions, which result in a diamagnetic ground state. The Mn_6 cluster was shown to be a molecular precursor to catalytically active nanoparticles, which displayed activities that are distinct from those of previously reported molecular Mn catalysts.

Substitution of the bulky amides in $M[N(SiMe_3)_2\}_2$ complexes (M = Fe, Co) with hydride atoms has recently enabled the preparation of soluble Fe and Co nanoclusters.[3] We surmised that an equimolar reaction of the related manganese complex $Mn[N(SiMe_3)_2\}_2$ (**1**)[6] with a hydride reagent would afford the coordinatively highly unsaturated species $[Mn\{N(SiMe_3)_2\}H]$. Oligomerization of this intermediate to higher aggregates constitutes a new entry into the nanoscale regime of Mn cluster growth and, in comparison with the related Fe and Co structures, provides new insight into the control of cluster topology by the nature of the 3d transition metal.

3.2 Cluster Synthesis and Characterization

Paralleling our work with Fe and Co clusters, we were mostly interested in the identification of small soluble nanoclusters that constitute snapshots on the nanoscale of the growth of nanoparticles from low-valent molecular Mn complexes. Indeed, the reaction of **1** with 1 equiv. HBpin (or Dibal-H) in *n*-hexane at 20 °C readily afforded the novel Mn_6 cluster $[Mn_6(\mu_3\text{-}H)_4(\mu_2\text{-}H)_2\{(\mu_2\text{-}N(SiMe_3)_2\}_4\{N(SiMe_3)_2\}_2]$ as brown single crystals in 18% yield after recrystallization (**2**; Scheme 3.1). Single-crystal X-ray analysis of **2** revealed an unprecedented ladder-type Mn_6 nanocluster containing four μ_2-bridging $N(SiMe_3)_2$ and two terminal $N(SiMe_3)_2$ ligands (Scheme 3.1, middle). The Mn_6 core is best described as a "flat chair" with four coplanar Mn centers (Mn_2, Mn_3, $Mn_{2'}$, and $Mn_{3'}$). Two Mn centers (Mn_1 and $Mn_{1'}$) cap two opposite edges of the central Mn_4 motif slightly above and below the plane (11.9°; see Scheme 3.1, right). Alternatively, this novel near-planar hexametallic architecture can be viewed as an array of four Mn_3 triangles sharing three common edges in a zigzag chain.

This structural interpretation could also suggest that the stepwise growth of the Mn_6 nanocluster proceeds through sequential formal [1+2] additions of Mn_1 units across Mn–Mn bonds. The resultant M_3 triangles are the common topological motif of all members of the $(hmds)_xM_yH_z$ family (hmds = $N(SiMe_3)_2$) with Mn_6, Fe_4, Fe_6, Fe_7, and Co_7 cores.[3] The unprecedented planar growth might be a direct consequence of the steric bulk of the hmds ligands, which effectively shield the half spaces above and below the metal plane. The Mn–Mn bond lengths (2.85622(3)–2.97627(3) Å) are in the range of Mn–Mn bonds in other Mn clusters.[7,8]

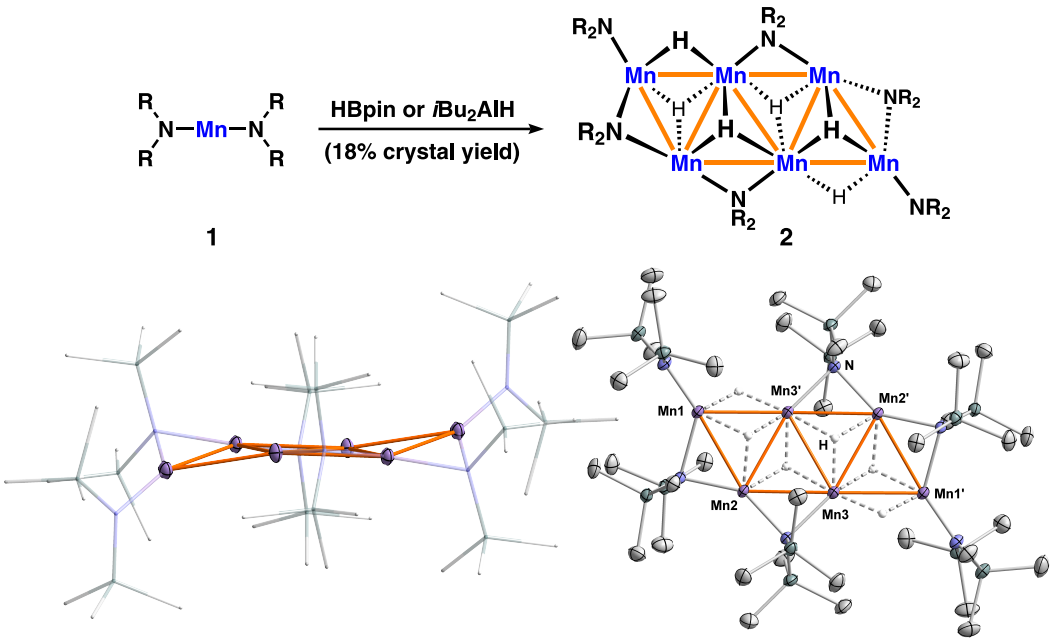

Scheme 3.1: Synthesis of the Mn_6 cluster **2** (top). Down: Crystal structure of **2**. Ellipsoids set at 50% probability. Hydrogen atoms omitted except for MnH.

The positions of the hydride ligands of **2** were determined from the electron density Fourier map. Four μ_3-H atoms coordinate the Mn_6 core in alternating up and down fashion. Two μ_2-H atoms span the sterically more hindered peripheral Mn–Mn bonds whereas the least hindered peripheral Mn–Mn edges are coordinated by the bulky hmds ligands.

In an effort to elucidate key properties of **2**, we further characterized the single crystals. In C_6D_6 solution, **2** is paramagnetic and ^{1}H-NMR silent. Solid **2** is thermally highly stable; decomposition was observed at 139 °C. The UV/Vis spectrum in *n*-hexane showed a featureless broad band tailing into the visible region (see Figure 3.4, p. 87). No significant absorption of the Mn–H moiety was detected in the expected region between 1500 and 2000 nm (Figure 3.5, p. 88). An effective magnetic moment μ_{eff} of 4.28 μ_B (or 2.29 $cm^3mol^{-1}K$, per Mn_6 cluster, in C_6D_6) was recorded, which is much lower than the spin-only value for six uncoupled S = 5/2 spins (14.49 μ_B or

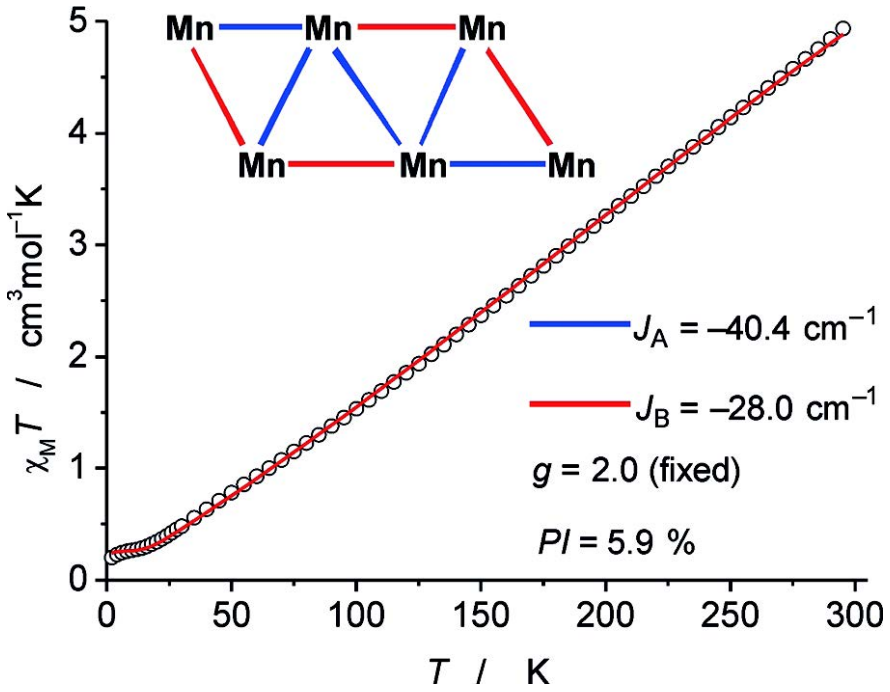

Figure 3.2: Temperature dependence of $\chi_M T$ for **2**. The solid red line is the best fit. See the main text and subsection 3.5.9 on p. 96 for details. Inset: magnetic coupling pattern used for the simulation.

26.25 $cm^3mol^{-1}K$). This may indicate the presence of strong antiferromagnetic interactions. Thus the temperature-dependent magnetism was analyzed by a SQUID measurement on solid **2** ($\chi_M T$ vs. T plot in Figure 3.2). Indeed, $\chi_M T$ drops rapidly and approaches zero at low temperatures, which supports the assumption of strong antiferromagnetic exchange and a diamagnetic ground state. Coupling constants were obtained from fitting the data on the basis of a simplified spin Hamiltonian that includes two coupling constants and Zeeman splitting, using the PHI program.[9] The coupling pattern shown in the inset in Figure 3.2 was derived from the structural data, where red lines represent coupling through amide and hydride ligands, and blue lines represent couplings only through hydride ligands. To avoid overparametrization, the g values for all Mn ions were fixed to 2.0. The obtained coupling constants J_A = -40.4 cm^{-1} and J_B = -28.0 cm^{-1} lie in the same range as for trinuclear Mn_3 clusters with comparable Mn–Mn distances.[8e] To date, all oligonuclear clusters with more than five Mn atoms reported in the literature contained carbonyl and multidentate N,O-ligands and adopted three-dimensional polyhedral geometries.[7,10,11] Two-dimensional Mn clusters are very rare;[8] no carbonyl-free 2D hexametal skeleton has ever been reported. Two planar Mn_7 wheels of type A (Figure 3.1) are contained within $[Mn][Mn_7(THF)_6(CO)_{12}]_2$, where each $Mn_7(THF)_6(CO)_{12}^-$ anion is coordinated to an isolated Mn^{2+} cation via three carbonyl oxygen atoms to give an octahedral coordination geometry about the central cation.[4c] A ladder-type hexametallic skeleton was observed in the complex $[Os_6(CO)_{18}(O_2CCF_3)]$.[5] The isolation

of the Mn_6 cluster **2** presents tangible advances over the current state-of-the-art of nanocluster topologies: **2** adopts a rare flat-chair geometry of six metal centers, it is free of strongly coordinating CO ligands, but contains labile amide and hydride ligands, the linear zigzag cluster growth is distinct from that of the recently reported Fe and Co clusters, and the manganese ions show strong antiferromagnetic interactions. Generally, discrete metal clusters receive great interest owing to their special optical, magnetic, and catalytic properties.[12] This first report of an easily accessible, soluble, planar oligo(hydridomanganese) nanosheet is of direct relevance for the design and understanding of hydrogen storage materials and hydrogenation catalysts.[3,13]

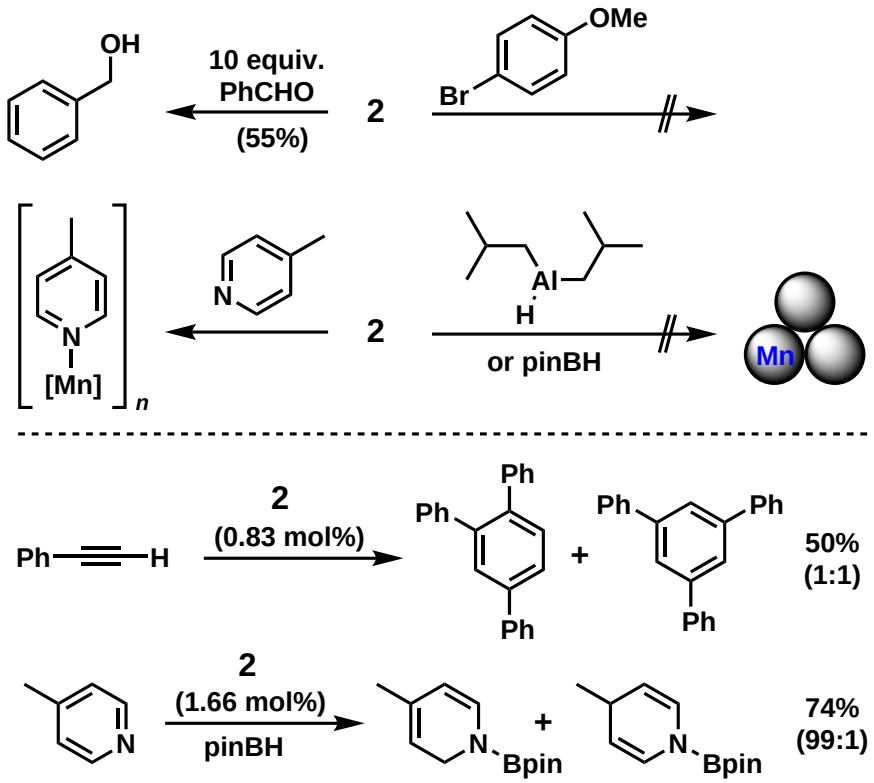

Scheme 3.2: Survey of stoichiometric (top) and catalytic (bottom) reactions of **2**.

An initial survey of the general reactivity pattern of **2** towards various reagents is shown in Scheme 3.2. The reaction of **2** with 10 equiv. benzaldehyde gave benzyl alcohol (55% vs. benzaldehyde), which indicates the presence of more than five active hydride ligands in **2**. The hydride reactivity was insufficient towards the poor electrophiles 4-bromoanisol (no debromination), diphenylacetylene (ca. 1% stilbene per Mn), and 1-octene. Upon addition of 4-methylpyridine (^{Me}Py, 6 equiv.), a yellow solution of **2** in C_6D_6 afforded a brown solution of a paramagnetic compound exhibiting broad ^{1}H-NMR resonances but no free ^{Me}Py. Further addition of ^{Me}Py (12 equiv.) shifted the broad ^{1}H-NMR resonances towards those of free ^{Me}Py, presumably owing to an equilibrium between coordinated and free ^{Me}Py. Addition

of 1 equiv. Dibal-H or pinBH to **2** resulted in a black solution, presumably owing to degradation of the complex to soluble Mn nanoparticles (see below). The first Mn-catalyzed cyclotrimerization of alkynes was observed. Phenylacetylene was converted into triphenylbenzene isomers (up to 50% yield) in the presence of 0.83 mol% **2**.[14] Sequential treatment of **2** (1.66 mol%) with ^{Me}Py and pinacolborane (HBpin) gave no hydroboration product, whereas the reverse order of addition (**2**, HBpin, ^{Me}Py) enabled selective 1,2-hydroboration (74% yield).[15] The *in situ* prepared cluster **2** (from $Mn(hmds)_2$ and HBpin) exhibited similar hydroboration activity. As hydride transfer appeared to be especially favorable with **2**, we turned our attention to the investigation of hydrogenations in the presence of catalytic amounts of **2**.

3.3 Hydrogenation Results

Hydrogenations of C=C and C=X bonds have mostly been performed with noble-metal catalysts.[16] The use of inexpensive, abundant, and non-toxic base metals has only recently been evaluated in the context of hydrogenations.[17] Manganese, as an early 3d transition metal, has largely been neglected in the development of potential hydrogenation catalysts, despite its high natural abundance (3rd most abundant transition metal in the Earth's crust after Fe, Ti) and biocompatibility.[18] In the past three years, only a handful of homogeneous pincer-type Mn complexes were applied to hydrogenations of polar C=X bonds, such as carbonyl and nitrile compounds as well as carbon dioxide, by the groups of Beller,[19] Kempe,[20] Milstein,[21] and others.[22] On the other hand, Mn-catalyzed hydrogenations of less polar C=X and non-polar C=C bonds have not been significantly explored.[18] There are two very early examples of the hydrogenation and isomerization of octenes with $Mn_2(CO)_{10}$ under harsh thermal conditions (207 bar H_2, 160 °C)[23] or with *cis*-$[(CO)_4(PPh_3)MnH]$ under UV light irradiation.[24] The trinuclear carbonyl cluster $[\{Mn(CO)_3\}_3H_3]$[25] was shown to coordinate alkenes and alkynes,[26] however, no further transformations were studied. To the best of our knowledge, there is no report on efficient Mn-catalyzed hydrogenations of less polar unsaturated substrates, such as alkenes, alkynes, or imines.

We investigated the hydrogenation of α-methylstyrene (**3**) and 1-phenyl-1-cyclohexene (**4**) under mild conditions (Table 3.1). Mn_6 cluster **2** (0.83 mol% = 5 mol% Mn) was inactive at 2 bar H_2 and 20 °C, but catalyzed full conversion of **3** at 5 bar H_2 and 60 °C. However, the latter conditions led to catalyst precipitation (in *n*-heptane) or a rapid color change from yellow to dark brown (in C_6D_6). Very good catalyst activity at 2 bar H_2 and 20 °C was observed when employing equimolar amounts of Dibal-H and **2** (entry 3). The same activity was achieved by *in situ* formation of **2** (from 5 mol% $Mn(hmds)_2$/Dibal-H in *n*-hexane) followed by addition of another 5 mol% of Dibal-H (entry 4). Further optimization with the more challenging trisubstituted substrate 1-phenyl-1-cyclohexene (**4**) was in full agreement with the fact that the binary catalyst

system $Mn(hmds)_2$/Dibal-H (1:2) was the most active hydrogenation catalyst in a non-polar solvent such as *n*-hexane (entry 7). Pinacolborane effected the formation of **2** (Scheme 3.1), but gave an inactive catalyst when mixed with $Mn(hmds)_2$ under the reaction conditions (entries 5 and 6). The optimized reaction conditions were applied to hydrogenate various alkenes (Table 3.3).

Mono- and disubstituted alkenes were hydrogenated at 5 bar H_2 and room temperature in high yields. Turnover frequencies of 65 and 24 h^{-1} were observed for the hydrogenation of 1-octene and α-methylstyrene, respectively, at 2 bar H_2 and 20 °C after 5 min. The mild reaction conditions tolerated fluoride, thioether, ether, amine, and benzyl substituents. Trisubstituted alkenes were quantitatively converted at 10 bar H_2 and 60 °C (entries 19–24). Alkynes underwent clean hydrogenation to the alkanes (entries 26– 28). A few key mechanistic experiments were performed:

Table 3.1: Optimization of the manganese-catalyzed alkene hydrogenation.

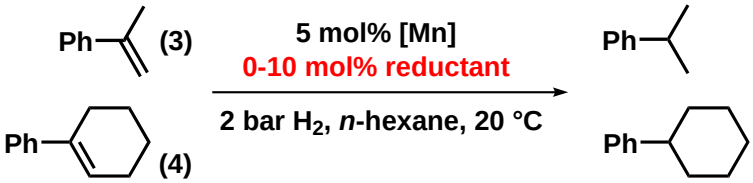

Entry	Catalyst	Reductant (mol%)	Ph-iPr [%]	Ph-Cy [%]
1	**2**	–	0	
2[a]	**2**	–	100	
3	**2**	*i*Bu_2AlH (5)	97	
4[b]	$Mn(hmds)_2$	*i*Bu_2AlH (10)	97	
5	$Mn(hmds)_2$	pinBH (5 or 10)		0
6	$Mn(hmds)_2$	*i*Bu_2AlH (5)		0
7	**$Mn(hmds)_2$**	***i*Bu_2AlH (10)**		**>99**
8	$Mn(hmds)_2$	–		0
9[c]	$MnBr_2$	*i*Bu_2AlH (10)		0
10[d]	$Mn(hmds)_2$	*i*Bu_2AlH (10)		2

General reactions conditions: alkene (0.2 mmol), [Mn] (5 mol%), reductant, hexane (1 ml), 2 bar H_2 (for **3**), 5 bar H_2 (for **4**), 20 °C, 20 h. [a] 5 bar H_2, 60 °C. [b] *In situ* formation of **2** from $Mn(hmds)_2$ and Dibal-H prior to addition of another 5 mol% Dibal-H. [c] $MnBr_2$ (5 mol%) in THF. [d] $MnBr_2$ (5 mol%), $LiN(SiMe_3)_2$ (10 mol%) in toluene instead of $Mn(hmds)_2$. Yields determined by quantitative GC-FID analysis with *n*-pentadecane as an internal standard.

Table 3.3: Manganese-catalyzed alkene hydrogenation.

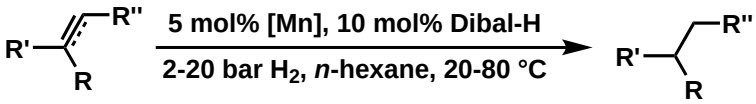

No.	Alkene	Subst.	Yield/%	No.	Alkene	Subst.	Yield/%
1	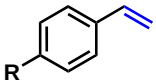	R = H	81	16[d]	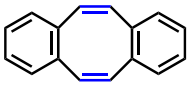		56 (70)
2		R = F	80				
3	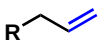	R = Ph	75	17			76
4[a]		R = C_5H_{11}	72 (94)				
5		R = Me	100	18	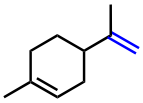		73[e]
6		R = *n*-Pr	94	19[f]	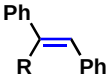	R = Me	97
7		R = *c*-Pr	91	20[f]		R = Ph	97
8		R = Ph	84	21		n = 1	100
9[b]		R = F	81 (81)	22	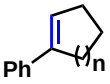	n = 2	>99
10[c]		R = Cl	8 (15)	23		n = 3	45 (47)
11	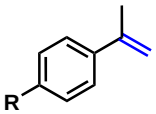	R = Br	0 (0)	24	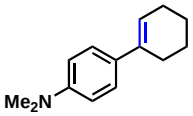		94 (94)
12		R = SMe	25 (38)				
13		R = OMe	99				
14		R = Me	96	25[g]	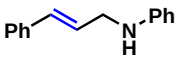		89[e]
15	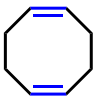		100	26		$R^1 = R^2 =$ Ph	96
				27		R^1 = Ph, R^2 = Me	77
				28		$R^1 = R^2 = C_5H_{11}$	87

Standard reaction conditions: alkene or alkyne (0.2 mmol), $Mn[N(SiMe_3)_2]_2$ (5 mol%), Dibal-H (10 mol%), *n*-hexane, 20 °C; 2 bar H_2, 3 h (entries 1–5); 5 bar H_2, 20 h (entries 6–28). If not otherwise noted, yields were determined by quantitative GC-FID analysis with *n*-pentadecane as an internal standard; conversions given in parentheses if not >95%. [a] Traces of isomerization. [b] 5 bar H_2, 3 h. [c] α-Methylstyrene (1%) formed. [d] Mixture of dihydro and tetrahydro products (4:1). [e] Yield of isolated product. [f] 10 bar H_2, *n*-heptane, 60 °C. [g] 20 bar H_2, *n*-heptane, 80 °C.

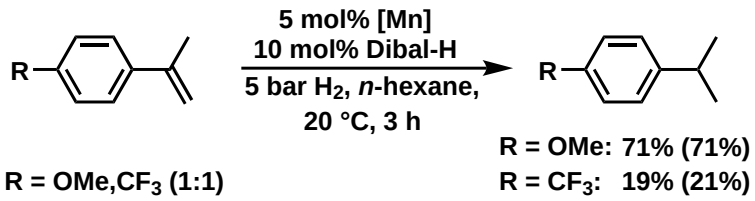

Scheme 3.3: Competitive hydrogenation of electron-rich versus electron-poor alkenes.

No adduct was obtained for the hydrogenation of **3** in the presence of the radical trap triphenylethylene. The catalyst activity was quenched in the presence of ethyl 3,3-dimethylacrylate. Employment of the radical clock α-cyclopropyl styrene generated a small amount of the ring-opened product (9%), but mainly the hydrogenation product (91%).[27] A competition experiment with 4-methoxy-α-methylstyrene and 4-trifluoromethyl-α-methylstyrene showed that the electron-rich alkene is hydrogenated more than three times faster (Scheme 3.3), which could be explained by the stronger coordination of the more Lewis basic substrate to the catalyst (see also Scheme 3.2).

Table 3.4: Manganese-catalyzed imine hydrogenation.

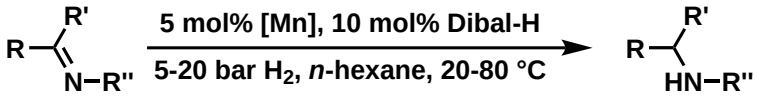

No.	Alkene	Substituents	Yield	No.	Alkene	Subst.	Yield
1	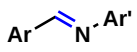	Ar = Ar′ = Ph	93	8	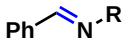	R = *t*-Bu	89
2		Ar = 4-MeOC$_6$H$_4$, Ar′ = Ph	96	9		R = Bn	50[d]
3[a]		Ar = Ph, Ar = 4-MeSC$_6$H$_4$	93	10[a]	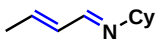		54
4[a]		Ar = Ph	96	11[a]		R = H	11[d]
5[a,b]	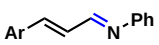	Ar = 4-MeOC$_6$H$_4$	89[c]	12[a]		R = Me	55
6[a,b]		Ar = 4-FC$_6$H$_4$	83[c]	13[a]	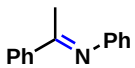		93
7[a,b]		Ar = 4-Me$_2$NC$_6$H$_4$	74[c]				

Standard reaction conditions: imine (0.2–0.5 mmol), Mn[N(SiMe$_3$)$_2$]$_2$ (5 mol%), Dibal-H (10 mol%), *n*-hexane, 5 bar H$_2$, 20 °C. If not otherwise noted, yields of isolated products are given. [a] 20 bar H$_2$, *n*-heptane, 80 °C, 20 h. [b] Ca. 10% alkene hydrogenation. [c] Yield determined by ^{1}H NMR spectroscopy. [d] Yield determined by quantitative GC-FID with *n*-pentadecane as an internal standard.

Following this observation, we extended the scope of the Mn-catalyzed hydrogenation to imines, which have not been studied in the literature. Very good conversions were achieved with *N*-aryl and *N*-alkyl aldimines (Table 3.4). Conjugated styrenyl aldimines underwent highly chemoselective C=N hydrogenation (entries 4–7), which suggests catalyst poisoning by the resulting amine. The higher reactivity of 8-methylquinoline versus quinoline might also be a direct consequence of unproductive σ-coordination of the latter to the catalyst (entries 11 and 12; see Scheme 3.1). The clear distinction between homogeneous and heterogeneous catalysis mechanisms is not trivial. However, kinetic studies are an instructive tool to discriminate between monometal and cluster catalysts by the analysis of selective poisoning experiments.[28] Addition of "sub-catalytic" amounts of trimethylphosphine at about 30% conversion of α-methylstyrene led to complete catalyst inhibition already at a catalyst/poison ratio of 5:1 (Figure 3.7, p. 97).[28] Hydrogenation of α-cyclopropyl styrene was only slightly slower in the presence of the homotopic poison dibenzo[*a*,*e*]cyclooctatetraene[29] (dct, 4 equiv. per Mn), which acted as a competing substrate (see subsection 3.5.10 on p. 97 and Table 3.3, entry 16). These results are strong indications of a heterotopic reaction mechanism involving polynuclear low-valent Mn species that are formed upon reductive activation of the nanocluster **2** with hydride reagents.

3.4 Conclusion

In summary, we have reported an unprecedented ladder-type $[XMnH]_6$ cluster that contains bulky amido ligands and active hydrides. This nanosheet complements the small family of planar 3d transition-metal clusters and presents a novel cluster topology. The cluster is soluble in organic solvents; its crystals were studied by X-ray crystallography and solid-state SQUID measurements. The latter evidences strong antiferromagnetic exchange interactions and a diamagnetic ground state for **2**. Under reducing conditions, the nanocluster displayed unprecedented catalytic activity in hydrogenations of alkenes, alkynes, and imines. Extensions of such nanocluster preparations and applications in small-molecule activation are currently being explored.

3.5 Experimental Section

3.5.1 General Information

All experiments for air-sensitive compounds were performed under an atmosphere of dry argon, by using standard Schlenk and glovebox techniques. Elemental analyses were determined by the analytical department of Regensburg University.

Analytical Thin-Layer Chromatography: TLC was performed using aluminum plates with silica gel and fluorescent indicator (Merck, 60, F254). Thin layer chromatography plates were visualized by exposure to ultraviolet light (366 or 254 nm) or by immersion in a staining solution of molybdatophosphoric acid in ethanol or potassium permanganate in water.

Column Chromatography: Flash column chromatography with silica gel 60 from KMF (0.040-0.063 mm). Mixtures of solvents used are noted in brackets.

Chemicals and Solvents: Commercially available olefins were distilled under reduced pressure prior use. Solvents (THF, Et_2O, *n*-hexane, toluene) were distilled over sodium and benzophenone and stored over molecular sieves (4 Å). Crystalline $LiN(SiMe_3)_2$ (Sigma-Aldrich, 97%) was used as received. Solvents used for column chromatography were distilled under reduced pressure prior use (ethyl acetate). DiBAl-H (1 M in *n*-hexane), DiBAl-H (1 M in toluene), $AlMe_3$ (2 M in toluene), $Al(iBu)_3$ were used as received from Sigma Aldrich or diluted before use.

High Pressure Reactor: Hydrogenation reactions were carried out in 160 and 300 ml high pressure reactors (ParrTM) in 4 ml glass vials. The reactors were loaded under argon, purged with H_2 (1 min), then three times with 2 bar H_2, sealed and the internal pressure was adjusted. Hydrogen (99.9992%) was purchased from Linde.

^{1}H- and ^{13}C-NMR-Spectroscopy: Nuclear magnetic resonance spectra were recorded on a Bruker Avance 300 (300 MHz) and Bruker Avance 400 (400 MHz). ^{1}H-NMR: The following abbreviations are used to indicate multiplicities: s = singlet; d = doublet; t = triplet, q = quartet; m = multiplet, dd = doublet of doublet, dt = doublet of triplet, dq = doublet of quartet, ddt = doublet of doublet of quartet. Chemical shift δ is given in ppm to tetramethylsilane.

Fourier-Transformations-Infrared-Spectroscopy (FT-IR): Spectra were recorded on a Agilent Cary 630 FTIR with ATR-device. All spectra were recorded at room temperature. Wave number is given in cm^{-1}. Bands are marked as s = strong, m = medium, w = weak and b = broad.

Gas Chromatography with FID (GC-FID): HP6890 GC-System with injector 7683B and Agilent 7820A System. Column: HP-5, 19091J-413 (30 m × 0.32 mm × 0.25 μm), carrier gas: N_2. GC-FID was used for reaction control and catalyst screening (calibration with internal standard *n*-pentadecane and analytically pure samples).

Gas Chromatography with Mass-Selective Detector (GC-MS): Agilent 6890N Network GC-System, mass detector 5975 MS. Column: HP-5MS (30m × 0.25 mm × 0.25 μm, 5% phenylmethylsiloxane, carrier gas: H_2. Standard heating procedure: 50 °C (2 min), 25 °C/min -> 300 °C (5 min)

High Resolution Mass Spectrometry (HRMS): The spectra were recorded by the Central Analytics Lab at the Department of Chemistry, University of Regensburg, on a MAT SSQ 710 A from Finnigan.

Gas-Uptake Reaction Monitoring: Gas-uptake was monitored with a Man On the Moon X201 kinetic system to maintain a constant reaction pressure. The system was purged with hydrogen prior use. Reservoir pressure was set to about 9 bar H_2. Calibration of the reservoir pressure drop in relation to H_2 consumption was performed by quantitative hydrogenation of various amounts of α-methylstyrene with a Pd/C catalyst in 1 ml of THF.

3.5.2 General Procedures

General Method for Catalytic Hydrogenation

In an argon-filled glove box an oven-dried 4 ml reaction vial was charged with the substrate (0.2 mmol). 10 ml catalyst solution in *n*-hexane or *n*-heptane was prepared from $Mn(hmds)_2$ (37.6 mg, 0.1 mmol) and Dibal-H (0.2 ml of 1 M Dibal-H in *n*-hexane) overnight. After addition of prepared catalyst solution (1 ml; 5 mol% [Mn]), the reaction vial was transferred to a high pressure reactor which was sealed and removed from the glovebox. The reactor was purged with H_2 (3 × 2 bar) and the reaction pressure and temperature were set. After the indicated reaction time, the vial was retrieved and hydrolyzed with a saturated aqueous solution of sodium hydrogen carbonate (0.5 ml). The reaction mixture was extracted with ethyl acetate (3 × 0.5 ml) and analyzed by GC-FID and GC-MS.

For product isolation, 0.5 to 1 mmol of the starting material was used. After quenching, the product was extracted with ethyl acetate (3 × 3 ml), dried over sodium sulfate and filtered over a pad of silica. Removal of the solvent at reduced pressure afforded the product in high purity.

For amine isolation as a free base, the product was filtered through a pad of aluminium oxide, eluted with ethyl acetate (3 × 2 ml) and dried under vacuum to remove all the volatiles to obtain the product. Product was further purified, where it is necessary, by chromatography using silica gel neutralized with Et_3N (10%) and pentane/ethyl acetate (10/1) as eluent.

For amine isolation as a chloride salt, the product was filtered through a pad of silica, eluted with ether and converted into the hydrochloride salt using a 1 M solution of HCl in ether (1 ml). The precipitate was collected via filtration or – if no precipitate formed – the solvent removed under reduced pressure.

General Method for *in situ* Catalyst Preparation with $LiN(SiMe_3)_2$

In an argon-filled glovebox an oven-dried 4 ml glass vial was charged with $MnBr_2$ (2.1 mg, 10 μmol) and $LiN(SiMe_3)_2$ (16.7 mg, 100 μmol). After dissolving the reagents in THF (1 ml), a solution of DiBAl-H in *n*-hexane (20 mM, 1 ml, 20 μmol) was added via syringe. The solution turned brown immediately and was stirred at room temperature for 5 minutes prior to use.

General Method for Kinetic Examination in Catalytic Hydrogenation

A flame-dried 10 ml two-neck flask was connected to a Man on the Moon X201 gas-uptake system. After purging with H_2, the system was set to a reaction pressure of 1.9 bar. A catalyst mixture was prepared by treatment of $Mn(hmds)_2$ (9.4 mg, 25 μmol in 2 ml *n*-hexane) with DiBAl-H (1 M, 50 μL, 50 μmol) and stirring for ca. 5 minutes. Monitoring of the hydrogen uptake started with the addition of the substrate (0.5 mmol).

3.5.3 Synthesis and Characterization of the Manganese Nanocluster $[Mn_6(\mu_3\text{-}H)_4(\mu_2\text{-}H)_2\{\mu_2\text{-}N(SiMe_3)_2\}_4\{N(SiMe_3)_2\}_2]$ (2)

Method 1: A solution of HBPin (0.39 ml in 5 ml of *n*-hexane, 2.69 mmol) was portionwise added to a light pinkish solution of $Mn\{N(SiMe_3)_2\}_2$ (1.00 g, 2.66 mmol) in *n*-hexane (5 ml) during 5 h. The obtained dark brown suspension was stirred further 1 h and filtered. The dark filtrate was stored at −35 °C for 2 days and the obtained crystalline solid was isolated by decanting the mother liquor and dried in vacuo affording complex **2** as a very air-sensitive brown solid. Yield: 102 mg (0.079 mmol, 18%). Elemental analysis calculated for $C_{36}H_{114}Mn_6N_6Si_{12}$ (1298.00 g/mol): C 33.31, H 8.85, N 6.47; found: C 33.54, H 8.62, N 6.43.

Method 2: A light pinkish solution of $Mn\{N(SiMe_3)_2\}_2$ (188 mg, 0.50 mmol) in *n*-hexane (2 ml) was treated with 0.5 ml of 1 M DiBAl-H solution (0.50 mmol) in *n*-hexane at ambient temperature. The color of the solution immediately turned to dark red-brown and it was stirred for ca. 10 minutes. The slightly turbid mixture was filtered and the filtrate was stored at −35 °C. A small amount of dark brown colored crystals suitable for X-ray crystallography were obtained. Formation of **2** was determined by single crystal X-ray crystallography.

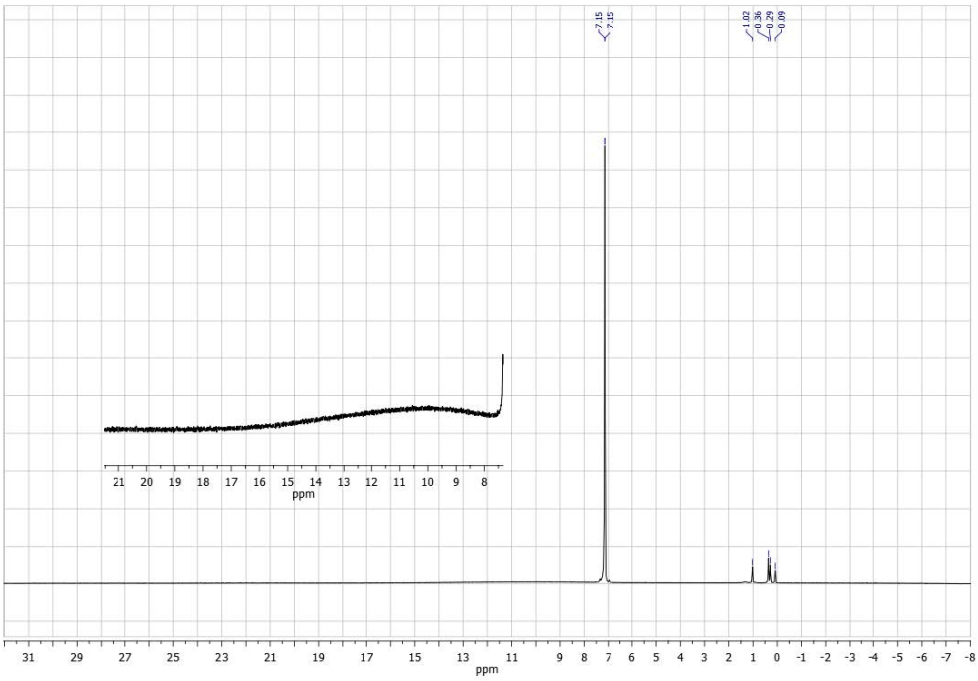

Figure 3.3: ^{1}H-NMR spectrum of **2** in C_6D_6.

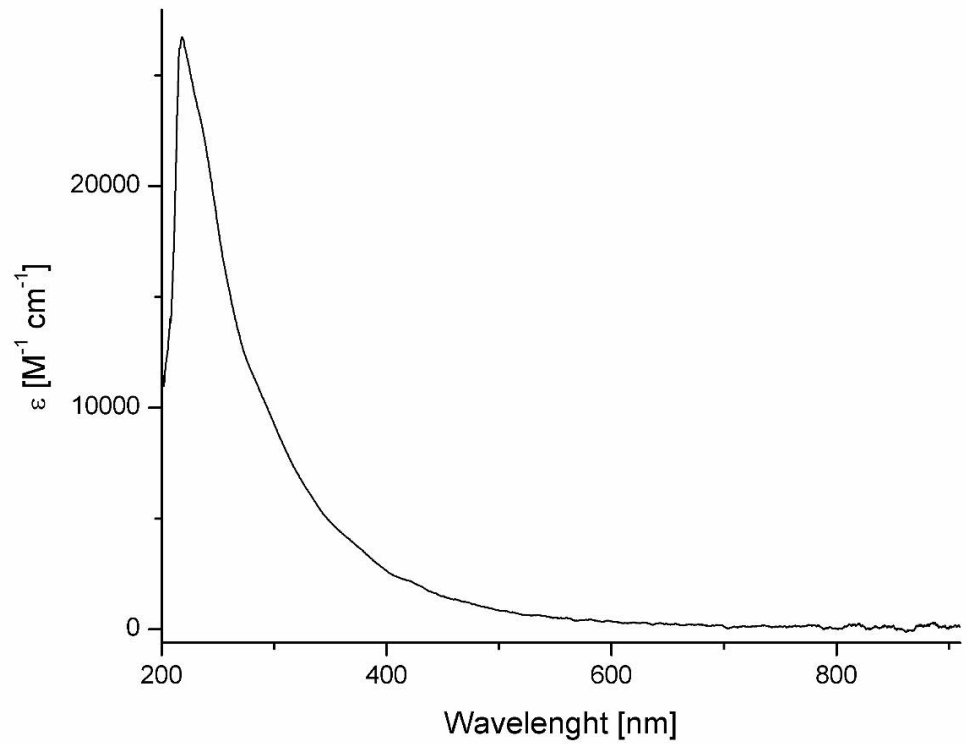

Figure 3.4: UV-vis spectrum of **2** in *n*-hexane.

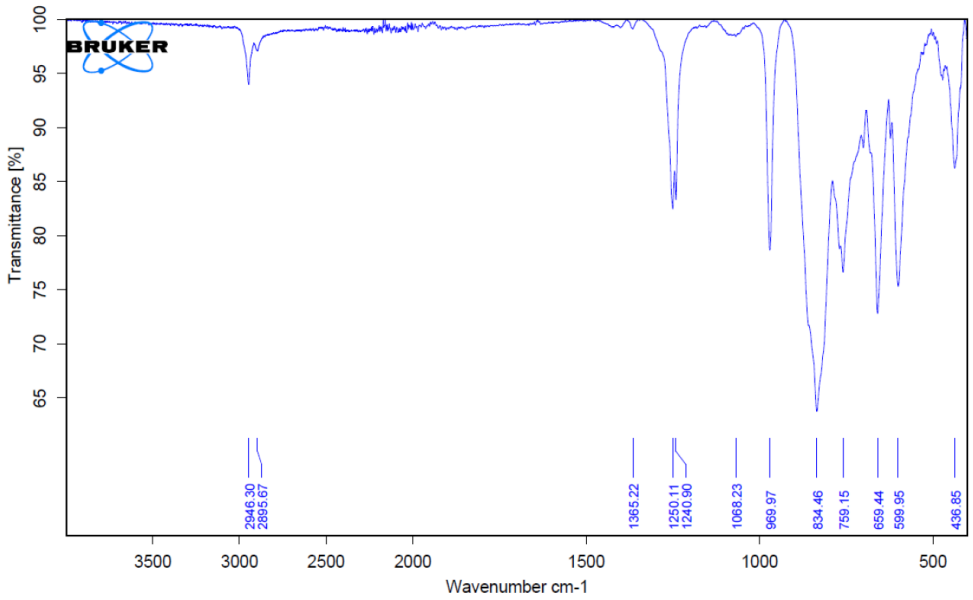

Figure 3.5: Solid IR (ATR) spectrum of **2**.

3.5.4 Radical clock reaction

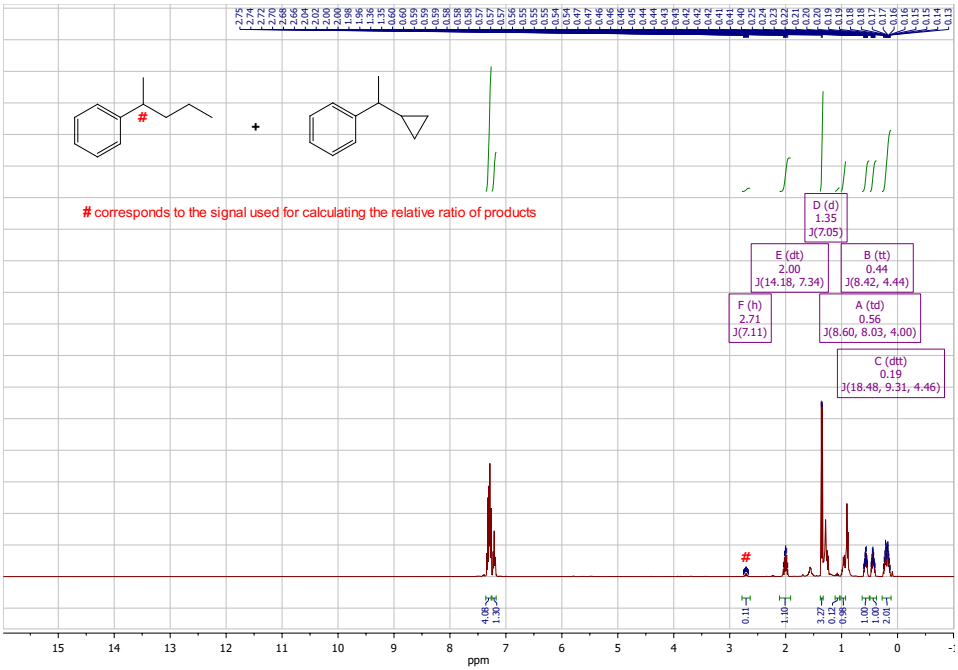

Figure 3.6: NMR analysis of the reaction mixture after hydrogenation of α-cyclopropylstyrene.

3.5.5 Cyclotrimerization Reactions of Phenyl Acetylene

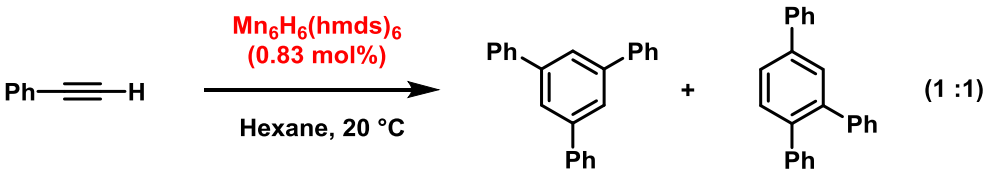

A mixture of phenylacetylene (44 μL, 40.92 mg, 0.4 mmol) and $Mn_6H_6(hmds)_6$ (4.3 mg, 3.3 μmol, 0.83 mol%) in 2 ml of hexane was stirred for three days at room temperature giving a black reation mixture with some amount of black particles. Reaction mixture was filtered over a plug of silica and the plug was eluted further with 3 × 2 ml of ethyl actetate. Solvent was removed under vacuum and the product was isolated by chromtagraphy using pentane and ethylactate mixture (95:5).

1,3,5-Triphenylbenzene and 1,2,4-triphenylbenzene (1:1)

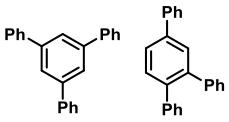

$C_{11}H_{18}Si$

178.35 g/mol

Appearance	Yellow oil
Yield	19 mg, 0.06 mmol (47%)
^{1}H-NMR	(300 MHz, $CDCl_3$) δ 7.81 (s, 3H), 7.75 – 7.65 (m, 10H), 7.56 – 7.35 (m, 15H), 7.28 – 7.17 (m, 5H).
^{13}C-NMR	(75 MHz, $CDCl_3$) δ 142.48, 141.61, 141.27, 141.24, 141.11, 140.72, 140.50, 139.67, 131.25, 130.05, 130.01, 129.56, 128.99, 128.07, 128.04, 127.69, 127.58, 127.50, 127.28, 126.74, 126.66, 126.27, 125.32.
GC-MS	t_R = 12.59 min, (EI, 70 eV): m/z = 306 [M^+], 291, 276, 265, 252, 239, 226, 215, 145, 113, 91, 77, 63, 52. t_R = 13.71 min, (EI, 70 eV): m/z = 306 [M^+], 302, 289, 276, 228, 207,189, 151, 113, 102, 91, 77, 63, 51.

Analytical data were in full agreement with A. Geny, N. Agenet, L. Iannazzo, M. Malacria, C. Aubert, V. Gandon, Angewandte Chemie International Edition 2009, 48, 1810–1813.

3.5.6 Reaction of 2 with 4-Me-Pyridine

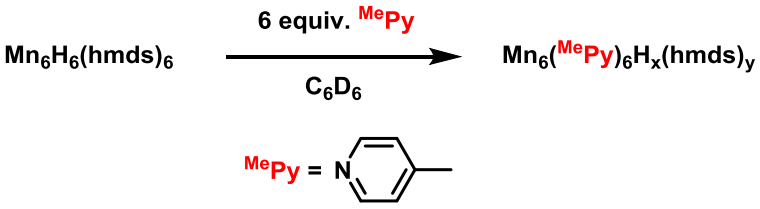

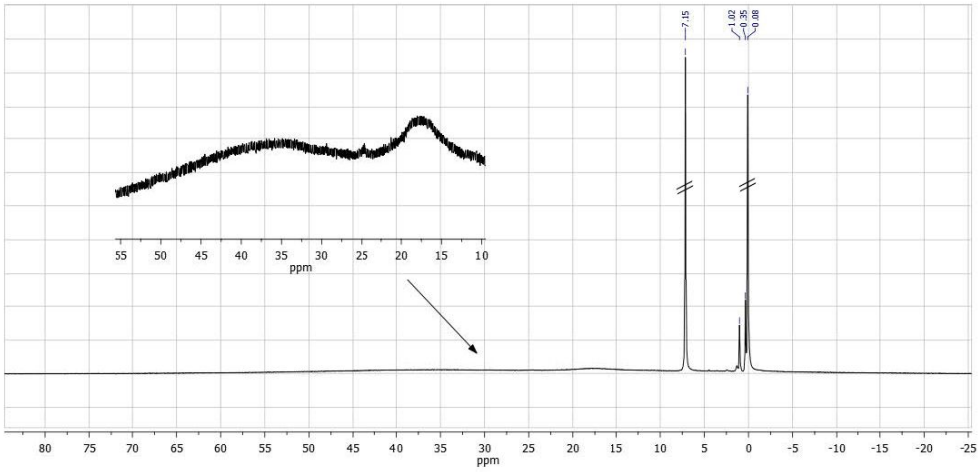

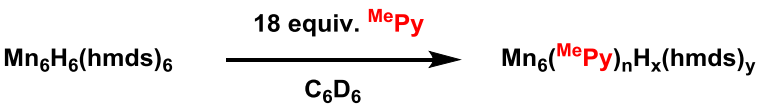

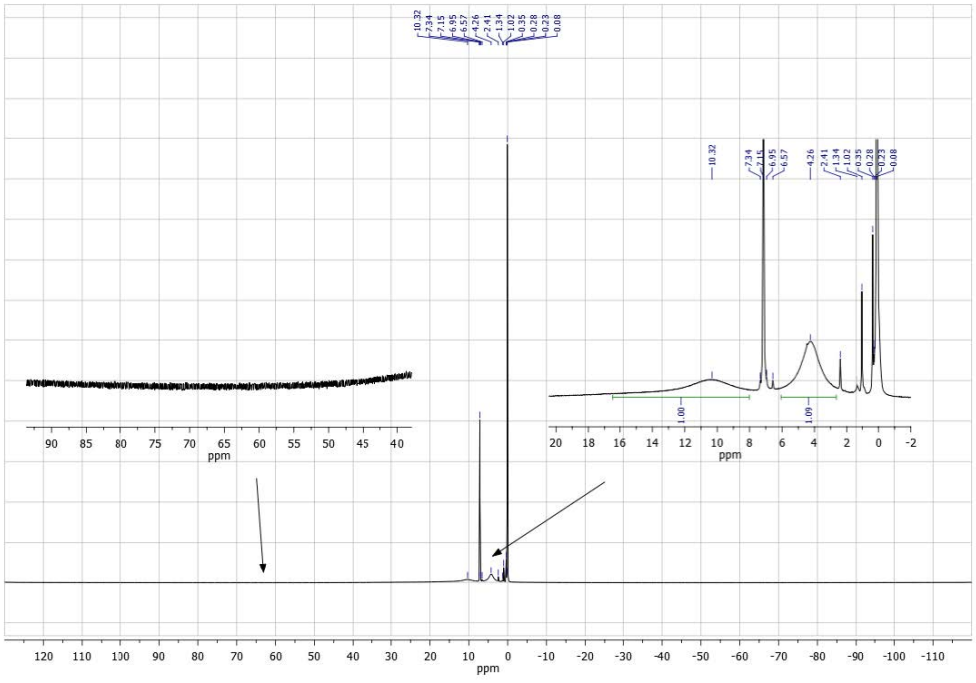

3.5.7 Hydroboration of Pyridine

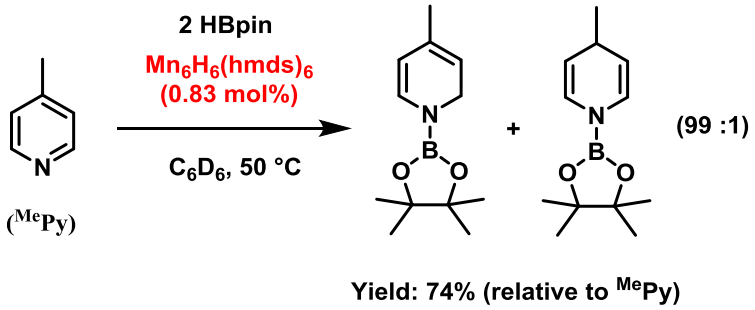

A screw-cap NMR tube was charged with **2** (2.2 mg, 1.7 μmol, 0.83 mol% compared to MePy) in 0.6 ml C_6D_6 and treated with HBpin (58 μL, 0.4 mmol) follwed by addition of MePy (19.5 μL, 0.2 mmol). The NMR tube was heated at 50 °C and the conversion of MePy was monitored by ^{1}H NMR spectroscopy.

1,2-addition product: ^{1}H NMR (400 MHz, C_6D_6) δ 6.70 (d, J = 7.4 Hz, 1H), 4.96 (dd, J = 7.4, 1.6 Hz, 1H), 4.89 – 4.82 (m, 1H), 4.16 (dd, J = 4.0, 1.7 Hz, 2H), 1.58 (dd, J = 7.3, 2.9 Hz, 3H), 1.01 (s, 12 H).

1,4-addition product: ^{1}H NMR (400 MHz, C_6D_6) δ 6.51 (d, J = 8.0 Hz, 2H, signals overlapped with 1,4-product), 4.60 – 4.53 (m, 2H), 3,02 (m, 2H), 1.01 (s, 12H, overlapped with the signal of 1,4- product), Me-Py protons are overlapped with the Bpin signals.

The data is in accordance with the reported values: M. Arrowsmith, M. S. Hill, T. Hadlington, G. Kociok-Köhn, C. Weetman, *Organometallics* **2011**, *30*, 5556–5559.

After 16 h:

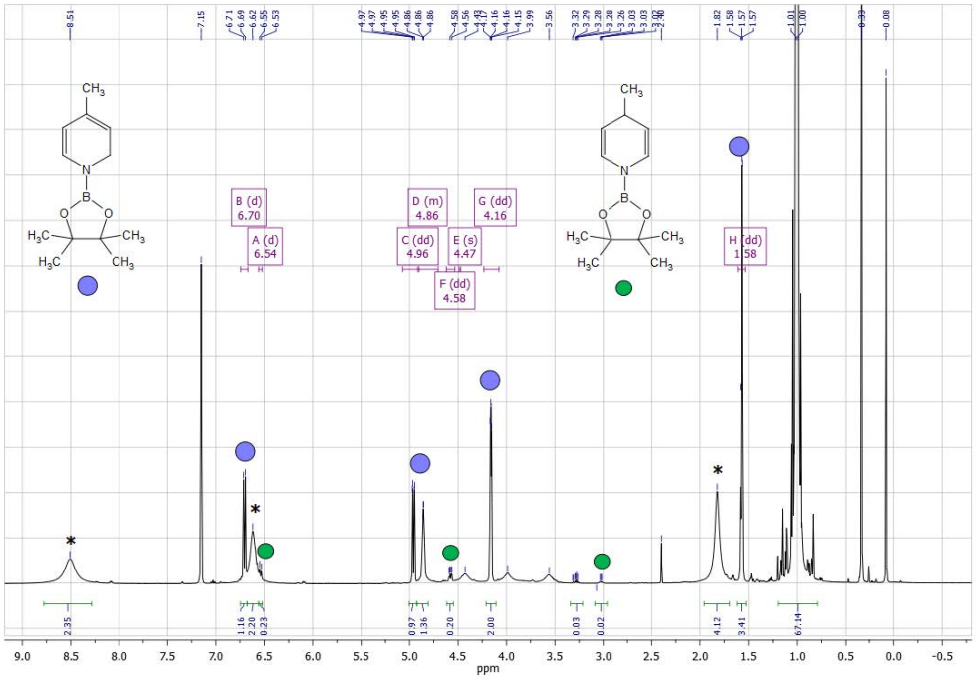

After 64 h:

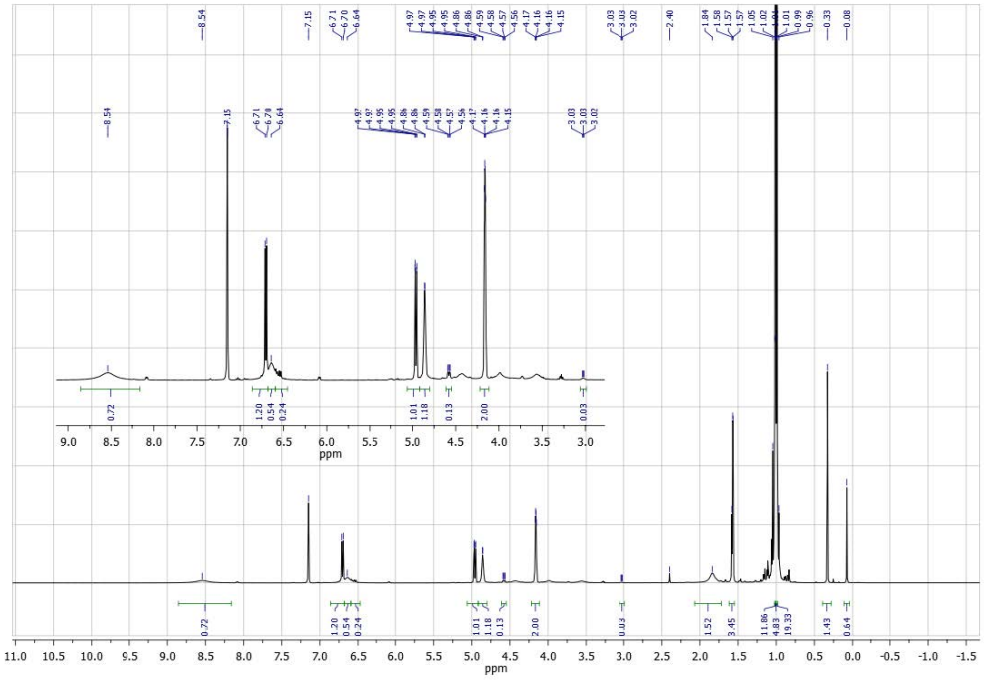

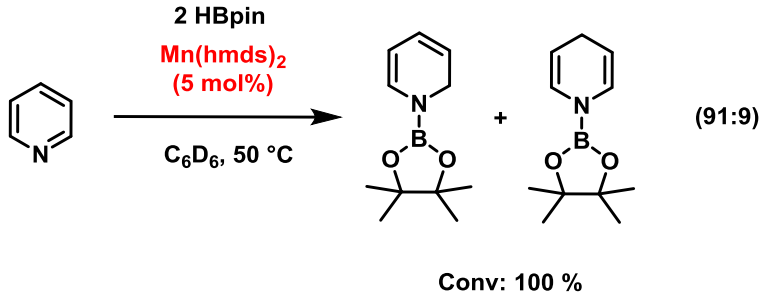

A screw-cap NMR tube was charged with $Mn(hmds)_2$ (3.8 mg, 0.01 mmol, 5 mol% compared to Py), Py (19.5 μL, 0.2 mmol) and HBpin (58 μL, 0.4 mmol). The NMR tube was heated at 50 °C and the conversion of Py was monitored by ^{1}H NMR spectroscopy.

1,2-addition product: ^{1}H NMR (400 MHz, C_6D_6) δ 6.69 (d, J = 7.4 Hz, 1H), 5.78 (dd, J = 9.0, 5.4 Hz, 1H), 5.17 – 5.03 (m, 2H), 4.14 (d, J = 2.9 Hz, 2H), 1.00 (s, 12H).

1,4-addition product: ^{1}H NMR (400 MHz, C_6D_6) δ 6.51 (d, J = 8.0 Hz, 2H), 4.60 – 4.53 (m, 2H), 2.81 (m, 2H), 0.97 (s, 12H).

The data is in accordance with the reported values: M. Arrowsmith, M. S. Hill, T. Hadlington, G. Kociok-Köhn, C. Weetman, *Organometallics* **2011**, *30*, 5556–5559.

After 16 h:

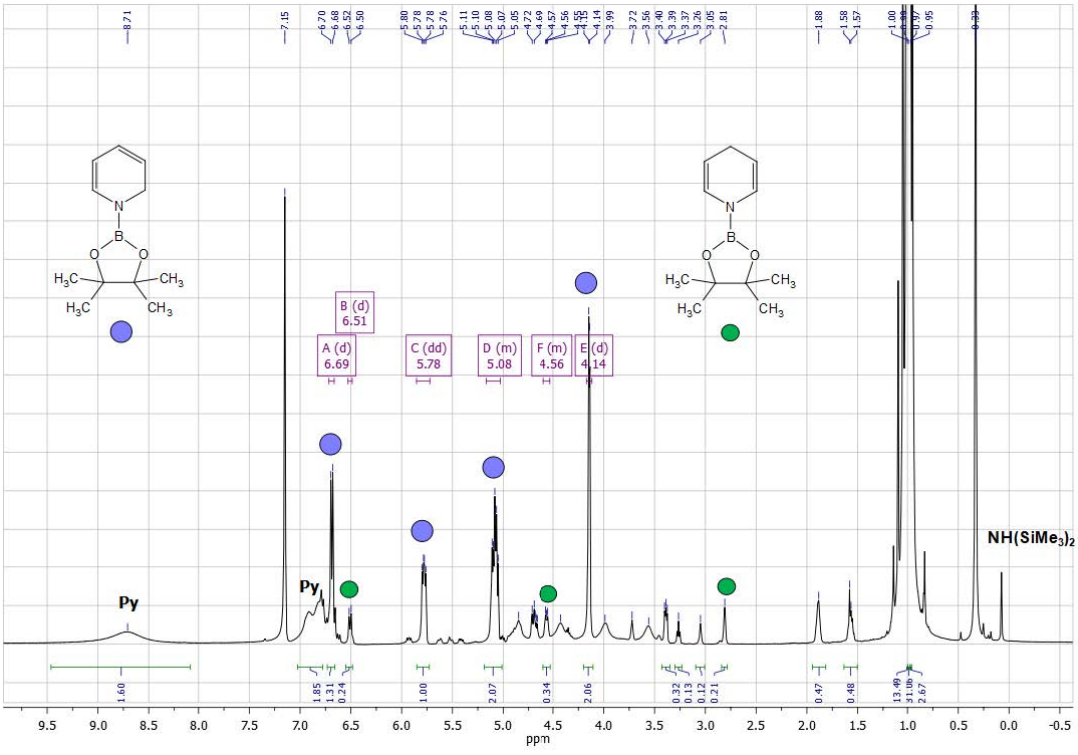

After 32 h:

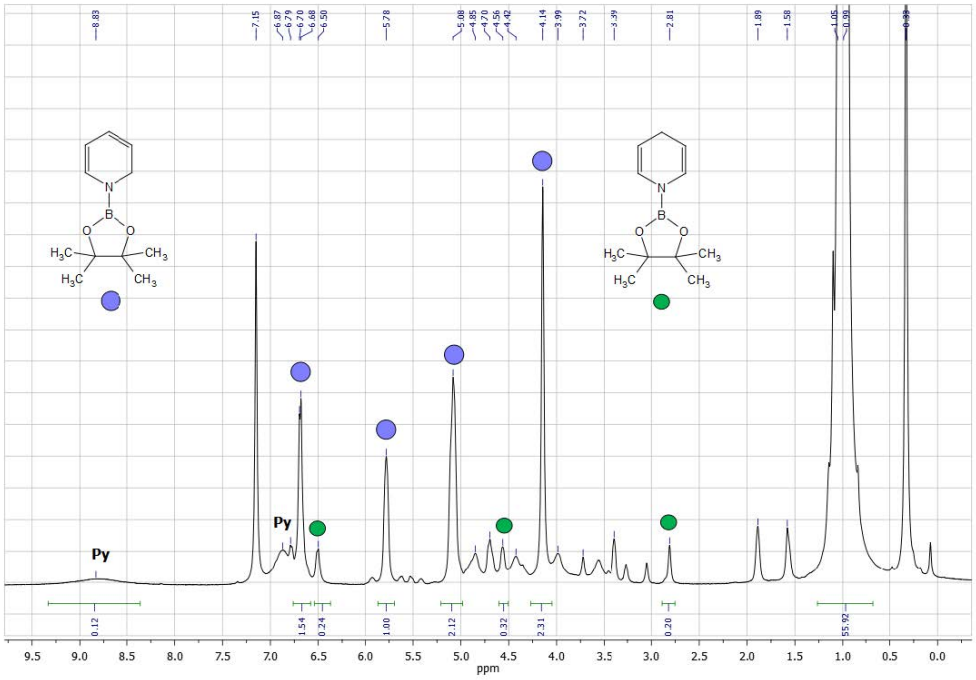

After 72 h:

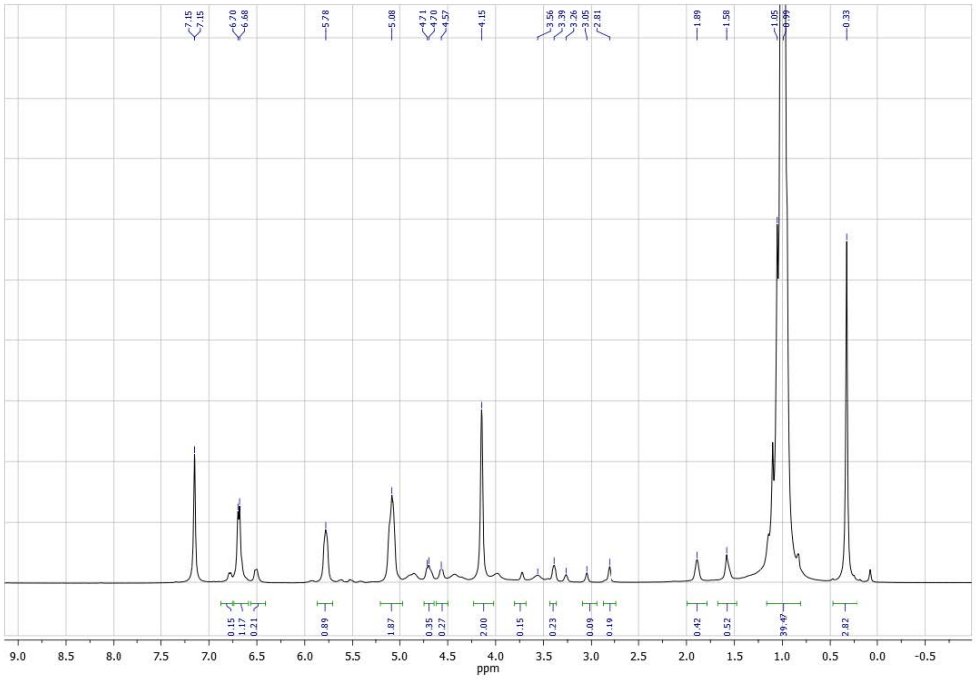

3.5.8 X-Ray Structure

$[Mn_6(\mu_3\text{-}H)_4(\mu_2\text{-}H)_2\{\mu_2\text{-}N(SiMe_3)_2\}_4\{N(SiMe_3)_2\}_2]$ crystallizes as *n*-hexane monosolvate. For X-Ray structure determination, a suitable crystal was selected and mounted on a MITIGEN holder with inert oil on a SuperNova, Single source at offset, Atlas diffractometer. The crystal was kept at T = 123.00(10) K during data collection. Using **Olex2** (Dolomanov *et al.*, 2009),[30] the structure was solved in the space group $P2_1/n$ by Direct Methods using the **ShelXT** (Sheldrick, 2015)[31] structure solution program and refined by Least Squares using version 2014/7 of **ShelXL** (Sheldrick, 2015).[32] All nonhydrogen atoms were refined anisotropically. Hydrogen atom positions were calculated geometrically and refined using the riding model. Data were measured using w scans of 1.0° per frame for 6.0 s using CuK_α radiation (micro-focus sealed X-ray tube). The total number of runs and images was based on the strategy calculation from the program CrysAlisPro (*Agilent*).

Cell parameters were retrieved using the CrysAlisPro (*Agilent*) software and refined using CrysAlisPro (*Agilent*). Data reduction was performed using the CrysAlisPro (*Agilent*) software which corrects for Lorentz polarization.

Crystal Data for $[Mn_6(\mu_3\text{-}H)_4(\mu_2\text{-}H)_2\{\mu_2\text{-}N(SiMe_3)_2\}_4\{N(SiMe_3)_2\}_2]$, *n*-hexane

Table 3.5: Crystal data and structure refinement for **2**.

Compound	**5**
Empirical formula	$C_{42}H_{128}Mn_6N_6Si_{12}$
Formula weight	1384.22
Temperature/K	123.0
Crystal system	monoclinic
Space group	$P2_1/n$
a [Å]	9.16670(10)
b [Å]	23.2172(3)
c [Å]	17.4631(3)
α [°]	90
β [°]	90.2310(10)
γ[°]	90

Volume [Å^3]	3716.56(9)
Z	2
ρcalc [g/cm^3]	1.237
μ [mm^{-1}]	10.124
F(000)	1480.0
Crystal size [mm^3]	0.2 × 0.1 × 0.07
Radiation	CuK$_\alpha$ (λ = 1.54184)
Range for data collection [°]	7.616 < 2Θ < 147.71
Index ranges	-11 $\leq$ h $\leq$ 11, -28 $\leq$ k $\leq$ 28, -21 $\leq$ l $\leq$ 21
Reflections collected	30226
Independent reflections	7438 [R_{int} = 0.0354, R_{sigma} = 0.0282]
Data/restraints/parameters	7438/72/357
Goodness-of-fit on F^2	1.019
Final R indexes [I $\geq 2\sigma$(I)]	R_1 = 0.0272, wR_2 = 0.0681
Final R indexes [all data]	R_1 = 0.0315, wR_2 = 0.0707
Largest diff. peak/hole [eÅ^{-3}]	0.44/-0.36

3.5.9 Magnetic Measurements

Temperature-dependent magnetic susceptibility measurements were carried out with a *Quantum-Design* MPMS-XL-5 SQUID magnetometer equipped with a 5 Tesla magnet in the range from 2 to 295 K in a magnetic field of 0.5 T. The polycrystalline sample was contained in a Teflon bucket and fixed in a non-magnetic sample holder. Each raw data file for the measured magnetic moment was corrected for the diamagnetic contribution of the Teflon bucket according to $M^{dia} = \chi_g \cdot m \cdot H$, with experimentally obtained gram susceptibility of Teflon bucket (g = $-3.80 \cdot 10^{-7}$ emu/(g·Oe)). The molar susceptibility data were corrected for the diamagnetic contribution according to χM^{dia}(sample) = $-0.5 \cdot M \cdot 10^{-6}$ cm^{3}mol^{-1}. Literature: O. Kahn *Molecular Magnetism*, VCH Publishers Inc., New York, **1993**.

Experimental χMT vs. T data were modelled using a fitting procedure to the spin Hamiltonian for six manganese (II) $S = 5/2$ ions with two coupling constants and additional term for Zeeman splitting:

$$\hat{H} = -2J_A(\hat{S_1}\hat{S_2} + \hat{S_2}\hat{S_5} + \hat{S_2}\hat{S_6} + \hat{S_3}\hat{S_5} + \hat{S_4}\hat{S_5}) - 2J_B(\hat{S_1}\hat{S_6} + \hat{S_2}\hat{S_3} + \hat{S_3}\hat{S_4} + \hat{S_5}\hat{S_6})$$

$$+g\mu_B \overrightarrow{B} \sum_{i=1}^{6} \overrightarrow{S_i}$$

3.5.10 Poisoning Studies

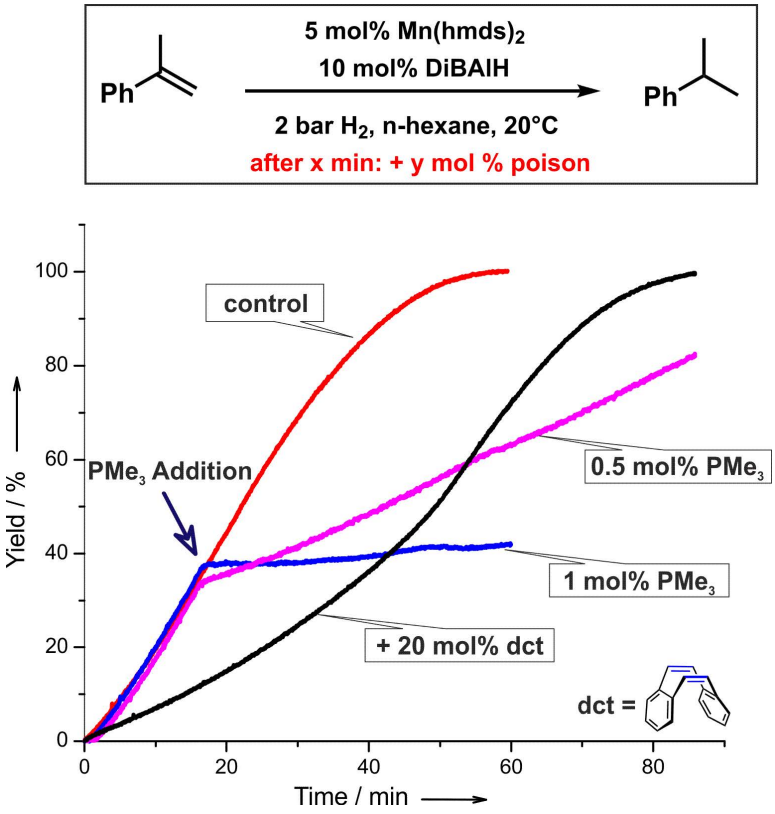

Figure 3.7: Poisoning studies with trimethylphosphine (PMe_3) and dibenzo[*a*,*e*]cyclooctatetraene (dct).

3.5.11 Synthesis of Starting Materials

General Procedure for Styrene Synthesis in a Wittig Reaction

A 50 ml flask was charged with a suspension of methyltriphenylphosphonium bromide (1 equiv.) in THF (0.7 M). Then, NaH-suspension in paraffine (60%, 1 equiv.) was added in small portions. The reaction mixture was stirred at room temperature for 20 h followed by a dropwise addition of a solution of a ketone/aldehyde derivative (1 equiv.) in THF (0.7 M). The reaction mixture was stirred for 2 d at room temperature, quenched with H_2O (15 ml) and extracted with Et_2O (3 × 15 ml). The combined organic layers were dried (Na_2SO_4), concentrated and subjected to silica gel flash chromatography (*n*-pentane).

(1-cyclopropylvinyl)benzene

Synthesis following the general procedure for styrene synthesis in a Wittig reaction.

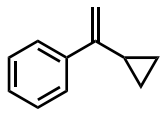

$C_{11}H_{12}$

144.22 g/mol

Appearance	colorless oil
Yield	1.27 g, 8.8 mmol (80%)
^{1}H-NMR	(300 MHz, $CDCl_3$) δ 7.67 – 7.57 (m, 2H), 7.42 – 7.26 (m, 3H), 5.30 (d, J = 1.0, 1H), 4.95 (t, J = 1.2, 1H), 1.67 (ttd, J = 8.3, 5.4, 1.2, 1H), 0.92 – 0.79 (m, 2H), 0.61 (ddd, J = 6.4, 5.4, 4.1, 2H).
^{13}C-NMR	(75 MHz, $CDCl_3$) δ 149.47, 141.75, 128.28, 127.58, 126.25, 109.15, 15.78, 6.83.
GC-MS	t_R = 6.31 min, (EI, 70 eV): m/z = 144 [M^+], 129, 115, 103, 91, 77, 63, 51.

Analytical data were in full agreement with C. Chatalova-Sazepin, Q. Wang, G. M. Sammis, J. Zhu, *Angew. Chem. Int. Ed.* **2015**, *54*, 5443–5446.

4-(Cyclohex-1-enyl)-*N*,*N*-dimethylaniline

Synthesis was performed by Schachtner, Josef, *Dissertation* **2016**, Regensburg.

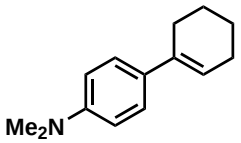

$C_{14}H_{19}N$

201.31 g/mol

Appearance	colorless oil
Yield	1.65 g, 8.20 mmol (82%)
^{1}H-NMR	(300 MHz, $CDCl_3$) δ 7.41 – 7.19 (m, 2H), 6.76 (ddd, J = 13.1, 6.8, 2.8 Hz, 2H), 6.06 – 6.00 (m, 1H), 2.96 (d, J = 2.8 Hz, 6H), 2.35 – 2.49 (m, 2H), 2.27 – 2.14 (m, 2H), 1.87 – 1.73 (m, 2H), 1.61 – 1.72 (m, 2H).
^{13}C-NMR	(75 MHz, $CDCl_3$) δ 149.4, 136.0, 129.1, 125.6, 121.7, 116.7, 112.7, 112.6, 40.8, 40.7, 27.4, 25.9, 23.2, 22.4.
GC-MS	t_R = 9.59 min, (EI, 70 eV): m/z = 202 [M^+], 180, 157, 129, 101, 77, 51.

Analytical data were in full agreement with K. Ishiuka, H. Seike, T. Hatakeyama, M. Nakamura, *J. Am. Chem, Soc.* **2010**, *132*, 13117-13119.

4-Bromo-α-methylstyrene

Synthesis following the general procedure for styrene synthesis in a Wittig reaction.

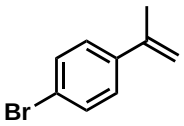

C_9H_9Br

197.08 g/mol

Appearance	colorless oil
Yield	1.06 g, 5.39 mmol (77%)
^{1}H-NMR	(400 MHz, $CDCl_3$) δ 7.50-7.35 (m, 2H), 7.42-7.29 (m, 2H), 5.36 (s, 1H), 5.10 (s, 1H), 2.12 (s, 3H).
^{13}C-NMR	(101 MHz, $CDCl_3$) δ 142.2, 140.1, 131.3, 127.2, 121.4, 113.1, 21.7.
GC-MS	t_R = 6.51 min, (EI, 70 eV): m/z = 197 [M^+], 183, 171, 156, 115, 102, 91, 75, 63, 51.

Analytical data were in full agreement with T. Taniguchi, A. Yajima, H. Ishibashi, *Adv. Synth. Catal.* **2011**, *353*, 2643–2647.

4-Methoxy-α-methylstyrene

Synthesis following the general procedure for styrene synthesis in a Wittig reaction.

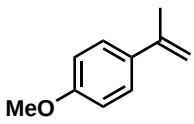

$C_{10}H_{12}O$

148.20 g/mol

Appearance	colorless oil
Yield	1.04 g, 7.02 mmol (35%)
TLC	R_f = 0.25 (SiO_2, *n*-pentane)
^{1}H-NMR	(300 MHz, $CDCl_3$) δ 7.42 (d, J = 8.9 Hz, 2H), 6.87 (d, J = 8.9 Hz, 2H), 5.29 (s, 1H), 4.99 (s, 1H), 3.82 (s, 3H), 2.13 (s, 3H).
^{13}C-NMR	(75 MHz, $CDCl_3$) δ 159.05, 142.56, 133.74, 126.60, 113.54, 110.68, 55.30, 21.94.
GC-MS	t_R = 6.39 min, (EI, 70 eV): m/z = 148 [M^+], 127, 133, 115, 105, 89, 77, 63, 51.

Analytical data were in full agreement with A. Fryszkowska, K. Fisher, J. M. Gardiner, G. M. Stephens, *J. Org. Chem.* **2008**, *73*, 4295-4298.

Methyl(4-(prop-1-en-2-yl)phenyl)sulfane

Synthesis following the general procedure for styrene synthesis in a Wittig reaction.

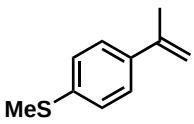

$C_{10}H_{12}S$

164.27 g/mol

Appearance	colorless solid
Yield	1.09 g, 6.63 mmol (33%)
TLC	R_f = 0.44 (SiO_2, *n*-pentane)
^{1}H-NMR	(300 MHz, $CDCl_3$) δ 7.45 – 7.35 (m, 2H), 7.25 – 7.18 (m, 2H), 5.36 (dq, J = 1.6, 0.8, 1H), 5.06 (dq, J = 1.5, 1.5, 1H), 2.49 (s, 3H), 2.14 (dd, J = 1.5, 0.8, 3H).
^{13}C-NMR	(75 MHz, $CDCl_3$) δ 142.51, 138.01, 137.49, 126.37, 125.90, 111.96, 21.75, 15.91.
GC-MS	t_R = 7.38 min, (EI, 70 eV): m/z = 164 [M^+], 149, 134, 115, 102, 91, 77, 69, 51.

Analytical data were in full agreement with G. Fraenkel, J. M. Geckle, *J. Am. Chem. Soc.* **1980**, *102*, 2869–2880.

Dibenzo[*a*,*e*]cyclooctatetraene (dct)

Synthesis following the procedure described by G. Franck, M. Brill, G. Helmchen, *J. Org. Chem.* **2012**, *89*, 55-65.

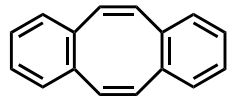

$C_{16}H_{12}$

204.27 g/mol

Appearance	colorless solid
Yield	912 mg, 4.46 mmol (47%)
TLC	R_f = 0.46 (SiO_2, hexanes)
^{1}H-NMR	(300 MHz, $CDCl_3$) δ 7.19–7.13 (m, 4H), 7.10–7.02 (m, 4H), 6.76 (s, 4H).
^{13}C-NMR	(75 MHz, $CDCl_3$) δ 137.1, 133.3, 129.1, 126.8.
GC-MS	t_R = 9.35 min, (EI, 70 eV): m/z = 204 [M^+].

Analytical data were in full agreement with G. Franck, M. Brill, G. Helmchen, *J. Org. Chem.* **2012**, *89*, 55-65.

1-Phenyl-1-cyclopentene

Synthesis was performed by Schachtner, Josef, *Dissertation* **2016**, Regensburg.

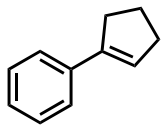

$C_{11}H_{12}$

144.22 g/mol

Appearance	colorless oil
Yield	1.99 g, 13.8 mmol (69%)
^{1}H-NMR	(300 MHz, $CDCl_3$) δ 7.48 – 7.42 (m, 2H), 7.36 – 7.27 (m, 2H), 7.25 – 7.18 (m, 1H), 6.19 (h, J = 2.1 Hz, 1H), 2.82 – 2.61 (m, 2H), 2.54 (tq, J = 7.6, 2.5 Hz, 2H), 2.15 – 1.93 (m, 2H).
^{13}C-NMR	(75 MHz, $CDCl_3$) δ 128.29, 128.27, 127.60, 126.82, 126.12, 125.91, 125.54, 66.45, 33.37, 33.18, 28.91, 28.08, 23.37, 19.35.
GC-MS	t_R = 6.94 min, (EI, 70 eV): m/z = 144 [M^+], 129, 115, 103, 91, 77, 63, 51.

Analytical data were in full agreement with W. Su, S. Urgaonkar, P. A. McLaughlin, J. G. Verkade, *J. Am. Chem. Soc.* **2004**, *126*, 16433–16439.

1-Phenyl-1-cycloheptene

Synthesis was performed by Schachtner, Josef, *Dissertation* **2016**, Regensburg.

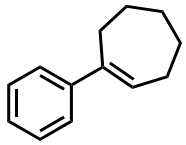

$C_{13}H_{16}$

172.27 g/mol

Appearance	colorless oil
Yield	2.89 g, 16.8 mmol (84%)
^{1}H-NMR	(300 MHz, $CDCl_3$) δ 7.42 – 7.16 (m, 5H), 6.13 (td, J = 6.8, 1.3 Hz, 1H), 2.75 – 2.52 (m, 2H), 2.43 – 2.25 (m, 2H), 1.94 – 1.80 (m, 2H), 1.74 – 1.50 (m, 4H).
^{13}C-NMR	(75 MHz, $CDCl_3$) δ 144.99, 130.45, 128.13, 126.26, 125.67, 32.86, 32.82, 28.92, 26.98, 26.85.
GC-MS	t_R = 7.97 min, (EI, 70 eV): m/z = 172 [M^+], 157, 144, 129, 115, 104, 91, 77, 63, 51.

Analytical data were in full agreement with G. Baddeley, J. Chadwick, H. T. Taylor, *J. Chem. Soc.* **1956**, 451.

3.5.12 Hydrogenation products

1,2-Diphenylpropane

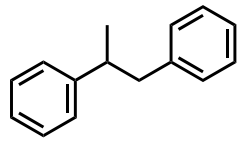

$C_{15}H_{16}$

196.29 g/mol

^{1}H-NMR (300 MHz, $CDCl_3$) δ 7.44 – 7.10 (m, 10H), 3.17 – 2.95 (m, 2H), 2.91 – 2.78 (m, 1H), 1.31 (d, J = 6.8 Hz, 3H).

^{13}C-NMR (75 MHz, $CDCl_3$) δ 147.05, 140.88, 129.23, 128.37, 128.17, 127.11, 126.09, 125.91, 45.13, 41.96, 21.23.

GC-MS t_R = 8.24 min, (EI, 70 eV): m/z = 196 [M^+], 178, 165, 152, 139, 128, 115, 105, 91, 77, 65, 51.

Analytical data were in full agreement with C. Metallinos, J. Zaifman, L. Van Belle, L. Dodge, M. Pilkington, *Organometallics* **2009**, *28*, 4534-4543.

Phenylcyclohexane

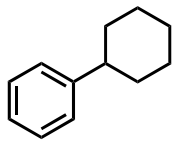

$C_{15}H_{16}$

160.26 g/mol

^{1}H-NMR (300 MHz, $CDCl_3$) δ 7.34 – 7.25 (m, 2H), 7.24 – 7.14 (m, 3H), 2.60 – 2.39 (m, 1H), 2.00 – 1.79 (m, 4H), 1.80 – 1.73 (m, 1H), 1.51 – 1.19 (m, 5H).

^{13}C-NMR (75 MHz, $CDCl_3$) δ 148.1, 128.3, 126.5, 125.8, 44.7, 34.52, 27.0, 26.2.

GC-MS t_R = 7.30 min, (EI, 70 eV): m/z = 160 [M^+], 143, 129, 115, 102, 91, 77, 63, 51.

Analytical data were in full agreement with W. M. Czaplik, M. Mayer, A. Jacobi von Wangelin, *Angew. Chem. Int. Ed.* **2009**, *48*, 607–610.

1,1-Diphenylethane

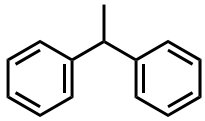

$C_{14}H_{14}$

182.27 g/mol

^{1}H-NMR	(300 MHz, $CDCl_3$) δ 7.35 – 7.11 (m, 10H), 4.15 (q, J = 7.1, 1H), 1.63 (d, J = 7.2, 3H).
GC-MS	t_R = 7.97 min, (EI, 70 eV): m/z = 182 [M^+], 167, 152, 139, 128, 115, 103, 89, 77, 63, 51.

Analytical data were in full agreement with F. Schoenebeck, J. A. Murphy, S.-z. Zhou, Y. Uenoyama, Y. Miclo, T. Tuttle, *J. Am. Chem. Soc.* **2007**, *129*, 13368–13369.

1-Cyclopropyl-1-phenylethane

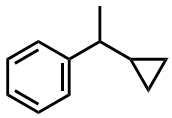

$C_{11}H_{14}$

146.23 g/mol

^{1}H-NMR	(300 MHz, $CDCl_3$) δ 7.41 – 7.26 (m, 4H), 7.25 – 7.17 (m, 1H), 1.99 (dq, J = 9.2, 7.0 Hz, 1H), 1.35 (d, J = 7.0 Hz, 3H), 0.96 (qt, J = 9.1, 8.0, 5.0 Hz, 1H), 0.65 – 0.36 (m, 2H), 0.27 – 0.09 (m, 2H).
^{13}C-NMR	(75 MHz, $CDCl_3$) δ 147.38, 128.23, 127.00, 125.89, 44.67, 21.62, 18.56, 4.64, 4.34.
GC-MS	t_R = 5.87 min, (EI, 70 eV): m/z = 146 [M^+], 131, 117, 105, 91, 77, 65, 51.

Analytical data were in full agreement with T. N. Gieshoff, M. Villa, A. Welther, M. Plois, U. Chakraborty, R. Wolf, A. Jacobi von Wangelin, *Green Chem.* **2015**, *17*, 1408–1413.

1,1,2-Triphenylethane

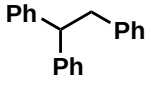

$C_{20}H_{18}$

258.36 g/mol

^{1}H-NMR	(300 MHz, $CDCl_3$) δ 7.30 – 7.09 (m, 13H), 7.05 – 6.95 (m, 2H), 4.24 (t, J = 7.8 Hz, 1H), 3.37 (d, J = 7.8 Hz, 2H).
^{13}C-NMR	(75 MHz, $CDCl_3$) δ 144.45, 140.26, 129.08, 128.34, 128.05, 126.19, 125.88, 53.11, 42.11.
GC-MS	t_R = 10.67 min, (EI, 70 eV): m/z = 258 [M^+], 167, 152, 139, 128, 115, 102, 91, 77, 65, 51.

Analytical data were in full agreement with T. C. Fessard, H. Motoyoshi, E. M. Carreira, *Angew. Chem. Int. Ed.* **2007**, *46*, 2078–2081.

1-Chloro-4-isopropylbenzene

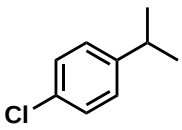

$C_9H_{11}Cl$

154.64 g/mol

^{1}H-NMR	(300 MHz, $CDCl_3$) δ 7.25 (m, 2H), 7.21–7.09 (m, 2H), 2.89 (m, 1H), 1.23 (d, J = 6.9 Hz, 6H).
^{13}C-NMR	(75 MHz, $CDCl_3$) δ 142.3, 131.3, 128.4, 127.8, 33.6, 23.9. 42.11.
GC-MS	t_R = 5.37 min, (EI, 70 eV): m/z = 154 [M^+], 139, 125, 119, 105, 89, 77, 63, 51.

Analytical data were in full agreement with S. S. Kim, C. S. Kim, *J. Org. Chem.* **1999**, *64*, 9261– 9264.

1-Isopropyl-4-methoxybenzene

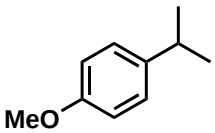

$C_{10}H_{14}O$

150.22 g/mol

^{1}H-NMR	(300 MHz, $CDCl_3$) δ 7.15 (d, J = 8.8 Hz, 2H), 6.84 (d, J = 8.7 Hz, 2H), 3.79 (s, 3H), 2.95 – 2.78 (m, 1H), 1.24 (s, 3H), 1.21 (s, 3H).
^{13}C-NMR	(75 MHz, $CDCl_3$) δ 156.86, 141.06, 127.26, 113.77, 55.27, 33.28, 24.24.

GC-MS t_R = 5.93 min, (EI, 70 eV): m/z = 150 [M^+], 120, 105, 91, 77, 65, 51.

Analytical data were in full agreement with Cahiez, G.; Foulgoc, L.; Moyeux, A. *Angew. Chem. Int. Ed.* **2009**, *48*, 2969–2972.

Methyl(4-(prop-2-yl)phenyl)sulfane

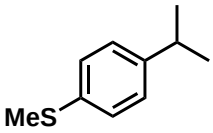

$C_{10}H_{14}S$

166.28 g/mol

^{1}H-NMR (300 MHz, $CDCl_3$) δ 7.26 – 7.19 (m, 2H), 7.19 – 7.13 (m, 2H), 2.88 (p, J = 6.9 Hz, 1H), 2.48 (s, 3H), 1.24 (d, J = 6.9 Hz, 6H).

^{13}C-NMR (75 MHz, $CDCl_3$) δ 146.11, 135.05, 127.20, 127.01, 77.47, 77.04, 76.62, 33.65, 24.00, 16.42.

GC-MS t_R = 7.20 min, (EI, 70 eV): m/z = 166 [M^+], 151, 136, 104, 91, 77, 51.

Analytical data were in full agreement with X.-m. Wu, J.-m. Lou, G.-b. Yan, *Synlett* **2016**, *27*, 2269–2273.

1-Phenyl-1-cycloheptene

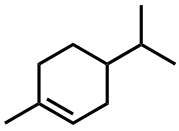

$C_{10}H_{18}$

138.25 g/mol

Appearance colorless oil

Yield 81 mg, 0.59 mmol (73%)

^{1}H-NMR (300 MHz, $CDCl_3$) δ 5.39 – 5.25 (m, 1H), 2.01 – 1.88 (m, 2H), 1.77 – 1.69 (m, 2H), 1.64 (br s, 3H), 1.50-1.40 (m, 2H), 1.26-1.17 (m, 2H), 0.89 (d, J = 4.3 Hz), 0.87 (d, J = 4.3Hz).

^{13}C-NMR (75 MHz, $CDCl_3$) δ 133.99, 121.03, 40.00, 32.30, 28.97, 26.49, 23.51, 20.02, 19.71.

GC-MS t_R = 4.92 min, (EI, 70 eV): m/z = 138 [M^+], 123, 95, 81, 67, 55.

Analytical data were in full agreement with D. F. Schneider, M. S. Viljoen, *Tetrahedron* **2002**, *58*, 5307–5315.

N-Cinnamylaniline hydrochloride

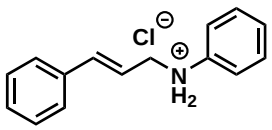

$C_{15}H_{16}ClN$

245.75 g/mol

Yield	119.1 mg, 0.48 mmol (96%)
^{1}H-NMR	(300 MHz, $CDCl_3$) δ 7.61 – 7.51 (m, 5H), 7.44 (ddt, J = 5.5, 2.6, 1.6 Hz, 2H), 7.38 – 7.29 (m, 3H), 6.84 (d, J = 16.2 Hz, 1H), 6.35 (dt, J = 15.9, 7.3 Hz, 1H), 4.20 (dd, J = 7.3, 1.2 Hz, 2H).
^{13}C-NMR	(75 MHz, $CDCl_3$) δ 140.74, 136.76, 136.25, 131.48, 131.09, 129.97, 129.82, 127.91, 124.16, 118.74, 55.34.
GC-MS	t_R = 10.29 min, (EI, 70 eV): m/z = 209 [M^+], 192, 132, 117, 106, 91, 77, 65, 51.
HRMS	Calcd. for $C_{15}H_{16}N^+$ 210.1277; found: 210.1274.
IR	3380 (b), 3060 (w), 2915 (m), 2661 (m), 2423 (m), 1588 (m), 1491 (m), 1446 (m), 969 (m), 738 (s), 690 (s) cm^{-1}.

1-Phenyl-1-cycloheptene

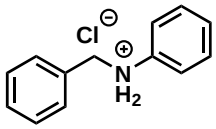

$C_{13}H_{14}ClN$

219.71 g/mol

Yield	106.9 mg, 0.49 mmol (98%)
^{1}H-NMR	(300 MHz, MeOD) δ 7.58 – 7.49 (m, 3H), 7.46 – 7.38 (m, 7H), 4.61 (s, 2H).
^{13}C-NMR	(75 MHz, MeOD) δ 136.36, 131.98, 131.47, 131.34, 130.83, 130.15, 124.15, 56.92.
GC-MS	t_R = 9.04 min, (EI, 70 eV): m/z = 183 [M^+], 154, 106, 91, 77, 65, 51.

Analytical data were in full agreement with T. Li, X. Cui, L. Sun, C. Li, *RSC Adv.* **2014**, *4*, 33599.

N-Benzyl-2-*tert*-butylamine hydrochloride

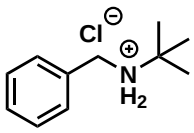

$C_{11}H_{18}ClN$

199.72 g/mol

Yield	35.4 mg, 0.18 mmol (89%)
^{1}H-NMR	(300 MHz, MeOD) δ 7.59 – 7.41 (m, 5H), 4.19 (s, 2H), 1.47 (s, 9H).
^{13}C-NMR	(75 MHz, MeOD) δ 133.15, 131.09, 130.59, 130.35, 58.71, 46.69, 27.93, 25.89.
GC-MS (freebase)	t_R = 6.25 min, (EI, 70 eV): m/z = 163 [M^+], 148, 106, 91, 77, 65, 51.
HRMS	Calcd. for $C_{11}H_{18}N^+$ 164.1434; found: 164.1432.
IR	3370 (b), 3038 (w), 2974 (m), 2192 (m), 2109 (m), 2050 (m), 1375 (s), 1204 (m), 1118 (m), 760 (s), 693 (s) cm^{-1}.

N-(4-Methoxybenzyl)aniline hydrochloride

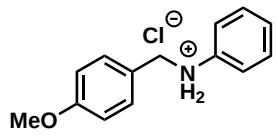

$C_{14}H_{16}ClNO$

249.74 g/mol

Yield	47.9 mg, 0.19 mmol (96%)
^{1}H-NMR	(300 MHz, MeOD) δ 7.61 – 7.49 (m, 3H), 7.44 – 7.37 (m, 2H), 7.36 – 7.29 (m, 2H), 7.03 – 6.89 (m, 2H), 4.54 (s, 2H), 3.80 (s, 3H).
^{13}C-NMR	(75 MHz, MeOD) δ 162.34, 136.10, 133.12, 131.40, 131.07, 124.43, 123.54, 115.45, 56.85, 55.86.
GC-MS (freebase)	t_R = 10.13 min, (EI, 70 eV): m/z = 213 [M^+], 168, 121, 106, 91, 77, 65, 51.
Elemental Analysis	Calcd. for $C_{14}H_{16}NO$: 214.1226; found: 214.1226.
IR	3060 (w), 2896 (m), 2840 (m), 2669 (s), 2550 (s), 2423 (s), 1595 (s), 1513 (s), 1305 (m), 1249 (s), 1033 (s), 815 (s), 795 (s) cm^{-1}.

_N_-Benzyl-4-(methylthio)aniline

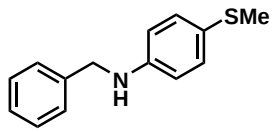

$C_{14}H_{15}NS$

229.34 g/mol

Yield	42.8 mg, 0.19 mmol (93%)
^{1}H-NMR	(300 MHz, $CDCl_3$) δ 7.39 – 7.33 (m, 4H), 7.25 – 7.19 (m, 2H), 6.63 – 6.56 (m, 2H), 4.32 (s, 2H), 2.41 (s, 3H).
^{13}C-NMR	(75 MHz, $CDCl_3$) δ 146.87, 139.08, 131.45, 128.69, 127.48, 127.34, 124.56, 113.53, 48.35, 19.13.
GC-MS	t_R = 10.91 min, (EI, 70 eV): m/z = 229 [M^+], 214, 180, 152, 138, 91, 77, 65, 51.

Analytical data were in full agreement with W. Zhou, M. Fan, J. Yin, Y. Jiang, D. Ma, *J. Am. Chem. Soc.* **2015**, *137*, 11942.

_N_-Cinnamylaniline

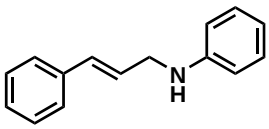

$C_{15}H_{15}N$

209.29 g/mol

^{1}H-NMR	(300 MHz, $CDCl_3$) δ 7.33 – 7.20 (m, 3H), 7.19 – 7.08 (m, 4H), 6.66 (tt, J = 7.3, 1.1 Hz, 1H), 6.63 – 6.51 (m, 3H), 6.26 (dt, J = 15.9, 5.7 Hz, 1H), 3.87 (dd, J = 5.7, 1.6 Hz, 2H), 3.78 (s, 1H).
^{13}C-NMR	(75 MHz, $CDCl_3$) δ 148.2, 137.0, 131.6, 129.4, 128.7, 127.7, 127.2, 126.5, 117.8, 113.2, 46.4.
GC-MS	t_R = 10.13 min, (EI, 70 eV): m/z = 209 [M^+], 192, 178, 165, 152, 132, 117, 106, 91, 77, 65, 51.

Analytical data were in full agreement with S. Karnakanti, Z.-L. Zang, S. Zhao, P.-L. Shao, P. Hu, Y. He, *Chem. Commun.* **2017**, *53*, 11205.

N-(4-Methoxycinnamyl)aniline

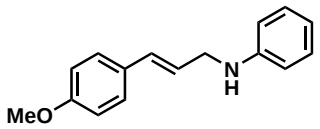

$C_{16}H_{17}NO$

239.32 g/mol

^{1}H-NMR (300 MHz, $CDCl_3$) δ 7.35 – 7.28 (m, 2H), 7.24 – 7.16 (m, 2H), 6.92 – 6.80 (m, 2H), 6.73 (tt, J = 7.4, 1.1 Hz, 1H), 6.70 – 6.65 (m, 2H), 6.58 (dt, J = 15.8, 1.6 Hz, 1H), 6.20 (dt, J = 15.8, 5.9 Hz, 1H), 3.92 (dd, J = 5.9, 1.6 Hz, 2H), 3.81 (s, 3H).

^{13}C-NMR (75 MHz, $CDCl_3$) δ 159.3, 148.2, 131.2, 129.7, 129.4, 127.6, 124.8, 117.7, 114.1, 113.2, 55.4, 46.4.

GC-MS t_R = 11.19 min, (EI, 70 eV): m/z = 239 [M^+], 222, 207, 190, 178, 165, 147, 133, 115, 103, 91, 77, 65, 51.

Analytical data were in full agreement with N. Nishina, Y. Yamamoto, *Tetrahedron* **2009**, *65*, 1799.

N-(4-Fluorocinnamyl)aniline

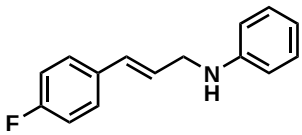

$C_{15}H_{14}FN$

227.28 g/mol

Yield 45.4 mg, 0.20 mmol (crude 83 %, isolated 50%)

^{1}H-NMR (300 MHz, $CDCl_3$) δ 7.40 – 7.27 (m, 2H), 7.24 – 7.16 (m, 2H), 7.08 – 6.93 (m, 2H), 6.74 (tt, J = 7.3, 1.1 Hz, 1H), 6.70 – 6.65 (m, 2H), 6.59 (dt, J = 15.8, 1.6 Hz, 1H), 6.25 (dt, J = 15.9, 5.7 Hz, 1H), 3.94 (dd, J = 5.8, 1.6 Hz, 2H), 3.87 (brs, 1H).

^{13}C-NMR (75 MHz, $CDCl_3$) δ 162.4 (d, J = 246.7 Hz), 148.1, 133.1 (d, J = 3.2 Hz), 130.4, 129.4, 127.9 (d, J = 8.0 Hz), 126.9 (d, J = 2.3 Hz), 117.8, 115.6 (d, J = 21.5 Hz), 113.2, 46.3.

GC-MS t_R = 10.10 min, (EI, 70 eV): m/z = 227 [M^+], 210, 196, 183, 165, 150, 135, 115, 109, 93, 77, 65, 51.

Analytical data were in full agreement with N. Nishina, Y. Yamamoto, *Tetrahedron* **2009**, *65*, 1799.

_N_-(4-_N'_,_N'_-Dimethylaminocinnamyl)aniline

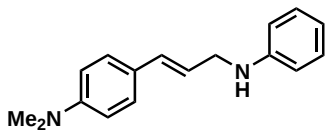

$C_{17}H_{20}N_2$

252.36 g/mol

Yield	34.1 mg, 0.14 mmol (crude 74 %, isolated 34%)
^{1}H-NMR	(300 MHz, $CDCl_3$) δ 7.29 (dd, J = 9.2, 2.4 Hz, 2H), 7.23 – 7.16 (m, 2H), 6.79 – 6.65 (m, 5H), 6.55 (d, J = 15.8 Hz, 1H), 6.14 (dt, J = 15.6, 6.0 Hz, 1H), 3.90 (dd, J = 6.0, 1.5 Hz, 2H), 3.70 (brs, 1H), 2.96 (s, 6H).
^{13}C-NMR	(75 MHz, $CDCl_3$) δ 150.2, 148.4, 131.9, 129.4, 127.4, 125.4, 122.5, 117.6, 113.2, 112.5, 46.7, 40.7.
GC-MS	t_R = 11.97 min, (EI, 70 eV): m/z = 252 [M^+], 234, 221, 207, 192, 173, 160, 146, 134, 115, 105, 93, 79, 66, 51.

_N_-Butylcyclohexanamine

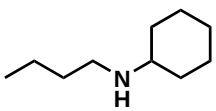

$C_{10}H_{21}N$

155.29 g/mol

Yield	34.7 mg, 0.22 mmol (54%)
^{1}H-NMR	(300 MHz, $CDCl_3$) δ 2.63 – 2.56 (m, 1H), 2.38 (ddd, J = 10.4, 7.0, 3.8 Hz, 1H), 1.88 – 1.84 (m, 2H), 1.72 – 1.68 (m, 2H), 1.50 – 0.99 (m, 10H), 0.89 (t, J = 7.2 Hz, 3H).
^{13}C-NMR	(75 MHz, $CDCl_3$) δ 57.05, 46.84, 33.76, 32.72, 26.31, 25.25, 20.70, 14.14.
GC-MS	t_R = 5.94 min, (EI, 70 eV): m/z = 155 [M^+], 126, 112, 98, 84, 70, 56.

Analytical data were in agreement with V. R. Jumde, E. Petricci, C. Petrucci, N. Santillo, M. Taddei, L. Vaccaro, *Org. Lett.* **2015**, *17*, 3990–3993.

N-(3-phenylpropyl)aniline

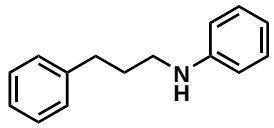

$C_{15}H_{17}N$

211.31 g/mol

Yield	27 mg, 0.13 mmol (89%)
^{1}H-NMR	(300 MHz, $CDCl_3$) δ 7.36 – 7.31 (m, 2H), 7.26 – 7.17 (m, 6H), 6.75 – 6.70 (m, 1H), 6.65 – 6.59 (m, 2H), 3.63 (s br, 1H), 3.18 (t, J = 7.0 Hz, 1H), 2.82 – 2.70 (m, 2H), 2.03 – 1.93 (m, 2H).
^{13}C-NMR	(75 MHz, $CDCl_3$) δ 148.46, 141.79, 129.35, 128.56, 128.53, 126.08, 117.33, 112.85, 43.51, 33.52, 31.19.
GC-MS	t_R = 9.74 min, (EI, 70 eV): m/z = 211 [M^+], 118, 106, 91, 77, 65, 51.

Analytical data were in agreement with Adam, J. R. Cabrero-Antonino, K. Junge, R. Jackstell, M. Beller, *Angew. Chem. Int. Ed.* **2016**, *55*, 11049–11053.

8-methyl-1,2,3,4-tetrahydroquinoline

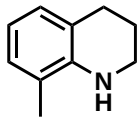

$C_{10}H_{13}N$

147.22 g/mol

Yield	16 mg, 0.11 mmol (55%)
^{1}H-NMR	(300 MHz, $CDCl_3$) δ 6.87 (t, J = 6.9 Hz, 2H), 6.57 (t, J = 7.0 Hz, 1H), 3.66 (s br, 1H), 3.38 (m, 2H), 2.80 (m, 2H), 2.09 (s, 3H), 1.95 (s, 2H).
^{13}C-NMR	(75 MHz, $CDCl_3$) δ 142.82, 127.96, 127.50, 121.31, 120.99, 116.52, 42.46, 27.40, 22.27, 17.30.
GC-MS	t_R = 7.36 min, (EI, 70 eV): m/z = 147 [M^+], 144, 132, 117, 103, 91, 77, 65, 51.

Analytical data were in agreement with J.-F. Zhang, R. Zhong, Q. Zhou, X. Hong, S. Huang, H.-Z. Cui, X.-F. Hou, *ChemCatChem* **2017**, *9*, 2496–2505.

3.6 References

[1] (a) Mannix, A. J.; Kiraly, B.; Hersam, M. C.; Guisinger, N. P. Synthesis and chemistry of elemental 2D materials. *Nat Rev Chem.* **2017**, *1*, 0014; (b) Geim, A. K.; Grigorieva, I. V. Van der Waals heterostructures. *Nature* **2013**, *499*, 419–425; (c) Geim, A. K.; Novoselov, K. S. The rise of graphene. *Nat. Mater.* **2007**, *6*, 183–191.

[2] Osada, M.; Sasaki, T. Two-Dimensional Dielectric Nanosheets: Novel Nanoelectronics From Nanocrystal Building Blocks. *Adv. Mater.* **2012**, *24*, 210–228.

[3] (a) Gieshoff, T. N.; Chakraborty, U.; Villa, M.; Jacobi von Wangelin, A. Alkene Hydrogenations by Soluble Iron Nanocluster Catalysts. *Angew. Chem. Int. Ed.* **2017**, *56*, 3585–3589; (b) Araake, R.; Sakadani, K.; Tada, M.; Sakai, Y.; Ohki, Y. [Fe_4] and [Fe_6] Hydride Clusters Supported by Phosphines: Synthesis, Characterization, and Application in N_2 Reduction. *J. Am. Chem. Soc.* **2017**, *139*, 5596–5606; (c) Ohki, Y.; Shimizu, Y.; Araake, R.; Tada, M.; Sameera, W. M. C.; Ito, J.-I.; Nishiyama, H. $Co_6H_8(PiPr_3)_6$: A Cobalt Octahedron with Face-Capping Hydrides. *Angew. Chem. Int. Ed.* **2016**, *55*, 15821–15825; (d) Brayshaw, S.; Green, J.; Edge, R.; McInnes, E.; Raithby, P.; Warren, J.; Weller, A. $[Rh_7(PiPr_3)_6H_{18}][BArF_4]_2$: A Molecular Rh(111) Surface Decorated with 18 Hydrogen Atoms. *Angew. Chem. Int. Ed.* **2007**, *46*, 7844–7848; (e) Cerrada, E.; Contel, M.; Valencia, A. D.; Laguna, M.; Gelbrich, T.; Hursthouse, M. B. A New, Simple Route to Novel Gold Clusters: Structure of an Au_6Ag Wheel with a Gold Rim. *Angew. Chem. Int. Ed.* **2000**, *39*, 2353–2356.

[4] (a) Adams, R. D.; Zhang, Q.; Yang, X. Two-Dimensional Bimetallic Carbonyl Cluster Complexes with New Properties and Reactivities. *J. Am. Chem. Soc.* **2011**, *133*, 15950–15953; (b) Du, S.; Hodson, B. E.; Lei, P.; McGrath, T. D.; Stone, F. G. A. Penta- and Hexaruthenium Carbonyl 'Raft' Complexes Supported by Monocarborane Cage Ligands. *Inorg. Chem.* **2007**, *46*, 6613–6620; (c) Kong, G.; Harakas, G. N.; Whittlesey, B. R. An Unusual Transition Metal Cluster Containing a Seven Metal Atom Plane. Syntheses and Crystal Structures of [Mn][$Mn_7(THF)_6(CO)_{12}]_2$, $Mn_3(THF)_2(CO)_{10}$, and [$Mn(THF)_6$][$Mn(CO)_5]_2$. *J. Am. Chem. Soc.* **1995**, *117*, 3502–3509; (d) Diebold, M. P.; Drake, S. R.; Johnson, B. F. G.; Lewis, J.; McPartlin, M.; Powell, H. Synthesis and X-ray analysis of unusual planar tetra- and hexa-nuclear osmium clusters containing trifluoroacetate ligands. *J. Chem. Soc., Chem. Commun.* **1988**, 1358; (e) Doyle, G.; Eriksen, K. A.; Engen, D. V. Mixed copper/iron clusters. The preparation and structure of the large planar cluster anions, $Cu_3Fe_3(CO)_{12}{}^{3-}$ and $Cu_5Fe_4(CO)_{16}{}^{3-}$. *J. Am. Chem. Soc.* **1986**, *108*, 445–451.

[5] Zacchini, S. Using Metal Carbonyl Clusters To Develop a Molecular Approach towards Metal Nanoparticles. *Eur. J. Inorg. Chem.* **2011**, *2011*, 4125–4145.

[6] Power, P. P. Stable Two-Coordinate, Open-Shell (d^1–d^9) Transition Metal Complexes. *Chem. Rev.* **2012**, *112*, 3482–3507.

[7] (a) Holloway, C. E.; Melnik, M. Manganese carbonyl and organometallic compounds: Analysis and classification of crystallographic and structural data. *J. Organomet. Chem.* **1990**, *396*, 129–246; (b) Mingos, D. M. P.; May, A. S. In *The Chemistry Of Metal Cluster Complexes*; Shriver, D. F., Kaesz, H. D., Adams, R. D., Eds.; VCH, New York, 1990; Chapter Structural and Bonding Aspects of Metal Cluster Chemistry, pp 11–120.

[8] (a) Abel, E. W.; Towle, I. D. H.; Cameron, T. S.; Cordes, R. E. Syntheses of nonacarbonylbis(μ^3-ethoxy)(μ^2-halogeno)trimanganese complexes, the crystal structures of the fluoride and iodide, and the crystal structure of octacarbonyl(dimethylphenylphosphine)bis(μ^3-ethoxy)(μ^2-ethoxy)trimanganese. *J. Chem. Soc., Dalton Trans.* **1979**, 1943–1949; (b) Legzdins, P.; Nurse, C. R.; Rettig, S. J. Organometallic nitrosyl chemistry. 18. Electrophile-induced reduction of coordinated nitrogen monoxide. Sequential conversion of a μ^3-nitrosyl group to μ^3-hydroxylimido and μ^3-imido ligands by protonic acids. *J. Am. Chem. Soc.* **1983**, *105*, 3727–3728; (c) Fang, Z. G.; Hor, T. S. A.; Mok, K. F.; Ng, S. C.; Liu, L. K.; Wen, Y. S. 5-Substituted 1,3,4-oxathiazol-2-ones as a sulfur source for a sulfido cluster: synthesis and molecular structure of the 48-electron equilateral triangular manganese cluster anion $[Mn_3(\mu^3\text{-}S)_2(CO)_9]^-$. *Organometallics* **1993**, *12*, 1009–1011; (d) Huang, K.-C.; Tsai, Y.-C.; Lee, G.-H.; Peng, S.-M.; Shieh, M. Syntheses and X-ray Structures of a Series of Chalcogen-Containing Manganese Carbonylates $[E_2Mn_3(CO)_9]^-$, $[E_8C_2Mn_2(CO)_6]^{2-}$, and $[E_2Mn_4(CO)_{12}]^{2-}$(E = Se, S). *Inorg. Chem.* **1997**, *36*, 4421–4425; (e) Fout, A. R.; Xiao, D. J.; Zhao, Q.; Harris, T. D.; King, E. R.; Eames, E. V.; Zheng, S.-L.; Betley, T. A. Trigonal Mn_3 and Co_3 Clusters Supported by Weak-Field Ligands: A Structural, Spectroscopic, Magnetic, and Computational Investigation into the Correlation of Molecular and Electronic Structure. *Inorg. Chem.* **2012**, *51*, 10290–10299.

[9] Chilton, N. F.; Anderson, R. P.; Turner, L. D.; Soncini, A.; Murray, K. S. PHI: A powerful new program for the analysis of anisotropic monomeric and exchange-coupled polynucleard- andf-block complexes. *J. Comput. Chem.* **2013**, *34*, 1164–1175.

[10] Fout, A. R.; Zhao, Q.; Xiao, D. J.; Betley, T. A. Oxidative Atom-Transfer to a Trimanganese Complex To Form $Mn_6(\mu^6\text{-}E)$ (E = O, N) Clusters Featuring Interstitial Oxide and Nitride Functionalities. *J. Am. Chem. Soc.* **2011**, *133*, 16750–16753.

[11] Eppley, H. J.; Tsai, H.-L.; de Vries, N.; Folting, K.; Christou, G.; Hendrickson, D. N. High-Spin Molecules: Unusual Magnetic Susceptibility Relaxation Effects in $[Mn_{12}O_{12}(O_2CEt)_{16}(H_2O)_3]$ (S = 9) and the One-Electron Reduction Product $(PPh_4)[Mn_{12}O_{12}(O_2CEt)_{16}(H_2O)_4]$ (S = $\frac{19}{2}$). *J. Am. Chem. Soc.* **1995**, *117*, 301–317.

[12] (a) Gates, B. C.; Guczi, L. *Metal Clusters in Catalysis (Studies in Surface Science & Catalysis)*; Elsevier Science Ltd, 1986; (b) Lamb, H. H.; Gates, B. C.; Knözinger, H.

Molecular Organometallic Chemistry on Surfaces: Reactivity of Metal Carbonyls on Metal Oxides. *Angew. Chem. Int. Ed.* **1988**, *27*, 1127–1144; (c) Braunstein, P. In *Metal Clusters in Chemistry*; Braunstein, P., Oro, L. A., Raithby, P. R., Eds.; Wiley-VCH, 1999; (d) de Smit, E.; Weckhuysen, B. M. The renaissance of iron-based Fischer–Tropsch synthesis: on the multifaceted catalyst deactivation behaviour. *Chem. Soc. Rev.* **2008**, *37*, 2758; (e) Sessoli, R.; Gatteschi, D.; Caneschi, A.; Novak, M. A. Magnetic bistability in a metal-ion cluster. *Nature* **1993**, *365*, 141–143; (f) Sessoli, R.; Tsai, H. L.; Schake, A. R.; Wang, S.; Vincent, J. B.; Folting, K.; Gatteschi, D.; Christou, G.; Hendrickson, D. N. High-spin molecules: $[Mn_{12}O_{12}(O_2CR)_{16}(H_2O)_4]$. *J. Am. Chem. Soc.* **1993**, *115*, 1804–1816; (g) Gatteschi, D.; Sessoli, R.; Villain, J. *Molecular Nanomagnets*; Oxford University Press, 2006; (h) Karotsis, G.; Teat, S.; Wernsdorfer, W.; Piligkos, S.; Dalgarno, S.; Brechin, E. Calix[4]arene-Based Single-Molecule Magnets. *Angew. Chem. Int. Ed.* **2009**, *48*, 8285–8288.

[13] (a) Shima, T.; Luo, Y.; Stewart, T.; Bau, R.; McIntyre, G. J.; Mason, S. A.; Hou, Z. Molecular heterometallic hydride clusters composed of rare-earth and d-transition metals. *Nat. Chem.* **2011**, *3*, 814–820; (b) Adams, R.; Captain, B. Hydrogen Activation by Unsaturated Mixed-Metal Cluster Complexes: New Directions. *Angew. Chem. Int. Ed.* **2008**, *47*, 252–257; (c) Weller, A. S.; McIndoe, J. S. Reversible Binding of Dihydrogen in Multimetallic Complexes. *Eur. J. Inorg. Chem.* **2007**, *2007*, 4411–4423; (d) Thomas, J. M.; Raja, R.; Johnson, B. F. G.; Hermans, S.; Jones, M. D.; Khimyak, T. Bimetallic Catalysts and Their Relevance to the Hydrogen Economy. *Ind. Eng. Chem. Res* **2003**, *42*, 1563–1570.

[14] Brenna, D.; Villa, M.; Gieshoff, T. N.; Fischer, F.; Hapke, M.; Jacobi von Wangelin, A. Iron-Catalyzed Cyclotrimerization of Terminal Alkynes by Dual Catalyst Activation in the Absence of Reductants. *Angew. Chem. Int. Ed.* **2017**, *56*, 8451–8454.

[15] Park, S.; Chang, S. Catalytic Dearomatization of *N*-Heteroarenes with Silicon and Boron Compounds. *Angew. Chem. Int. Ed.* **2017**, *56*, 7720–7738.

[16] (a) de Vries, J. G., Elsevier, C. J., Eds. *The Handbook of Homogeneous Hydrogenation*; Wiley-VCH Verlag GmbH, 2007; (b) Nishimura, S. *Handbook of Heterogeneous Catalytic Hydrogenation for Organic Synthesis*; Wiley-VCH: New York, 2001.

[17] (a) Bullock, R. M., Ed. *Catalysis without Precious Metals*; Wiley-VCH Verlag GmbH & Co. KGaA, 2010; (b) Chirik, P. J. Iron- and Cobalt-Catalyzed Alkene Hydrogenation: Catalysis with Both Redox-Active and Strong Field Ligands. *Acc. Chem. Res.* **2015**, *48*, 1687–1695; (c) Junge, K.; Schröder, K.; Beller, M. Homogeneous catalysis using iron complexes: recent developments in selective reductions. *Chem. Commun.* **2011**, *47*, 4849; (d) Bailly, B. A. F. L.; Thomas, S. P. Iron-catalysed reduction of carbonyls and olefins. *RSC Adv.* **2011**, *1*, 1435.

[18] Valyaev, D. A.; Lavigne, G.; Lugan, N. Manganese organometallic compounds in homogeneous catalysis: Past, present, and prospects. *Coord. Chem. Rev.* **2016**, *308*, 191–235.

[19] (a) Elangovan, S.; Topf, C.; Fischer, S.; Jiao, H.; Spannenberg, A.; Baumann, W.; Ludwig, R.; Junge, K.; Beller, M. Selective Catalytic Hydrogenations of Nitriles, Ketones, and Aldehydes by Well-Defined Manganese Pincer Complexes. *J. Am. Chem. Soc.* **2016**, *138*, 8809–8814; (b) Elangovan, S.; Garbe, M.; Jiao, H.; Spannenberg, A.; Junge, K.; Beller, M. Hydrogenation of Esters to Alcohols Catalyzed by Defined Manganese Pincer Complexes. *Angew. Chem. Int. Ed.* **2016**, *55*, 15364–15368; (c) Perez, M.; Elangovan, S.; Spannenberg, A.; Junge, K.; Beller, M. Molecularly Defined Manganese Pincer Complexes for Selective Transfer Hydrogenation of Ketones. *ChemSusChem* **2016**, *10*, 83–86.

[20] Kallmeier, F.; Irrgang, T.; Dietel, T.; Kempe, R. Highly Active and Selective Manganese C=O Bond Hydrogenation Catalysts: The Importance of the Multidentate Ligand, the Ancillary Ligands, and the Oxidation State. *Angew. Chem. Int. Ed.* **2016**, *55*, 11806–11809.

[21] Espinosa-Jalapa, N. A.; Nerush, A.; Shimon, L. J. W.; Leitus, G.; Avram, L.; Ben-David, Y.; Milstein, D. Manganese-Catalyzed Hydrogenation of Esters to Alcohols. *Chem. Eur. J.* **2016**, *23*, 5934–5938.

[22] (a) van Putten, R.; Uslamin, E. A.; Garbe, M.; Liu, C.; de Castro, A. G.; Lutz, M.; Junge, K.; Hensen, E. J. M.; Beller, M.; Lefort, L.; Pidko, E. A. Non-Pincer-Type Manganese Complexes as Efficient Catalysts for the Hydrogenation of Esters. *Angew. Chem. Int. Ed.* **2017**, *56*, 7531–7534; (b) Dubey, A.; Nencini, L.; Fayzullin, R. R.; Nervi, C.; Khusnutdinova, J. R. Bio-Inspired Mn(I) Complexes for the Hydrogenation of CO_2 to Formate and Formamide. *ACS Cat.* **2017**, *7*, 3864–3868; (c) Kallmeier, F.; Kempe, R. Manganese Complexes for (De)Hydrogenation Catalysis: A Comparison to Cobalt and Iron Catalysts. *Angew. Chem. Int. Ed.* **2017**, *57*, 46–60.

[23] Weil, T. A.; Metlin, S.; Wender, I. The $Mn_2(CO)_{10}$ catalyzed hydrogenation and hydroformylation of olefins. *J. Organomet. Chem.* **1973**, *49*, 227–232.

[24] Bogdan, P. L.; Sullivan, P. J.; Donovan, T. A.; Atwood, J. D. Photocatalysis of hydrogenation and isomerization of alkenes by cis-$HMn(CO)_4PPh_3$. *J. Organomet. Chem.* **1984**, *269*, c51–c54.

[25] Kirtley, S. W.; Olsen, J. P.; Bau, R. Location of the hydrogen atoms in dodecarbonyltrihydromanganese. Crystal structure determination. *J. Am. Chem. Soc.* **1973**, *95*, 4532–4536.

[26] King, R. B.; Ackermann, M. N. Organometallic chemistry of the transition metals. XXVIII. Novel olefinic manganese carbonyl derivatives. *Inorg. Chem.* **1974**, *13*, 637–644.

[27] (a) Bullock, R. M.; Samsel, E. G. Hydrogen atom transfer reactions of transition-metal hydrides. Kinetics and mechanism of the hydrogenation of .alpha.-cyclopropylstyrene by metal carbonyl hydrides. *J. Am. Chem. Soc.* **1990**, *112*, 6886–6898; (b) Masnovi, J.; Samsel, E. G.; Bullock, R. M. Cyclopropylbenzyl radical clocks. *J. Chem. Soc., Chem. Commun.* **1989**, 1044.

[28] Crabtree, R. H. Resolving Heterogeneity Problems and Impurity Artifacts in Operationally Homogeneous Transition Metal Catalysts. *Chem. Rev.* **2011**, *112*, 1536–1554.

[29] (a) Anton, D. R.; Crabtree, R. H. Dibenzo[*a*,*e*]cyclooctatetraene in a proposed test for heterogeneity in catalysts formed from soluble platinum-group metal complexes. *Organometallics* **1983**, *2*, 855–859; (b) Franck, G.; Brill, M.; Helmchen, G. Dibenzo[*a*,*e*]cyclooctene: Multi-gram Synthesis of a Bidentate Ligand. *Org. Synth.* **2012**, *89*, 55.

[30] Dolomanov, O. V.; Bourhis, L. J.; Gildea, R. J.; Howard, J. A. K.; Puschmann, H. OLEX2: a complete structure solution, refinement and analysis program. *Journal of Applied Crystallography* **2009**, *42*, 339–341.

[31] Sheldrick, G. M. Crystal structure refinement withSHELXL. *Acta Crystallographica Section C Structural Chemistry* **2015**, *71*, 3–8.

[32] Sheldrick, G. M. SHELXT– Integrated space-group and crystal-structure determination. *Acta Crystallographica Section A Foundations and Advances* **2015**, *71*, 3–8.

Chapter 4

Alkene Metalates as Hydrogenation Catalysts

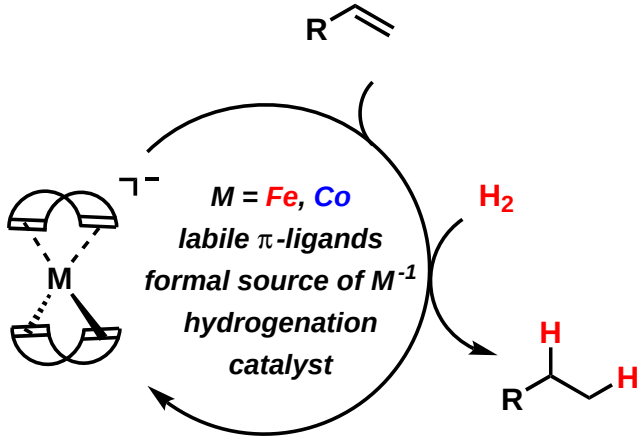

Abstract: First-row transition-metal complexes hold great potential as catalysts for hydrogenations and related reductive reactions. Homo- and heteroleptic arene/alkene metalates(1-) (M = Co, Fe) are a structurally distinct catalyst class with good activities in hydrogenations of alkenes and alkynes. The first syntheses of the heteroleptic cobaltates [K([18]crown-6)][Co(η^4-cod)(η^2-styrene)$_2$] (**5**) and [K([18]crown-6)][Co(η^4-dct)(η^4-cod)] (**6**), and the homoleptic complex [K(thf)$_2$][Co(η^4-dct)$_2$] (**7**; dct = dibenzo[*a*,*e*]cyclooctatetraene, cod = 1,5-cyclooctadiene), are reported. For comparison, two cyclopentadienylferrates(1-) were synthesized according to literature procedures. The isolated and fully characterized monoanionic complexes were competent precatalysts in alkene hydrogenations under mild conditions (2 bar H_2, r.t., thf). Mechanistic studies by NMR spectroscopy, ESI mass spectrometry, and poisoning experiments documented the operation of a homogeneous mechanism, which was initiated by facile redox-neutral π-ligand exchange with the substrates followed by H_2 activation. The substrate scope of the investigated precatalysts was also extended to polar substrates (ketones and imines).

4.1 Introduction

Metal-catalyzed hydrogenations are among the largest technical processes and constitute key operations in numerous chemical syntheses.[1] In recent decades, the use of highly active platinum-group metal catalysts has grown to maturity and enabled efficient hydrogenations of unsaturated C=C and C=X bonds.[2] Apart from nickel,[3] 3d transition-metal catalysts have received much less attention, despite their higher abundance and often lower toxicity.[4] The emphasis on stringent economic and environmental criteria has placed the development of sustainable hydrogenation methods with base-metal catalysts into the limelight of current research activities.[5] Great progress was only recently made with the development of low-valent iron-group metal catalysts (Fe, Co, Ni) for olefin hydrogenations under very mild reaction conditions. Special ligand architectures allowed the stabilization of catalytically active species in low oxidation states.

Budzelaar and co-workers reported the first application of (pyridyldiimine)cobalt catalysts to hydrogenations of mono- and disubstituted olefins (Figure 4.1, top left).[6] Significantly, Chirik and co-workers introduced new catalyst derivatives and expanded the scope to include bulky alkenes; they were also able to hydrogenate geminal-disubstituted olefins enantioselectively (Figure 4.1, top left).[7] Hanson and co-workers reported PNP pincer cobalt complexes to be active in the hydrogenation of alkenes, aldehydes, ketones, and imines and to undergo transfer hydrogenations (Figure 4.1, top center).[8] Iron and cobalt complexes with bis(phosphine) ligands were also used for (asymmetric) alkene hydrogenation (Figure 4.1, top right), whereas a catalyst with a tridentate tris(phosphane) (= triphos) ligand was shown to reduce esters and carboxylic acids.[9,10]

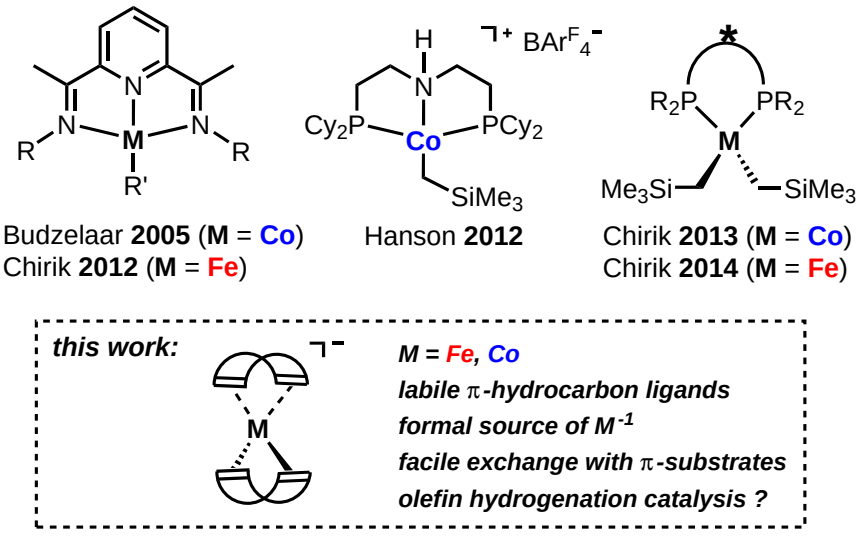

Figure 4.1: Cobalt- and iron-based hydrogenation catalysts (top) and the design concept of alkene metalate catalysts (bottom). $BAr^F_4^-$ = tetrakis[3,5-bis(trifluoromethyl)phenyl]borate.

To date, there have been many more examples, especially for PNP pincer complexes, that show impressive catalytic activities.[11] Recently, the groups of Kempe and Kirchner used PNP pincer cobalt and iron complexes for selective hydrogenations of polar bonds with high tolerance of other unsaturated bonds.[12] Moreover, effective cobalt catalysts based on NNP, PBP, and CCC pincers have been reported.[13–15]Arenes are one of the most abundant and versatile classes of unsaturated organic compounds and also entertain a rich coordination chemistry with low-valent transition metals.[16,17]

Our groups recently initiated a research program with the aim of developing metalate catalysts with simple and cheap arenes as stabilizing ligand motifs (Figure 4.1, bottom).[18] Initial experiments focused on homoleptic bis(η^4-anthracene) metalates **1** (M = Co) and **2** (M = Fe) originally reported by Ellis and co-workers.[19,20] The closed-shell 18-electron complex **1** and the open-shell 17-electron complex **2** constitute two isolable representatives of homogeneous Fe^- and Co^- sources.[17] The bis(η^4-anthracene)metalates **1** and **2** exhibited good activity in hydrogenations of various alkenes under mild conditions; cobaltate **1** was also active in catalytic hydrogenations of alkynes, ketones, and imines.[18]

Based on our preliminary mechanistic investigations with the precatalysts **1** and **2**, we postulated a new catalytic approach to hydrogenation reactions that involved 1) facile synthetic access to a variety of modular catalyst compositions from simple starting materials (alkene/arene, metal salt, reductant); 2) the presence of highly reduced, anionic iron or cobalt species, providing sufficient reducing power for the key H_2 activation; and 3) the presence of a cheap hydrocarbon ligand that could be easily replaced with structurally very similar substrates of olefin hydrogenations. The exchange of labile π-ligands with the substrates is redox-neutral, requires only little structural reorganization, and can, in principle, be traceless if the ligands undergo complete hydrogenation themselves under the reaction conditions (Scheme 4.1).

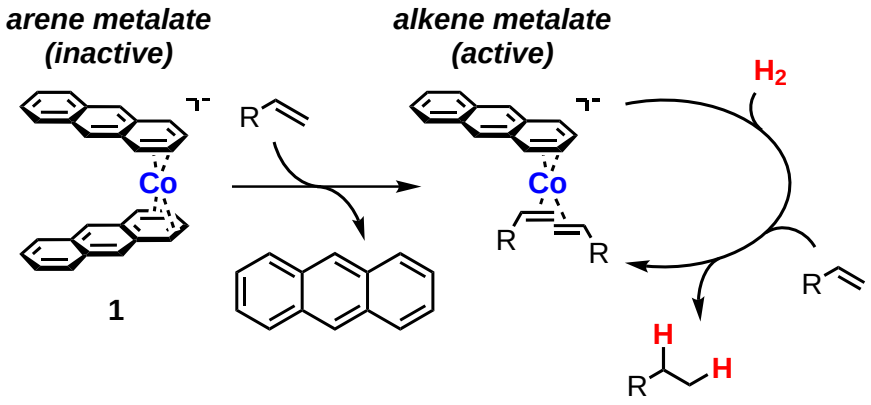

Scheme 4.1: Catalytic concept: activation of arene metalate precatalysts for hydrogenation reactions by π-ligand exchange with olefinic substrates.

In an effort to explore the scope of this new mechanistic paradigm further, we prepared a series of monoanionic alkene/arene metalates (M = Co, Fe) and studied their catalytic activity in alkene hydrogenations. Herein, we give a full account of these catalytic studies and describe the results of reaction monitoring and poisoning experiments designed to reveal the catalyst activation step and the homo- or heterogeneous nature of the catalytically active species.

4.2 Results and Discussion

4.2.1 Precatalyst Syntheses

The potassium bis(η^4-anthracene)metalates **1** (M = Co) and **2** (M = Fe) were prepared in good yields, according to the method by Ellis and co-workers, through the reduction of metal dibromides with potassium in the presence of anthracene (Scheme 4.2).[19–21] In a similar manner, treatment of the *in situ* prepared [Co(η^4-naphthalene)$_2$]$^-$ with one equivalent of 1,5-cyclooctadiene (cod) gave the heteroleptic complex [K([18]crown-6)][Co(η^4-naphthalene)(η^4-cod)] (**3**).[22] Following a protocol of Jonas and co-workers, we synthesized homoleptic [K(thf)$_x$][Co(η^4-cod)$_2$] (**4**) by the reduction of cobaltocene with a slight excess of potassium in the presence of cod (3 equiv.) in thf.[23] Upon ligand exchange of **3** and **4** with styrene, we succeeded in the first preparation of the heteroleptic complex [K([18]crown-6)][Co(η^4-cod)(η^2-styrene)$_2$] (**5**), which constituted a potential intermediate of styrene hydrogenations with cobaltate precatalysts (see below).

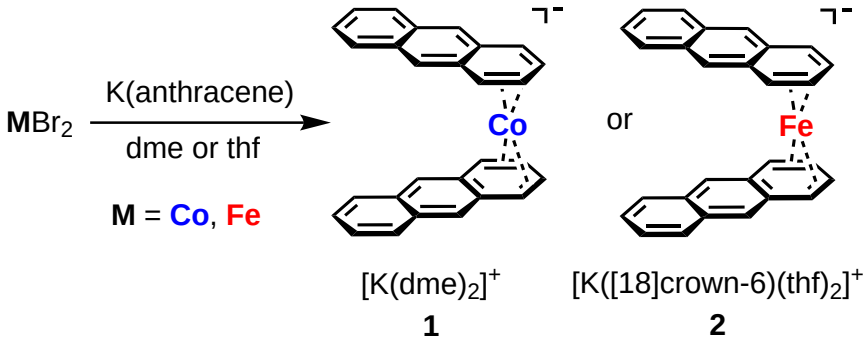

Scheme 4.2: Synthesis of bis(anthracene) metalates **1** and **2**; dme = dimethoxyethane.[19–21]

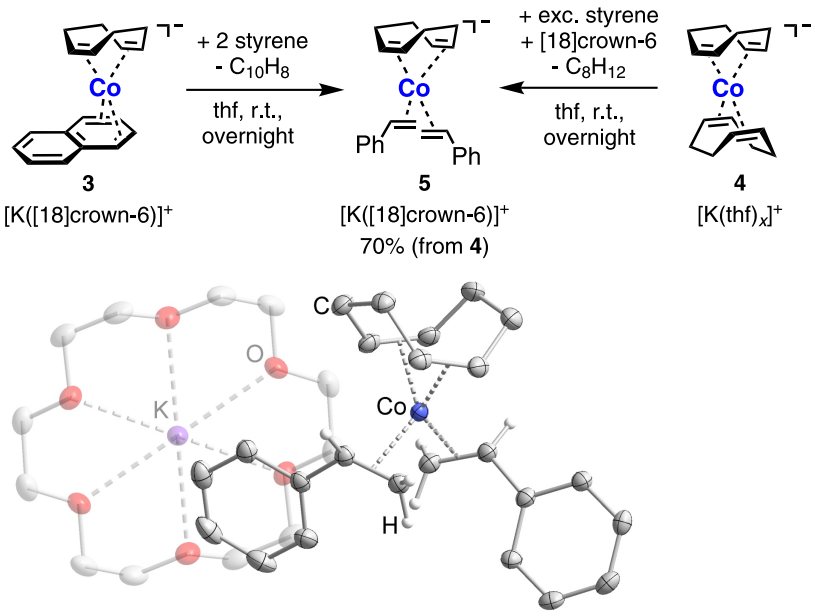

Scheme 4.3: Synthesis and molecular structure of **5**. Ellipsoids are at the 50% probability level; H atoms are omitted for clarity.

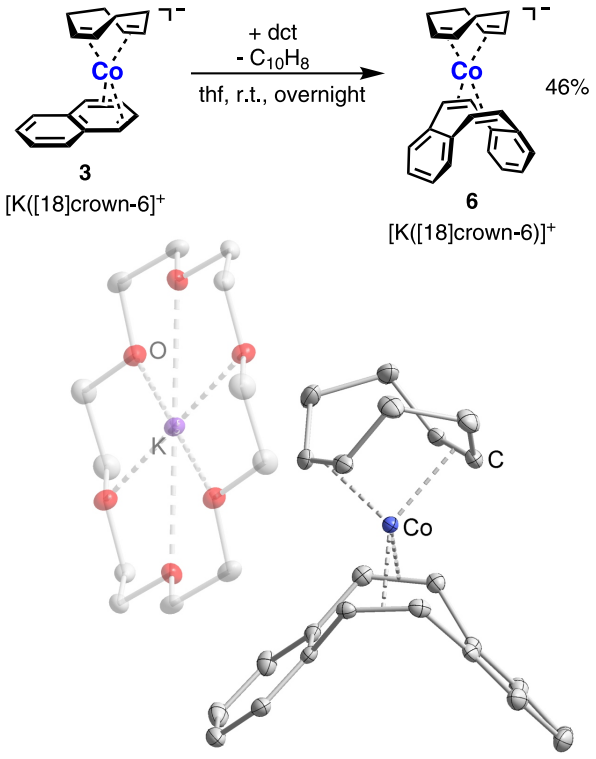

Scheme 4.4: Synthesis and molecular structure of **6**. Ellipsoids are at the 50% probability level; H atoms are omitted for clarity.

Reaction of **3** with 2.2 equivalents of styrene in thf at room temperature gave the bis(η^2-styrene) complex **5** in 61% yield (Scheme 4.3, top). The analogous reaction of **4** with styrene in thf at room temperature required a large excess of styrene (30 equiv.) and addition of [18]crown-6 to allow the isolation of bis(η^2-styrene) complex **5** in 70% yield. Isolation of a solid product was not possible in the absence of the crown ether. The formation of a putative homoleptic complex [Co(η^2-styrene)$_4$]$^-$ was not observed. Complex **5** crystallized as bright orange blocks from a solution in thf layered with *n*-hexane and was characterized by single-crystal XRD (Scheme 4.3, bottom), NMR spectroscopy, and elemental analysis. The compound is very air sensitive. Exposure of solid **5** to air is followed by immediate decomposition to a dark brown solid. A dark precipitate is formed in solution upon contact with air or moisture.

In the molecular structure of **5**, the coordination environment of the cobalt atom is distorted tetrahedral with a twist angle of 56.3°, which is somewhat smaller than that for [K([2,2,2]cryptand)][Co(η^4-cod)$_2$] (67.3°) reported by Ellis *et al.*[19b] The bite angle of the codligand is 90.0(3)°, and the angle between the two styrene ligands and Co is 104.3(3)°. The average C=C bond length of the styrene ligands is 1.423(1) Å, which is 0.08 Å longer than that of free styrene.[24]

The ^{1}H-NMR spectrum of **5** ([D$_8$]thf) shows two sets of signals with different intensities, which indicates the presence of a major and a minor isomer in solution (Figure 4.11, p. 120). These isomers are likely to arise from species with differing relative orientations of the phenyl rings, but the same overall composition.[25] According to ^{1}H-NMR integration, the ratio between the major and minor isomers is 4:1.

Similar to the preparation of **5**, [K([18]crown-6)][Co(η^4-cod)(η^4-dct)] (**6**; dct = dibenzo[*a*,*e*]cyclooctatetraene), containing the rigid, nonplanar, tub-like diene ligand dct,[26,27] was synthesized by adding one equivalent of dct to **3** in thf at room temperature (Scheme 4.4, top). Ligand exchange is incomplete; thus, complex **6** could not be obtained as a pure compound. Various samples were contaminated with a minimum of 18% [K([18]crown-6)][Co(η^4-dct)$_2$], even after several recrystallizations. X-ray-quality crystals of yellow–orange **6** were obtained from a solution in thf layered with diethyl ether. The crystallographically determined molecular structure (Scheme 4.4, bottom) is similar to those of **5** and [K([2,2,2]cryptand)][Co(η^4- cod)$_2$].[19b] Cobalt has a distorted tetrahedral coordination environment with a twist angle of 59.0°. The average C=C bond length (1.419 Å) of the coordinated dct molecules is very similar to the value found for cod in [K([2,2,2]cryptand)][Co(η^4- cod)$_2$].[19b]

The ^{1}H-NMR spectrum of the isolated product mixture recorded in [D$_8$]thf corroborates the composition of **6**. The spectrum clearly shows one set of signals assigned to **6** with the expected broad multiplets for dct and cod ligands in a 1:1 ratio, including the typical AA'BB' spin system arising from the arene protons of dct (multiplets at δ = 6.45 and 6.32 ppm). In addition, a second set of minor signals can be assigned to [K([18]crown-6)][Co(η^4-dct)$_2$].

Treatment of **4** with dct (1.2 equiv.) resulted in a mixture of unreacted **4**, the mono-substitution product [K(solv)][Co(η^4-cod)(η^4-dct)], and homoleptic [K(thf)$_2$][Co(η^4-dct)$_2$] (**7**). The formation of such a mixture is probably due to ligand-exchange equilibria, which need to be considered when using dct as a catalyst poison (see below).[27]

The desired homoleptic complex **7** was cleanly produced by reacting **1** with two equivalents of dct in thf at room temperature (Scheme 4.5, top) and was isolated in 19% yield by recrystallization from thf/*n*-hexane. The relatively low yield is explained by the need for several recrystallizations to remove free anthracene and dct. It seems noteworthy that the yield of **7** considerably increased when styrene (2 equiv.) was added to the reaction mixture. In this case, pure **7** was isolated in 62% yield after only one crystallization step from the clear orange reaction solution. The higher yield in this case might be due to the formation of an intermediary styrene complex, such as **5**, which is subsequently converted into **7** by reaction with dct.

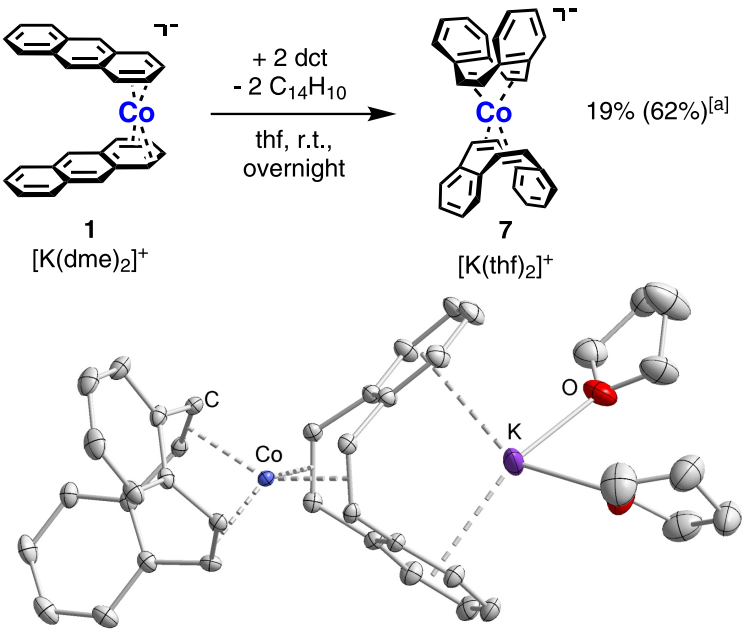

Scheme 4.5: Synthesis and molecular structure of **7**. Ellipsoids are at the 50% probability level; H atoms are omitted for clarity.

Orange blocks of **7** suitable for X-ray crystallography were obtained from thf/Et$_2$O. Single-crystal X-ray analysis revealed an ion-contact structure (Scheme 4.5, bottom) in which the coordination environment of cobalt is overall similar to that in [K([2,2,2]cryptand)][Co(η^4-cod)$_2$].[19b] The twist angle of 55.0(1)° is significantly smaller than that of the former compound (67.3°). One set of dct signals is observed in the ^{1}H-NMR spectrum of **7** in [D$_8$]thf, which is consistent with the homoleptic structure of the complex.

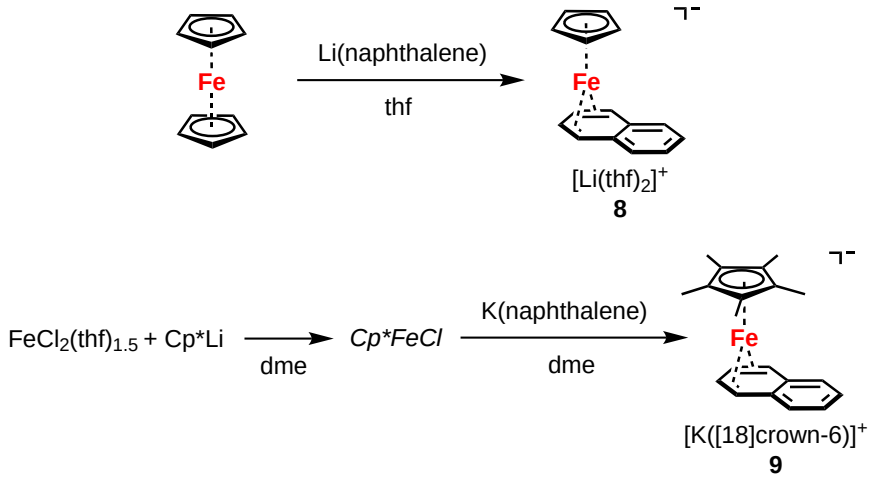

Scheme 4.6: Synthesis of cyclopentadienylferrates **8** and **9**.

The aforementioned series of arene and alkene metalates was complemented with two cyclopentadienyl iron complexes (Scheme 4.6). $[Li(thf)_2][CpFe(\eta^4\text{-naphthalene})]$ (**8**; Cp = C_5H_5) was prepared according to a method reported by Jonas from ferrocene by reduction with Li in the presence of naphthalene.[28] The compound was isolated in 60% yield. Its purity was confirmed by ^{1}H-NMR spectroscopy and elemental analysis. The synthesis of the related complex $[K([18]crown\text{-}6)][Cp^*Fe(\eta^4\text{-naphthalene})]$ (**9**; Cp* = C_5Me_5) was reported previously by our group.[29] The reduction of Cp*FeCl, *in situ* prepared from $FeCl_2(thf)_{1.5}$ and Cp*Li in dme, with potassium naphthalenide (2 equiv.) in the presence of [18]crown-6 at -60 °C in dme gave **9** in 40% yield.

4.2.2 Catalytic Hydrogenations

Our preliminary study of catalytic hydrogenations with 1 mol% of the potassium bis(η^4-anthracene) metalates(1-) **1** and **2** revealed superior activity of cobaltate **1** (Table 4.1).[18] Various α-, β-, and ring-substituted styrenes were hydrogenated in excellent yields in toluene at 2 bar H_2 and room temperature. The conversion of terminal, internal, and di- and trisubstituted aliphatic alkenes and alkynes required a higher catalyst loading, as well as elevated pressure and temperature (5 mol%, 10 bar H_2 , 60 °C). The 17 valence electron precatalyst **2** exhibited good activity only with unbiased styrenes and 1-alkenes, but fared much poorer with deactivated olefins (electron-donating group (EDG)-substituted styrenes, internal alkenes). Rapid deactivation and unwanted side reactions were observed when the substrate contained ester and free amino groups. No significant effect of the crown ether coordinated to the potassium counterion on the catalytic activity was observed.

Table 4.1: Hydrogenation of alkenes with bis(anthracene) complexes **1** and **2**.[a]

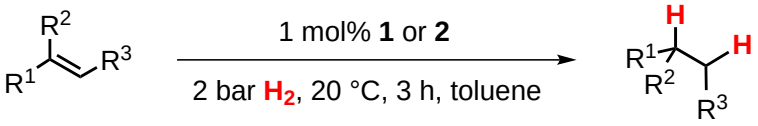

			Yield [%]	
Entry	Alkene	R	**1**	**2**
1		H	95	89
2		4-F	100	100
3	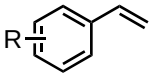	4-CO_2Me	89	2
4		2-OMe	95	50
5		3-Me	96	27
6		4-NH_2	27	0
7	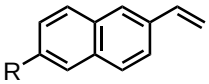	OMe	97[b]	58
8		OAc	69	-
9	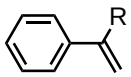	Me	100[c]	-
10		Ph	100[d]	-
11	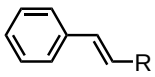	Me	100[c]	-
12		Ph	100[c]	-
13		CO_2Et	76[d]	-
14	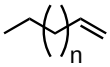	n=8	88[d,e]	73[d,e]
15		n=12	92[d,e]	72[d,e]
16	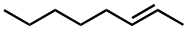		92[d]	-
17			100[c]	-
18	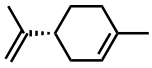		63[d,f]	-

19	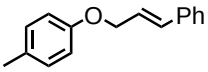	79[d]	<5[d]
20		99[d,g]	<5[d,gh]

[a] Standard conditions: substrate (0.5 mmol) in toluene (2 ml); yields of hydrogenation products were determined by quantitative GC versus the internal reference *n*-pentadecane. [b] 2 bar. [c] 60 °C, 2 bar, 24 h. [d] 5 mol% cat., 60 °C, 10 bar, 24 h. [e] <8% 2-alkene. [f] 1-Menthene. [g] Bibenzyl. [h] (*E*)-Stilbene.

We then set out to evaluate the series of monoanionic alkene and arene metalates **1**–**9** as precatalysts in parallelized olefin hydrogenations under identical conditions. Styrene and 1-dodecene (dod) were chosen as model substrates (Table 4.2).

The standard conditions involved reaction with 5 mol% precatalyst under an atmosphere of 2 bar H_2 in thf (due to the better solubility of the complexes compared with that in toluene) at room temperature for 24 h in a stainless-steel Parr TM reactor (Figure 4.2). In general, styrene was converted in excellent yields with most precatalysts, except **6** and **7**, containing dct as a ligand. This observation is in accordance with the postulate that dct is a competent catalyst poison for homogeneous low-valent monometal species (see above).[27] The strong coordination of dct, and to a lesser extent of cod, to the formal Co^- catalytic center slows down ligand exchange with the substrate styrene. At the same time, dct is not hydrogenated and the hydrogenation of cod is slow.

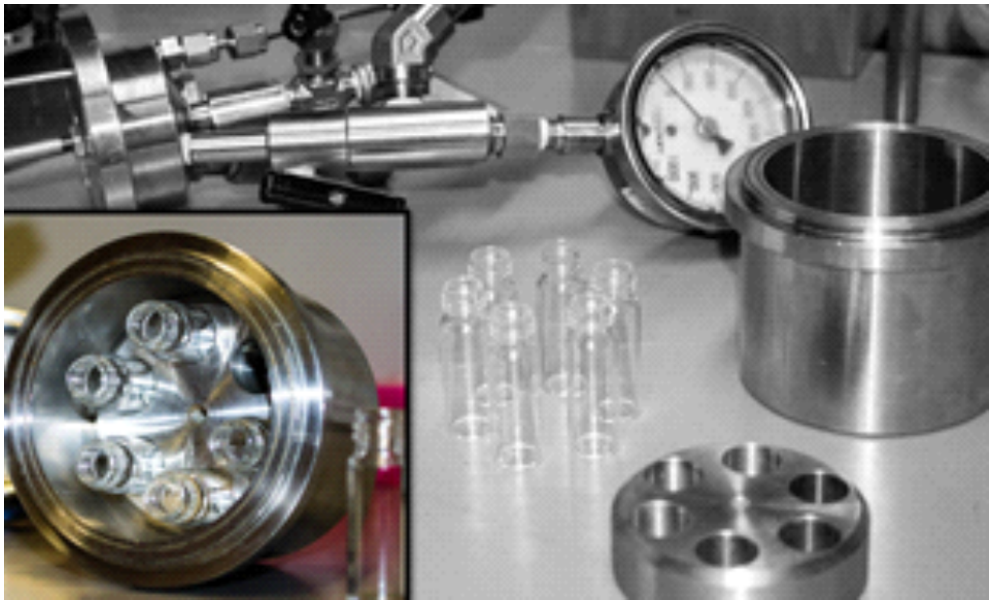

Figure 4.2: Parallelized hydrogenation setup in Parr^{TM} pressure reactors.

Table 4.2: Hydrogenation of alkenes with precatalysts **1**–**9**.[a]

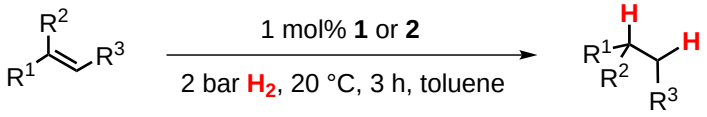

Precatalyst			Precatalyst		
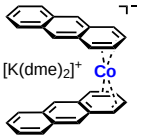	94	58 (27)	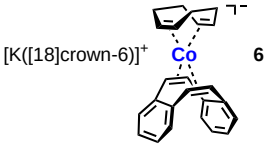	36	71 (24)
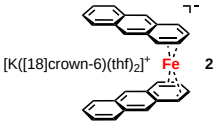	72	15 (7)	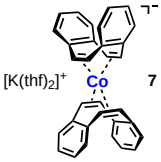	0	0 (0)
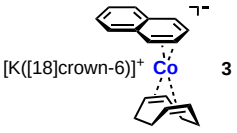	99	93 (0)	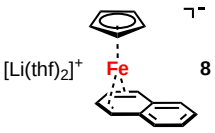	90	84 (15)
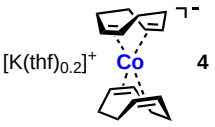	93	62 (29)	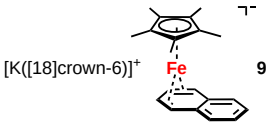	6	72 (24)
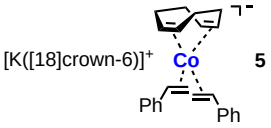	72	85 (8)			

[a] Standard conditions: substrate (0.5 mmol) in thf (2 ml); yields of hydrogenation products were determined by quantitative GC versus the internal reference *n*-pentadecane. In parentheses: yields of alkene isomerization products.

The iron complexes **2**, **8**, and **9** showed slightly lower activity. With dod, similarly good catalytic hydrogenation activities were observed for the precatalysts **1**, **3**, **4**, **5**, and **8** with up to 93% alkene hydrogenation and < 29% alkene isomerization. The best activity and selectivity was determined in the reaction with **3**, which resulted in no observable isomerization to internal alkenes. Again, bis(η^4-dct)cobaltate **7** was catalytically inactive due to strong dct coordination to the Co center, which rendered this complex inert with respect to ligand substitution and ligand hydrogenation.[27]

From both model reaction series, it became clear that, despite only small stereoelectronic differences between precatalysts **1**–**9**, the nature of the π-hydrocarbon ligands and the central metal ion had a strong influence on the overall catalytic activity. Precatalysts containing naphthalene or anthracene exhibited generally higher activity, presumably due to the reestablishment of aromaticity upon exchange of the polyarene ligand with the better π*-accepting alkenes.[30] Cobaltate complexes were more active and selective than their iron counterparts.

4.2.3 Mechanistic Studies

The investigated precatalysts **1** and **2** did not react with dihydrogen at ambient temperature (J. Young NMR tube experiment, up to 4 bar H_2, [D_8]thf). We therefore believe that the proposed mechanism of alkene hydrogenation is initiated by the substitution of the labile arene ligand by the π-substrate followed by reaction of the

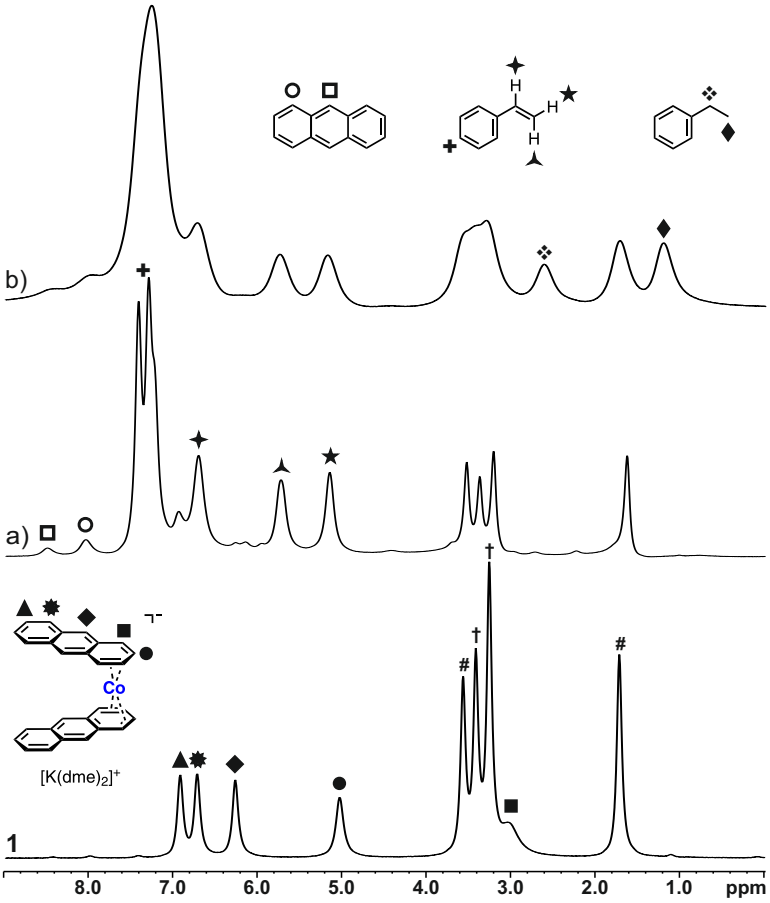

Figure 4.3: ^{1}H-NMR spectroscopy monitoring ([D_8]thf: #) of styrene hydrogenation with precatalyst **1** (dme: †): a) 3 h after the addition of styrene (20 equiv.); and b) 3 h after the addition of hydrogen.

resulting metal catalyst with dihydrogen (Scheme 4.1). In preliminary studies with bis(η^4-anthracene)cobaltate **1**, we monitored this catalyst activation step by redox-neutral π-ligand exchange in homogeneous phase through H-NMR spectroscopy experiments.

Figure 4.3 shows the ^{1}H-NMR spectra of precatalyst **1** in [D_8]thf after the addition of styrene (20 equiv.) to the solution of the complex at room temperature and the reaction mixture after 3 h under 4 bar H_2 pressure. The observation of resonances of noncoordinated anthracene in spectra a and b in Figure 4.3 clearly supports the notion of ligand exchange prior to styrene hydrogenation. The signals of ethylbenzene are apparent in spectrum b in Figure 4.3. There were no further resonances observed in the high-field section that would indicate the formation of hydride complexes under a dihydrogen atmosphere. The observed line broadening is tentatively attributed to the slow formation of cobalt nanoparticles.

We extended the ^{1}H-NMR spectroscopy monitoring studies to complexes **3** and **4**. When assuming precatalyst activation by π-ligand exchange of the weakest ligand with the substrate, both **3** and **4** should funnel through the same catalytic intermediate. We tested this mechanistic hypothesis by adding 20 equivalents of styrene to solutions of **3** and **4** in [D_8]thf (Figures 4.4 and 4.5, respectively). Indeed, the

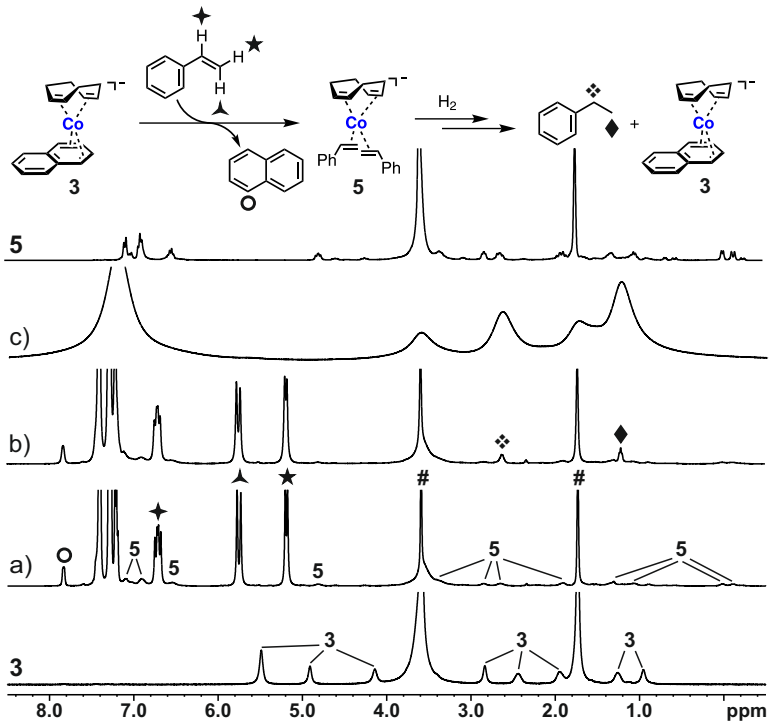

Figure 4.4: ^{1}H-NMR spectroscopy monitoring ([D_8]thf: #) of styrene hydrogenation with precatalyst **3**: a) 1.5 h after the addition of styrene (20 equiv.), and b) 1.5 and c) 24 h after the addition of hydrogen; the spectrum of a clean sample of **5** is shown on top.

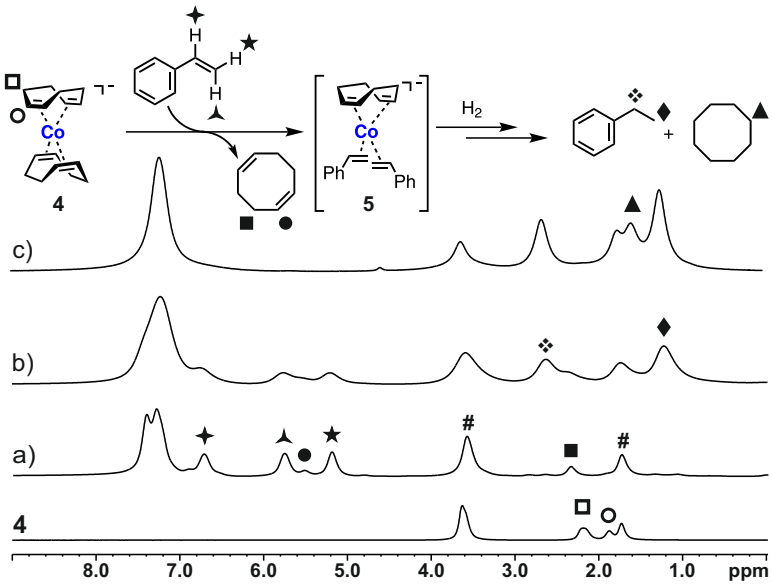

Figure 4.5: ^{1}H-NMR spectroscopy monitoring ([D$_8$]thf: #) of styrene hydrogenation with precatalyst **4**: a) 1.5 h after the addition of styrene (20 equiv.), and b) 1.5 and c) 96 h after the addition of hydrogen.

recorded ^{1}H-NMR spectra showed the clean formation of the anticipated bis(η^2-styrene)cobaltate **5** in both cases, alongside resonances of free naphthalene (from **3**) and cod (from **4**). This observation strongly supports our mechanistic proposal. Upon application of an atmosphere of H_2 to the NMR-scale reactions, clean conversion of the substrate styrene was observed (Figures 4.4 and 4.5). Furthermore, the rate of substrate conversion can be qualitatively assessed from these experiments.

The loss of the styrene π-ligand upon complete hydrogenation with precatalyst **3** after 24 h at 2 bar H_2 and a significantly slower conversion of cod (and naphthalene) resulted in the reconstitution of the original precatalyst **3** by naphthalene coordination, as indicated by the red color of the complex. This complex is difficult to detect in the reaction mixture by ^{1}H-NMR spectroscopy, but its formation was clearly proven by a separate experiment (Scheme 4.7). NMR spectroscopy monitoring of the related

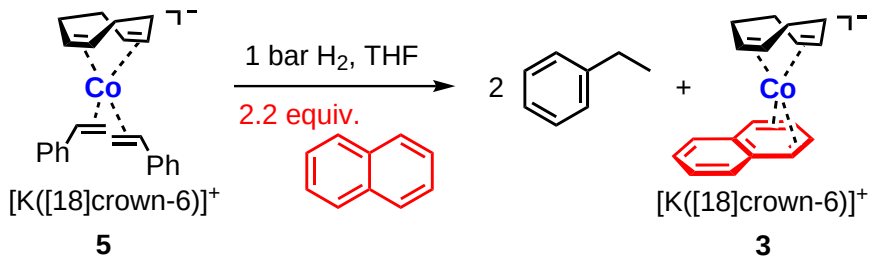

Scheme 4.7: Demonstration of the ligand release-catch concept by the conversion of **5** into **3** upon chemoselective hydrogenation of styrene.

4-catalyzed hydrogenation of styrene showed full conversion of the substrate and the ligand cod after 96 h (Figure 4.5). Likewise, as in the case of **1**, NMR spectroscopy monitoring of complexes **3** and **4** did not show any high-field signals of hydride species.

We prepared and fully characterized the catalytically active bis(η^4-styrene) complex **5** (Scheme 4.3, p. 123), the role of which as a key intermediate in styrene hydrogenations with alkene cobaltate precatalysts was clear from the NMR spectroscopy experiments discussed above (Figures 4.4 and 4.5). Application of an H_2 atmosphere (1 bar) to a bright orange solution of **5** in [D_8]thf effected an immediate color change to black due to the hydrogenative consumption of the π-ligands that stabilize this cobaltate species (Figures 4.14, p. 150).

^{1}H-NMR spectra of the crude mixture and GC analyses confirmed the instantaneous formation of major amounts of ethylbenzene and cyclooctane and only minor amounts of cyclooctene. With precatalyst **3**, with a much less reactive naphthalene ligand, sufficiently differing rates of hydrogenation, styrene > cod ≫ naphthalene, allowed the reconstitution of the original precatalyst by a release–catch mechanism after the complete hydrogenation of the reactive alkenes (Figure 4.4, top). A similar outcome was observed in reactions of bis(η^2-styrene) complex **5** with excess naphthalene under 1 bar H_2 pressure (Scheme 4.7). The chemoselective conversion of styrene and inertness of naphthalene under the mild hydrogenation conditions also led to the formation of **3**, which was isolated as a dark red solid by evaporation of the volatile compounds (Figure 4.15, p. 150).

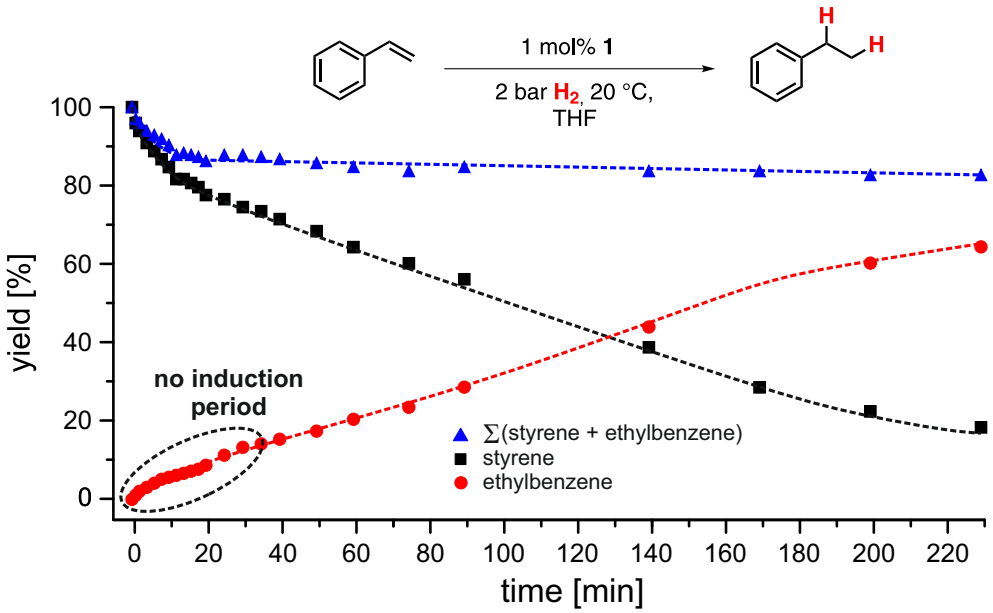

Figure 4.6: Reaction progress analysis: **1**-catalyzed hydrogenation of styrene under standard conditions without any detectable induction period. Dashed lines are only visual guides.

Because the above mentioned results do not rule out the operation of a heterogeneous catalytic pathway as a background reaction,[27] we turned to reaction progress analyses by quantitative GC analysis of all reaction components (Figure 4.6). The early reaction phase of the **1**-catalyzed hydrogenation of styrene (< 20 min) showed no induction period and no sigmoidal curvature, which would indicate a nucleation step en route to nanoclusters and nanoparticles. Identical behavior was observed from the hydrogenation of styrene with 5 mol% of pre-catalyst **3**. Without any detectable induction period, styrene was completely hydrogenated within 45 min at 2 bar H_2. The conversion of the ligands cod and naphthalene largely commenced after the substrate styrene had been entirely converted into ethylbenzene (Figure 4.8).

To gain further information with respect to the homo- versus heterogeneous nature of the operating catalyst, we performed kinetic poisoning studies with a scavenger reagent selective for mononuclear late-transition-metal species in low oxidation states: dct.[26,27] Upon addition of only 2 mol% dct to a catalytic hydrogenation of styrene with 1 mol% **1** after 35 min (≈ 17% conversion), complete inhibition of catalyst turnover was observed; this is indicative of a homogeneous mechanism (Figure 4.7). Inhibition of a potential heterogeneous reaction pathway by amalgamation was not observed.[27] In an extended study, we performed the two model reactions (styrene, dod) with the two most active precatalysts, **1** and **3**, in the presence of scavengers (Hg, PMe_3, and dct; Table 4.3). Filtration of the freshly prepared precatalyst solution through a polytetrafluoroethylene (PTFE) syringe filter (pore size < 0.1 mm) prior to the addition of the substrate gave unaltered hydrogenation activity of precatalyst **1**. The addition of 300 mol% mercury only slightly affected the catalyst activity. However, the formation of amalgams between mercury and 3d transition metals is very slow.[31]

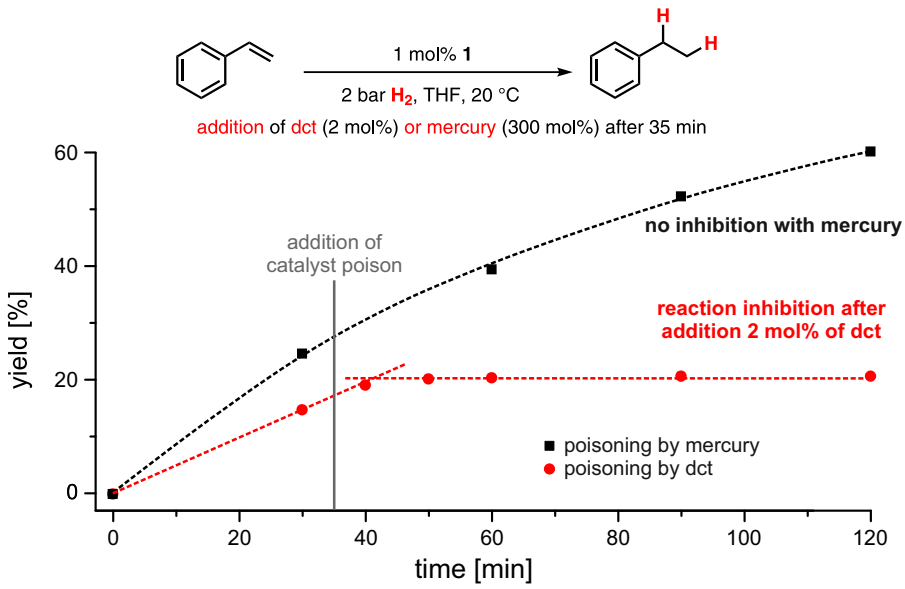

Figure 4.7: Poisoning studies with precatalyst **1** by the addition of 300 mol% Hg and 2 mol% dct, respectively. Dashed lines are only visual guides.

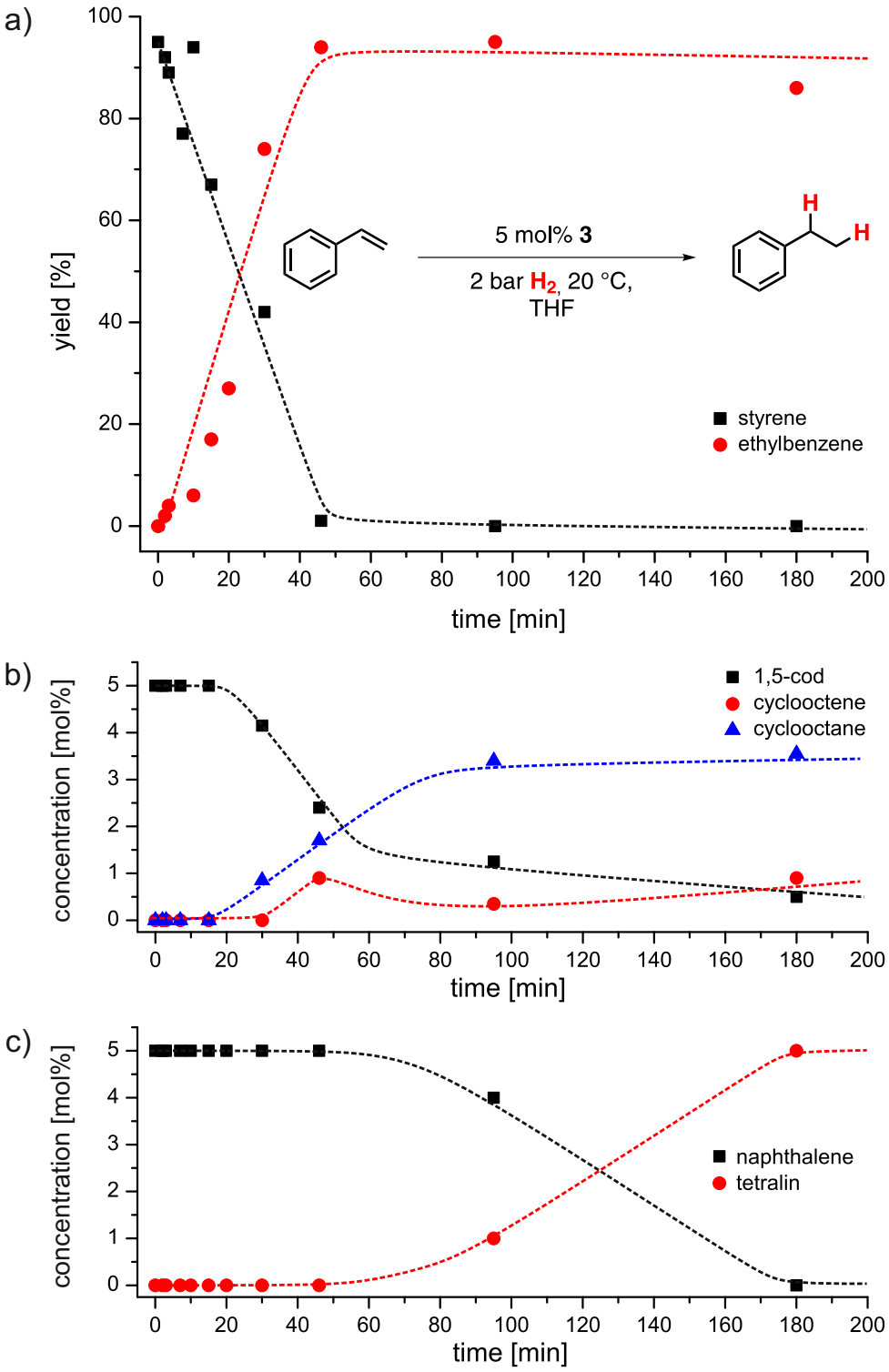

Figure 4.8: Reaction progress analysis: **3**-catalyzed hydrogenation. Conversions of styrene (a), cod (b), and naphthalene (c). Dashed lines are only visual guides.

A pronounced reaction inhibition was only observed by the addition of dct to the catalytic hydrogenation with precatalyst **1**. This suggests the formation of a catalytically inactive homoleptic cobaltate containing dct ligands, which is in perfect agreement with the observation of 0% conversion in alkene hydrogenations with precatalyst **7** (see Table 4.2). The rapid formation of **7** from **1** and dct was already demonstrated (Scheme 4.6). Further support comes from ^{1}H-NMR spectroscopy experiments of a solution of **7** in thf with 20 equivalents of styrene, which showed no substitution of the dct ligands over the course of 1.5 h (Figure 4.9).

The observation of good catalytic activity of a mixture of precatalyst **3** and dct in Table 4.3 is a direct consequence of the presence of the strongly coordinating ligand cod in **3**, which undergoes little or no substitution with equimolar dct. This results in the exclusive substitution of the naphthalene ligand of **3** by dct and formation of the heteroleptic cobaltate **6** as the dominant catalyst species. Our catalytic experiments showed that **6** had good activity in hydrogenations of styrene and dod (Table 4.2, p. 129).

Given the anionic nature of the putative catalyst species, we also used negative-ion mode ESI-MS for their selective detection and analysis. Under carefully optimized conditions, this method is capable of detecting even highly reactive organometallics in intact form,[32] including low-valent transition-metal complexes.[33] Indeed, negative-ion mode ESI of a solution of **1** in thf afforded the free $[Co(anthracene)_2]^-$ anion with high signal intensity (Figure 4.16, p. 4.16). In addition, the potassium-bound dimer $[K\{Co(anthracene)_2\}_2]^-$ was also observed. Presumably, this species was not present in the diluted sample solution, but formed due to the concentration increase during the ESI process; similar behavior has been found in other cases as well.[34] ESI of a solution of heteroleptic complex **3** produced not only $[Co(\eta^4\text{-cod})(\eta^4\text{-naphthalene})]^-$, as well as small quantities of $[K\{Co(\eta^4\text{-cod})(\eta^4\text{-naphthalene})\}_2]^-$, but also its homoleptic counterpart $[Co(\eta^4\text{-cod})_2]^-$ (Figure 4.17, p. 4.17). This observation clearly demonstrates the operation of an intermolecular exchange process in solution. ESI-MS analysis of solutions of **4** and **5** also resulted in the detection of the expected anionic complexes as the main signals Figures 4.18 and 4.19, respectively, on p. 4.16).

After treating solutions of **1** and **3** with an excess of styrene, we observed the formation of cobaltates **10** and **5**, respectively (Figure 4.10a and b). In both complexes, two styrene molecules replaced one of the originally bound ligands (also compare Figure 4.4). For the heteroleptic complex **3**, only naphthalene, but not the cod ligand, was released. This behavior is fully in line with the higher binding energy of the latter, which we had already derived from NMR spectroscopic experiments. The reaction of **1** with styrene also gave the homoleptic complex $[Co(styrene)_3]^-$ in very small abundance. The lack of any detectable $[Co(styrene)_4]^-$ suggested that this species did not form in solution or that its stability was too low to survive the ESI process. When **1** was treated with an excess of dod, the replacement of naphthalene by dod proceeded only to a small extent (Figure 4.10c). This finding is consistent with the lower reactivity of dod observed in the synthetic studies (see above). Interestingly,

the cobaltate complexes incorporating two molecules of styrene were accompanied by ions, the m/z ratios of which were shifted by two units to lower values, which clearly resulted from dehydrogenation reactions. According to the principle of microscopic reversibility, the catalytic activity of the cobaltatecomplexes with respect to hydrogenation reactions implies that they can also catalyze dehydrogenations.[35]

Table 4.3: Poisoning experiments of hydrogenations with arene cobaltate precatalysts **1** and **3**.[a]

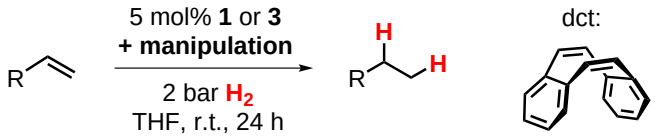

Catalyst manipulation	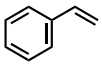 **1**	**3**	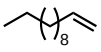 **1**	**3**
none	94	99	58[b]	93
<0.1 μm filter	91	-	46[c]	-
300 mol% Hg	81	75	29[d]	40
1.25 mol% PMe_3	69	91	47[e]	94
11 mol% dct	14	81	3[f]	66

[a] Standard conditions: substrate (0.5 mmol) in thf (2 ml). [b] 27% isomerization. [c] 34% isomerization. [d] 34% isomerization. [e] 6% isomerization. [f] 31% isomerization.

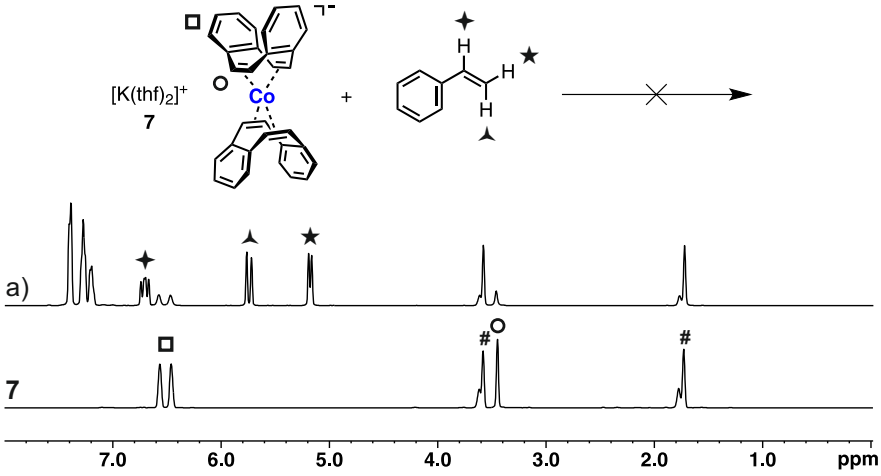

Figure 4.9: ^{1}H-NMR spectrum ([D_8]thf: #) of complex **7**, and a) 1.5 h after the addition of styrene (20 equiv.).

The absence of any ions with m/z ratios shifted by four units moreover indicates that the dehydrogenation reactions involve a coupling of two styryl units, which most likely result in 1,4-diphenylbuta-1,3-diene. Possibly, this diene originated from the dehydrogenation of one cobalt-bound styrene molecule and the addition of a second cobalt-bound styrene to the resulting C≡C triple bond. Low-valent cobalt complexes are known to catalyze related C–H activation reactions.[36]

Finally, we probed the unimolecular gas-phase reactivity of the mass-selected cobaltate complexes. These experiments have the advantage of excluding any interference from dynamic equilibria, counterion, or solvent effects, which may operate in solution. Gas-phase fragmentation of **3** led to the loss of cod and naphthalene, whereas **5** and **10** only released styrene (Figures 4.20-4.23, respectively, on pp. 153-154). In conclusion, our investigations on catalytic alkene hydrogenations documented the formation of 18 valence electron (18e) bis(alkene) complexes in the reaction mixtures. These species are presumably resting states, which serve as the reservoir for the catalytically active cobalt species. One may speculate that H_2 activation is initiated by loss of an alkene ligand, forming an unsaturated and reactive 16e monoalkene complex.

4.2.4 Methodology Extensions

We also applied precatalysts **1**–**9** to hydrogenations of ketones and imines. Generally, hydrogenations of such polar unsaturated compounds are accelerated by the presence of a Lewis acidic catalyst in higher oxidation states. However, the precatalyst complexes contain a weakly Lewis acidic K^+ counterion. We observed very poor catalytic activities under standard conditions at 2 bar H_2 and room temperature. Elevated pressure and temperature (10 bar H_2 , 60 °C, see Table 4.4) led to good activity of potassium bis(anthracene)cobaltate **1** in the hydrogenation of dibenzylketone and *N*-benzylideneaniline (>91% yield). The cod-containing complexes **3** and **4** exhibited moderate activity in the ketone hydrogenation (60–65%). Surprisingly, both complexes were rather inactive in the hydrogenation of the imine. The most active ketone hydrogenation catalyst **1** was subjected to a series of other carbonyl compounds (Table 4.6).[18]

Good catalytic activity was only observed at elevated temperature and pressure. Importantly, the employment of carbonyl compounds as hydrogenation substrates could, in principle, trigger three unwanted side reactions: deprotonation at the α-carbonyl position, direct reduction of the carbonyl moiety by metalate addition or single-electron transfer (SET), and deprotonation of any formed alcohol. Indeed, we have observed the operation of the last two pathways under the present reaction conditions.

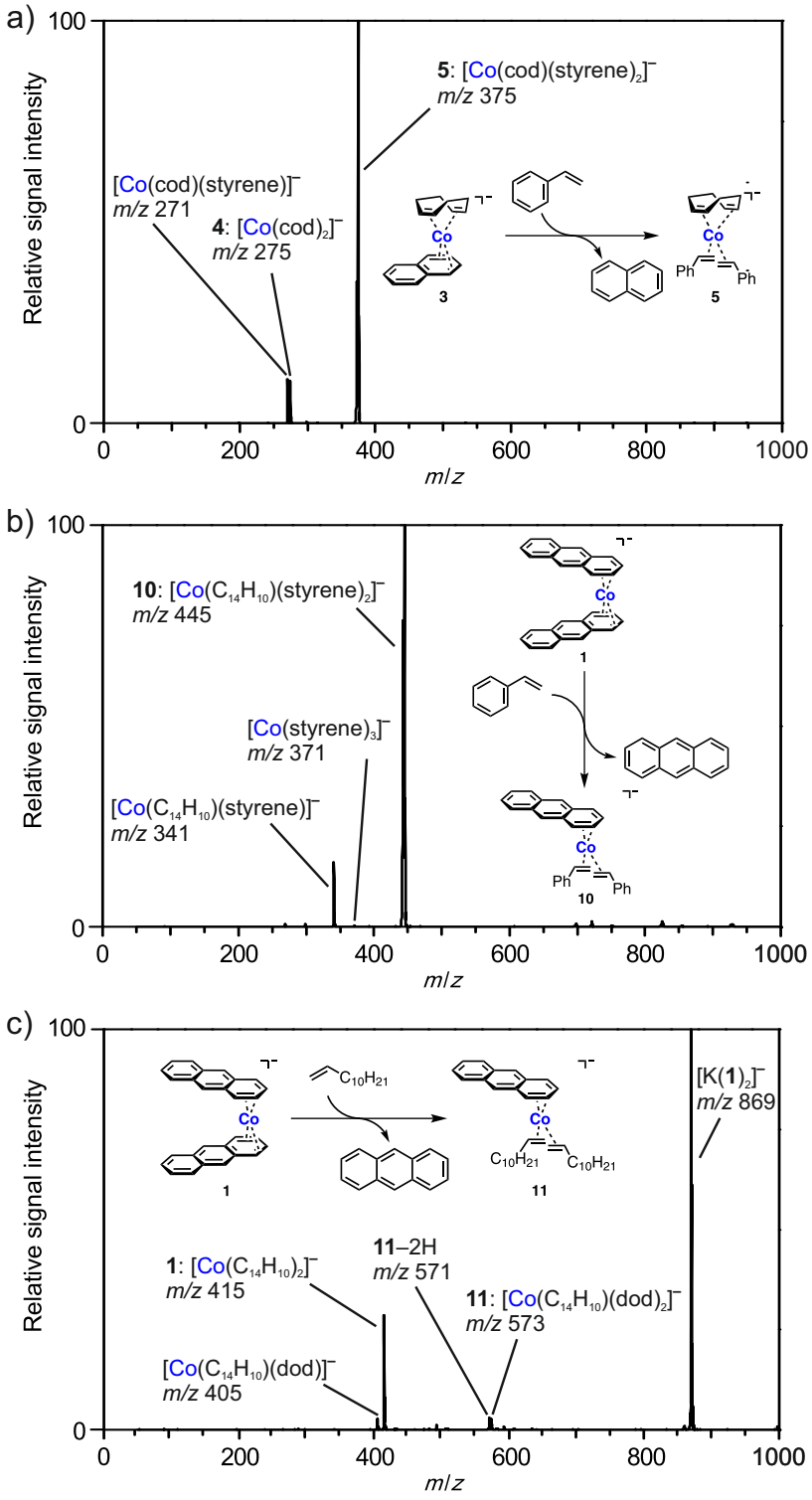

Figure 4.10: Negative-ion mode ESI mass spectra of the products formed upon reaction of a) **3** (7.5 mM) with 10 equivalents of styrene; b) **1** (7.5 mM) with 20 equivalents of styrene; c) **1** (7.5 mM) with 20 equivalents of 1-dodecene (dod) in thf.

Table 4.4: Hydrogenation of ketone and imine with precatalysts **1**–**9**.[a]

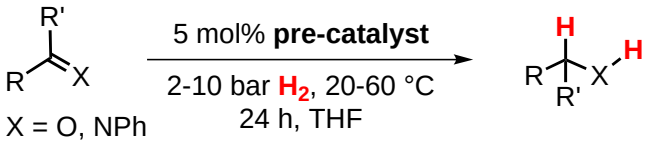

Precatalyst	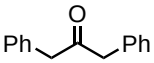	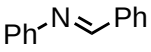
1	11 (91)	0 (99)
2	14 (14)	0 (2)
3	4 (65)	0 (15)
4	5 (60)	0 (3)
5	5	3 (3)
7	0 (17)	0 (26)
8	6 (4)	0 (15)
9	2 (4)	4 (6)

[a] Standard conditions: substrate (0.5 mmol) in thf (2 ml); yields of hydrogenation products determined by quantitative GC versus the internal reference *n*-pentadecane. Yields from reactions at 10 bar H_2, 60 °C, in parentheses.

Table 4.6: Hydrogenation of ketones and imines with cobaltate precatalysts **1**.

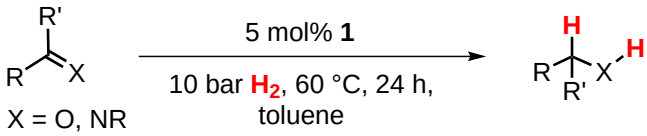

Entry	Substrate	R	Yield [%]
1	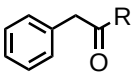	Me	99, 91[b]
2		Bn[c]	96
3	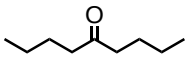		100
4	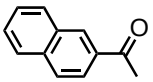		88

5	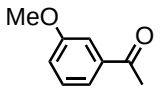		71
6	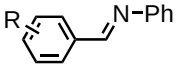	H	96, 99[b]
7		2-Me	98
8		3-Me	100
9		4-OMe	100
10	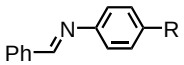	CO_2Et	79[d]
11		Br	0

[a] Standard conditions: substrate (0.5 mmol) in toluene (2 ml); yields of hydrogenation products determined by quantitative GC versus the internal reference *n*-pentadecane. [b] Solvent: thf. [c] Bn=benzyl. [d] 7.5 mol% **1**, 70 °C, 10 bar H_2.

The catalytic hydrogenation reaction generates an acidic proton in the resulting alcohol and amine products, both with pK_a values of about 29 (in DMSO).[37] After the first turnover, this is very likely to alter the catalytic mechanism by catalyst oxidation and H_2 evolution (Scheme 4.8).[38] Considering catalyst oxidation after direct electron transfer to the ketone or after the first hydrogenation catalysis turnover, we postulate the formation of a cobalt(+I) catalyst that displays lower catalytic activity, and therefore, requires harsher conditions.

The formation of dihydrogen was observed by ^{1}H-NMR spectroscopy in an equimolar reaction between **1** and 1,3-diphenyl-2-propanol. Furthermore, a transfer hydrogenation experiment between 4-methylstyrene and 4 equivalents of 1,3-diphenyl-2-propanol afforded 18% yield of ethylbenzene in the presence of 5 mol% **1**.[18] Direct SET reduction of acetophenone was observed in the presence of **1** and **2**, respectively, to give the pinacol product in good yields (Scheme 4.9a).[39] With an olefinic radical probe, such behavior was much less pronounced under standard reaction conditions (Scheme 4.9b). Catalyst **1** showed no ring opening of α-cyclopropylstyrene, but clean hydrogenation of the double bond. Significant radical character was observed in reactions with the cod-bearing catalysts **3** and **4**.

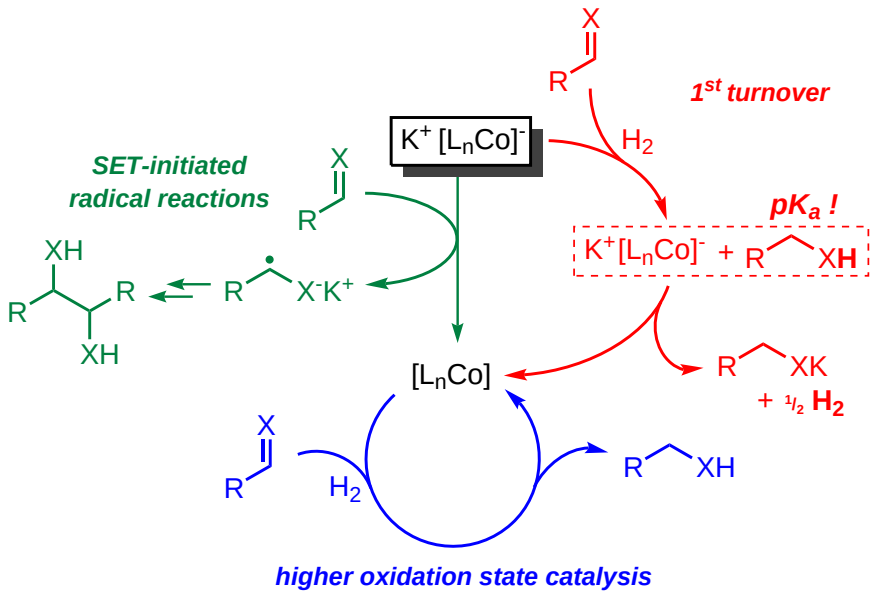

Scheme 4.8: Change of mechanism, H_2 evolution, and catalyst oxidation in the hydrogenation of polar substrates.

a) Pinacol coupling:

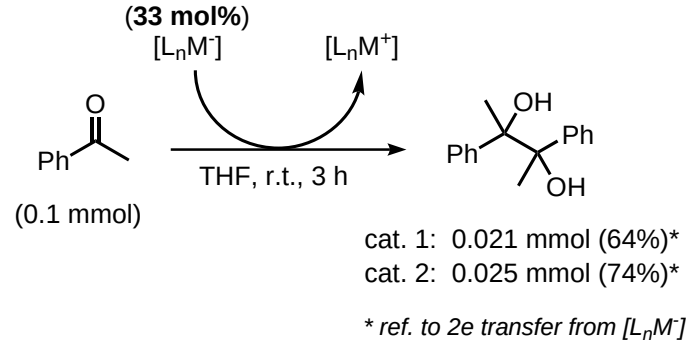

b) Ring opening:

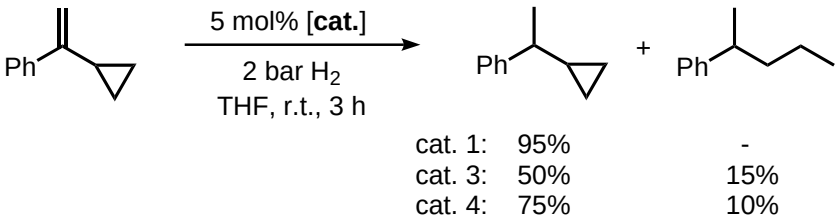

Scheme 4.9: Observation of radical side reactions.

4.3 Conclusions

We showed that bis(η^4-anthracene)metalates **1** and **2** exhibited good activity in catalytic hydrogenation reactions. The bis(η^4- anthracene)cobaltate **1** was a highly active precatalyst for the hydrogenation of a variety of alkenes, ketones and, imines at ambient H_2 pressure and temperatures. The iron analogue, **2**, showed significantly lower catalytic activity.[18] In a greatly extended study, we have now compared the catalytic activity of **1** and **2** with that of structurally related alkene and arene metalates **3**–**9**. Complexes **5**–**7** were synthesized for the first time. Complexes **1**–**6**, as well as **8** and **9**, were competent precatalysts for the hydrogenation of alkenes under mild conditions. Unlike **1** and **2**, bis(η^4-styrene) complex **5** rapidly reacts with H_2 (1 bar) with release of ethylbenzene. Kinetic studies and ^{1}H-NMR spectroscopy monitoring experiments presented herein now lead to the conclusion that the olefin hydrogenation reaction is initiated by the substitution of one labile arene ligand by a π-acceptor substrate. Furthermore, we proved the concept of the release–catch mechanism of catalyst activation by ^{1}H-NMR spectroscopy monitoring of π-ligand exchange reactions and by negative-ion mode ESI-MS investigations. The selective formation of a bis(η^2-monoalkene)cobaltate is believed to be key to rapid dihydrogen activation because, unlike coordinated cod and naphthalene or anthracene, the monoalkene ligands of such a species are readily hydrogenated.

Poisoning experiments with dct and mercury supported the hypothesis that the active species had a homogeneous nature. The validity of the Crabtree dct test for cobaltate complexes was confirmed by the formation of **7** and **6**. Bis(η^4-dct) complex **7** was not a competent precatalyst, presumably because the dct ligands were not substituted or hydrogenated under the reaction conditions. By contrast, complex **6** still showed some catalytic activity because of its more labile cod ligand. Extensions to polar substrates (ketones and imines) were also investigated, but these reactions most likely proceeded through a different mechanism than that of alkene hydrogenations because of the operation of unwanted radical and acid–base reactions. Both pathways most likely involve oxidation of the metalate complexes to a higher oxidation manifold, which ultimately exhibits lower catalytic activity. However, the rapid onset of SET reactions with polar substrates appears to be a promising entry to future studies of radical reactions catalyzed by such alkene metalates. The general concept of redox-neutral alkene ligand substitution with metalate complexes has only recently been tapped for catalytic reaction developments. Further variations of this motif in the context of small-molecule hydrogenation and hydrofunctionalization will be reported in due course.

4.4 Experimental Section

4.4.1 General Information

All experiments were performed under an atmosphere of dry argon by using standard Schlenk and glove box techniques. Solvents were purified, dried, and degassed by standard techniques. NMR spectra were recorded (300 K) with Bruker Avance 300 and Avance 400 spectrometers internally referenced to residual solvent resonances. NMR spectroscopy assignments were based on COSY, HSQC, and NOESY 2D-NMR spectroscopy experiments. Melting points were measured on samples in sealed capillaries and are uncorrected. Elemental analyses were determined by the Analytical Department of the University of Regensburg. Precatalysts **1**,[19,21] **2**,[20] **3**,[22] **4**,[23] **8**,[28] and **9**[29] were prepared according to procedures reported in the literature. The thf content of **4** varied, according to ^{1}H-NMR spectroscopy and elemental analysis (x=0.15–0.3).

Elemental Analyses: Elemental analyses were determined by the analytical department of the University of Regensburg with a Micro Vario Cube (Elementar).

ESI-MS: Sample solutions were transferred into a gas-tight syringe and infused into the ESI source of a HCT quadrupole ion trap mass spectrometer (BrukerDaltonik) at a flow rate of 8 μLmin^{-1}. For the ESI process and the transfer of ions into the helium-filled quadrupole ion trap, mild conditions similar to those reported previously were applied.[32] Mass spectra were recorded over a typical range of *m/z* 50–1000. Gas-phase fragmentation was accomplished by subjecting the mass-selected ions to excitation voltages of amplitudes, V_{exc}, and allowing them to collide with the helium gas.

Gas Chromatography with FID: *Agilent* 7820A GC-Systems. Column: HP 5 19091J-413 (30 m x 0.32 mm x 0.25 μm) from *Agilent*, carrier gas: N_2. GC-FID was used for catalyst screening (calibration with internal standard *n*-pentadecane and analytically pure samples). Standard heating procedure: 50 °C (0.5 min), 25 °C/min (9.2 min) => 280 °C (3 min); 2.0 ml/min. Heating procedure for reactions with 1-dodecene: 50 °C (0 min), 5 °C/min (21 min), 30 °C/min (4.3 min) => 250 °C (1 min); 2.0 ml/min.

Gas Chromatography with Mass-Selective Detector: *Agilent* 6890N Network GC-System, mass detector 5975 MS. Column: BPX5 (30 m x 0.25 mm x 0.25 μm), from SGE, carrier gas: H_2 (1.0 ml/min). Standard heating procedure: 50 °C (2 min), 25 °C/min (10 min) => 300 °C (5 min).

NMR Spectroscopy: ^{1}H- and ^{13}C-NMR spectra were recorded with a *Bruker* Avance 300 (300.13 MHz ^{1}H; 75.47 MHz ^{13}C) and *Bruker* Avance 400 (400.13 MHz ^{1}H; 100.61 MHz ^{13}C) spectrometers. Chemical shifts are reported in ppm (δ) relative to internal tetramethylsilane (TMS). Coupling constants (J) are reported in Hertz (Hz). Following abbreviations are used for spin multiplicities: s (singlet), d (doublet), t (triplet), m (multiplet), dd = (doublet of dublets).

^{1}H NMR Spectroscopy Reaction Monitoring: Reaction monitoring by ^{1}H-NMR spectroscopy was carried out in a sealed J. Young NMR tube. A solution of the pre-catalyst (5 x 10^{-3} mmol, 5 mol%) in [D_8]thf (0.5 ml) was transferred to a NMR tube, and the first ^{1}H-NMR spectrum was measured. In the glove box, styrene (10 mg, 0.1 mmol, 1.0 equiv.) was added to the solution of precatalyst. After storing the sample for 90 min, the second ^{1}H-NMR spectrum was recorded. Subsequently, the atmosphere was exchanged with dihydrogen by the freeze–pump–thaw technique. Subsequent spectra were recorded after further 90 min and then at irregular intervals until the substrate was fully consumed or until no further consumption was detected.

Melting Points: Determination of melting points was carried out with a SMP10 (*Stuart*) device. Samples were sealed in a glass ampoule under reduced pressure. The values are not corrected.

Reaction Progress Analysis: Reaction progress was monitored in a 50 ml Schlenk flask. A solution of styrene (260 mg, 2.50 mmol, 1.00 equiv.) in thf (5 ml) was added to a solution of the precatalyst (0.125 mmol, 5 mol%) in thf (5 ml). For quantitative GC-FID analysis, *n*-pentadecane was added as an internal standard. The reaction was started by replacing the atmosphere in the Schlenk flask by dihydrogen (2 bar). Samples of 0.1 ml were taken at regular intervals through a septum. Each sample was worked up according to the general procedure for hydrogenation reactions. Quantification of starting material and hydrogenation products was performed by GC-FID analysis.

X-Ray Crystallography: The single-crystal XRD data were recorded on an *Agilent Technologies* SuperNova diffractometer in case of compound **5** and on an *Agilent Technologies* Gemini Ultra diffractometer in case of **6** and **7**, by using $Cu_{K\alpha}$ radiation for **5** and **6** and $Mo_{K\alpha}$ radiation for **7**. Empirical multiscan and analytical absorption corrections were applied to the data.[40,41] By using Olex2,[42] the structures were solved with SHELXS or SHELXT.[43,44] Least-squares refinements were carried out with SHELXL.[43] CCDC 1513657, 1513658, and 1513659 contain the supplementary crystallographic data for this chapter. These data are provided free of charge by The Cambridge Crystallographic Data Centre.

4.4.2 General Procedures

Hydrogenation Reactions: A dry 5 ml vial with a screw cap and PTFE septum was charged with a magnetic stirrer bar and a solution of the precatalyst (0.025 mmol) in thf (1 ml). After adding a solution of the substrate (0.5 mmol) in thf (1 ml) with a pipette, the vial was closed and the septum was punctured with a short needle (*Braun*). The vial was placed into a high-pressure reactor (*Parr Instr.*), which was sealed, removed from the glove box, placed on a magnetic stirrer plate, and purged with hydrogen. After 24 h at room temperature under an atmosphere of hydrogen (2 bar), the pressure was released, the vial was removed, and the reaction was quenched with a saturated aqueous solution of $NaHCO_3$ (1 ml). For quantitative GC-FID analysis, *n*-pentadecane was added as an internal standard. The mixture was extracted with diethyl ether and the combined organic layers were dried over Na_2SO_4.

Poisoning and Filtration Experiments: The poisoning experiments were carried out according to the general procedure for hydrogenation reactions. In the case of poisoning with PMe_3, the precatalyst was dissolved in thf (0.5 ml) before a stock solution of the phosphane (0.5 ml; c = 1.25 x 10^{-2} $molL^{-1}$) in thf was added. For experiments with dct, the catalyst poison was added to the solid precatalyst before dissolving both together in thf. When using elementary mercury as the catalyst poison, the liquid metal was added directly to the dissolved precatalyst with a syringe before the addition of the substrate solution. For the filtration experiments, the precatalyst solution was filtered through a PTFE syringe filter (Puradisc 13, *Whatman*, pore size < 0.1 μm) before the substrate solution was added.

Syntheses of [K([18]crown-6)][Co(η^4-cod)(η^2-styrene)$_2$] (5)

Method 1 (from 3): A solution of styrene (57.4 mg, 0.551 mmol, 2.20 equiv.) in thf (2 ml) was added dropwise to a solution of **3** (150 mg, 0.251 mmol, 1.00 equiv.) in thf (5 ml) at room temperature. The resulting clear, orange solution was stirred overnight. Afterwards, the solvent was removed in vacuo. The solid, orange residue was washed several times with diethyl ether (10 ml overall). The crude product was dissolved in thf (5 ml); the resulting solution was filtered and concentrated. Orange, X-ray-quality crystals of **5** (105 mg, 62%) formed after layering of the solution in thf with *n*-hexane (1:2). M.p. 125 °C (decomp); ^{1}H-NMR (300.13 MHz, [D_8]thf): major isomer: δ = -0.15 (d, J = 11.1 Hz, 2H; styrene CH_2), -0.02 (d, J = 7.3 Hz, 2H; styrene CH_2), 0.92–1.16 (m, 2H; cod CH), 1.22–1.44 (m, 2H; cod CH_2), 1.78–2.04 (m, 2H; cod CH_2), 2.62 (dd, J = 13.4, 7.9 Hz, 2H; cod CH_2), 2.27–2.93 (m, 2H; cod CH), 3.27–3.39 (m, 2H; cod CH_2), 4.77 (dd, J = 11.1, 7.3 Hz, 2H; styrene CH), 6.38– 6.64 (m, 2H; styrene *p*-Ar-H), 6.89 (t, J = 7.4 Hz, 4H; styrene *m*-Ar- H), 7.15–6.97 ppm (m, 4H; styrene *o*-Ar-H); minor isomer: -0.63 (d, J = 6.8 Hz), -0.26 (d, J = 11.2 Hz), 0.55 (d, J = 11.2 Hz), 0.65 (d, J = 6.8 Hz), 0.87–0.89 (m), 2.29–2.39 (m), 3.02–3.10 (m), 4.17–4.27

(m), 4.50–4.62 ppm (m); $^{13}C\{^1H\}$-NMR (100.61 MHz, 300 K, [D_8]thf): δ = 29.4 (cod CH_2), 37.8 (cod CH_2), 47.0 (styrene CH_2), 60.4 (styrene CH), 71.0 ([18]crown-6 CH_2), 81.6 (cod CH), 89.5 (cod CH), 117.7 (styrene *p*-Ar-CH), 124.2 (styrene *m*-Ar-CH), 127.0 (styrene *o*-Ar-CH), 154.6 ppm (styrene $C_{quart.}$-Ar); minor isomer: δ = 29.0, 29.4, 38.5, 117.6, 118.0, 124.4, 126.9, 127.5 ppm; elemental analysis calcd (%) for $C_{36}H_{52}O_6CoK$ (678.84): C 63.70, H 7.72; found: C 63.04, H 7.47.

Method 2 (from 4): Styrene (2.09 ml, 18.2 mmol, 30.0 equiv.) was added to a solution of **4** (200 mg, 0.608 mmol, 1.00 equiv.) and [18]crown-6 (162.5 mg, 0.608 mmol, 1.00 equiv.) in thf (5 ml) at room temperature. The resulting clear, orange solution was stirred for 5 h. All volatile components were removed in vacuo afterwards. The resulting orange solid was washed with diethyl ether (5 ml), taken up in thf, and layered with *n*-hexane. Compound **5** was obtained as orange blocks by storage at room temperature (290 mg, 70%). The ^{1}H-NMR spectrum of the sample prepared by method 2 was identical to that prepared by method 1.

Synthesis of [K([18]crown-6)][Co(η^4-cod)(η^4-dct)] (6)

A solution of dct (73.6 mg, 0.360 mmol, 1.50 equiv.) in thf (7 ml) was added dropwise to **3** (143.7 mg, 0.240 mmol, 1.00 equiv.) in thf (10 ml) at room temperature. The resulting clear, yellow solution was stirred overnight. Afterwards, the solvent was removed in vacuo. The yellow–orange solid residue was washed three times with diethyl ether (15 + 10 + 5 ml). The crude product was dissolved in thf (7 ml) and filtered. Yellow–orange, X-ray-quality crystals of **6** formed after layering the filtrate with diethyl ether (1:1). Compound **6** was contaminated with varying amounts of **7** that could not be removed by recrystallization. A minimum of 18% impurity was observed. Yield: 76.3 mg (46%), referring to a mixture of **6** (82%) and **7** (18%); ^{1}H-NMR (400.13 MHz, [D_8]thf): δ=1.98– 2.06 (m, 4H; CH_2 of cod or dct), 2.24–2.34 (m, 4H; CH_2 of cod or dct), 2.71 (brs, 4H; alkene-CH of cod or dct), 2.93 (s, 4H; alkene-CH of cod or dct), 6.27–6.36 (m, 4H; Ar-H), 6.42–6.49 ppm (m, 4H; dct Ar-H); in addition, one set of signals assigned to the $[Co(dct)_2]^-$ anion of [K([18]crown-6)][Co(h 4 -$dct)_2$] was observed.

Syntheses of [K(thf)$_2$][Co(η^4-dct)$_2$] (7)

Method 1 (from 1): A solution of dct (733 mg, 3.59 mmol, 2.00 equiv.) in thf (60 ml) was added to a solution of **1** (1.14 g, 1.79 mmol, 1.00 equiv.) in thf (100 ml) at -80 °C, and the mixture was slowly warmed to room temperature. The resulting black suspension was concentrated, filtered, and layered with *n*-hexane. A dark precipitate was isolated after 3 days. Repeated recrystallization (3 x from thf/*n*-hexane 1:3) was necessary to remove remaining dct and anthracene. Compound **7** was obtained as bright orange crystals (220 mg, 19%). M.p. 112 °C (decomp); ^{1}H-NMR (400.13 MHz,

[D_8]thf): δ = 1.77 (m, thf), 3.45 (s, 8H; dct CH), 3.61 (m, thf), 6.45–6.48 (m, 8H; dct Ar-H), 6.56–6.58 ppm (m, 8H; dct Ar-H); $^{13}C\{^1H\}$-NMR (100.61 MHz, 300 K, [D_8]thf): δ = 26.3 (thf), 68.1 (thf), 87.6 (CH), 122.8 (C-Ar), 124.9 (C-Ar), 152.9 ppm (C_{quart}-Ar); elemental analysis calcd (%) for $C_{40}H_{40}O_2CoK$ (650.79): C 73.82, H 6.20; found: C 73.45, H 6.04.

Method 2 (from 1): A solution of dct (600 mg, 2.94 mmol, 2.00 equiv.) and styrene (612 mg, 5.88 mmol, 4.00 equiv.) in thf (50 ml) was added to a solution of **1** (932 mg, 1.47 mmol, 1.00 equiv.) in thf (120 ml) at room temperature. The mixture was stirred overnight and filtered. Concentration of the clear orange solution to 60 ml and layering with diethyl ether (1:1) gave **7** as orange crystals. The isolated compound had the composition [K(thf)$_{0.75}$][Co(η^4-dct)$_2$] after drying in vacuo for 1 h, according to ^{1}H-NMR spectroscopy and elemental analysis. Yield: 512 mg (62%). The ^{1}H-NMR spectrum of samples prepared by this method was identical to that of samples prepared by method 1.

4.4.3 ^{1}H-NMR Spectra of the New Complexes 5–7

[K([18]crown-6)][Co(cod)(styrene)$_2$] (5)

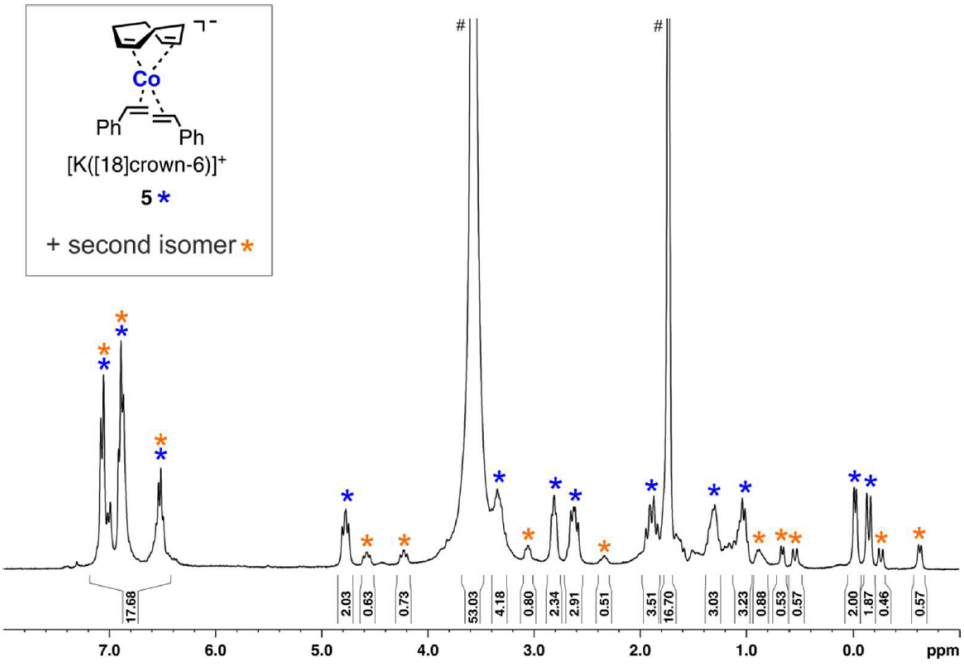

Figure 4.11: ^{1}H-NMR spectrum (300.13 MHz, 300 K, thf-d_8: #) of [K([18]crown-6)][Co(cod)(styrene)$_2$] (**5**) and its second isomer.

[K([18]crown-6)][Co(cod)(dct)] (6)

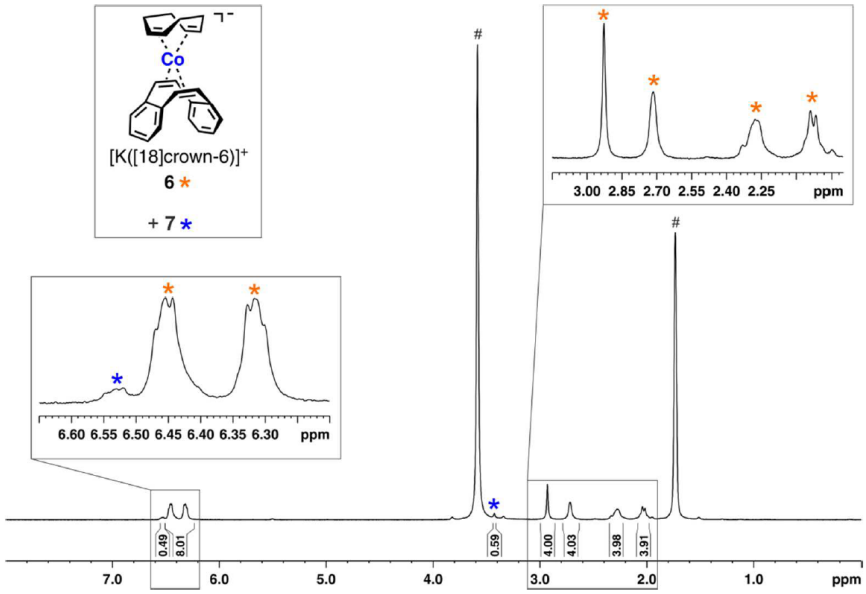

Figure 4.12: ^{1}H-NMR spectrum (300.13 MHz, 300 K, thf-d_8: #) of [K([18]crown-6)][Co(cod)(dct)] (**6**) contaminated with **7**.

[K(thf)$_{0.75}$][Co(dct)$_2$] (7b)

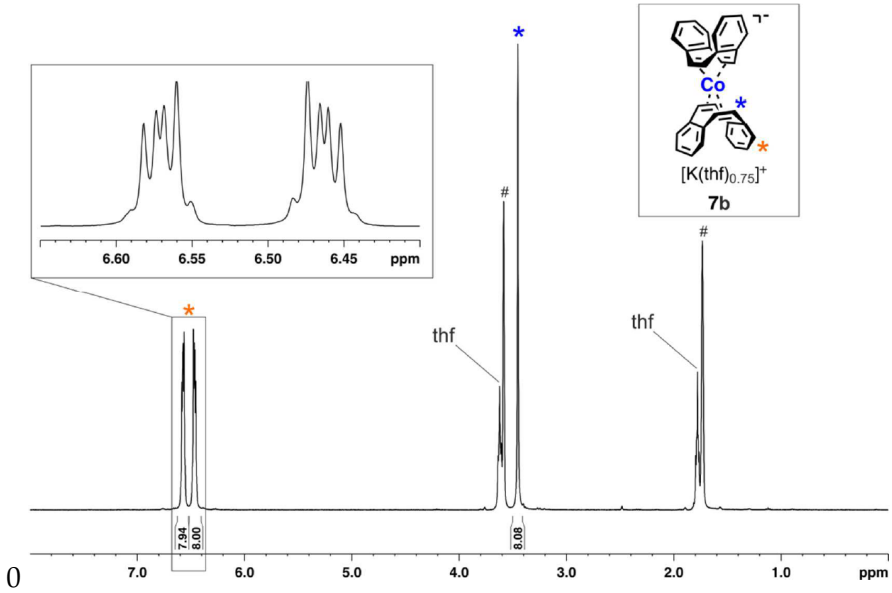

Figure 4.13: ^{1}H-NMR spectrum (300.13 MHz, 300 K, thf-d_8: #) of [K(thf)$_{0.75}$][Co(dct)$_2$] (**7b**).

4.4.4 Photographic Images of Monitoring Experiments

Figure 4.14: A solution of [K([18]crown-6][Co(cod)(styrene)$_2$] (**5**) in thf in an NMR (a). Image of the solution taken immediately after H_2 was admitted to the NMR (b). The formation of a black precipitate, presumably metallic cobalt, is observed. Image of the solution recorded 5 minutes after H_2 was admitted (c). The solution has turned colorless and copious amounts of a black precipitate are observed. A ^{1}H-NMR spectrum of the mixture recorded at this point exclusively showed the signals of ethylbenzene and cycloctane and only minor amounts of cyclooctene. The black precipitate was isolated by decantation of the solvent (d).

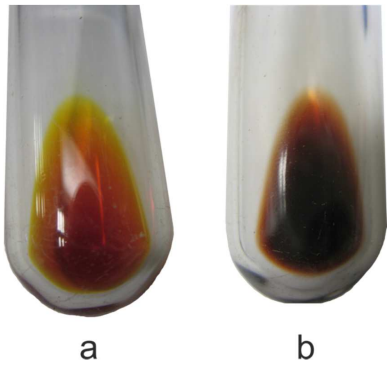

Figure 4.15: Demonstration of the ligand release-catch concept: Image (a) displays a solution of [K([18]crown-6][Co(cod)(styrene)$_2$] (**5**) and naphthalene (2.2 equiv.) in thf in a Schlenk tube. Image (b) shows the same solution 15 min after H_2 was admitted to the Schlenk tube. K([18]crown-6][Co(naphthalene)(cod)] (**3**) is formed due to hydrogenation the styrene ligands of **5**.

4.4.5 Negative-Ion Mode ESI Spectra

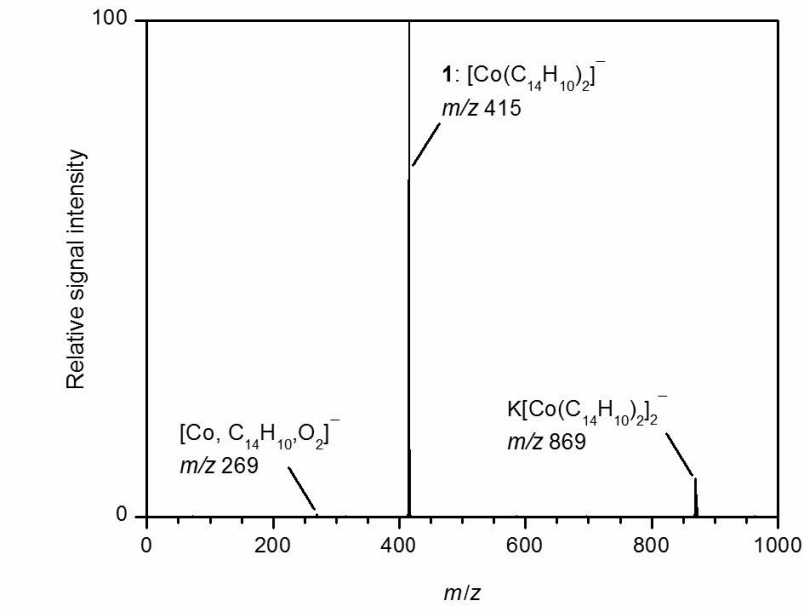

Figure 4.16: Negative-ion mode ESI spectrum of **1** (10 mM) in thf.

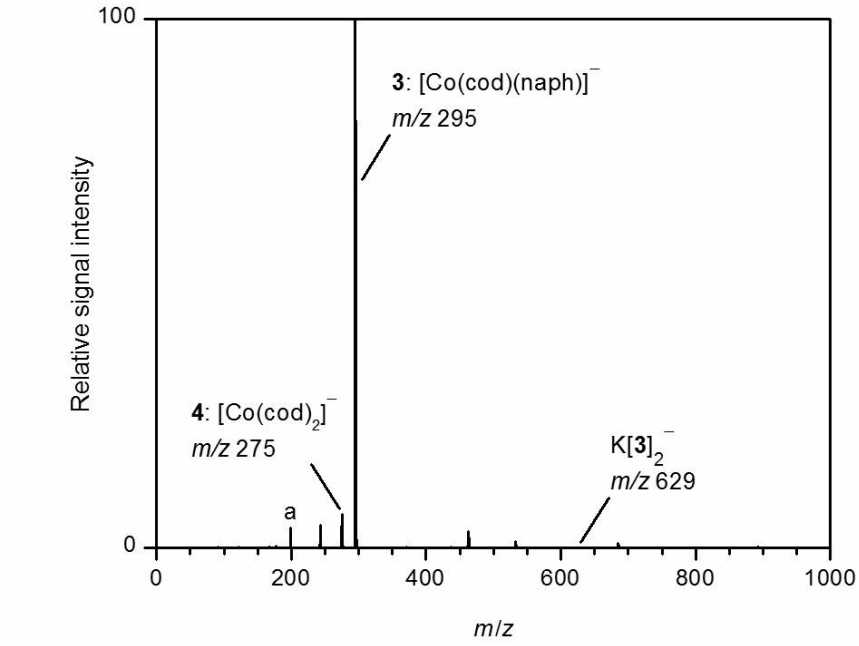

Figure 4.17: Negative-ion mode ESI spectrum of **3** (7.5 mM) in thf.

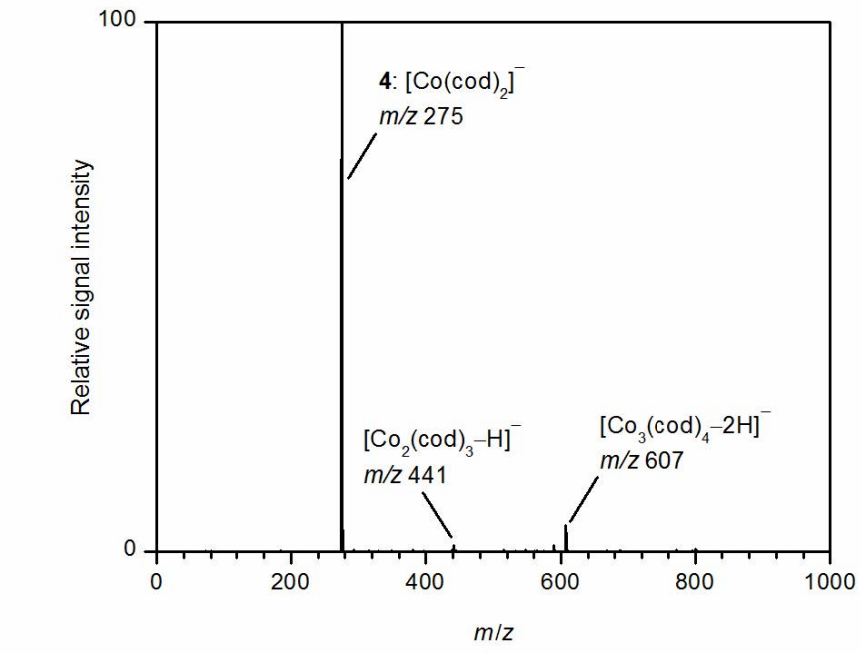

Figure 4.18: Negative-ion mode ESI spectrum of **4** (7.5 mM) in thf.

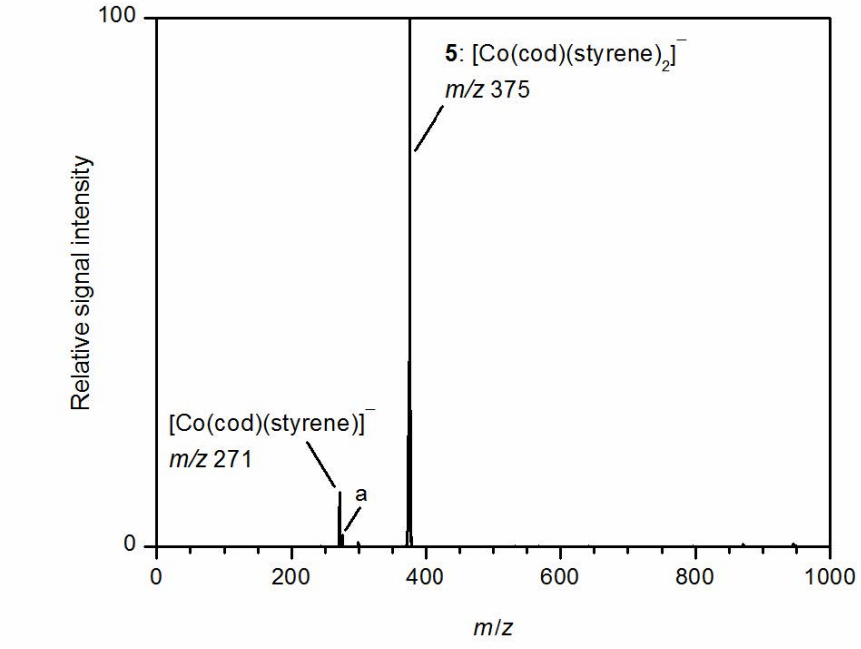

Figure 4.19: Negative-ion mode ESI spectrum of **5** (10 m M) in thf; a = $[Co(cod)_2]^-$.

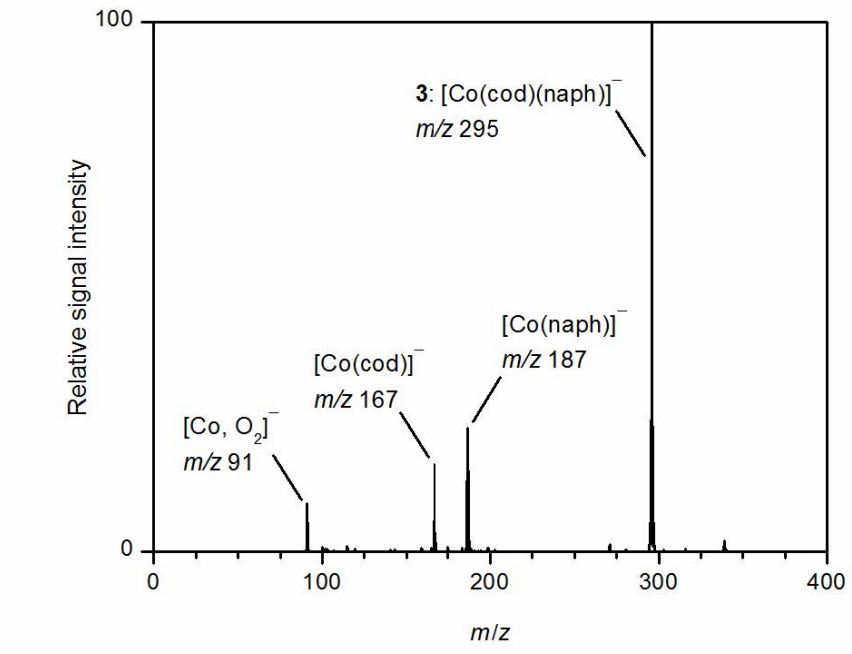

Figure 4.20: Mass spectrum of mass selected **3** and its fragment ions produced upon collision-induced dissociation at V_{exc} = 0.65.

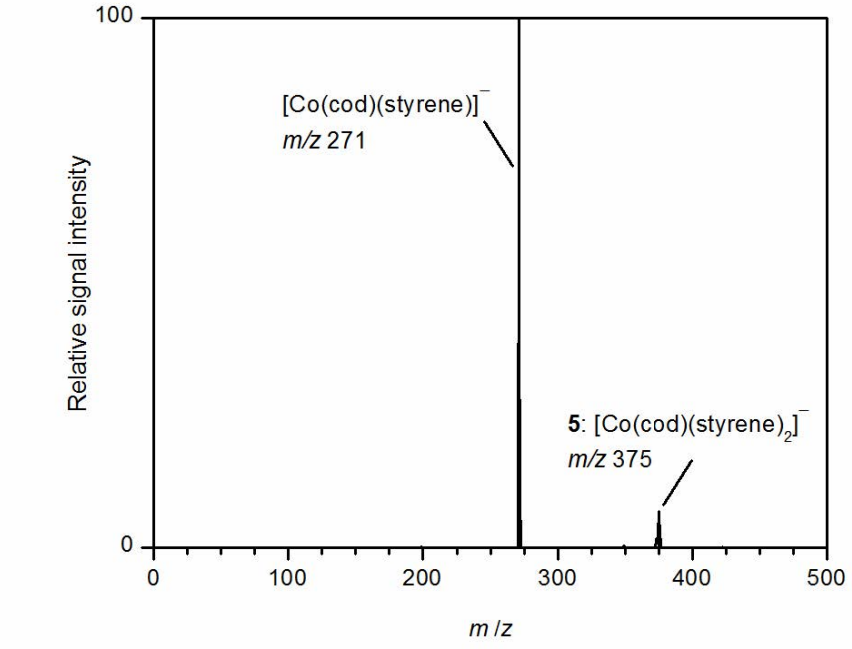

Figure 4.21: Mass spectrum of mass selected **5** and its fragment ions produced upon collision-induced dissociation at V_{exc} = 0.35.

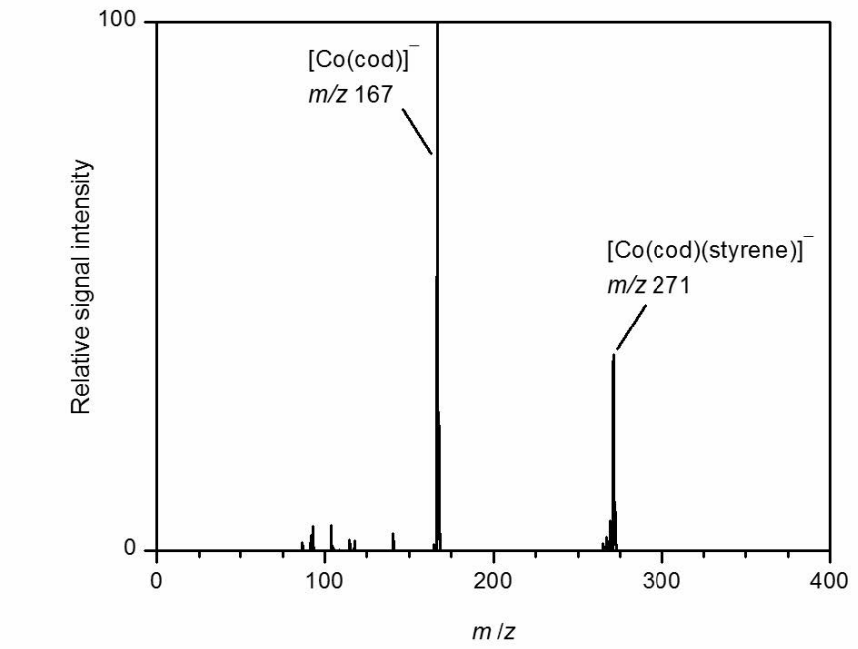

Figure 4.22: Mass spectrum of mass selected $[Co(cod)(styrene)]^-$ and its fragment ions produced upon collision-induced dissociation at V_{exc} = 0.55.

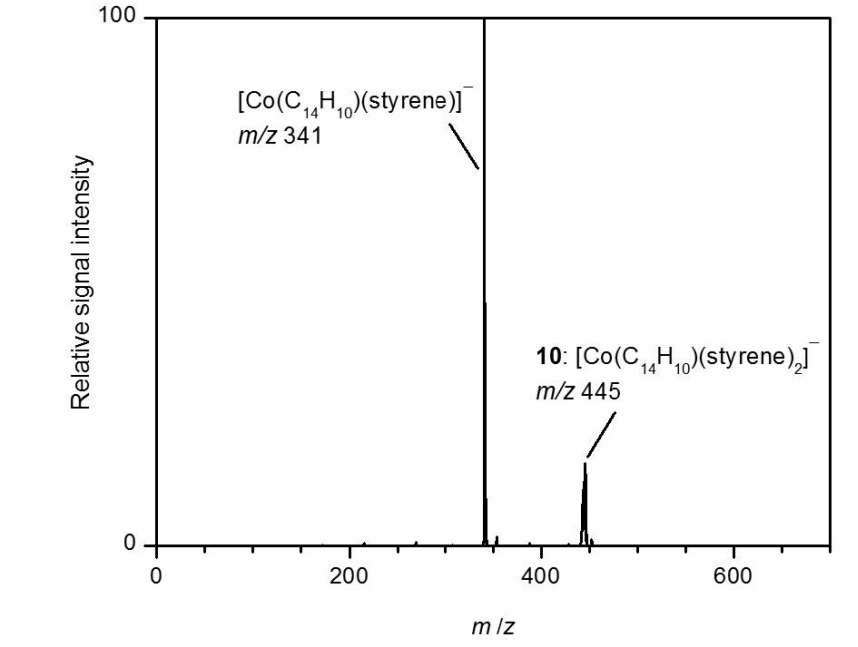

Figure 4.23: Mass spectrum of mass selected **10** and its fragment ions produced upon collision-induced dissociation at V_{exc} = 0.25.

4.4.6 X-Ray Crystallography

Table 4.7: Crystal data and structure refinement for compounds **5**, **6**, and **7**.

Compound	**5**	**6**	**7**
Empirical formula	$C_{36}H_{52}CoKO_6$	$C_{36}H_{48}CoKO_6$	$C_{40}H_{40}CoKO_2$
Formula weight	678.80	674.77	650.75
Temperature [K]	123.0(1)	123.0(1)	123(1)
Crystal system	triclinic	monoclinic	monoclinic
Space group	*P*-1	$P2_1/c$	$P2_1/c$
a [Å]	8.6684(3)	10.13736(6)	15.1339(4)
b [Å]	9.2481(2)	21.30324(13)	15.3434(3)
c [Å]	22.0306(8)	15.32401(9)	14.9559(4)
α [°]	79.000(3)	90	90.00
β [°]	89.777(3)	96.1754(6)	115.835(3)
γ[°]	83.456(3)	90	90.00
Volume [$Å^3$]	1722.09(10)	3290.15(4)	3125.77(14)
Z	2	4	4
ρcalc [g/cm^3]	1.309	1.362	1.383
μ [mm^{-1}]	5.330	5.579	0.718
F(000)	724.0	1432.0	1368.0
Crystal size [mm^3]	0.1726 × 0.1347 × 0.0951	0.5154 × 0.2368 × 0.141	0.2 × 0.15 × 0.1
Radiation	CuK_α (λ = 1.54184)	CuK_α (λ = 1.54184)	MoK_α (λ = 0.71073)
Range for data collection [°]	8.178 < 2Θ < 146.904°	7.134 < 2Θ < 133.484°	6.62 < 2Θ < 60.5°
Index ranges	$-9 \leq h \leq 10$ $-10 \leq k \leq 11$ $-27 \leq l \leq 24$	$-12 \leq h \leq 12$ $-24 \leq k \leq 25$ $-18 \leq l \leq 18$	$-21 \leq h \leq 21$ $-20 \leq k \leq 21$ $-21 \leq l \leq 21$
Reflections collected	16144	42504	86933

Independent reflections	6726 R_{int} = 0.0303 R_{sigma} = 0.0369	5815 R_{int} = 0.0336 R_{sigma} = 0.0173	8906 R_{int} = 0.0423 R_{sigma} = 0.0295
Data/restraints/ parameters	6726/91/427	5815/0/592	8906/36/426
Goodness-of-fit on F^2	1.094	1.023	1.030
Final R indexes [$I \geq 2\sigma(I)$]	R_1 = 0.0358 wR_2 = 0.0849	R_1 = 0.0239 wR_2 = 0.0608	R_1 = 0.0533 wR_2 = 0.1389
Final R indexes [all data]	R_1 = 0.0399 wR_2 = 0.0873	R_1 = 0.0252 wR_2 = 0.0616	R_1 = 0.0693 wR_2 = 0.1481
Largest diff. peak/hole [eÅ^{-3}]	0.41/-0.33	0.21/-0.44	1.00/-0.60
CCDC	1513657	1513658	1513659

4.5 References

[1] (a) Cerveny, L., Ed. *Catalytic Hydrogenation (Studies in Surface Science & Catalysis)*; Elsevier Science Ltd, 1986; (b) de Vries, J. G., Elsevier, C. J., Eds. *The Handbook of Homogeneous Hydrogenation*; Wiley-VCH Verlag GmbH, 2007.

[2] (a) Osborn, J. A.; Jardine, F. H.; Young, J. F.; Wilkinson, G. The preparation and properties of tris(triphenylphosphine)halogenorhodium(I) and some reactions thereof including catalytic homogeneous hydrogenation of olefins and acetylenes and their derivatives. *J. Chem. Soc. A: Inorg., Phys., Theor.* **1966**, 1711; (b) Knowles, W. S.; Sabacky, M. J.; Vineyard, B. D.; Weinkauff, D. J. Asymmetric hydrogenation with a complex of rhodium and a chiral bisphosphine. *J. Am. Chem. Soc.* **1975**, *97*, 2567–2568; (c) Doucet, H.; Ohkuma, T.; Murata, K.; Yokozawa, T.; Kozawa, M.; Katayama, E.; England, A. F.; Ikariya, T.; Noyori, R. *trans*-[$RuCl_2$(phosphane)$_2$(1,2-diamine)] and Chiral *trans*-[$RuCl_2$(diphosphane)(1,2-diamine)]: Shelf-Stable Precatalysts for the Rapid, Productive, and Stereoselective Hydrogenation of Ketones. *Angew. Chem. Int. Ed.* **1998**, *37*, 1703–1707; (d) Molnár, Á.; Sárkány, A.; Varga, M. Hydrogenation of carbon–carbon multiple bonds: chemo-, regio- and stereo-selectivity. *J. Mol. Catal. A: Chem.* **2001**, *173*, 185–221.

[3] (a) Raney, M. Method of Producing Finely-Divided Nickel. 1927; (b) Angulo, I. M.; Kluwer, A. M.; Bouwman, E. Fast and selective homogeneous hydrogenation with nickel(II) phosphane catalysts. *Chem. Commun.* **1998**, 2689–2690; (c) Kuhl, S.; Schneider, R.; Fort, Y. Transfer Hydrogenation of Imines Catalyzed by a Nickel(0)/NHC Complex. *Organometallics* **2003**, *22*, 4184–4186; (d) Hibino, T.; Makino, K.; Sugiyama, T.; Hamada, Y. Homogeneous Chiral Nickel-Catalyzed Asymmetric Hydrogenation of Substituted Aromatic α-Aminoketone Hydrochlorides through Dynamic Kinetic Resolution. *ChemCatChem* **2009**, *1*, 237–240.

[4] (a) Hess, W.; Treutwein, J.; Hilt, G. Cobalt-Catalysed Carbon-Carbon Bond-Formation Reactions. *Synthesis* **2008**, *2008*, 3537–3562; (b) Holzwarth, M. S.; Plietker, B. Biorelevant Metals in Sustainable Metal Catalysis-A Survey. *ChemCatChem* **2013**, *5*, 1650–1679; (c) Bauer, I.; Knölker, H.-J. Iron Catalysis in Organic Synthesis. *Chem. Rev.* **2015**, *115*, 3170–3387; (d) Röse, P.; Hilt, G. Cobalt-Catalysed Bond Formation Reactions – Part 2. *Synthesis* **2016**, *48*, 463–492.

[5] Enthaler, S.; Junge, K.; Beller, M. Sustainable Metal Catalysis with Iron: From Rust to a Rising Star? *Angew. Chem. Int. Ed.* **2008**, *47*, 3317–3321.

[6] Knijnenburg, Q.; Horton, A. D.; van der Heijden, H.; Kooistra, T. M.; Hetterscheid, D. G.; Smits, J. M.; de Bruin, B.; Budzelaar, P. H.; Gal, A. W. Olefin hydrogenation using diimine pyridine complexes of Co and Rh. *J. Mol. Catal. A: Chem.* **2005**, *232*, 151–159.

[7] (a) Monfette, S.; Turner, Z. R.; Semproni, S. P.; Chirik, P. J. Enantiopure C1-Symmetric Bis(imino)pyridine Cobalt Complexes for Asymmetric Alkene Hydrogenation. *J. Am. Chem. Soc.* **2012**, *134*, 4561–4564; (b) Yu, R. P.; Darmon, J. M.; Hoyt, J. M.; Margulieux, G. W.; Turner, Z. R.; Chirik, P. J. High-Activity Iron Catalysts for the Hydrogenation of Hindered, Unfunctionalized Alkenes. *ACS Catal.* **2012**, *2*, 1760–1764.

[8] (a) Zhang, G.; Scott, B. L.; Hanson, S. K. Mild and Homogeneous Cobalt-Catalyzed Hydrogenation of C=C, C=O, and C=N Bonds. *Angew. Chem. Int. Ed.* **2012**, *51*, 12102–12106; (b) Zhang, G.; Vasudevan, K. V.; Scott, B. L.; Hanson, S. K. Understanding the Mechanisms of Cobalt-Catalyzed Hydrogenation and Dehydrogenation Reactions. *J. Am. Chem. Soc.* **2013**, *135*, 8668–8681; (c) Zhang, G.; Hanson, S. K. Cobalt-catalyzed transfer hydrogenation of C=O and C=N bonds. *Chem. Commun.* **2013**, *49*, 10151.

[9] (a) Friedfeld, M. R.; Shevlin, M.; Hoyt, J. M.; Krska, S. W.; Tudge, M. T.; Chirik, P. J. Cobalt Precursors for High-Throughput Discovery of Base Metal Asymmetric Alkene Hydrogenation Catalysts. *Science* **2013**, *342*, 1076–1080; (b) Friedfeld, M. R.; Margulieux, G. W.; Schaefer, B. A.; Chirik, P. J. Bis(phosphine)cobalt Dialkyl Complexes for Directed Catalytic Alkene Hydrogenation. *J. Am. Chem. Soc.* **2014**, *136*, 13178–13181; (c) Hoyt, J. M.; Shevlin, M.; Margulieux, G. W.; Krska, S. W.; Tudge, M. T.; Chirik, P. J. Synthesis and Hydrogenation Activity of Iron Dialkyl Complexes with Chiral Bidentate Phosphines. *Organometallics* **2014**, *33*, 5781–5790.

[10] Korstanje, T. J.; van der Vlugt, J. I.; Elsevier, C. J.; de Bruin, B. Hydrogenation of carboxylic acids with a homogeneous cobalt catalyst. *Science* **2015**, *350*, 298–302.

[11] (a) Yang, X. Hydrogenation of Carbon Dioxide Catalyzed by PNP Pincer Iridium, Iron, and Cobalt Complexes: A Computational Design of Base Metal Catalysts. *ACS Catal.* **2011**, *1*, 849–854; (b) Bauer, G.; Kirchner, K. A. Well-Defined Bifunctional Iron Catalysts for the Hydrogenation of Ketones: Iron, the New Ruthenium. *Angew. Chem. Int. Ed.* **2011**, *50*, 5798–5800; (c) Langer, R.; Leitus, G.; Ben-David, Y.; Milstein, D. Efficient Hydrogenation of Ketones Catalyzed by an Iron Pincer Complex. *Angew. Chem. Int. Ed.* **2011**, *50*, 2120–2124; (d) Xu, R.; Chakraborty, S.; Yuan, H.; Jones, W. D. Acceptorless, Reversible Dehydrogenation and Hydrogenation of N-Heterocycles with a Cobalt Pincer Catalyst. *ACS Catal.* **2015**, *5*, 6350–6354; (e) Spentzos, A. Z.; Barnes, C. L.; Bernskoetter, W. H. Effective Pincer Cobalt Precatalysts for Lewis Acid Assisted CO_2 Hydrogenation. *Inorg. Chem.* **2016**, *55*, 8225–8233.

[12] (a) Rösler, S.; Obenauf, J.; Kempe, R. A Highly Active and Easily Accessible Cobalt Catalyst for Selective Hydrogenation of C=O Bonds. *J. Am. Chem. Soc.* **2015**, *137*, 7998–8001; (b) Gorgas, N.; Stöger, B.; Veiros, L. F.; Kirchner, K. Highly Efficient and Selective Hydrogenation of Aldehydes: A Well-Defined Fe(II) Catalyst Exhibits Noble-Metal Activity. *ACS Catal.* **2016**, *6*, 2664–2672.

[13] (a) Srimani, D.; Mukherjee, A.; Goldberg, A. F. G.; Leitus, G.; Diskin-Posner, Y.; Shimon, L. J. W.; Ben David, Y.; Milstein, D. Cobalt-Catalyzed Hydrogenation of Esters to Alcohols: Unexpected Reactivity Trend Indicates Ester Enolate Intermediacy. *Angew. Chem. Int. Ed.* **2015**, *54*, 12357–12360; (b) Shao, Z.; Fu, S.; Wei, M.; Zhou, S.; Liu, Q. Mild and Selective Cobalt-Catalyzed Chemodivergent Transfer Hydrogenation of Nitriles. *Angew. Chem. Int. Ed.* **2016**, *55*, 14653–14657; (c) Fu, S.; Chen, N.-Y.; Liu, X.; Shao, Z.; Luo, S.-P.; Liu, Q. Ligand-Controlled Cobalt-Catalyzed Transfer Hydrogenation of Alkynes: Stereodivergent Synthesis of *Z*- and *E*-Alkenes. *J. Am. Chem. Soc.* **2016**, *138*, 8588–8594.

[14] (a) Lin, T.-P.; Peters, J. C. Boryl-Mediated Reversible H_2 Activation at Cobalt: Catalytic Hydrogenation, Dehydrogenation, and Transfer Hydrogenation. *J. Am. Chem. Soc.* **2013**, *135*, 15310–15313; (b) Lin, T.-P.; Peters, J. C. Boryl–Metal Bonds Facilitate Cobalt/Nickel-Catalyzed Olefin Hydrogenation. *J. Am. Chem. Soc.* **2014**, *136*, 13672–13683.

[15] Tokmic, K.; Markus, C. R.; Zhu, L.; Fout, A. R. Well-Defined Cobalt(I) Dihydrogen Catalyst: Experimental Evidence for a Co(I)/Co(III) Redox Process in Olefin Hydrogenation. *J. Am. Chem. Soc.* **2016**, *138*, 11907–11913.

[16] (a) Choe, S.-B.; Klabunde, K. J. New η^6-arene complexes of nickel(II): polyarene and fused arene systems. *J. Organomet. Chem.* **1989**, *359*, 409–418; (b) Sun, S.; Dullaghan, C. A.; Carpenter, G. B.; Rieger, A. L.; Rieger, P. H.; Sweigart, D. A. Synthesis and Structure of Bimetallic η^4,η^6-Naphthalene Complexes Containing a Mn-Mn Moiety Bonded in asyn-Facial Manner: A General Route to Homo- and Heteronuclear Bimetallic Complexes of Polyarenes. *Angew. Chem. Int. Ed.* **1995**, *34*, 2540–2542; (c) Sun, S.; Yeung, L. K.; Sweigart, D. A.; Lee, T.-Y.; Lee, S. S.; Chung, Y. K.; Switzer, S. R.; Pike, R. D. (η^6-Polyarene)$Mn(CO)_3^+$ Complexes as Manganese Tricarbonyl Transfer Reagents. A Convenient and General Synthetic Route to (arene)$Mn(CO)_3^+$ Complexes. *Organometallics* **1995**, *14*, 2613–2615; (d) Seaburg, J. K.; Fischer, P. J.; Victor G. Young, J.; Ellis, J. E. First Isolation and Structural Characterization of Bis(Anthracene)Metal Complexes: [Ti(η^6-$C_{14}H_{10}$)(η^4-$C_{14}H_{10}$)(η^2-dmpe)] and [Ti(η^4-$C_{14}H_{10}$)(η^2-$C_{14}H_{10}$)(η^5-C_5Me_5)]$^-$. *Angew. Chem. Int. Ed.* **1998**, *37*, 155–158.

[17] Ellis, J. E. Adventures with Substances Containing Metals in Negative Oxidation States†. *Inorg. Chem.* **2006**, *45*, 3167–3186.

[18] Gärtner, D.; Welther, A.; Rad, B. R.; Wolf, R.; Jacobi von Wangelin, A. Heteroatom-Free Arene-Cobalt and Arene-Iron Catalysts for Hydrogenations. *Angew. Chem. Int. Ed.* **2014**, *53*, 3722–3726.

[19] (a) Brennessel, W. W.; Victor G. Young, J.; Ellis, J. E. Bis(1,2,3,4-η^4-anthracene)cobaltate(1-). *Angew. Chem. Int. Ed.* **2002**, *41*, 1211–1215; (b) Brennessel, W. W.; Ellis, J. E. Naphthalene and Anthracene Cobaltates(1-): Useful Storable Sources of an Atomic Cobalt Anion. *Inorg. Chem.* **2012**, *51*, 9076–9094.

[20] Brennessel, W.; Jilek, R.; Ellis, J. Bis(1,2,3,4-η^4-anthracene)ferrate(1-): A Paramagnetic Homoleptic Polyarene Transition-Metal Anion. *Angew. Chem. Int. Ed.* **2007**, *46*, 6132–6136.

[21] Compound 1 was prepared according to a slightly modified procedure detailed in ref. [18].

[22] Brennessel, W. W.; Young, V. G.; Ellis, J. E. Towards Homoleptic Naphthalenemetalates of the Later Transition Metals: Isolation and Characterization of Naphthalenecobaltates(1-). *Angew. Chem. Int. Ed.* **2006**, *45*, 7268–7271.

[23] (a) Jonas, K.; Mynott, R.; Krüger, C.; Sekutowski, J. C.; Tsay, Y.-H. Bis(η-1,5-cyclooctadien)cobaltlithium. *Angew. Chem.* **1976**, *88*, 808–809; (b) Jonas, K. Method of Preparing Transition Metal-Olefin Complex Compounds and Alkali Metal-Transition Metal-Olefin Complex Compounds. 1979.

[24] Caminati, W.; Vogelsanger, B.; Bauder, A. Rotational spectrum of styrene observed by microwave Fourier transform spectroscopy. *J. Mol. Spectrosc.* **1988**, *128*, 384–398.

[25] In total, four isomers with differing relative orientations of the phenyl groups are conceivable for **5**, two of which have C_2 symmetry and two have C_s symmetry.

[26] (a) Chaffins, S.; Brettreich, M.; Wudl, F. An Efficient Synthesis of Dibenzocycloocta-4a,6a,-diene-5,11-diyne and its Precursors. *Synthesis* **2002**, *2002*; (b) Franck, G.; Brill, M.; Helmchen, G. Dibenzo[*a*,*e*]cyclooctene: Multigram Synthesis of a Bidentate Ligand. *Org. Synth.* **2012**, *89*, 55.

[27] (a) Anton, D. R.; Crabtree, R. H. Dibenzo[*a*,*e*]cyclooctatetraene in a proposed test for heterogeneity in catalysts formed from soluble platinum-group metal complexes. *Organometallics* **1983**, *2*, 855–859; (b) Widegren, J. A.; Finke, R. G. A review of the problem of distinguishing true homogeneous catalysis from soluble or other metal-particle heterogeneous catalysis under reducing conditions. *J. Mol. Catal. A: Chem.* **2003**, *198*, 317–341; (c) Crabtree, R. H. Resolving Heterogeneity Problems and Impurity Artifacts in Operationally Homogeneous Transition Metal Catalysts. *Chem. Rev.* **2011**, *112*, 1536–1554.

[28] Jonas, K. New findings in the arene chemistry of the 3d transition metals. *Pure Appl. Chem.* **1990**, *62*, 1169–1174.

[29] Schnöckelborg, E.-M.; Khusniyarov, M. M.; de Bruin, B.; Hartl, F.; Langer, T.; Eul, M.; Schulz, S.; Pöttgen, R.; Wolf, R. Unraveling the Electronic Structures of Low-Valent Naphthalene and Anthracene Iron Complexes: X-ray, Spectroscopic, and Density Functional Theory Studies. *Inorg. Chem.* **2012**, *51*, 6719–6730.

[30] (a) Zhang, S.; Shen, J. K.; Basolo, F.; Ju, T. D.; Lang, R. F.; Kiss, G.; Hoff, C. D. Ground-State versus Transition-State Effects in Arene Displacement Reactions

of the Complexes (η^6-arene)Cr(CO)$_3$: Linear Dependence of Transition-State Energies and Resonance Energies of the Arene Ligands. *Organometallics* **1994**, *13*, 3692–3702; (b) Zhu, G.; Janak, K. E.; Figueroa, J. S.; Parkin, G. Oxidative Addition of Dihydrogen to (η^6-Arene)Mo(PMe$_3$)$_3$Complexes: Origin of the Naphthalene and Anthracene Effects. *J. Am. Chem. Soc.* **2006**, *128*, 5452–5461.

[31] Paklepa, P.; Woroniecki, J.; Wrona, P. Transformations in cobalt amalgam—from a homogeneous Co amalgam to nanocrystallites. *J. Electroanal. Chem.* **2001**, *498*, 181–191.

[32] (a) Lipshutz, B. H.; Keith, J.; Buzard, D. J. An Electrospray Ionization Mass Spectrometry Study of the Aggregation States of Organocopper Complexes in Solution. *Organometallics* **1999**, *18*, 1571–1574; (b) Koszinowski, K.; Böhrer, P. Aggregation and Reactivity of Organozincate Anions Probed by Electrospray Mass Spectrometry. *Organometallics* **2009**, *28*, 100–110; (c) Putau, A.; Koszinowski, K. Association and Dissociation of Lithium Cyanocuprates in Ethereal Solvents. *Organometallics* **2011**, *30*, 4771–4778; (d) Trefz, T. K.; Henderson, M. A.; Linnolahti, M.; Collins, S.; McIndoe, J. S. Mass Spectrometric Characterization of Methylaluminoxane-Activated Metallocene Complexes. *Chem. Eur. J.* **2015**, *21*, 2980–2991; (e) Schnegelsberg, C.; Bachmann, S.; Kolter, M.; Auth, T.; John, M.; Stalke, D.; Koszinowski, K. Association and Dissociation of Grignard Reagents RMgCl and Their Turbo Variant RMgCl·LiCl. *Chem. Eur. J.* **2016**, *22*, 7752–7762.

[33] Parchomyk, T.; Koszinowski, K. Ate Complexes in Iron-Catalyzed Cross-Coupling Reactions. *Chem. Eur. J.* **2016**, *22*, 15609–15613.

[34] (a) Tsierkezos, N. G.; Roithová, J.; Schröder, D.; Ončák, M.; Slavíček, P. Can Electrospray Mass Spectrometry Quantitatively Probe Speciation? Hydrolysis of Uranyl Nitrate Studied by Gas-Phase Methods. *Inorg. Chem.* **2009**, *48*, 6287–6296; (b) Putau, A.; Brand, H.; Koszinowski, K. Tetraalkylcuprates(III): Formation, Association, and Intrinsic Reactivity. *J. Am. Chem. Soc.* **2012**, *134*, 613–622.

[35] We also analyzed sample solutions prepared under a hydrogen atmosphere (1 bar), which should disfavor dehydrogenation reactions. However, we still observed signals of the dehydrogenated complexes. Possibly, these species formed in the ESI source, where no hydrogen atmosphere could be maintained.

[36] Fallon, B. J.; Derat, E.; Amatore, M.; Aubert, C.; Chemla, F.; Ferreira, F.; Perez-Luna, A.; Petit, M. C–H Activation/Functionalization Catalyzed by Simple, Well-Defined Low-Valent Cobalt Complexes. *J. Am. Chem. Soc.* **2015**, *137*, 2448–2451.

[37] (a) 2016; http://www.chem.wisc.edu/areas/reich/pkatable/; (b) Olmstead, W. N.; Margolin, Z.; Bordwell, F. G. Acidities of water and simple alcohols in dimethyl sulfoxide solution. *J. Org. Chem.* **1980**, *45*, 3295–3299; (c) Bordwell, F. G.; Algrim, D. J. Acidities of anilines in dimethyl sulfoxide solution. *J. Am. Chem. Soc.* **1988**, *110*, 2964–2968.

[38] (a) Dobereiner, G. E.; Crabtree, R. H. Dehydrogenation as a Substrate-Activating Strategy in Homogeneous Transition-Metal Catalysis. *Chem. Rev.* **2010**, *110*, 681–703; (b) Zhang, G.; Hanson, S. K. Cobalt-Catalyzed Acceptorless Alcohol Dehydrogenation: Synthesis of Imines from Alcohols and Amines. *Org. Lett.* **2013**, *15*, 650–653.

[39] (a) Terra, B. S.; Macedo Jr., F. Progress in the intermolecular pinacol cross coupling methodologies. *Arkivoc* **2011**, *2012*, 134; (b) Kahn, B. E.; Rieke, R. D. Carbonyl coupling reactions using transition metals, lanthanides, and actinides. *Chem. Rev.* **1988**, *88*, 733–745.

[40] (a) SCALE3ABS, CrysAlisPro, Aglient Technologies Inc., Oxford, UK, 2015; (b) G. M. Sheldrick, SADABS, BrukerAXS, Madison, USA, 2007.

[41] (a) Clark, R. C.; Reid, J. S. The analytical calculation of absorption in multifaceted crystals. *Acta Crystallogr. A* **1995**, *51*, 887–897; (b) CrysAlisPro, version 171.37.35, Agilent Technologies Inc., Oxford, UK, 2015.

[42] Dolomanov, O. V.; Bourhis, L. J.; Gildea, R. J.; Howard, J. A. K.; Puschmann, H. OLEX2: a complete structure solution, refinement and analysis program. *J. Appl. Crystallogr.* **2009**, *42*, 339–341.

[43] Sheldrick, G. M. A short history of SHELX. *Acta Crystallogr. A* **2008**, *64*, 112–122.

[44] Sheldrick, G. M. SHELXT– Integrated space-group and crystal-structure determination. *Acta Crystallogr. A* **2015**, *71*, 3–8.

Iron-Catalyzed Cross-Coupling of Secondary Alkyl Chlorides

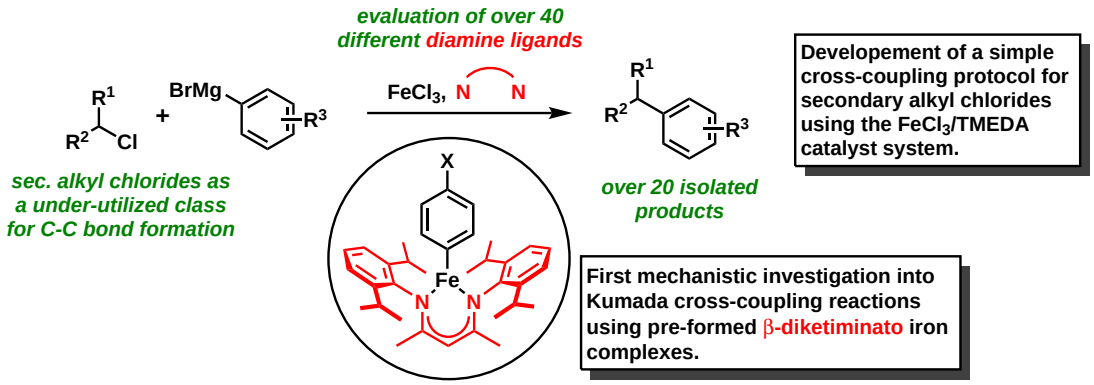

Abstract: Organochlorides are an under-utilized class of electrophiles in catalytic C-C bond formations due to the strong C-Cl linkage. Cross-coupling reactions of secondary alkyl chlorides, which can be easily prepared from various alcohols, require strong nucleophiles and highly electron-rich metal catalysts. We have realized selective iron-catalyzed arylations of secondary alkyl chlorides in the presence of simple iron/diamine catalysts under mild conditions. The selection of the reaction medium seemed to influence the reaction mechnism significantly. As a platform for further mechnistical studies, a set of β-diketiminato iron complexes have been synthesized and, for the first time, subjected to Kumada cross-coupling conditions. Mechanistical studies and analytical data have furnished a proposed catalytic cycle operating by a single electron transfer to the organic electrophile.

5.1 Introduction

Iron-catalyzed cross-coupling reactions have recently gained a strong foothold in the repertoire of arene functionalizations.[1] Due to environmental considerations and regulatory constraints there has been a shift to substitute the commonly used precious metals for more ecological and economical alternatives. Because of its low toxicity, cost and widespread availability, iron has been studied extensively as a promising option in this context.[2] As one of only a few base metals, iron has been used successfully to catalyze cross-coupling reactions in multikilogram scale underlining its importance for modern and sustainable industrial applications.[3]

Most effort has been directed at reactions with sp^2-hybridized electrophiles whereas alkyl halides have received much less attention. This is mostly a consequence of their propensity to undergo metal or base mediated eliminations when bearing β-hydrogen atoms. Furthermore, successful applications of alkyl halides to iron-catalyzed cross-coupling reactions largely employed primary and secondary alkyl bromides and iodides whereas activation of the corresponding chlorides is still a challenging task for which only a few isolated examples were reported.[4] Nakamura *et al.* developed an optimized procedure with iron/N-heterocyclic carbene (NHC) catalysts.[5] We now report synthetic and mechanistic aspects of an operationally facile iron-catalyzed cross-coupling of *sec*-alkyl chlorides in the absence of NHC ligands with a reduced amount of Grignard reagents under mild conditions (Scheme 5.1).

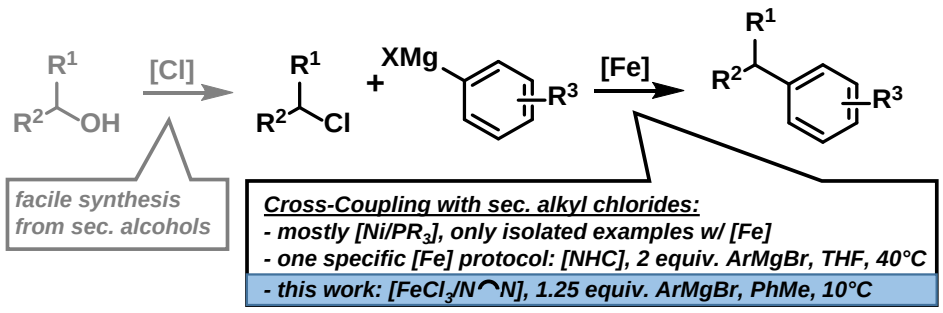

Scheme 5.1: Iron-catalyzed arylative cross-coupling of sec-alkyl chlorides.

We were especially interested to replace the NHC ligand which can constitute a major limitation of cross-coupling reactions from an economic perspective. In comparison to simple amines, NHC ligands exhibit a high molecular mass and associated cost (either from an additional synthesis step or from commercial sources[1]). Amines, meanwhile, can draw on reliable aqueous extraction methods used for separation. Thus, the use of NHC complexes on industrial scale to date is quite

[1]Comparison of the cost of the commonly used NHC ligand IPr·HCl (1,3-Bis(2,6-diisopropylphenyl)imidazolium chloride) and the amine ligand TMEDA from the commercial vendor Sigma-Aldrich (accessed on 10/2018): IPr: 43,775 €/mol, TMEDA: 60 €/mol.

limited.[6] The beneficial effect of NHC ligands was rationalized to enhance the generation of highly electron-rich catalysts, possibly even arylferrates.[7] However, several protocols of iron-catalyzed cross-couplings showed that a similar effect can be exerted by electron-rich chelating diamine ligands (e.g. TMEDA, *N*,*N*,*N*',*N*'-tetramethylethylenediamine).[4]

5.2 Results and Discussion

We initiated our studies with the use of the $FeCl_3$/TMEDA catalyst system for the cross-coupling between chlorocyclohexane (**1**) and 4-tolylmagnesium bromide to give 4-cyclohexyltoluene (**2**, see Table 5.1). The presence of LiCl was shown to accelerate the cross-coupling reactions which is in full accord with earlier postulations of the critical role of nucleophilic catalyst and/or Grignard species, presumably also involving ate complex formation (*vide infra*).[8] Using toluene as the reaction medium, high selectivitiy was shown for the slow addition (~1 h) of a LiCl-Grignard reagent complex[9] (entry 1). Meanwhile, a reduction in the amount of TMEDA or lithium chloride employed led to a decrease in reaction yield (entries 2-5). The opposite trend was shown for the reaction in THF, where high yields could only be achieved by omitting either TMEDA, LiCl or both from the reaction mixture (entries 9-13).

As previously reported, the iron/TMEDA catalyst system likely produces a main catalytic cycle with the homoleptic iron ate complexes $[FeR_3]^-$ or $[FeR_4]^{2-}$ as the active catalytic species.[10] This applies especially in cases where Grignard reagents without β-hydrogen are involved since low-valent Fe species can not be accessed by the initial reduction of the iron salt via β-hydrogen elimination.[11] Kinetically unstable iron intermediates can produce unselective or unproductive iron species off-cycle (e.g. iron nanoparticles and -clusters). TMEDA, meanwhile, is purportedly able to generate an adduct with these critical iron intermediates and to reintroduce them into the main cycle. However, the iron nanoparticles itself can be catalytically active under certain conditions. Bedford *et al.* were able to stabilize iron nanoparticles from the *in situ* reduction of $FeCl_3$ using polyethyleneglycol (PEG) to produce an active cross-coupling catalyst.[12] Therefore, the reaction can proceed in different pathways either via homogeneous ate complexes, nanoparticulate iron species or a combination thereof. The higher stabilization of catalytically active nanoparticles by the more strongly coordinating etheral solvent may explain the findings of our optimization study, as agglomeration of metal nanoparticles represent one of their major deactivation pathways. Our group already reported on the formation of small, catalytically active iron clusters by the reduction of $FeCl_3$ with EtMgBr and their stabilization by THF-coordination.[13]

Additionally, we investigated the influence of rapid Grignard addition to the reaction mixture. The slow addition of the reducing agent has been shown to avoid

Table 5.1: Selected optimization experiments.

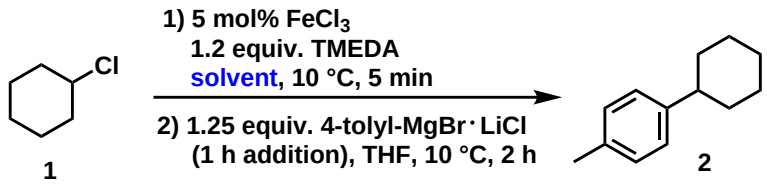

	PhMe			THF	
Entry	Deviation from optimized conditions [a]	**2** [%]	Entry	Deviation from optimized conditions [a]	**2** [%]
1	–	97	9	–	23, 44 [b]
2	20 mol% TMEDA	72	10	20 mol% TMEDA	62, 68 [b]
3	w/o TMEDA	46	11	w/o TMEDA	72, 99 [b]
4	w/o LiCl	62, 99 [b]	12	w/o LiCl	99
5	w/o LiCl, w/o TMEDA	3	13	w/o LiCl, w/o TMEDA	99[b]
6	rapid addition of 4-tolylMgBr·LiCl	72	14	rapid addition of 4-tolylMgBr, w/o LiCl, r.t.	99
7	0 °C	58, 79 [b]	15	-10 °C, 20 mol% TMEDA	50
8	$Fe(acac)_3$	35	16	$Fe[N(SiMe_3)_2]_2$, w/o TMEDA	76

[a] Conditions: $FeCl_3$ (0.1 mmol), PhMe or THF (4 ml), TMEDA (2.4 mmol), 10°C, then **1** (2 mmol), 5 min; then slow addition (~1 h) of 4-tolylmagnesium bromide/ lithium chloride (freshly prepared, 2.5 mmol, 1 M in THF); 10 °C, 1 h. [b] 4 h reaction time.

over-reduction of the iron catalyst and allow the formation of a homogeneous iron-TMEDA complex.[10,14] The results were in accordance with our previous assumptions, explaining the need for slow Grignard addition in toluene while rapid addition was tolerated well in THF (entries 6, 14). Using lower reaction temperatures or different iron sources generally reduced the yields (entries 7-8, 15-16).

The optimized set of conditions was then transferred to various combinations of arylmagnesium bromides and secondary alkyl chlorides (Table 5.3). The best results were achieved using electron-rich Grignard reagents typically leading to good or excellent yields. When the electron-poor 4-fluorophenyl magnesium bromide was employed in the cross coupling reaction, however, only a moderate reaction yield was observed (entry 6). In this case the exclusion of TMEDA was neccessary to achieve complete

conversion.[2] 4-Chlorotetrahydro-2*H*-pyrans[15] showed good stereoselectivities in favour of the 2,4-*cis* diastereomers (entries 14-16). Primary alkyl chlorides gave only moderate yields which is presumably a direct consequence of the lower stabilization of the free radical intermediates (entries 17-20).

Table 5.3: Cross-coupling of alkyl chlorides with arylmagnesium bromides.[a]

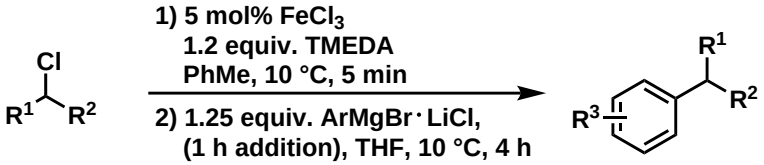

Entry	Product	R	Yield [%]
1	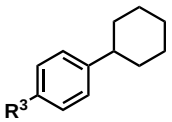	R^3 = H	90
2		R^3 = Me	91, 99[b]
3		R^3 = *t*-Bu	89
4		R^3 = OMe	95
5		R^3 = NMe_2	90
6		R^3 = F	62, 94[c]
7	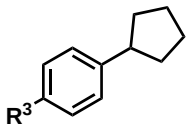	R^3 = Me	78
8		R^3 = OMe	27 [d]
9	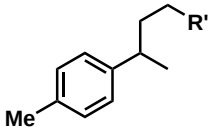	R′ = H	97
10		R′ = Ph	71 , 82[b]
11	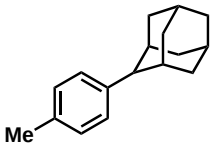		74
12	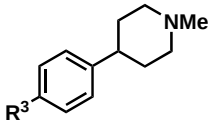	R^3 = Me	69[e]
13		R^3 = OMe	66[b]

[2]See subsection 5.4.6.2 on p. 190 for further information on the effects of different additives using electron poor Grignard reagents.

14	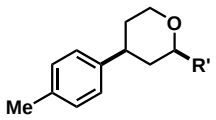	R′ = Bn	83 (5/1)[b,f]
15		R′ = *t*-Bu	78 (49/1)[b,f]
16	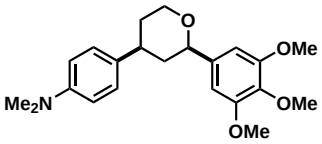		78 (4/1)[b,f]
17	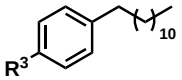	R^3 = H	47[b,g]
18		R^3 = Me	58[b,g]
19	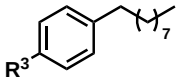	R^3 = Me	86[d]
20		R^3 = OMe	31[d]

[a] Conditions: $FeCl_3$ (0.1 mmol), PhMe (4 ml), TMEDA (2.4 mmol), 10°C, then alkyl chloride (2 mmol), 5 min; then slow addition (~1 h) of arylmagnesium bromide/lithium chloride (freshly prepared, 2.5 mmol, 1 M in THF); 10°C, 3 h; [b] 10 mol% $FeCl_3$, 1.5 equiv. ArMgBr · LiCl. [c] without TMEDA; [d] without LiCl; [e] NMR yield (vs. internal hexamethyldisiloxane); [f] cis/trans diastereomer ratio. [g] r.t., THF.

As was the case for aryl magnesium bromides bearing electron withdrawing substituents, the addition of TMEDA led to a decrease in reaction rate for *ortho*-methyl substituted Grignard reagents. For a few selected examples, simplified reaction conditions without the use of a *N*-donor ligand, LiCl and with rapid addition of the reducing agent afforded significantly higher reaction yields compared to the optimized reaction conditions (Table 5.4). An increase in reactivity towards more sterically hindered aryl magnesium bromides was also found by Sun *et al.* They were able to show that the iron complex [(depe)Fe(Mes)$_2$] (depe = 1,2-bis(diethylphosphino)ethane) is a highly effective precatalyst for the cross-coupling of *o*-tolyl magnesium bromide with primary alkyl bromides. The use of less bulky *p*-tolMgBr or PhMgBr, however, led to a reduction in reaction yields as well as a higher biphenyl formation. They concluded a higher kinetic stability of the transient [(depe)FeAr$_2$] species in favour of the sterically more hindered arenes.[16]

Using ligand-free conditions, a fast reaction rate and immidiate darkening of the reaction solution was observed upon addition of the reducing agent. The addition of the homogeneous catalyst poison dibenzo[*a*,*e*]cyclooctatetraene (DCT) did not lead to a complete inhibition of the coupling reaction, indicating the involvement of iron-nanoparticles as the active catalyst under these conditions.[3] The reaction with 2-chloroadamantane afforded only moderate yield and a high amount of the hydrodehalogenation product (entry 4).

[3]See subsection 5.4.7.2 on p. 200 for experimental details and the reaction progress analysis of the poisoning study.

Table 5.4: Simplified reaction conditions using *o*-tolyl magnesium bromide.

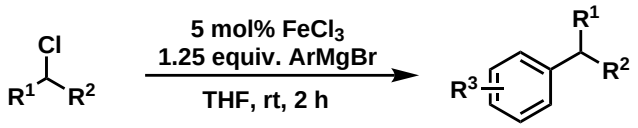

Entry	Product	Yield [%]
1	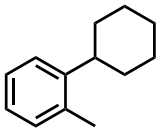	91 (14) [a]
2	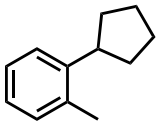	55 (10) [a]
3	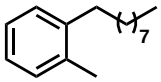	73 (1) [a]
4	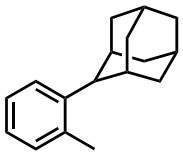	22 (42) [c]

[a] Yields for standard optimized reaction conditions shown in parantheses; [b] slow addition of arylmagnesium bromide, 10 °C, 4 h; [c] yield for hydrodehalogenation product (adamantane) in parentheses.

To gain insight into the mechanistical differences between the ligand-free and optimized conditions, a reaction progress analysis with addition of TMEDA was performed. It documented an induction period during which the active catalyst formed upon reduction with the Grignard reagent (Figure 5.1). Approximately 8-10% of 4,4'-bitolyl (**3**) were formed by addition of 4-tolylmagnesium bromide (ArMgBr) to a solution of **1**, 10 mol% $FeCl_3$, and 120 mol% TMEDA prior to the onset of cross-coupling. When assuming a homogeneous system in the absence of oxidants, this observation is indicative of reduction to catalytically active Fe(II) or Fe(I) species which are coordinated by two Ar substituents.[17,18]

We further investigated the role of *N*-ligands which can modulate the catalyst composition and activity as ligands and alter the effective concentration and nucleophilicity of the Grignard reagent by Mg^{2+} coordination.[19] Looking into the selectivity of

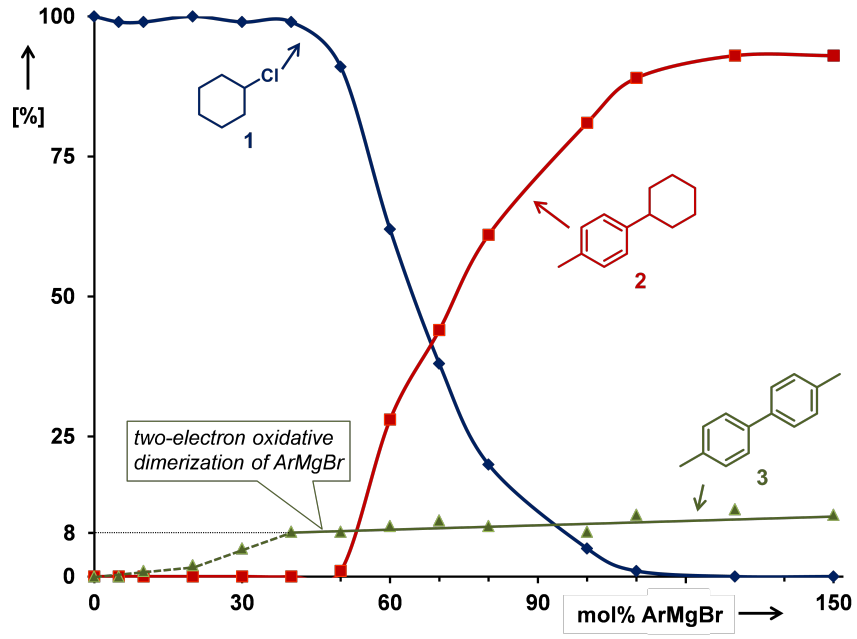

Figure 5.1: Reaction progress analysis with slow addition of 1.5 equiv. ArMgBr over 90 min (Ar = 4-tolyl).

a catalyst system, the sterical properties, chelating abilities and the stereoelectronic effects of the ligand have to be taken into consideration. Although a strong correlation between donor strength and reaction yield could not be shown for different NHC ligands in iron catalyzed Kumada couplings (sterics was shown to have major influence over the reaction outcome),[20] we could not find conclusive literature reports regarding other ligand classes.

Besides the advantages that sterically demanding ligand systems are known to have (e.g. higher stability of the formed metal complexes, suppression of unproductive side-reactions, shielding of coordination sites),[4k] strong donor ligands should i) favour the activation of the electrophilic alkyl chloride by single electron transfer (SET)

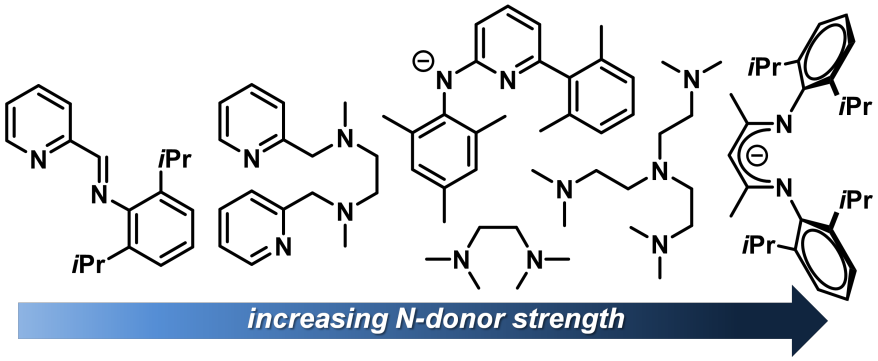

Scheme 5.2: Summary of the *N*-donor strenght for various amine ligand types.

reduction, ii) enhance coordination of less stable (primary) radical species, and iii) prevent over-reduction and formation of Fe(0) precipitates.[21] To elucidate this effect, we employed a wide range of chelating amines, amides, and imines with differing chelate motifs and *N*-donor abilities (Table 5.5).

Following our previous assumptions, the 2-iminopyridine ligands in entries 1-5 displayed increased activity for ligands bearing electron-donating groups. As mentioned above, the ligand containing 2,6-diisopropyl substituents (entry 4) performs better due to its steric bulk. The addition of TMEDA to several catalyst solutions reduced the amount of the biphenyl side-product but did not influence the reaction yield. We also compared the efficiency of the cross-coupling reaction involving either preformed iron-complexes or an *in situ* protocol. This did not affect the reactions with TMEDA (entries 6-7) but catalyst preformation afforded minor advantages for the tetradentate ligand in entries 8 and 9. In general, the performance of tetradentate amine ligands (entries 8-10) was not on par with TMEDA. This finding is in accordance with recent results from Bedford *et al.* comparing the catalytic activity of iron catalyzed Kumada couplings using amine ligands of varying lability.[22] In their experiments, the more strongly chelating amines showed the lowest reactivity which was explained by the need for ligand dissociation in the formation of the active catalyst species.

Consistent with our expectations (Scheme 5.2 and Table 5.5, entry 17), the strong *N*-donor and sterically hindered β-diketiminato ligand dipp$_2$nacnac (dipp = 2,6-diisopropylphenyl; L^{Me}) showed high cross-coupling activity. Ligands in entries 14–16 showed exeptional results yet did not produce significant advantages over TMEDA in further studies[4] and was not investigated further.

Table 5.5: Cross-coupling efficiency of selected *N*-donor ligands and preformed iron complexes.

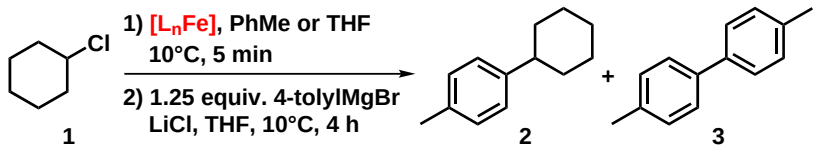

Entry	Ligand [L]		**2** [%]	**3** [%]
1 [a]	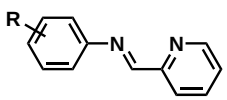	R = 3,4,5-(OMe)$_3$	61 (60) [c]	25 (9) [c]
2 [a]		R = 2-OMe	55 (58) [c]	22 (6) [c]
3 [a]		R = H	17 (25) [c]	20 (9) [c]
4 [a]		R = 2,6-(*i*Pr)$_2$	76	20

[4]See subsection 5.4.6.5 on p. 196 for experimental details on reactions comparing the activity of selected ligands.

5 [a]	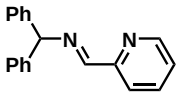		52	36
6 [a]	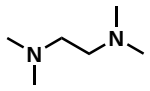		82	10
7 [b]			83	8
8 [a]	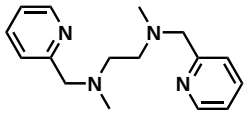		68	9
9 [b]			49	20
10 [d]	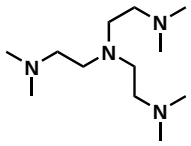		29	14
11 [d]	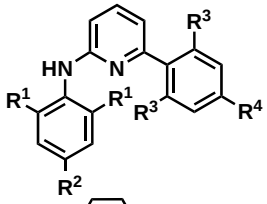	R^1,R^2,R^3,R^4 = Me	77	5
12 [d]		R^1,R^3,R^4 = *i*Pr, R^2=H	75	7
13 [d]		R^1=*i*Pr, R^2, R^4 = H, R^3=Me	78	9
14 [d]	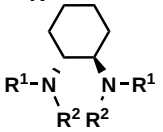	R^1=*i*Bu, R^2= Me	100	16
15 [d]		R^1=C(O)CF_3, R^2= H	100	17
16 [b]	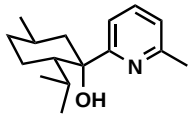		100	18
17 [d]	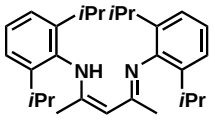		93 (40) [c]	13 (29) [c]
18 [b]	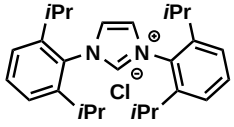		53	36

[a] Method A: a) [Fe] complex formation: $FeCl_2$, 2 equiv. [N_2]-ligand (or 1 equiv. [N_4]-ligand), CH_2Cl_2/CH_3CN, r.t., 12 h; b) 5 mol% [Fe] complex, PhMe, **1**, 10°C, 5 min, then addition of 1.25 equiv. 4-tolylMgBr · LiCl in THF over 1h, then 3 h at 10°C. [b] Method B: 10 mol% $FeCl_3$, 20 mol% [N_2]-ligand (or 10 mol% [N_4]-ligand), THF, **1**, 10°C, 5 min, then 1.25 equiv. 4-tolylMgBr · LiCl in THF over 1 h, then 3 h at 10°C. [c] in parentheses yields of reactions with added TMEDA (1 equiv.). [d] method B with 5 mol% $FeCl_3$, 10 mol% ligand.

The β-diketiminato ligand scaffold was studied extensively for their ability to stabilize metal centers in low oxidation states and to generate coordinatively unsaturated complexes which plays a major role in their catalytic activity.[23] Due to the high reducing power of many metal-nacnac complexes they have been shown to be competent catalyst systems for the activation of small molecules (e.g. N_2, O_2, P_4).[24] While their cross-coupling capability was shown for a range of Pd-containing nacnac complexes,[25] we are not aware of any application to aryl-alkyl cross-coupling reactions. We aimed at the preparation of related iron-complexes which i) could allow the observation of potential aryliron catalysts with various aryl moieties and ii) possibly enhance the reductive activation of even less reactive electrophiles (e.g. *n*-alkyl chlorides).

The Fe(II) complexes **5a–c** have been obtained according to a literature procedure.[26] $FeCl_2$·1.5 THF was reacted with $L^{Me}Li$ in toluene to give **4** as orange solid. Without isolation, the β-diketiminato iron(II) complex **4** was treated with different arylmag-

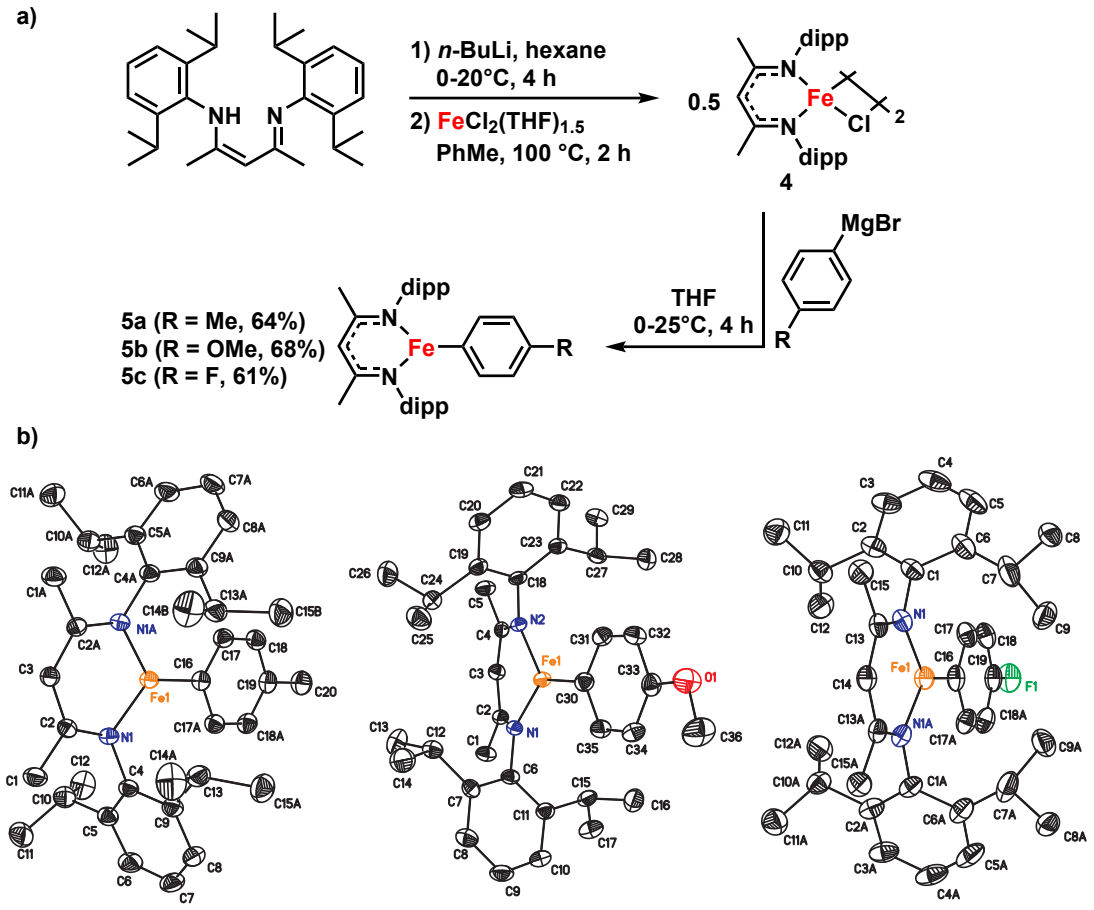

Scheme 5.3: a) Synthesis of aryliron complexes **5a-c**; b) ORTEP diagrams (50% probability level) of the molecular structure of **5a** (left), **5b** (middle) and **5c** (right) with the atom-numbering scheme. All H atoms were omitted for clarity.

nesium bromides to give the aryliron complexes **5a**–**c** as orange solids in good overall yields (60-70% over three steps, Scheme 5.3a). Upon addition of the Grignard reagent, the reaction solution immediately darkened due to some reduction of Fe(II) to low-valent complexes or nanoparticles. The corresponding oxidation event is the homocoupling of the arylmagnesium bromide to the biphenyl derivative. Analysis of an aliquot of the reaction mixture by GC-FID documented that - irrespective of the Grignard reagent employed - 8–9 % of the 4,4´-disubstituted 1,1´-biphenyl were formed. In the syntheses of **5a**,**c**, the respective biaryls could be removed completely by recrystallization from *n*-hexane, whereas this methodology proved unsuccessful for **5b** because of the low solubility of 4,4´-dimethoxy-1,1´-biphenyl in hexane.[27]

5a–**c** were characterized by ^{1}H NMR spectroscopy, mass spectrometry, and single crystal X-ray diffraction. The proton NMR spectra measured in C_6D_6 showed broad resonances in the range of 170 to –140 ppm, which could be fully interpreted based on integration and comparison to $L^{Me}Fe(C_6H_5)$.[26,28] The aryliron complexes **5a**–**c** are paramagnetic compounds exhibiting solution magnetic moments of 5.8–6.0(2) μB in C_6D_6 (Evans method). These values are higher than the spin-only value expected for four unpaired electrons (4.90 μB), which may be caused by a significant orbital contribution to the angular momentum due to spin-orbit coupling as observed for other three-coordinate Fe(II) complexes.[29] The sensitivity of **5a**–**c** toward air and moisture complicated the recording of mass spectra. Nevertheless, peaks close to the calculated m/z for [**5a**–**c**]$^+$ were observed displaying the calculated isotope patterns using liquid injection field desorption ionization mass spectrometry (LIFDI-MS). The aryl complexes and two minor side products were characterized by single crystal X-day diffraction. Single crystals were obtained by recrystallization from *n*-hexane upon storing the filtrate at –15 °C for 2–3 days.[5] The NCCCN backbone of the β-diketiminate ligand is essentially planar for all compounds (rms deviations 0.0021–0.0409 Å), with the dipp substituents being nearly perpendicular to this plane.

Table 5.6 show stochiometric cross-coupling reactions using the prepared iron(II) complexes. Treatment of **5a**–**c** with equal amounts of cyclohexyl bromide in THF at 20°C gave no cross-coupling product after 3 h (entries 1, 9, 12). On the other hand, we observed rapid cross-coupling between 4-tolylmagnesium bromide and bromocyclohexane in the presence of 5 mol% $FeCl_2$ and 7.5 mol% H-L^{Me} (85% yield). We then evaluated the effect of different additives which are present during the catalytic experiments onto the reactivity of **5a** toward bromocyclohexane. The addition of $MgBr_2$ lead to a significant increase in the amount of the coupling product in the reaction with bromocyclohexane (entry 4). Reaction monitoring by UV/Vis spectroscopy showed that the addition of $MgBr_2$ did not affect the absorption bands of **5a**. Upon addition of the alkyl bromide, almost complete quenching of the characteristic absorption at 490 nm and appearance of a shoulder at 430 nm was observed.[6] Furthermore, the addition of $MgBr_2$ did not lead to a change in the ^{1}H NMR spectrum

[5] The molecular structures are displayed in scheme 5.3b. For crystal data, selected bond distances, and angles see subsection 5.4.12 on p. 221.

[6] The characteristic absorption band at 490 nm was also observed for **5b**,**c** with an extinction coefficient of approx. 500 $L{\cdot}mol^{-1}{\cdot}cm^{-1}$ in THF. The UV/Vis spectra for the stoichiometric reactions of **5a**-**c** and cyclohexyl bromide in presence of different additives before and after the addition of cyclohexyl bromide are displayed in subsection 5.4.10 on p. 218.

of **5a**.[7] After the addition of bromocyclohexane, however, a rapid and complete consumption of **5a** was observed and the resulting spectrum is in full accordance with the formation of 1-cyclohexyl-4-methylbenzene and $L^{Me}FeBr(THF)$.[30]

Table 5.6: Stoichiometric cross-coupling reactions using aryliron complexes **5a–c**.

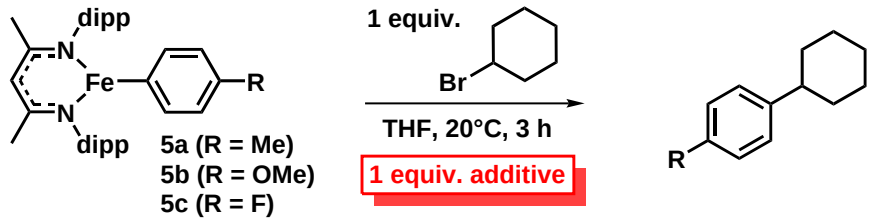

Entry	Fe complex	Additive	Yield [%][a]
1		–	< 5 (0)
2		$[N(n\text{-}Bu)_4]Br$	< 1
3		$Mg(OTf)_2$	5
4	**5a**	$MgBr_2$	52, 66[b] (0)
5		$MgBr_2$ & LiCl	56 (3)
6		$[(4\text{-tolyl})_2B(pin)]MgBr$[c]	63
7		$(4\text{-tolyl})_2Zn$[d]	92
8		4-tolylMgBr	96 (95)
9		–	< 5 (0)
10	**5b**	$MgBr_2$	37, 52[e] (0)
11		4-anisylMgBr	96 (62, 84[f])
12		–	< 5 (0)
13	**5c**	$MgBr_2$	12 (0)
14		$4\text{-}FC_6H_4MgBr$	75 (26)

[a] GC yields (vs. *n*-pentadecane as internal reference). Reaction yield using cyclohexyl chloride in parentheses; [b] 24 h; [c] Generated *in-situ* by the reaction of (4-tolyl)B(pin) and 4-tolylMgBr; [d] Generated *in-situ* by the reaction of $ZnCl_2$ and 2 equiv. 4-tolylMgBr; [e] 5 equiv. of $MgBr_2$; [f] 4-anisylMgBr · LiCl.

[7] Proton NMR spectra for the reaction progress analysis of **5a** with different additives can be found in subsection 5.4.11 on p. 219.

Under identical conditions, the addition of [N(*n*-Bu)$_4$]Br and Mg(OTf)$_2$, respectively, gave only low conversions of bromocyclohexane (entries 3,4). Addition of the Grignard reagent to **5a** caused rapid darkening of the reaction solution. The respective UV/Vis spectrum showed the development of a weak shoulder at approx. 610 nm. In contrast, the ^{1}H NMR spectra was not affected by the addition of 4-tolylmagnesium bromide. The darkening of the reaction solution was reversible, as the addition of 1 equiv. bromocyclohexane restored the original colour within minutes. GC-FID analysis after 3 h documented the full consumption of the organic electrophile and formation of the cross-coupling product in 96 % yield (entry 8). ^{1}H NMR and UV/Vis spectroscopy showed the presence of **5a** after 3 h reaction time (approx. 75 % of the aryl complex was regenerated according to the ^{1}H NMR spectrum). Zinc- and boron-based nucleophiles were also competent reagents and afforded the cross-coupling product with bromocyclohexane in good yields (entries 6,7). The cross-coupling with the less electrophilic chlorocyclohexane, on the other hand, was only possible in the presence of equal amounts of 4-tolylmagnesium bromide.

For the 4-anisyl iron complex **5b**, similar reactivity was observed. Addition of equal amounts of $MgBr_2$ to **5b** produced only moderate conversion in the coupling with bromocyclohexane which could be increased in the presence of 5 equiv. $MgBr_2$ (entry 10), possibly due to complexation of $MgBr_2$ to the methoxy function. Clean conversion of cyclohexyl bromide and effective activation of cyclohexyl chloride was achieved only with the addition of the corresponding Grignard reagent.

The electron-poorer fluorophenyl complex **5c** was the least reactive toward bromo- and chlorocyclohexane and showed a distinct behavior when adding another equiv. of Grignard reagent. The addition of 1 equiv. 4-fluorophenylmagnesium bromide led to a more pronounced darkening of the reaction than with **5a** and **5b**, and the UV/Vis spectrum displayed the shoulder at 590 nm with five fold intensity. The addition of the organic electrophile did not restore the original orange color of the solution. After 3 h reaction, the disappearance of the characteristic absorption at 490 nm indicated the decomposition of **5c**. This might explain the relatively low yields of cross-coupling reactions (entry 14).

To further investigate the reactivity of β-diketiminato iron complexes, stoichiometric coupling reactions involving a selection of different organic electrophiles was performed (Table 5.8). Cyclopropyl bromide as well as benzyl bromide converted cleanly to the coupling product (entries 1,3). Using the radical clock (bromomethyl)cyclopropane, however, only the ring-opened coupling product was observed[8] (entry 2), indicating the involvement of a single-electron activation of the C-Br bond and hence the presence of an organic radical in the catalytic cycle. As an example for sp^2-electrophiles, naphthalenes containing either bromide or oxygen-based leaving groups were subjected to the cross-coupling conditions. In all cases only trace-amounts of the desired coupling product was observed (entries 4-6), possibly owing to the low stability of the naphthyl radical.

[8] For experimental data as well as NMR analysis of the coupling reaction see subsection 5.4.7.3 on p. 200.

Table 5.8: Stoichiometric coupling reactions using **5a** in presence of 4-tolylmagnesium bromide.

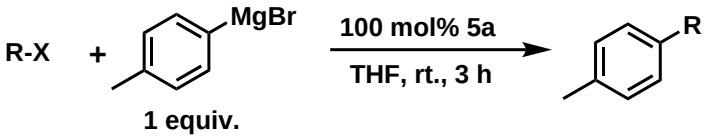

Entry	substrate	X	yield[a] [%]
1	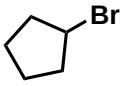		84
2	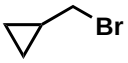		68[b]
3	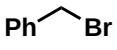		95
4	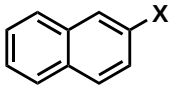	Br	8
5		OMs	1
6		OTs	3

[a] yield determined via GC-FID vs. internal standard; [b] yield of ring-opening product.

Further evidence for the formation of radical species during the catalytic cycle was afforded in coupling reactions of cyclohexyl bromide with 4-tolylmagnesium bromide and substoichiometric amounts of **5a**. GC-MS analysis of the reaction mixtures after 3 h identified the formation of a compound with a molecular ion peak of 162, the amount of which increased with lower catalyst loadings. The molecular mass and fragmentation pattern suggest the formation of 2-(4-tolyl)tetrahydrofurane, indicating a radical reaction mechanism involving H atom transfer from THF (scheme 5.4).

Next, competition reactions were performed to provide further insight into the composition of the active catalyst species. Herein, bromocyclohexane was coupled with 1 equiv. 4-*n*-butylphenyl- and 4-methoxyphenylmagnesium bromide, respectively, in presence of equal amounts of **5a**.[9] Both reactions afforded the cross-coupling

[9]Experimental deteils of the competition reaction can be found in subsection 5.4.7.4 on p. 201.

products in almost statistical ratios (transfer of the aryl moiety of **5a** as well as of the Grignard reagents) along with minor amounts of the biaryls (each < 2%). These experiments indicate that facile exchange of the aryl ligands at Fe is operative which could also involve diarylferrate complexes or low amounts of 'naked' Fe species/-particles.[10]

In general, we assume that the complexes **5a–c** form a new, catalytically active species in the presence of $MgBr_2$ and of their respective arylmagnesium bromides. The identity of this species remained untraceable by NMR spectroscopy and ESI-MS (the latter due to lability toward air, moisture). However, the reactions darkened when adding arylmagnesium bromides and the UV/Vis spectra showed characteristic bands at 610 nm (with **5a**,**b**) and 590 nm (with **5c**). The former observation is most likely a consequence of the partial presence of low-valent Fe complexes or Fe(0) particles (from the reduction of the iron complexes with the Grignard reagent) which is indirectly supported by the concurrent formation the respective 4,4´-disubstituted-1,1´-biphenyls (~5-10%, from the oxidative homocoupling of the Grignard reagent). However, Fe(0) particles are not accountable for the aforementioned optical properties (absorption at ~600 nm), although the partial dissolution of particles in the presence of organic electrophiles has been reported.[10]

We postulate a reaction mechanism that is initiated by activation of the formal Fe(II) pre-catalyst (**5a-c**) by the use of ArMgBr or $MgBr_2$. The acitve catalyst species is then

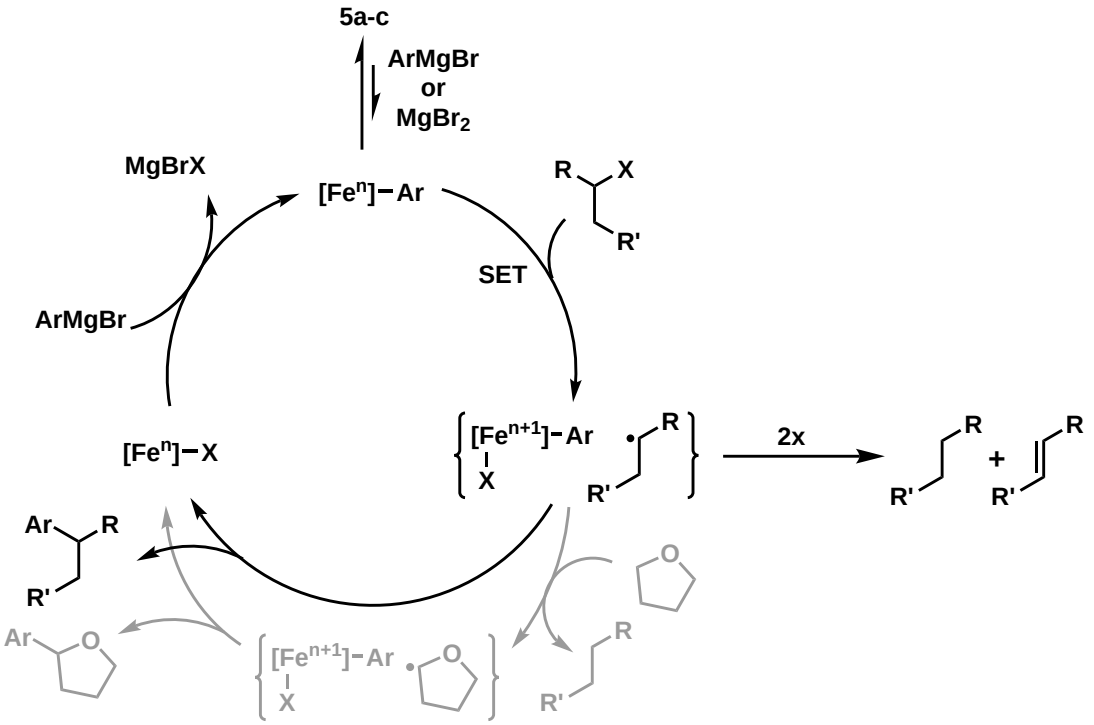

Scheme 5.4: Postulated mechanism for the Kumada cross-coupling of secondary alkyl halides using the aryliron complexes **5a-c**.

able to activate the alkyl bromide and chlorde by single electron transfer (SET) and generate a *sec*-alkyl radical. Radical recombination with an aryliron complex gives the desired cross-coupling product. However, with lower catalyst concentrations, H atom transfer from the solvent becomes competitive which results in the formation of the alkane and the heteroatom-stabilized THF radical. Reaction of the latter with an aryliron species furnishes the observed side product. In presence of the Grignard reagent, the acive catalyst is regenerated otherwise the formation of $L^{Me}FeBr(THF)$ is observed. UV/Vis spectra as well as the formation of the homocoupling product indicate the presence of low-valent Fe complexes or Fe(0) particles and their involvement in the reaction could not be ruled out. Catalyst poisoning studies may provide further evidence into the composition of the acive catalyst.

5.3 Conclusion

In summary, we have reported an operationally simple cross-coupling protocol which can take advantage of the under-utilized class of secondary alkyl chlorides. This has been achieved with the use of the environmentally friendly catalyst system $FeCl_3$/TMEDA and lithium chloride was established to play a crucial role in catalytic activity. The polarity of the reaction medium had a high influence on the efficiency of the coupling reaction which seemed to indicate a change in reaction mechanism in etheral solvents due to the participation of nanoparticulate iron species. In a quest to broaden the mechanistical understanding of this reaction type, over 40 different di- and tetraamine, -imine, and -amide ligands were evaluated in correlation to their stereoelectronic properties. As a testbench for further mechanistic investigations, a set of β-diketiminato(aryl)iron complexes were synthesized and, to our knowlege, for the first time subjected to Kumada cross-coupling conditions. On the basis of analytical data (UV/Vis, NMR, and LIFDI-MS) as well as radical clock and competition reactions, we were able to get a better understanding of the species involved in the catalytic cycle and to postulate a reaction mechanism that is initiated by single electron transfer.

5.4 Experimental Section

5.4.1 General Information

Analytical Thin-Layer Chromatography: TLC was performed using aluminum plates with silica gel and fluorescent indicator (Merck, 60, F254). Thin layer chromatography plates were visualized by exposure to ultraviolet light (366 or 254 nm) or by immersion in a staining solution of molybdatophosphoric acid in ethanol or potassium permanganate in water.

Column Chromatography: Flash column chromatography with silica gel 60 from KMF (0.040-0.063 mm). Mixtures of solvents used are noted in brackets.

Chemicals and Solvents: Unless noted otherwise, all commercially available compounds were used as provided without further purification. TMEDA was distilled over KOH under argon atmosphere. $Fe(acac)_3$ (>97%), $FeCl_3$ (98%), and anhydrous LiCl (>99%) from Aldrich were stored and handled in a glove box. $FeCl_2$ [31] and $dipp_2$nacnacLi[32] were synthesized according to published procedures. $FeCl_2 \cdot 1.5$ THF has been prepared by heating $FeCl_2$ to reflux in tetrahydrofuran overnight and subsquently removing the solvent by filtration. All experiments were performed under an atmosphere of dry argon or nitrogen using standard Schlenk and glovebox techniques. Anhydrous toluene was purchased from Sigma-Aldrich in Sure/Seal^{TM} bottles. *n*-Hexane was dried and deoxygenated with an MBraun SPS800 solvent purication system. Diethylether and tetrahydrofuran were distilled from sodium benzophenone ketyl. Benzene-d_6 and tetrahydrofuran-d_8 werde distilled from sodium and sodium benzophenone ketyl, respectively and degassed by three freeze-pump-thaw cycles. All solvents were stored over molecular sieves (3A) in an argon-filled glovebox.

High Pressure Reactor: Hydrogenation reactions were carried out in 160 and 300 ml high pressure reactors (ParrTM) in 4 ml glass vials. The reactors were loaded under argon, purged with H_2 (1 min), then three times with 2 bar H_2, sealed and the internal pressure was adjusted. Hydrogen (99.9992%) was purchased from Linde.

^{1}H-and ^{13}C-NMR-Spectroscopy: Nuclear magnetic resonance spectra were recorded on a Bruker Avance 300 (300 MHz) and Bruker Avance 400 (400 MHz). ^{1}H-NMR: The following abbreviations are used to indicate multiplicities: s = singlet; d = doublet; t = triplet, q = quartet; m = multiplet, dd = doublet of doublet, dt = doublet of triplet, dq = doublet of quartet, ddt = doublet of doublet of quartet. ^{13}C-APT/DEPTQ-NMR data: u = up (CH_3 or CH), d = down (CH_2 or Cq). Chemical shift δ is given in ppm to tetramethylsilane.

Fourier-Transformations-Infrared-Spectroscopy (FT-IR): Spectra were recorded on a Agilent Cary 630 FTIR with ATR-device. All spectra were recorded at room temperature. Wave number is given in cm^{-1}. Bands are marked as s = strong, m = medium, w = weak and b = broad.

Gas Chromatography with FID (GC-FID): HP6890 GC-System with injector 7683B and Agilent 7820A System. Column: HP-5, 19091J-413 (30 m × 0.32 mm × 0.25 μm), carrier gas: N_2. GC-FID was used for reaction control and catalyst screening (calibration with internal standard *n*-pentadecane and analytically pure samples).

Gas Chromatography with Mass-Selective Detector (GC-MS): Agilent 6890N Network GC-System, mass detector 5975 MS. Column: HP-5MS (30m × 0.25 mm × 0.25 μm, 5% phenylmethylsiloxane, carrier gas: H_2. Standard heating procedure: 50 °C (2 min), 25 °C/min -> 300 °C (5 min)

High Resolution Mass Spectrometry (HRMS): The spectra were recorded by the Central Analytics Lab at the Department of Chemistry, University of Regensburg, on a MAT SSQ 710 A from Finnigan.

Melting Point: Melting points were determined on a Büchi apparatus after Dr. Tottoli and are uncorrected.

UV/Vis-Spectroscopy: Spectra were recorded on a Varian Cary 50 spectrometer.

5.4.2 General Procedures

General Procedure 1 – Synthesis of Starting Materials

To a solution of 3-buten-1-ol (10 mmol, 885 μL) in dry CH_2Cl_2 (0.1 M, 100 ml) was added 7 mol% $Fe(acac)_3$ (0.7 mmol, 178 mg) and chlorotrimethylsilane (1.2 equiv., 12 mmol, 1.5 ml). Aldehyde (1 equiv.) was then added to the reaction. The reaction was stirred at room temperature until analysis via GC-MS showed complete formation of the product. The reaction was then quenched by addition of water under stirring and extracted with DCM. The combined organic layers were dried over $MgSO_4$, and the solvent was removed under reduced pressure. This crude reaction mixture was purified by silica gel column chromatography. According to: P. O. Miranda, R. M. Carballo, V. S. Martín, J. I. Padrón, Org. Lett. 2009, 11, 357-360.

General Procedure 2 – Cross-Coupling of Secondary Alkyl Chlorides

Under an inert atmosphere, a Schlenk tube was charged with $FeCl_3$ (5-10 mol%) and treated with 4 ml dry THF or toluene and distilled TMEDA (1.2 equiv.). The resulting yellow solution was put in a water bath at 10 °C and the sec. alkyl chloride (2 mmol) was added via syringe, followed by the freshly prepared arylmagnesium bromide solution (1.5 equiv., 1 M in THF) over 1 h. The mixture was stirred at 10 °C for 4 h. Then saturated aqueous NH_4Cl was added, and the mixture was extracted with ethyl acetate. The combined organic layers were dried ($MgSO_4$) and concentrated under reduced pressure. Silica gel column chromatography resulted in the pure coupling products.

General Procedure 3 - Preparation of Arylmagnesium Bromides

Under an inert atmosphere, a 20 ml Schlenk flask was placed in an ice/water bath at 0 °C, charged with magnesium turnings (292 mg, 12 mmol) and LiCl (509 mg, 12 mmol), fitted with a rubber septum, and purged with argon. Dry THF (~9 ml) was added via syringe followed by aryl bromide. The mixture was stirred at 0 °C to r.t. for 3 h. According to: F. M. Piller, P. Appukkuttan, A. Gavryushin, M. Helm, P. Knochel, *Angew. Chem.* **2008**, *120*, 6907-6911; *Angew. Chem. Int. Ed.* **2008**, *47*, 6802-6806.

The concentration of the solution has been determined by titration against a known mass of iodine dissolved in anhydrous tetrahydrofuran.

General Procedure 4 - Preparation of $Dipp_2$nacnacFe-Ar Complexes

The complexes **5a-c** were synthesized following a procedure of Holland and coworkers.[26] To a Schlenk tube were added $Dipp_2$nacnacLi (500 mg, 1.18 mmol), $FeCl_2 \cdot 1.5$ THF (277 mg, 1.18 mmol, 1.0 equiv.), and toluene (10 ml). The mixture was stirred at 100 °C for 12 h, upon which an orange precipitate formed. After cooling to 0 °C arylmagnesium bromide (1.0 equiv., solution in THF) was added dropwise, which resulted in an immediate colorchange from orange to black. The reaction mixture was stirred for 4 h at room temperature after which the solvent was removed in vacuo. The solid material obtained was extracted with *n*-hexane (55 ml); the yellow-orange filtrate was concentrated under reduced pressure to approx. 5 ml. Upon cooling to 40 °C an orange solid precipitated, which was collected by filtration. Single crystals of the complexes could be obtained by storing the filtrate in a freezer for 23 days.

5.4.3 Synthesized Starting Materials

2-Chloro-4-phenylbutane

A 100 ml 3-neck flask was fitted with a dropping funnel and a reflux condenser. The flask was charged with 12.4 ml 4-phenyl-2-butanol (80 mmol, 1 equiv.) in 6.5 ml pyridine (80 mmol, 1 equiv.). To the stirring solution, 8.75 ml thionyl chloride (120 mmol, 1.5 equiv.) were added slowly via dropping funnel. Then it was refluxed for 2 h. After cooling to rt, the mixture was quenched by adding ice water, and the suspension was extracted three times with chloroform. The combined organic layers were washed with saturated aqueous $NaHCO_3$, dried over Na_2SO_4 and concentrated under reduced pressure. The crude reaction mixture was purified by silica gel column chromatography (*n*-pentane).

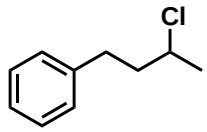

Yellow oil

$C_{10}H_{13}Cl$

168.66 g/mol

Yield 6.68 g (40 mmol, 93%)

TLC R_f = 0.43 (SiO_2, *n*-pentane)

^{1}H-NMR (300 MHz, $CDCl_3$) δ 1.60 (d, J = 6.6 Hz, 3H), 2.05-2.13 (m, 2H), 2.77-2.98 (m, 2H), 4.01-4.12 (m, 1H), 7.27-7.40 (m, 5H).

^{13}C-APT-NMR (75 MHz, $CDCl_3$) δ 25.4 (u), 32.8 (d), 41.9 (d), 57.9 (u), 126.0 (u), 128.4 (u), 141.0.

GC-MS t_R = 5.80 min, (EI, 70 eV): m/z = 168 [M^+], 133, 117, 91, 65, 51.

HR-MS (EI, 70 eV, m/z): 168.071, calcd: 168.0706.

FT-IR (ATR film) $1/\lambda$ [cm^{-1}] = 3440 (w), 3354 (w, b), 3086 (w), 3063 (m), 3027 (m), 2971 (m), 2928 (m), 2862 (m), 1496 (m), 913 (s), 780 (s), 700 (s), 629 (s).

(2*S*,4*R*)-2-*tert*-Butyl-4-chloro-tetrahydro-2*H*-pyrane

According to general procedure 1: Using 1.1 ml trimethylacetaldehyde (10 mmol, 1 equiv.). Purification by SiO_2 column chromatography (cyclohexane/ethyl acetate 4:1).

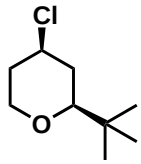

Colorless oil

$C_9H_{17}ClO$

176.68 g/mol

Yield 742 mg (4.20 mmol, 42%)

TLC R_f = 0.50 (SiO_2, cyclohexane/ethyl acetate (4:1))

^{1}H-NMR (300 MHz, $CDCl_3$) δ 0.88 (s, 9H), 1.54 (q, J = 11.8 Hz, 1H), 1.79 (qd, J = 12.3, 4.8 Hz, 1H), 2.03 (ddt, J = 12.7, 4.4, 2.0, 1H), 2.12 (ddt, J = 12.6, 4.2, 1.9, 1H), 2.84 (dd, J = 11.3, 1.7 Hz, 1H), 3.33 (td, J = 12.6, 2.2 Hz, 1H), 3.89-4.08 (m, 2H).

^{13}C-APT-NMR (75 MHz, $CDCl_3$) δ 26.1 (u), 34.2 (d), 37.4 (d), 37.6 (d), 57.3 (u), 67.3 (d), 85.2 (u).

GC-MS t_R = 4.98 min, (EI, 70 eV): m/z = 176 [M^+], 161, 141, 119, 111, 87, 83, 69, 62, 55, 51.

(2*S*,4*R*)-4-Chloro-2-(3,4,5-trimethoxyphenyl)-tetrahydro-2*H*-pyrane

According to general procedure 1: Using 1.96 g 3,4,5-trimethoxybenzaldehyde (10 mmol, 1 equiv.). Purification by SiO_2 column chromatography (cyclohexane/ethyl acetate 5:2).

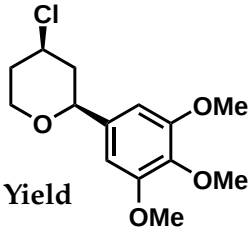

	Colorless oil
	$C_{14}H_{19}ClO_4$
	286.75 g/mol
Yield	2.12 g (7.40 mmol, 74%)
TLC	R_f = 0.29 (SiO_2, cyclohexane/ethyl acetate (5:2))
^{1}H-NMR	(300 MHz, $CDCl_3$) δ 1.21 (td, J = 7.2, 1.4 Hz, 1H), 1.82-2.16 (m, 4H), 3.54 (tt, J = 12.1, 1.9 Hz, 1H), 3.78 (s, 3H), 3.83 (s, 6H), 4.02-4.18 (m, 2H), 6.57 (m, 2H).
^{13}C-APT-NMR	(75 MHz, $CDCl_3$) δ 36.8 (d), 44.6 (d), 56.0 (u), 60.7 (u), 67.3 (d), 73.8 (u), 79.4 (u), 102.8 (u), 136.9 (d), 137.4 (d), 137.6 (d), 153.2 (d).
GC-MS	t_R = 4.98 min, (EI, 70 eV): m/z = 176 [M^+], 161, 141, 119, 111, 87, 83, 69, 62, 55, 51.
HR-MS	(EI, 70 eV, m/z): 286.097, calcd: 286.0972.
FT-IR	(ATR film) $1/\lambda$ [cm^{-1}] = 3008 (m), 2957 (m), 2932 (m), 2839 (m), 1712 (w), 1589 (s), 1506 (s), 1460 (s), 1417 (s), 1364 (m), 1327 (m), 1233 (s), 1122 (s), 1074 (s), 1003 (m), 966 (m), 825 (m), 745 (s).

(2*S*,4*R*)-2-Benzyl-4-chloro-tetrahydro-2*H*-pyrane

According to general procedure 1: Using 1168 μL phenylacetaldehyde (10 mmol, 1 equiv.). Purification by SiO_2 column chromatography (cyclohexane/ethyl acetate 6:1).

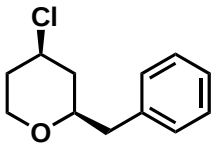

	Yellow oil
	$C_{12}H_{15}ClO$
	210.70 g/mol
Yield	1.30 g (6.18 mmol, 62%)
TLC	R_f = 0.51 (SiO_2, cyclohexane/ethyl acetate (6:1))

^{1}H-NMR	(300 MHz, $CDCl_3$) δ 1.66 (q, J = 11.8 Hz, 1H), 1.88-2.00 (m, 1H), 2.05-2.25 (m, 2H), 2.70-2.82 (m, 1H), 2.97 (ddd, J = 17.5, 13.8, 6.9 Hz, 1H), 3.43 (td, J = 12.2, 2.2 Hz, 1H); 3.55 (dtd, J = 11.1, 6.5, 1.9 Hz, 1H), 3.92-4.12 (m, 2H), 7.25-7.40 (m, 5H).
^{13}C-APT-NMR	(75 MHz, $CDCl_3$) δ 37.0 (d), 42.3 (d), 42.5 (d), 55.9 (u), 67.0 (d), 78.1 (u), 126.5 (u), 128.4 (u), 129.4 (u), 137.6 (d).
GC-MS	t_R = 7.55 min, (EI, 70 eV): m/z = 210 [M^+], 119, 91, 77, 55.
HR-MS	(EI, 70 eV, m/z): 210.081, calcd: 210.0811.
FT-IR	(ATR film) $1/\lambda$ [cm^{-1}] = 3082 (w), 3059 (w), 3024 (m), 2923 (m), 2954 (m), 2845 (m), 2740 (w), 2358 (w), 2339 (w), 1947 (w), 1887 (w), 1732 (w), 1602 (m), 1492 (s), 1452 (s), 1331 (s), 1249 (s), 1153 (s), 1141 (s), 1081 (s), 1063 (s), 1027 (s), 984 (m), 876 (m), 804 (m), 765 (s), 742 (s).

Naphthalen-2-yl methanesulfonate

A 50 ml flask was charged with 2-naphthol (5 mmol, 720 mg) and triethylamine (1.35 equiv., 6.75 mmol, 950 μL) in 20 ml THF. The reaction mixture was cooled to 0 °C and a solution of mesityl chloride (1.2 equiv., 6 mmol, 465 μL) in 5 ml THF was added over a period of 1 h using a syringe pump. After stirring for an additional 2 h, the reaction was quenched with destilled water and 3 times extracted with ethyl acetate. The combined organic layers were dried over Na_2SO_4 , filtered and concentrated under reduced pressure. The crude reaction mixture was purified by silica gel column chromatography (*n*-pentane/ethyl acetate (6:1)) and recrystallized from a mixture of *n*-pentane and ethyl acetate to obtain short white needles in 69% yield.

The procedure was modified from C. K. Lau, P. C. Belanger, C. Dufresne, J. Scheigetz, *J. Org. Chem.* **1987**, *52*, 1670-1673.

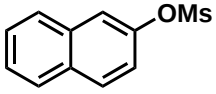

	White needles
	$C_{11}H_{10}O_3S$
	222.26 g/mol
Yield	767 mg (3.5 mmol, 69%)
TLC	R_f = 0.38 (SiO_2, *n*-pentane/ethyl acetate (6:1))
^{1}H-NMR	(300 MHz, $CDCl_3$) δ 7.94 – 7.83 (m, 3H), 7.77 (dd, *J* = 2.5, 0.7 Hz, 1H), 7.59 – 7.49 (m, 2H), 7.41 (dd, *J* = 8.9, 2.4 Hz, 1H), 3.19 (s, 3H).

^{13}C-NMR	(75 MHz, $CDCl_3$) δ 146.9, 133.7, 132.2, 130.4, 128.0, 128.0, 127.3, 126.7, 120.9, 119.6, 37.5.
GC-MS	t_R = 9.84 min, (EI, 70 eV): m/z = 222 [M^+], 143, 128, 115, 102, 89, 79, 63, 51.

Analytical data in accordance with literature data: D. A. Wilson, C. J. Wilson, C. Moldoveanu, A.-M. Resmerita, P. Corcoran, L. M. Hoang, B. M. Rosen and V. Percec, *J. Am. Chem. Soc.* **2010**, *132*, 1800–1801.

Naphthalen-2-yl 4-methylbenzenesulfonate

A 50 ml flask was charged with 2-naphthol (5 mmol, 720 mg) and triethylamine (1.35 equiv., 6.75 mmol, 950 μL) in 20 ml THF. The reaction mixture was cooled to 0 °C and a solution of tosyl chloride (1.2 equiv., 6 mmol, 1.15 g) in 5 ml THF was added over a period of 1 h using a syringe pump. After stirring for an additional 2 h, the reaction was quenched with destilled water and 3 times extracted with ethyl acetate. The combined organic layers were dried over Na_2SO_4 , filtered and concentrated under reduced pressure. The crude reaction mixture was purified by silica gel column chromatography (*n*-pentane/ethyl acetate (19:1)) and recrystallized from a mixture of *n*-pentane and ethyl acetate to obtain pale yellow needles in 65% yield.

The procedure was modified from C. K. Lau, P. C. Belanger, C. Dufresne, J. Scheigetz, *J. Org. Chem.* **1987**, *52*, 1670-1673.

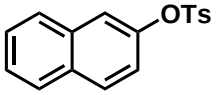

	Pale yellow needles
	$C_{17}H_{14}O_3S$
	298.36 g/mol
Yield	966 mg (3.2 mmol, 65%)
TLC	R_f = 0.45 (SiO_2, *n*-pentane/ethyl acetate (19:1))
^{1}H-NMR	(300 MHz, $CDCl_3$) δ 7.85 – 7.79 (m, 1H), 7.78 – 7.69 (m, 4H), 7.53 – 7.45 (m, 3H), 7.33 – 7.27 (m, 2H), 7.09 (dd, *J* = 8.9, 2.4 Hz, 1H), 2.44 (s, 3H).
^{13}C-NMR	(75 MHz, $CDCl_3$) δ 147.3, 145.5, 133.6, 132.5, 132.0, 129.9, 129.9, 128.7, 128.0, 127.9, 127.0, 126.5, 121.3, 120.1, 21.9.
GC-MS	t_R = 12.20 min, (EI, 70 eV): m/z = 298 [M^+], 234, 218, 206, 191, 178, 155, 143, 131, 115, 103, 91, 75, 65, 51.

Analytical data in accordance with literature data: D. A. Wilson, C. J. Wilson, C. Moldoveanu, A.-M. Resmerita, P. Corcoran, L. M. Hoang, B. M. Rosen and V. Percec, *J. Am. Chem. Soc.* **2010**, *132*, 1800–1801.

5.4.4 Ligand Synthesis

N,N'-Dimethyl-*N,N'*-bis(pyridine-2-ylmethyl)-1,2-diaminoethane

According to the literature, to a solution of *N,N'*-dimethylethylenediamine (6.5 mmol, 700 μL) and KOH (25 mmol, 1.4 g) in nitrogen flushed methanol (25 ml) was slowly added 2-chloromethylpyridine hydrochloride (13 mmol, 12.1 g) dissolved in methanol (25 ml) under nitrogen atmosphere. The mixture was stirred for 30 min, heated under reflux for 1 h, and then cooled to room temperature. After the methanol was evaporated under reduced pressure, water was added, followed by KOH to raise the pH to 13. The product was extracted with dichloromethane, and the organic layer was then dried ($MgSO_4$). Subsequently, the solvent was evaporated and a yellow oil was obtained. Purification by SiO_2 column chromatography (methanol/toluene/NEt_3 88:10:2).

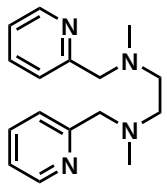

Yellow oil

$C_{16}H_{22}N_4$

270.37 g/mol

Yield	n.d.
TLC	R_f = 0.48 (SiO_2, methanol/toluene/NEt_3 88:10:2)
^{1}H-NMR	(300 MHz, $CDCl_3$) δ 2.22 (m, 6H), 2.60 (m, 4H), 3.64 (m, 4H), 7.10 (m, 2H), 7.38 (m, 2H), 7.58 (m, 2H), 8.48 (m, 2H).
^{13}C-APT-NMR	(75 MHz, $CDCl_3$) δ 42.9, 55.5, 64.2, 121.9, 123.1, 136.4, 149.0, 159.4.

Analytical data in accordance with literature data: T. Pandiyan, H. J. Guadalupe, J. Cruz, S. Bernès, V. M. Ugalde-Salvdivar, I. González, Eur. J. Inorg. Chem. 2008, 3274-3285.

Tris[2-(dimethylamino)ethyl]amine

According to the literature, aqueous formaldehyde (37 wt%, 220 mmol, 16.3 ml) was added to a solution of tris[2-aminoethyl]-amine (6.6 mmol, 992 μL) and acetic acid (45 ml) in acetonitrile (200 ml) and allowed to be stirred for 1 h. Subsequently, the reaction mixture was cooled to 0 °C and sodium borohydride (4.5 mmol, 3.3 g) slowly added. After being stirred for 48 h, all solvents were removed under reduced pressure, the residue was made strongly basic with 3 M aqueous sodium hydroxide and extracted several times with DCM. The organic layers were combined, dried and

the solvent removed. The residue was dissolved in *n*-pentane, filtered and the filtrate reduced to dryness to obtain the product as yellow oil.

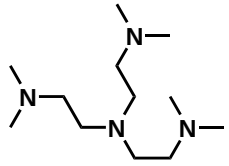

	Yellow oil
	$C_{12}H_{30}N_4$
	230.39 g/mol
Yield	1.23 g (5.3 mmol, 81%)
^{1}H-NMR	(300 MHz, $CDCl_3$) δ 2.17 (s, 18H), 2.32 (m, 6H), 2.55 (m, 6H).
^{13}C-APT-NMR	(75 MHz, $CDCl_3$) δ 45.8, 53.0, 57.4.
GC-MS	t_R = 11.95 min, (EI, 70 eV): m/z = 230 [M^+], 172, 114, 89, 72, 58, 42.

Analytical data in accordance with literature data: G. J. P. Britovsek, J. England, A. J. P. White, Inorg. Chem. 2005, 44, 8125-8134.

5.4.5 Synthesis of β-Ketiminato Iron Complexes

Dipp$_2$nacnacFe(4-Me-C$_6$H$_4$) (5a)

According to general procedure 4: using dipp$_2$nacnacLi (500 mg), $FeCl_2$·1.5 THF (277 mg), and 4-tolylmagnesium bromide (1.29 ml, 0.91 M in THF).

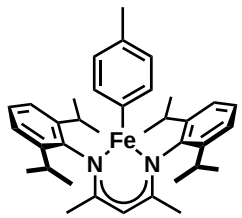

	Orange powder
	$C_{36}H_{48}FeN_2$
	564.64 g/mol
Yield	423 mg (0.75 mmol, 64%)
M.p.	190 °C (decomp.)
^{1}H-NMR	(400 MHz, C_6D_6) δ 161 (2H; H-3/C_6H_4Me), 157 (3H; Me/C_6H_4Me), 124 (1H; CH/nacnac), 44 (6H; Me/nacnac), -10 (4H; H-3/C_6H_3(*i*-Pr)$_2$), -21 (12H; Me/*i*-Pr), -81 (2H; H-4/C_6H_3(*i*-Pr)$_2$), -117 (4H; CH/*i*-Pr), -123 (12H; Me/*i*-Pr).
Elemental Anal.	calcd. (%) for $C_{36}H_{48}FeN_2$: C 76.58, H 8.57, N 4.96; found: C 76.06, H 8.29, N 4.84.
LIFDI-MS	*m*/*z* calcd. for $C_{36}H_{48}FeN_2$: 564.32; found: 564.31.

Dipp$_2$nacnacFe(4-MeO-C$_6$H$_4$) (5b)

According to general procedure 4: using dipp$_2$nacnacLi (500 mg), $FeCl_2$·1.5 THF (277 mg), and 4-methoxyphenylmagnesium bromide (1.42 ml, 0.83 M in THF).

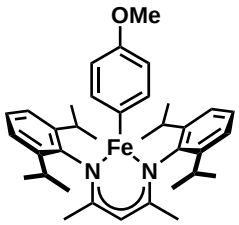

Orange powder

$C_{36}H_{48}FeN_2O$

580.64 g/mol

Yield 464 mg (0.80 mmol, 68%)

M.p. 182 °C (decomp.)

^{1}H-NMR (400 MHz, C_6D_6) δ 151 (2H; H-3/C_6H_4OMe), 125 (1H; CH/n-acnac), 53 (3H; Me/C_6H_4OMe), 42 (6H; Me/nacnac), -11 (4H; H-3/C_6H_3(*i*-Pr)$_2$), -21 (12H; Me/*i*-Pr), -82 (2H; H-4/C_6H_3(*i*-Pr)$_2$), -118 (4H; CH/*i*-Pr), -123 (12H; Me/*i*-Pr).

Elemental Anal. calcd. (%) for $C_{36}H_{48}FeN_2O$: C 74.47, H 8.33, N 4.82; found: C 74.31, H 8.16, N 4.53.

LIFDI-MS *m*/*z* calcd. for $C_{36}H_{48}FeN_2O$: 580.31; found: 580.38.

Dipp$_2$nacnacFe(4-F-C$_6$H$_4$) (5c)

According to general procedure 4: using dipp$_2$nacnacLi (500 mg), $FeCl_2$·1.5 THF (277 mg), and 4-fluorophenylmagnesium bromide (1.31 ml, 0.90 M in THF).

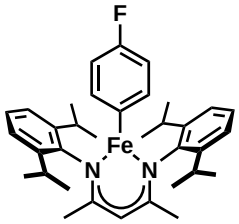

Orange powder

$C_{35}H_{45}FFeN_2$

568.60 g/mol

Yield 409 mg (0.72 mmol, 61%)

M.p. 220 °C (decomp.)

^{1}H-NMR (400 MHz, C_6D_6) δ 148 (2H; H-3/C_6H_4F), 123 (1H; CH/nacnac), 45 (6H; Me/nacnac), -9 (4H; H-3/C_6H_3(*i*-Pr)$_2$), -20 (12H; Me/*i*-Pr), -83 (2H; H-4/C_6H_3(*i*-Pr)$_2$), -116 (4H; CH/*i*-Pr), -123 (12H; Me/*i*-Pr).

Elemental Anal. calcd. (%) for $C_{35}H_{45}FFeN_2$: C 73.93, H 7.98, N 4.93; found: C 73.19, H 7.71, N 4.88.

LIFDI-MS *m*/*z* calcd. for $C_{35}H_{45}FFeN_2$: 568.29; found: 568.35.

5.4.6 Optimization Experiments

5.4.6.1 Catalyst Loading Experiments

The 4-tolylmagnesium bromide was synthesized as described in general procedure 3. The reaction was performed following general procedure 2. Cyclohexyl chloride (0.5 mmol), the additive, a $FeCl_3$ stock solution in THF ($1.25 \cdot 10^{-2}$ M) and THF was added for a total volume of 2 ml.

Table 5.11: Effect of catalyst loading with different amounts of additives on Kumada cross-couplings.

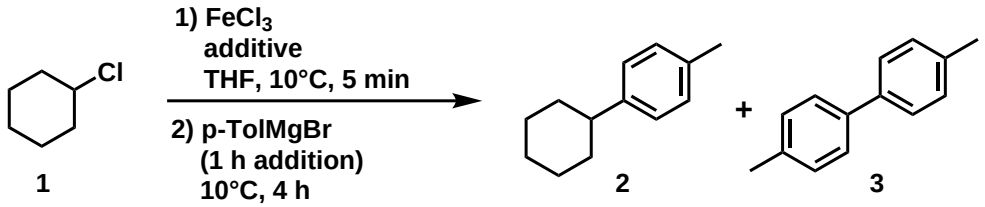

Entry	$FeCl_3$[mol%]	additive	**2**[a] [%]	**3**[a] [%]
1	0	–	0	11
2	2.5	–	98	8
3	5	–	100	11
4	0	20 mol% LiCl	0	0
5	0.5	20 mol% TMEDA	37	14
6	1	20 mol% TMEDA	62	14
7	2	20 mol% TMEDA	96	12
8	5	20 mol% TMEDA	100	12

[a] GC yields (vs. *n*-pentadecane as internal reference).

5.4.6.2 Optimization Experiments Using Electron Withdrawing Aryl Grignard Reagents

The 4-fluorophenylmagnesium bromide was synthesized as described in general procedure 3. Under an inert atmosphere, a Schlenk tube was charged with $FeCl_3$ (10 mol%) and treated with 2 ml dry THF and distilled TMEDA (1.2 equiv.). The resulting yellow solution was put in a water bath at 10 °C and chlorocyclohexane (1 mmol) was added via syringe, followed by the freshly prepared 4-fluorophenylmagnesium

bromide solution (1.5 equiv., 1 M in THF) over 1 h. The mixture was stirred at 10 °C for 4 h. Then, saturated aqueous NH_4Cl was added, and the mixture was extracted with ethyl acetate. The combined organic layers were dried ($MgSO_4$) and analyzed by quantitative GC-FID.

Table 5.13: Optimization experiments using fluorinated aryl Grignard reagents.

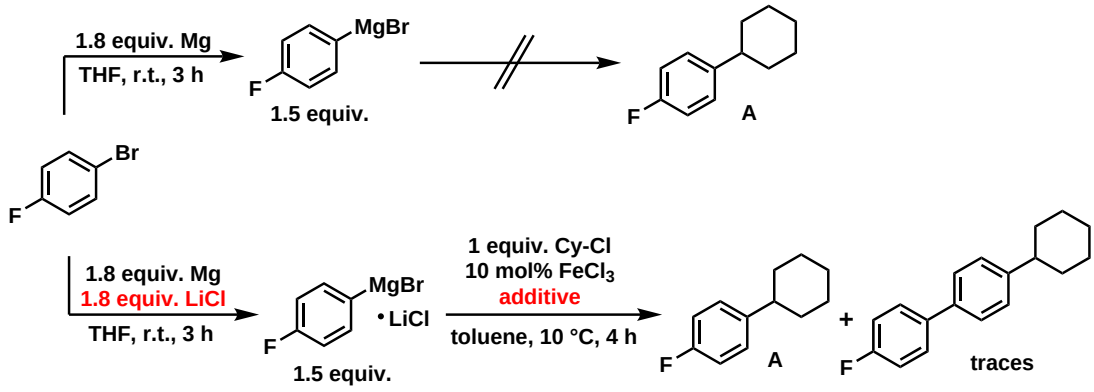

No.	Additive (equiv.)	Yield of A [%][a]
1	–	94
2	TMEDA (1.2)	62
3	TMEDA (1.2 + 1.5 (to the Grignard))	30
4	*n*-BuLi in hexane (1.5)	27
5	4-(trifluoromethyl)styrene (0.1)	71

[a] GC yields (vs. *n*-pentadecane as internal reference).

5.4.6.3 Effect of Fluorinated Substrates as Additive

The 4-tolylmagnesium bromide was synthesized as described in general procedure 3. Under an inert atmosphere, a Schlenk tube was charged with $FeCl_3$ (5 mol%) and treated with 2 ml dry THF and fluorinated additive (1 equiv.). The resulting solution was put in a water bath at 10 °C and chlorocyclohexane (1 mmol) was added via syringe, followed by the freshly prepared 4-tolylmagnesium bromide solution (1.25 equiv., 1 M in THF) over 1 h. The mixture was stirred at 10 °C for 4 h. Then, saturated aqueous NH_4Cl was added, and the mixture was extracted with ethyl acetate. The combined organic layers werde dried ($MgSO_4$) and analyzed by quantitative GC-FID.

Table 5.14: Effect of fluorinated substrates as addive in cross-coupling of sec. alkyl chlorides.

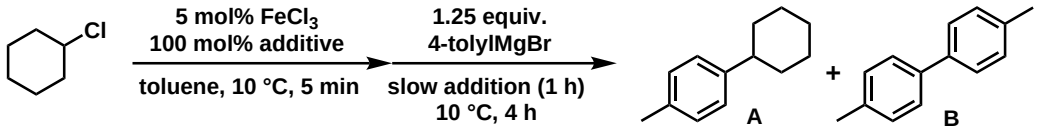

No.	Fluorinated additive	Yield of A [%][a]	Yield of B [%][a]
1	1-fluorododecane	68	7
2	1,4-difluorobenzene	75	12
3	TMEDA	91	4

[a] GC yields (vs. *n*-pentadecane as internal reference).

5.4.6.4 Amine and Amide Ligand Screening

In a glovebox a flame-dried centrifuge vial containing a stir bar was charged with an iron(III) chloride solution in dry THF (0.0125 M, 0.025 mmol, 2 ml), cyclohexyl chloride (0.5 mmol, 59 μL) and 5-10 mol% of the amine/amide ligand. The vial was capped with a rubber septum, transferred to a temperature-controlled cooling bath atop a magnetic stirrer and connected to a Schlenk line via a cannula. The reaction flask was cooled to 10 °C and 1.25-1.45 equiv. of a freshly prepared 4-tolylmagnesium bromide solution in THF (0.74 M, 0.65-0.725 mmol) was added over 1 h using a syringe pump. The reaction mixture was stirred for further 3 h at 10 °C and then quenched with 2 ml sat. ammonium chloride. The aqueous phase was extracted 3 times with ethyl acetate (1 ml each), the combined organic layers dried over sodium sulfate and the reaction yield determined via GC-FID.

Table 5.15: Screening of various amine, imine, and amide ligands.

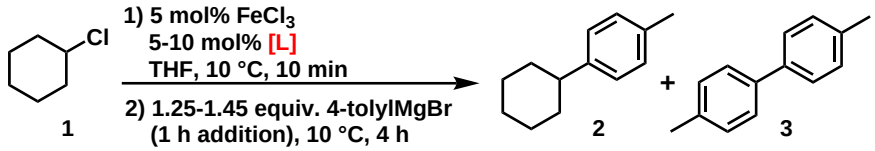

Entry	Ligand [L]		**2** [%]	**3** [%]
1[a]	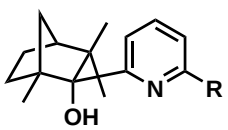	R = H	76	20
2[a]		R = Me	100	9
3[a]		R = Ph	98	9

4[a]	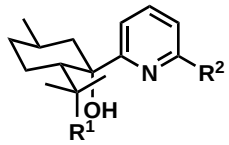	R^1 = H, R^2 = Br	62	34
5[a]		R^1 = H, R^2 = Me	100	8
6[a]		R^1 = H, R^2 = Ph	100	10
7[a]		R^1 = Ph, R^2 = Br	76	18
8[a]		R^1 = Ph, R^2 = Me	100	9
9[a]		R^1 = Ph, R^2 = Ph	95	12
10[b]		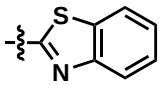	51	26
11[b]	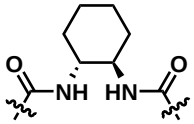	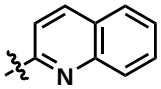	83	19
12[b]		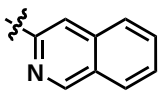	69	19
13[b]		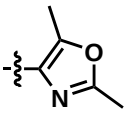	67	20
14[b]	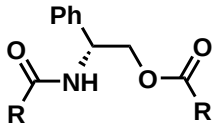	R = 2-pyridyl	80	19
15[c]	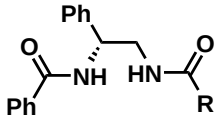	R = 2-pyridyl	42	27
16[c]	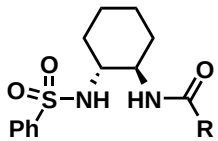		91	14
17[b]	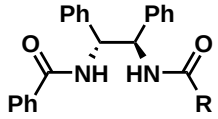		59	17

18[a]	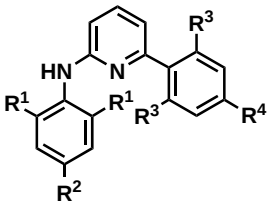	R^1,R^2,R^3,R^4= Me	89	13
19[a]		R^1,R^3,R^4= *i*Pr, R^2= H	81	16
20[a]		R^1= *i*Pr, R^2,R^4= H, R^3= Me	56	23
21[b]	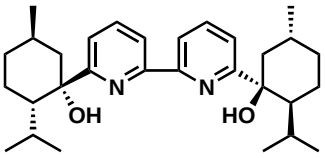		72	19
22[b]	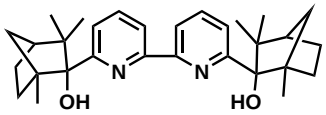		78	17
23[d]	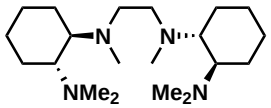		98	11
24[e]	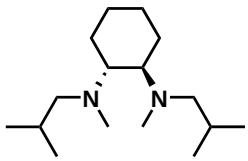		100	9
25[c]	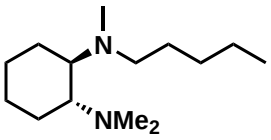		82	14
26[c]	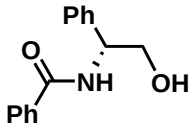		98	11
27[c]	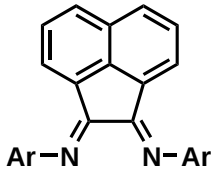	Ar = Ph	58	32
28[c]		Ar = 2,6-diisopropylphenyl	1	12
29[c]		Ar = 4-$MeOC_6H_4$	58	31

30[c]	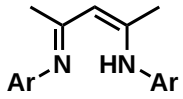	Ar = 2,6-diisopropylphenyl	68	19
31[c]	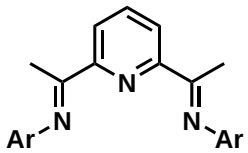	Ar = 2,6-diisopropylphenyl	63	27
32[c]	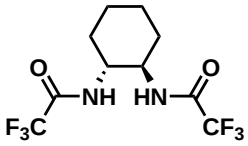		100	9
33[c]	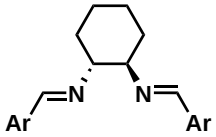	Ar = 2-pyridyl	68	21
34[b]	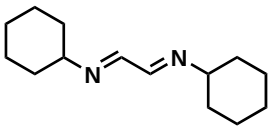		26	22
35[e]	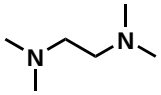		93	11

[a] 10 mol% [L], 1.35 equiv. 4-tolylMgBr. [b] 5 mol% [L], 1.35 equiv. 4-tolylMgBr. [c] 10 mol% [L], 1.45 equiv. 4-tolylMgBr. [d] 5 mol% [L], 1.25 equiv. 4-tolylMgBr. [e] 10 mol% [L], 1.25 equiv. 4-tolylMgBr.

5.4.6.5 Further Investigation into Ligand Activity

Table 5.16: Comparison of the cross-coupling efficiency of selected ligand systems with TMEDA.

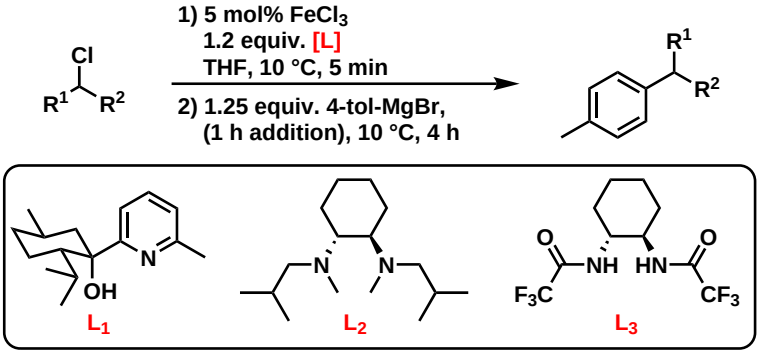

Entry	Product	Ligand [L]	Yield [%] [a]
1	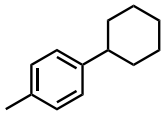	–	40 [b]
2		TMEDA	50 [b]
3		L_1	83 [b]
4		L_2	54 [b]
5		L_3	72 [b]
6	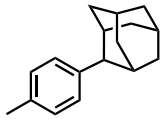	TMEDA	18
7		L_1	19
8		L_2	15
9		L_3	14
10	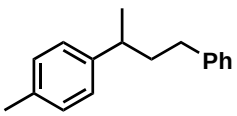	–	46 [b]
11		TMEDA	63, 22 [b]
12		L_1	64, 50 [b]
13		L_2	70, 39 [b]
14		L_3	40

[a] GC yields (vs. *n*-pentadecane as internal reference), [b] -10 °C.

5.4.6.6 Use of Well-Defined Iron(II) Complexes

The 4-tolylmagnesium bromide was synthesized like described in general procedure 3. Under an inert atmosphere, a Schlenk tube was charged with iron(II) complex (5 mol%) (Figure 5.2) and treated with 2 ml dry toluene. The resulting solution was put in a water bath at 10 °C and chlorocyclohexane (1 mmol) was added via syringe, followed by the freshly prepared 4 tolylmagnesium bromide solution (1.5 equiv., 1 M in THF), mixed with TMEDA (1.35 equiv.) unless noted otherwise, over 1 h. The mixture was stirred at 10 °C for 4 h. Then, saturated aqueous NH_4Cl was added, and the mixture was extracted with ethyl acetate. The combined organic layers were dried ($MgSO_4$) and analyzed by quantitative GC FID.

Table 5.17: Results of cross-coupling using well-defined iron(II) complexes.

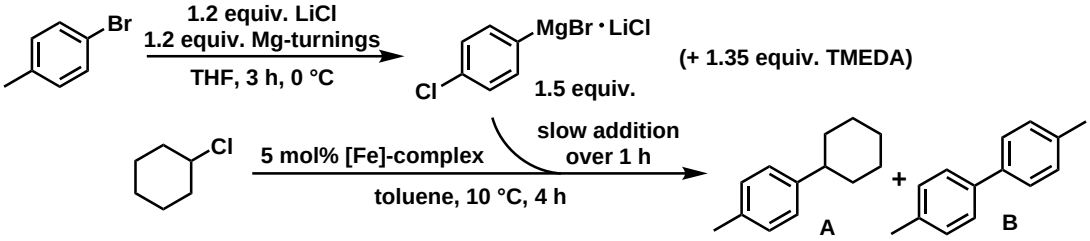

Entry	Complex	TMEDA	Yield of **A** (%) [a]	Yield of **B** (%) [a]
1	K1a	no	0	0
2	K1a	yes	0	6
3	K1b	no	34	18
4	K1c	no	11	15
5	K1d	no	17	20
6	K1d	yes	25	10
7	K2a	no	48	35
8	K2a	yes	75	10
9	K2b	no	50	25
10	K3a	yes	11	10
11	K3b	yes	60	9
12	K4	yes	0	11
13	K5	no	55	22
14	K5	yes	58	6

15	K6	yes	25	12
16	K7	no	15	22
17	K8	yes	68	9
18	K9	yes	21	8

[a] GC yields (vs. *n*-pentadecane as internal reference)

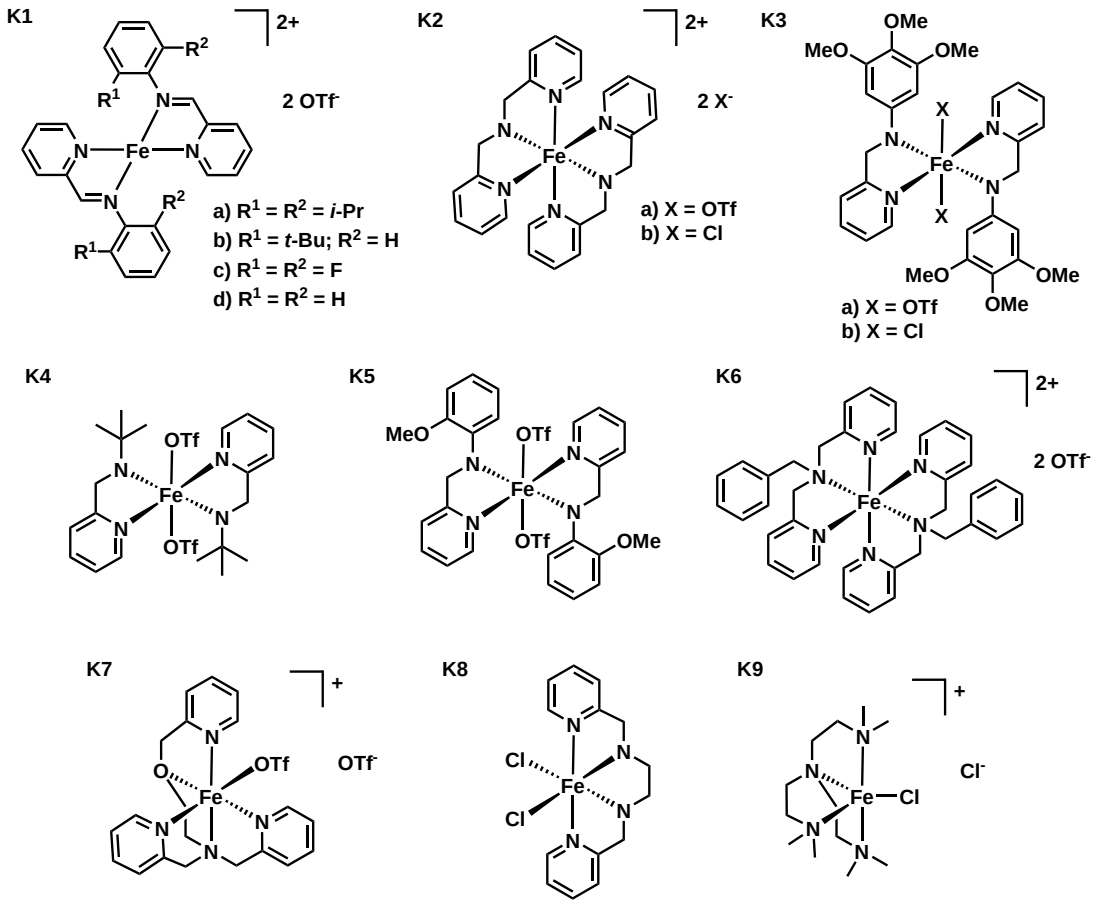

Figure 5.2: Selection of preformed iron(II) complexes.

5.4.7 Mechanistical Investigations

5.4.7.1 Using 4-Chlorophenylmagnesium Bromide

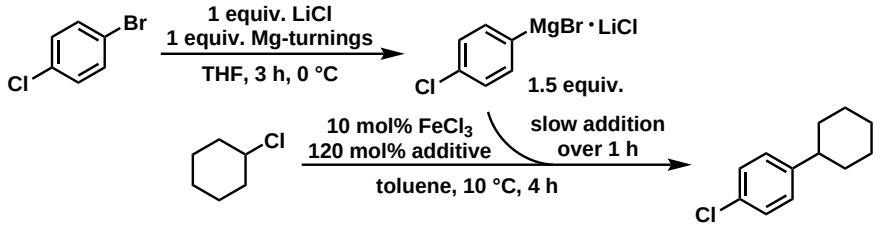

Scheme 5.5: 4-Chlorophenyl Grignard reagents in iron-catalyzed cross-coupling of sec. alkyl chlorides.

The 4-chlorophenylmagnesium bromide was synthesized like described in general procedure 3 using just 1 equiv. Mg-turnings and 1 equiv. LiCl. Under an inert atmosphere, a Schlenk tube was charged with $FeCl_3$ (10 mol%) and treated with 2 ml dry toluene and distilled TMEDA (1.2 equiv.). The resulting yellow solution was put in a water bath at 10 °C and chlorocyclohexane (1 mmol) was added via syringe, followed by the freshly prepared 4 chlorophenylmagnesium bromide solution (1.5 equiv., 1 M in THF) over 1 h. The mixture was stirred at 10 °C for 4 h. Then, saturated aqueous NH_4Cl was added, and the mixture was extracted with ethyl acetate. The combined organic layers were dried ($MgSO_4$) and analyzed by GC-MS.

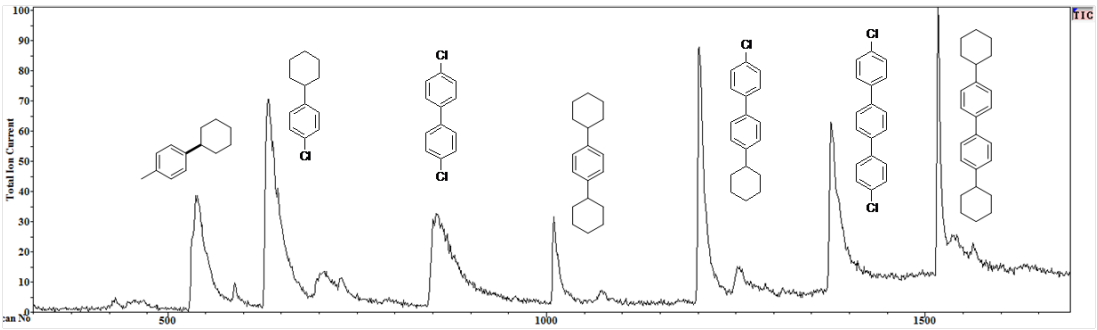

Figure 5.3: GC-MS spectrum of iron-catalyzed cross coupling using 4-chlorophenyl Grignard reagent.

5.4.7.2 Catalyst Poisoning Experiments Under Ligand-Free Conditions

In a glovebox an oven-dried 4 ml autoclave vial with PTFE screw cap containing a stir bar was charged with $FeCl_3$ (0.025 mmol, 4.1 mg) which was dissolved in 2 ml THF. After addition of chlorocyclohexane (0.5 mmol, 59.3 μL) and *n*-pentadecane (50 μL) as internal standard, the vial was transferred to a cooling bath. After the reaction mixture was cooled to 10 °C, a freshly prepared solution of 4-tolyl magnesium bromide in THF (1.24 M, 0.625 mmol, 0.92 μL) was added and the reaction stirred for 1 h. To monitor the reaction, aliquots of the reaction mixture were taken after certain time intervalls, quenched in sat. NH_4Cl solution, extracted with ethyl acetate and analyzed via GC-FID. At 50% conversion (17 min; determined in a previous reaction progress analysis) a solution of DCT (10 mol%, 10.2 mg) in THF was added to the reaction mixture.

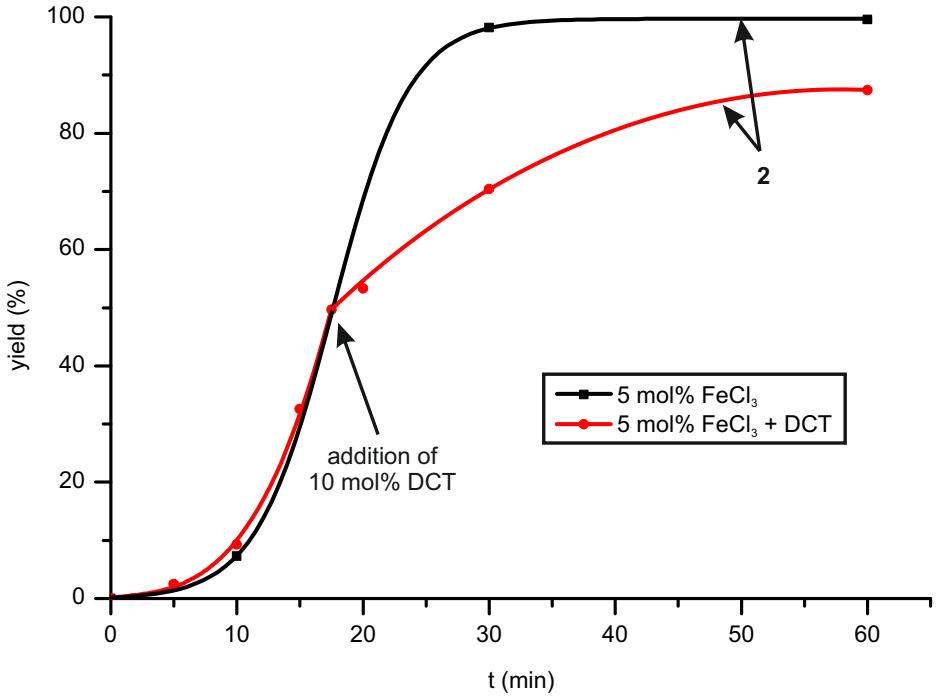

Figure 5.4: Influence of the addition of DCT in the cross coupling reaction of **1** with 4-tol-MgBr.

5.4.7.3 Radical Clock Experiments

In a glovebox an oven-dried 4 ml autoclave vial with PTFE screw cap containing a stir bar was charged with dipp$_2$nacnacFe(*p*-tol) (0.02 mmol, 11.3 mg) which was dissolved in a 0.33 M solution of *n*-pentadecane in dry THF (0.02 mmol, 600 μL). Previously prepared stock solutions of (bromomethyl)cyclopropane in dry THF (0.1 M, 0.02 mmol, 200 μL) and of 4-tolylmagnesium bromide in dry THF (0.1 M, 0.02 mmol,

200 μL) were added to the reaction vial and the mixture stirred for 3 h at room temperature. The reaction was then quenched with the addition of a couple drops of an aqueous ammonium chloride solution and eluted over a short silica gel column directly into a GC vial using ethyl acetate. The product yield was determined via quantitative GC-FID and the reaction mixture analyzed with NMR.

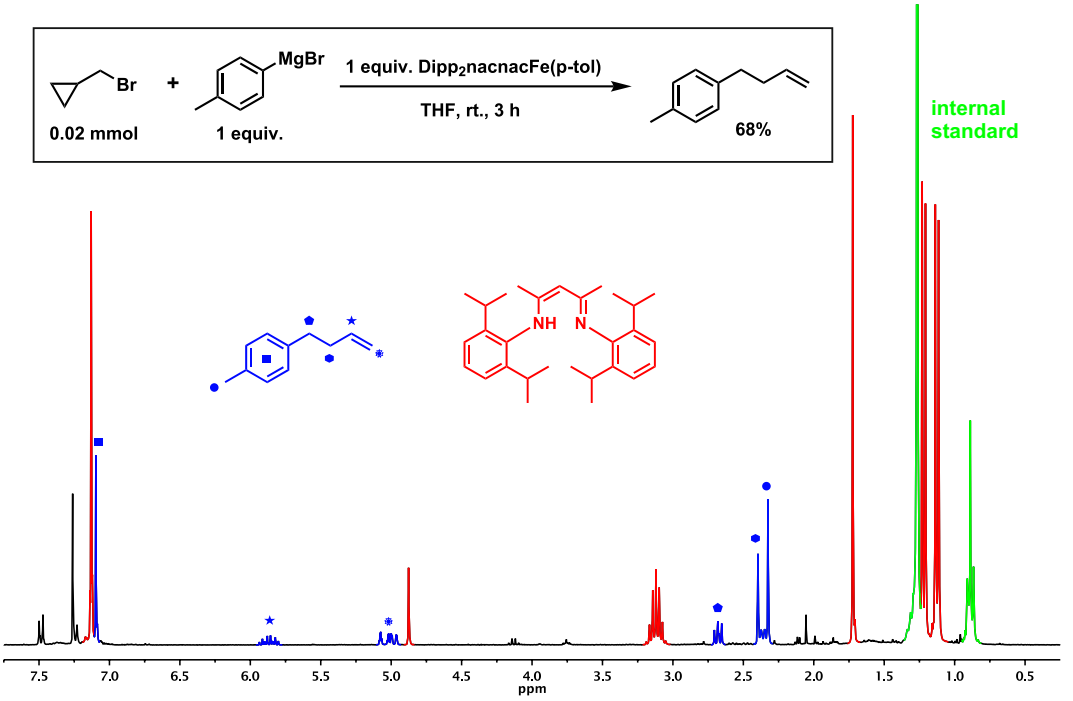

Figure 5.5: NMR analysis of radical clock experiment.

5.4.7.4 Competition Reactions Between $L^{Me}FeAr$ and Ar'MgBr

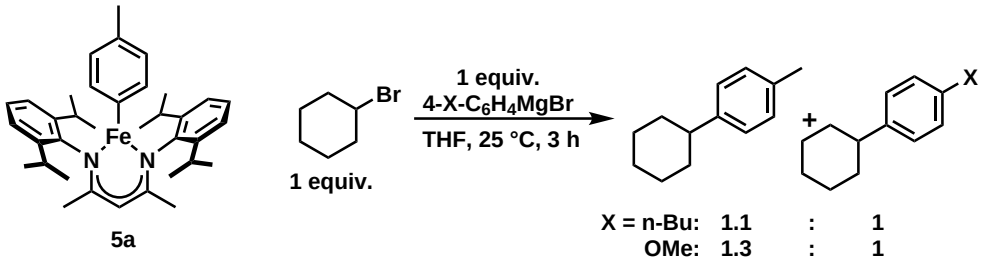

Figure 5.6: Competition reactions between $L^{Me}FeAr$ and Ar'MgBr.

5.4.8 Isolated Coupling Products

1-Cyclohexyl-4-methylbenzene

According to general procedure 2: Using 5 mol% $FeCl_3$ (0.1 mmol, 16.2 mg), 4 ml toluene, chlorocyclohexane (2 mmol, 237 μL) and 1.5 equiv. 4-tolylmagnesium bromide (3 mmol, 3 ml). Purification by SiO_2 column chromatography (cyclohexane).

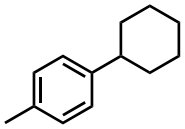

Colorless oil

$C_{13}H_{18}$

174.14 g/mol

Yield 91% (GC-FID)

TLC R_f = 0.49 (SiO_2, cyclohexane)

^{1}H-NMR (300 MHz, $CDCl_3$) δ 1.48-1.64 (m, 5H), 1.89-2.01 (m, 5H), 2.48 (s, 3H), 2.62 (m, 1H), 7.27 (s, 4H).

^{13}C-APT-NMR (75 MHz, $CDCl_3$) δ 21.0 (u), 26.2 (d), 27.0 (d), 34.6 (d), 44.2 (u), 126.6 (u), 128.9 (u), 135.1 (d), 145.1 (d).

GC-MS t_R = 6.73 min, (EI, 70 eV): m/z = 174 [M^+], 159, 131, 105, 91, 77, 65, 51.

HR-MS (EI, 70 eV, m/z): 174.141, calcd: 174.1409.

Analytical data in accordance with literature data: M. Nakamura, K. Matsuo, S. Ito, E. Nakamura, J. Am. Chem. Soc. 2004, 126, 3686-3687.

1-Methyl-4-(4-phenylbutane-2-yl)benzene

According to general procedure 2: Using 5 mol% $FeCl_3$ (0.1 mmol, 16.2 mg) and 10 mol% $FeCl_3$ (0.2 mmol, 32.4 mg), 4 ml toluene, 2-chloro-4-phenylbutane (2 mmol, 325 μL) and 1.5 equiv. 4-tolylmagnesium bromide (3 mmol, 3 ml). Purification by SiO_2 column chromatography (cyclohexane).

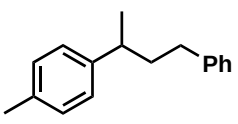

Colorless oil

$C_{17}H_{20}$

224.16 g/mol

Yield 66% (GC-FID)

TLC R_f = 0.45 (SiO_2, cyclohexane)

^{1}H-NMR	(300 MHz, $CDCl_3$) δ 1.29 (d, J = 6.9 Hz, 3H), 1.93 (m, 2H), 2.37 (s, 3H), 2.54 (t, J = 7.9 Hz, 2H), 2.72 (m, 1H), 7.11-7.32 (m, 9H).
^{13}C-APT-NMR	(75 MHz, $CDCl_3$) δ 21.0 (u), 22.6 (u), 33.9 (d), 39.1 (u), 40.0 (d), 125.6 (u), 127.0 (d), 128.2 (d), 128.4 (d), 129.1 (d).
GC-MS	t_R = 8.42 min, (EI, 70 eV): m/z = 224 [M^+], 133, 119, 91, 65.
HR-MS	(EI, 70 eV, m/z): 224.156, calcd: 224.1565.

1-Methyl-4-(4-phenylbutane-2-yl)benzene

According to general procedure 2: Using 5 mol% $FeCl_3$ (0.1 mmol, 16.2 mg) and 10 mol% $FeCl_3$ (0.2 mmol, 32.4 mg), 4 ml toluene, 2-chloro-4-phenylbutane (2 mmol, 325 μL) and 1.5 equiv. 4-tolylmagnesium bromide (3 mmol, 3 ml). Purification by SiO_2 column chromatography (cyclohexane).

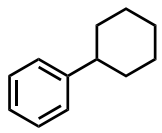

	Colorless oil
	$C_{12}H_{16}$
	160.26 g/mol
Yield	229 mg (1.42 mmol, 71%)
TLC	R_f = 0.56 (SiO_2, cyclohexane)
^{1}H-NMR	(300 MHz, $CDCl_3$) δ 1.47 (m, 5H), 1.92 (m, 5H), 2.60 (m, 1H), 7.33 (m, 5H).
^{13}C-APT-NMR	(75 MHz, $CDCl_3$) δ 26.2 (d), 26.9 (d), 34.5 (d), 44.6 (u), 125.7 (u), 126.8 (u), 128.2 (u), 148.0 (d).
GC-MS	t_R = 6.15 min, (EI, 70 eV): m/z = 160 [M^+], 154, 129, 117, 104, 91, 82, 78, 74, 51.

Analytical data in accordance with literature data: N. A. Strotman, S. Sommer, G. C. Fu, Angew. Chem. 2007, 119, 3626-3628; Angew. Chem. Int. Ed. 2007, 46, 3556-3558.

1-(2-Butyl)-4-methylbenzene

According to general procedure 2: Using 5 mol% $FeCl_3$ (0.1 mmol, 16.2 mg), 4 ml toluene, 2 chlorobutane (2 mmol, 212 μL) and 1.5 equiv. 4-tolylmagnesium bromide (3 mmol, 3 ml). Purification by SiO_2 column chromatography (cyclohexane).

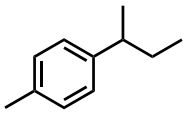

Colorless oil

$C_{11}H_{16}$

148.24 g/mol

Yield 140 mg (0.94 mmol, 47%); 97% (GC-FID)

TLC R_f = 0.61 (SiO_2, cyclohexane)

^{1}H-NMR (300 MHz, $CDCl_3$) δ 0.86 (t, J = 7.4 Hz, 3H), 1.26 (m, 3H), 1.62 (m, 2H), 2.36 (s, 3H), 2.60 (m, 1H), 7.11 (m, 4H).

^{13}C-APT-NMR (75 MHz, $CDCl_3$) δ 12.3 (u), 21.0 (u), 21.9 (u), 31.2 (d), 41.3 (u), 127.0 (u), 128.9 (u), 135.1 (d), 144.6 (d).

GC-MS t_R = 4.80 min, (EI, 70 eV): m/z = 148 [M^+], 133, 119, 105, 91, 77, 65, 51.

Analytical data in accordance with literature data: J. Bayardon, J. Holz, B. Schäffner, V. Andrushko, S. Verkin, A. Preets, A. Börner, Angew. Chem. 2007, 119, 6075-6078; Angew. Chem. Int. Ed. 2007, 46, 5971-5974.

1-Cyclopentyl-4-methylbenzene

According to general procedure 2: Using 5 mol% $FeCl_3$ (0.1 mmol, 16.2 mg), 4 ml toluene, chlorocyclopentane (2 mmol, 208 μL) and 1.5 equiv. 4-tolylmagnesium bromide (3 mmol, 3 ml). Purification by SiO_2 column chromatography (cyclohexane).

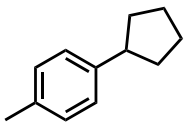

Colorless oil

$C_{12}H_{16}$

160.13 g/mol

Yield 170 mg (1.06 mmol, 53%); 61% (GC-FID)

TLC R_f = 0.61 (SiO_2, cyclohexane)

^{1}H-NMR (300 MHz, $CDCl_3$) δ 1.66-195 (m, 6H), 2.20 (m, 2H), 2.46 (s, 3H), 3.10 (m, 1H), 7.26 (m, 4H).

^{13}C-APT-NMR (75 MHz, $CDCl_3$) δ 20.9 (u), 25.5 (d), 34.7 (d), 45.6 (u), 126.9 (u), 128.9 (u), 135.0 (d), 143.4 (d).

GC-MS t_R = 6.20 min, (EI, 70 eV): m/z = 160 [M^+], 131, 115, 91, 65.

Analytical data in accordance with literature data: M. P. D. Mahindaratne, K. Wimalasena, J. Org. Chem. 1998, 63, 2858-286.

1-Cyclohexyl-4-methoxybenzene

According to general procedure 2: Using 5 mol% $FeCl_3$ (0.1 mmol, 16.2 mg), 4 ml THF, chlorocyclohexane (2 mmol, 237 μL) and 1.5 equiv. 4-methoxyphenylmagnesium bromide (3 mmol, 3 ml). Purification by SiO_2 column chromatography (cyclohexane/ethyl acetate 99:1).

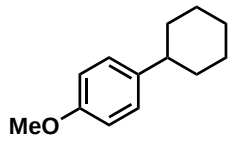

	Colorless oil
	$C_{13}H_{18}O$
	190.28 g/mol
Yield	361 mg (1.89 mmol, 95%)
TLC	R_f = 0.53 (SiO_2, cyclohexane/ethyl acetate (99:1))
^{1}H-NMR	(300 MHz, $CDCl_3$) δ 1.48 (m, 6H), 1.99 (m, 4H), 2.59 (m, 1H), 3.89 (s, 3H), 6.97 (d, J = 8.7 Hz, 2H), 7.26 (d, J = 8.9 Hz, 2H).
^{13}C-APT-NMR	(75 MHz, $CDCl_3$) δ 26.1 (d), 26.9 (d), 34.7 (d), 43.6 (u), 55.0 (u), 113.6 (u), 127.5 (u), 140.2 (d), 157.6 (d).
GC-MS	t_R = 7.53 min, (EI, 70 eV): m/z = 174 [M^+], 159, 131, 105, 91, 77, 65, 51.
HR-MS	(EI, 70 eV, m/z): 190.135, calcd: 190.1358.

Analytical data in accordance with literature data: M. Nakamura, K. Matsuo, S. Ito, E. Nakamura, J. Am. Chem. Soc. 2004, 126, 3686-3687.

1-Dodecyl-4-methylbenzene

According to general procedure 2: Using 10 mol% $FeCl_3$ (0.2 mmol, 32.4 mg), 4 ml toluene, 1 chlorododecane (2 mmol, 472 μL) and 1.5 equiv. 4-tolylmagnesium bromide (3 mmol, 3 ml). Purification by SiO_2 column chromatography (cyclohexane).

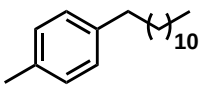

	Colorless oil
	$C_{19}H_{32}$
	260.46 g/mol
Yield	38% (GC-FID)
TLC	R_f = 0.44 (SiO_2, cyclohexane)
^{1}H-NMR	(300 MHz, $CDCl_3$) δ 0.94 (t, J = 6.0 Hz, 3H), 1.31 (m, 18H), 1.64 (m, 2H), 2.36 (s, 3H), 2.61 (t, J = 7.6 Hz, 2H), 7.12 (m, 4H).

^{13}C-APT-NMR	(75 MHz, $CDCl_3$) δ 14.1 (u), 21.0 (u), 22.7 (d), 29.4 (d), 29.6 (d), 29.7 (d), 31.7 (d), 32.0 (d), 35.5 (d), 128.3 (u), 128.9 (u), 134.9 (d), 139.9 (d).
GC-MS	t_R = 9.22 min, (EI, 70 eV): m/z = 260 [M^+], 147, 131, 105, 79, 55.

Analytical data in accordance with literature data: G. Cahiez, V. Habiak, C. Duplais, A. Moyeux, Angew. Chem. 2007, 119, 4442-4444; Angew. Chem. Int. Ed. 2007, 46, 4364-4366.

1-Dodecylbenzene

According to general procedure 2: Using 10 mol% $FeCl_3$ (0.2 mmol, 32.4 mg), 4 ml toluene, 1 chlorododecane (2 mmol, 472 μL) and 1.5 equiv. 4-tolylmagnesium bromide (3 mmol, 3 ml). Purification by SiO_2 column chromatography (cyclohexane).

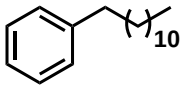

	Colorless oil
	$C_{18}H_{30}$
	246.43 g/mol
Yield	15% (GC-FID)
TLC	R_f = 0.51 (SiO_2, cyclohexane)
^{1}H-NMR	(300 MHz, $CDCl_3$) δ 0.94 (t, J = 6.3 Hz, 3H), 1.33 (m, 18H), 1.66 (m, 2H), 2.65 (t, J = 7.6 Hz, 2H), 7.21-7.34 (m, 5H).
^{13}C-APT-NMR	(75 MHz, $CDCl_3$) δ 14.1 (u), 22.7 (d), 29.4 (d), 29.7 (d), 31.5 (d), 31.9 (d), 36.0 (d), 125.5 (u), 128.2 (u), 128.4 (u), 142.9 (d).
GC-MS	t_R = 8.81 min, (EI, 70 eV): m/z = 247 [M^+], 134, 119, 92, 57.
HR-MS	(EI, 70 eV, m/z): 246.235, calcd: 246.2348.

Analytical data in accordance with literature data: T. Brenstrum, D. A. Gerristma, G. M. Adjabeng, C. S. Frampton, J. Britten, A. J. Robertson, J. McNulty, A. Capretta, J. Org. Chem. 2004, 69, 7635-7639.

1-Cyclohexyl-4-tert-butylbenzene

According to general procedure 2: Using 5 mol% $FeCl_3$ (0.1 mmol, 16.2 mg), 4 ml THF, chlorocyclohexane (2 mmol, 237 μL) and 1.5 equiv. 4-tert-butylphenylmagnesium bromide (3 mmol, 3 ml). Purification by SiO_2 column chromatography(cyclohexane).

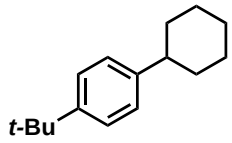

	Colorless oil
	$C_{16}H_{24}$
	216.36 g/mol
Yield	381 mg (1.76 mmol, 88%)
TLC	R_f = 0.50 (SiO_2, cyclohexane)
^{1}H-NMR	(300 MHz, $CDCl_3$) δ 1.41 (s, 9H), 1.45-1.62 (m, 5H), 1.82-2.00 (m, 5H), 2.57 (m, 1H), 7.24 (d, J = 8.4 Hz, 2H), 7.41 (d, J = 8.4 Hz, 2H).
^{13}C-APT-NMR	(75 MHz, $CDCl_3$) δ 26.4 (d), 27.1 (d), 31.6 (u), 34.5 (u), 34.6 (d); 44.1 (u), 125.3 (u), 126.6 (u), 145.1 (d), 148.5 (d).
GC-MS	t_R = 9.54 min, (EI, 70 eV): m/z = 216 [M^+], 201, 159, 145, 128, 105, 91, 77, 55.
FT-IR	(ATR film) $1/\lambda$ [cm^{-1}] = 3051 (w), 2957 (s), 2920 (s), 2848 (s), 2357 (w), 1898 (w), 1783 (w), 1651 (w), 1518 (m), 1506 (m), 1446 (s), 1360 (m), 1268 (m), 1107 (m), 997 (m), 822 (s), 759 (m).

Analytical data in accordance with literature data: E. Grovenstein, P.-C. Lu, J. Org. Chem. 1982, 47, 2928-2939.

2-(4-Tolyl)-adamantane

According to general procedure 2: Using 5 mol% $FeCl_3$ (0.1 mmol, 16.2 mg), 4 ml toluene, 2-chloroadamantane (2 mmol, 341 mg) and 1.5 equiv. 4-tolylmagnesium bromide (3 mmol, 3 ml). Purification by SiO_2 column chromatography (cyclohexane).

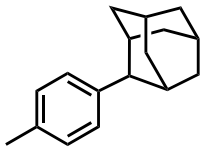

	Colorless oil
	$C_{17}H_{22}$
	226.36 g/mol
Yield	276 mg (1.22 mmol, 61%)
Melting point:	55 °C
TLC	R_f = 0.55 (SiO_2, cyclohexane)
^{1}H-NMR	(300 MHz, $CDCl_3$) δ 1.58 (m, 2H), 1.80-2.01 (m, 10H), 2.37 (s, 3H), 2.48 (s, 2H), 3.00 (s, 1H), 7.17 (d, J = 8.0 Hz, 2H), 7.29 (d, J = 8.0 Hz, 2H).
^{13}C-APT-NMR	(75 MHz, $CDCl_3$) δ 21.0 (u), 28.0 (u), 28.2 (u), 31.2 (u), 32.1 (d), 38.1 (d), 39.3 (d), 46.6 (u), 126.8 (u), 129.0 (u), 134.6 (d), 141.5 (d).

GC-MS	t_R = 9.54 min, (EI, 70 eV): m/z = 216 [M^+], 201, 159, 145, 128, 105, 91, 77, 55.
HR-MS	(EI, 70 eV, m/z): 226.172, calcd: 226.1722.
FT-IR	(ATR film) $1/\lambda$ [cm^{-1}] = 3020 (w), 2896 (s), 2844 (s), 2668 (w), 1892 (w), 1572 (w), 1512 (s), 1466 (m), 1447 (s), 1353 (m), 1189 (m), 1127 (m), 1098 (s), 1068 (m), 967 (m), 827 (s), 758 (s).

Analytical data in accordance with literature data: G. A. Olah, A. Wu, O. Farooq, J. Org. Chem. 1988, 53, 5143-5145.

N,N-Dimethylamino-4-cyclohexylbenzene

According to general procedure 2: Using 10 mol% $FeCl_3$ (0.2 mmol, 32.4 mg), 4 ml THF, chlorocyclohexane (2 mmol, 237 μL) and 1.5 equiv. 4-(N,N-dimethylamino)-phenylmagnesium bromide (3 mmol, 3 ml). Purification by SiO_2 column chromatography (methanol/toluene/NEt_3 88:10:2).

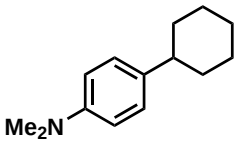

Brown oil

$C_{14}H_{21}N$

203.32 g/mol

Yield	246 mg (1.22 mmol, 61%); 88% (NMR with hexamethyldisiloxane as internal standard)
TLC	R_f = 0.78 (SiO_2, methanol/toluene/NEt_3 88:10:2)
^{1}H-NMR	(300 MHz, $CDCl_3$) δ 1.26-1.61 (m, 5H), 1.78-2.07 (m, 5H), 2.44-2.63 (m, 1H), 3.02 (s, 6H), 6.82 (d, J = 8.4 Hz, 2H), 7.22 (d, J = 8.4 Hz, 2H).
^{13}C-APT-NMR	(75 MHz, $CDCl_3$) δ 26.34 (d), 27.13 (d), 34.83 (d), 40.99 (u), 43.59 (u), 113.03 (u), 127.38 (u), 136.62 (d), 149.07 (d).
GC-MS	t_R = 8.22 min, (EI, 70 eV): m/z = 203 [M^+], 174, 160, 134, 115, 91, 77, 56.
HR-MS	(EI, 70 eV, m/z): 203.167, calcd: 203.1674.
FT-IR	(ATR film) $1/\lambda$ [cm^{-1}] = 3420 (b), 2917 (s), 2845 (s), 2793 (m), 1868 (w), 1709 (w), 1611 (s), 1517 (s), 1477 (m), 1444 (s), 1339 (s), 1223 (m), 1161 (s), 1127 (s), 1058 (m), 946 (s), 809 (s).

Analytical data in accordance with literature data: W. M. Czaplik, M. Mayer, A. Jacobi von Wangelin, Angew. Chem. 2009, 121, 616-620; Angew. Chem. Int. Ed. 2009, 48, 607-610.

1-Methyl-4-(4-tolyl)piperidine

According to general procedure 2: Using 10 mol% $FeCl_3$ (0.2 mmol, 32.4 mg), 4 ml toluene, 4-chloro-1-methylpiperidine (2 mmol, 267 mg) and 1.5 equiv. 4-tolylmagnesium bromide (3 mmol, 3 ml). Purification by SiO_2 column chromatography (methanol/toluene/NEt_3 88:10:2).

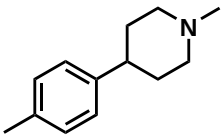

Yellow oil

$C_{13}H_{19}N$

189.30 g/mol

Yield 246 mg (1.22 mmol, 61%); 88% (NMR with hexamethyldisiloxane as internal standard)

TLC R_f = 0.44 (SiO_2, methanol/toluene/NEt_3 88:10:2)

^{1}H-NMR (300 MHz, $CDCl_3$) δ 1.83-1.86 (m, 4H), 2.03-2.12 (m, 2H), 2.34 (s, 6H), 2.41-2.52 (m, 1H), 2.98-3.02 (m, 2H), 7.14-7.28 (m, 4H).

^{13}C-APT-NMR (75 MHz, $CDCl_3$) δ 21.1 (u), 33.7 (d), 41.7 (u), 46.6 (u), 56.5 (d), 126.9 (u), 129.2 (u), 135.8 (d), 143.4 (d).

GC-MS t_R = 7.10 min, (EI, 70 eV): m/z = 189 [M^+], 174, 160, 146, 131, 117, 97.

HR-MS (EI, 70 eV, m/z): 189.152, calcd: 189.1517.

4-(4-Methoxyphenyl)-1-methylpiperidine

According to general procedure 2: Using 10 mol% $FeCl_3$ (0.2 mmol, 32.4 mg), 4 ml THF, 4 chloro-1-methylpiperidine (2 mmol, 267 mg) and 1.5 equiv. 4-methoxyphenylmagnesium bromide (3 mmol, 3 ml). Purification by SiO_2 column chromatography (methanol/toluene/NEt_3 88:10:2).

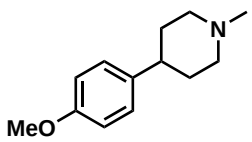

Brown oil

$C_{13}H_{19}NO$

205.15 g/mol

Yield 224 mg (1.10 mmol, 55%)

TLC R_f = 0.80 (SiO_2, methanol/toluene/NEt_3 88:10:2)

^{1}H-NMR (300 MHz, $CDCl_3$) δ 1.70-1.90 (m, 5H), 1.99-2.15 (m, 2H), 2.33 (s, 3H), 2.99 (d, J = 11.2, 2H), 3.78 (s, 3H), 6.86 (d, J = 8.0 Hz, 2H), 7.16 (d, J = 8.1 Hz, 2H).

^{13}C-APT-NMR	(75 MHz, $CDCl_3$) δ 33.5 (d), 41.1 (u), 46.3 (u), 55.2 (u), 56.3 (d), 113.9 (u), 127.8 (u), 133.5 (d), 157.9 (d).
GC-MS	t_R = 7.84 min, (EI, 70 eV): m/z = 205 [M^+], 134, 119, 97, 82, 70, 57.
FT-IR	(ATR film) $1/\lambda$ [cm^{-1}] = 2934 (m), 2837 (w), 2782 (w), 2679 (w), 1673 (w), 1607 (m), 1512 (s), 1465 (m), 1445 (m), 1378 (w), 1272 (m), 1244 (s), 1178 (s), 1133 (w), 1039 (s), 824 (s), 776 (w), 637 (m), 604 (m), 549 (m), 494 (m), 459 (w), 416 (m).

1-Cyclohexyl-4-fluorbenzene

According to general procedure 2: Using 10 mol% $FeCl_3$ (0.2 mmol, 32.4 mg), 4 ml THF, no TMEDA, chlorocyclohexane (2 mmol, 237 mg) and 1.5 equiv. 4-fluorophenylmagnesium bromide (3 mmol, 3 ml). Purification by SiO_2 column chromatography (cyclohexane/ethyl acetate 88:1).

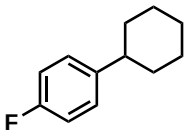

	Colorless oil
	$C_{12}H_{15}F$
	178.25 g/mol
Yield	94% (GC-FID)
TLC	R_f = 0.60 (SiO_2, cyclohexane/ethyl acetate 88:1)
^{1}H-NMR	(300 MHz, $CDCl_3$) δ 1.27-1.48 (m, 10H), 2.49 (m, 1H), 6.99 (m, 2H), 7.18 (m, 2H).
^{13}C-APT-NMR	(75 MHz, $CDCl_3$) δ 26.2 (d), 27.1 (d), 34.8 (d), 44.0 (u), 115.0 (d, J = 20.8 Hz; u), 126.6 (d, J = 7.6 Hz; u), 144.0 (d, J = 3.4 Hz; d), 161.6 (d, J = 242.3 Hz; d).
GC-MS	t_R = 6.08 min, (EI, 70 eV): m/z = 178 [M^+], 163, 149, 135, 121, 109, 83, 67, 51.
HR-MS	(EI, 70 eV, m/z): 178.116, calcd: 178.1158.

Analytical data in accordance with literature data: S. K. Ghorai, M. Jin, T. Hatakeyama, M. Nakamura, *Org. Lett.* **2012**, *14*, 1066-1069.

(*S*)-2-Benzyl-4-(4-tolyl)-tetrahydro-2*H*-pyrane

According to general procedure 2: Using 10 mol% $FeCl_3$ (0.2 mmol, 32.4 mg), 4 ml toluene, (2*S*,4*R*)-2-benzyl-4-chloro-tetrahydro-2*H*-pyrane (2 mmol, 421.4 mg) and 1.5 equiv. 4 tolylmagnesium bromide (3 mmol, 3 ml). Purification by SiO_2 column chromatography (cyclohexan/ethyl acetate 5:1).

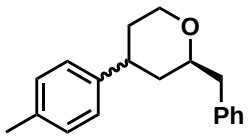

	Colorless oil
	$C_{19}H_{22}O$
	266.38 g/mol
Yield	430 mg (1.61 mmol, 81% (75 : 25))
TLC	*major:* R_f = 0.50 (SiO_2, cyclohexane/ethyl acetate 5:1)
^{1}H-NMR	*major:* (300 MHz, $CDCl_3$) δ 1.75-1.92 (m, 2H), 1.94-2.10 (m, 2H), 2.35-2.44 (m, 3H), 2.67-2.83 (m, 1H), 2.89-3.26 (m, 2H), 3.49-3.76 (m, 1H), 3.79-4.02 (m, 1H), 4.11-4.25 (m, 1H), 7.16-7.19 (m, 1H), 7.20 (s, 2H), 7.26-7.40 (m, 6H).
^{13}C-APT-NMR	*major:* (75 MHz, $CDCl_3$) δ 21.0 (u), 33.6 (d), 39.0 (d), 41.4 (u), 43.2 (d), 68.4 (d), 78.8 (u), 126.3 (u), 126.7 (u), 127.1 (u), 128.3 (u), 128.5 (u), 129.2 (u), 129.5 (u), 135.9 (d), 139.0 (d), 142.9 (d).
GC-MS	*major:* t_R = 9.93 min, (EI, 70 eV): m/z = 266 [M^+], 248, 175, 119, 105, 91.
HR-MS	*major:* (EI, 70 eV, m/z): 266.168, calcd: 266.1671.

(*S*)-2-*tert*-Butyl-4-*p*-tolyl-tetrahydro-2*H*-pyrane

According to general procedure 2: Using 10 mol% $FeCl_3$ (0.2 mmol, 32.4 mg), 4 ml toluene, (2*S*,4*R*)-2-benzyl-4-chloro-tetrahydro-2*H*-pyrane (2 mmol, 421.4 mg) and 1.5 equiv. 4 tolylmagnesium bromide (3 mmol, 3 ml). Purification by SiO_2 column chromatography (cyclohexan/ethyl acetate 5:1).

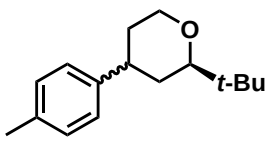

	Colorless oil
	$C_{16}H_{24}O$
	232.36 g/mol
Yield	74% (97 : 3) (GC-FID)
TLC	*major:* R_f = 0.66 (SiO_2, cyclohexane/ethyl acetate 4:1)

^{1}H-NMR	*major:* (300 MHz, $CDCl_3$) δ 1.07 (s, 9H), 1.55 (td, J = 12.5, 11.1 Hz, 1H), 1.77-1.87 (m, 2H), 2.51 (s, 3H), 2.75-2.90 (m, 1H); 3.15 (dd, J = 11.1, 1.8 Hz, 1H), 3.58-3.71 (m, 1H), 4.21-4.33 (m, 1H), 7.35 (d, J = 7.8 Hz, 2H), 7.61 (d, J = 8.1 Hz, 2H).
^{13}C-APT-NMR	*major:* (75 MHz, $CDCl_3$) δ 21.1 (u), 26.3 (u), 33.8 (d), 34.2 (d), 42.0 (u), 68.7 (d), 85.9 (u), 126.8 (u), 129.3 (u), 135.8 (d), 143.5 (d).
GC-MS	*major:* t_R = 7.97 min, (EI, 70 eV): m/z = 232 [M^+], 217, 175, 157, 145, 131, 119, 105, 91, 51.
HR-MS	*major:* (EI, 70 eV, m/z): 232.183, calcd: 266.1827.

(*S*)-*N*,*N*-Dimethyl-4-(2-(3,4,5-trimethoxyphenyl)tetrahydro-2*H*-pyran-4-yl)aniline

According to general procedure 2: Using 10 mol% $FeCl_3$ (0.2 mmol, 32.4 mg), 4 ml THF, (2*S*,4*R*)-4-chloro-2-(3,4,5-trimethoxyphenyl)-tetrahydro-2*H*-pyrane (2 mmol, 573.5 mg) and 1.5 equiv. 4-(*N*,*N*-dimethylamino)-phenylmagnesium bromide (3 mmol, 3 ml). Purification by SiO_2 column chromatography (methanol/toluene/NEt_3 88:10:2).

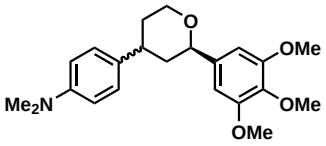

	Yellow oil
	$C_{22}H_{29}NO_4$
	371.47 g/mol
Yield	465 mg (1.25 mmol, 63% (75 : 25))
TLC	*major:* R_f = 0.68 (SiO_2, methanol/toluene/NEt_3 88:10:2)
^{1}H-NMR	*major:* (300 MHz, $CDCl_3$) δ 0.95-1.00 (t, J = 8 Hz, 1H), 1.47-2.24 (m, 4H), 2.49-2.56 (quart., J = 7.5 Hz, 1H), 2.80-2.84 (m, 6H), 3.41-3.65 (m, 1H), 3.74-3.76 (s, 9H), 4.11-4.33 (m, 1H), 6.47-6.69 (m, 4H), 7.02-7.37 (m, 2H).
^{13}C-APT-NMR	*major:* (75 MHz, $CDCl_3$) δ 10.4 (u), 33.3 (d), 40.5 (u), 41.5 (d), 45.6 (d), 55.8 (u), 60.5 (u), 68.5 (d), 79.8 (u), 102.6 (u), 112.7 (u), 127.0 (u), 128.8 (u), 132.2 (d), 133.3 (d), 136.8 (d), 138.5 (d), 149.1 (d), 152.9 (d).
GC-MS	*major:* t_R = 12.95 min, (EI, 70 eV): m/z = 371 [M^+], 219, 196, 181, 161, 147, 131, 117, 91, 77, 53.
HR-MS	*major:* (EI, 70 eV, m/z): 371.210, calcd: 371.2097.
FT-IR	(ATR film) $1/\lambda$ [cm^{-1}] = 3505 (b), 2934 (m), 2836 (m), 1713 (w), 1609 (m), 1588 (s), 1505 (s), 1453 (s), 1415 (s), 1326 (s), 1230 (s), 1121 (s), 1084 (s), 1005 (s), 963 (m), 945 (m), 817 (s), 748 (s).

1-Cyclohexyl-2-methylbenzene

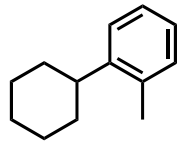

Colorless oil

$C_{13}H_{18}$

174.29 g/mol

Yield 78.6 mg (0.45 mmol, 91%)

TLC R_f = 0.65 (SiO_2, *n*-pentane)

^{1}H-NMR (300 MHz, $CDCl_3$) δ 7.25 – 7.19 (m, 1H), 7.19 – 7.12 (m, 2H), 7.12 – 7.05 (m, 1H), 2.80 – 2.63 (m, 1H), 2.34 (s, 3H), 1.92 – 1.72 (m, 5H), 1.47 – 1.35 (m, 5H).

^{13}C-NMR (75 MHz, $CDCl_3$) δ 146.0, 135.3, 130.3, 126.2, 125.6, 125.5, 40.2, 33.8, 27.3, 26.5, 19.5.

GC-MS t_R = 7.59 min, (EI, 70 eV): m/z = 174 [M^+], 159, 145, 131, 117, 105, 91, 77, 65, 56.

Analytical data in accordance with literature data: F. González-Bobes, and G. C. Fu, *J. Am. Chem. Soc.* **2006**, *128*, 5360–5361.

1-Cyclopentyl-2-methylbenzene

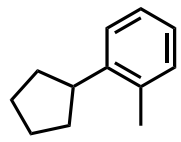

Colorless oil

$C_{12}H_{16}$

160.26 g/mol

Yield 44.5 mg (0.28 mmol, 55%)

TLC R_f = 0.60 (SiO_2, *n*-pentane)

^{1}H-NMR (300 MHz, $CDCl_3$) δ 7.26 (dd, *J* = 7.6, 1.5 Hz, 1H), 7.16 (ddd, *J* = 13.4, 6.4, 1.9 Hz, 2H), 7.12 – 7.04 (m, 1H), 3.19 (ddd, *J* = 16.6, 9.2, 7.4 Hz, 1H), 2.36 (s, 3H), 2.11 – 1.97 (m, 2H), 1.91 – 1.78 (m, 2H), 1.77 – 1.65 (m, 2H), 1.65 – 1.52 (m, 2H).

^{13}C-NMR (75 MHz, $CDCl_3$) δ 144.7, 136.1, 130.2, 126.2, 125.6, 125.4, 41.8, 33.7, 25.7, 20.0

GC-MS t_R = 7.11 min, (EI, 70 eV): m/z = 160 [M^+], 145, 131, 117, 105, 91, 77, 65, 51.

Analytical data in accordance with literature data: Z. Duan, W. Li, A. Lei, *Org. Lett.* **2016**, *18*, 4012–4015.

1-Cyclopentyl-4-methoxybenzene

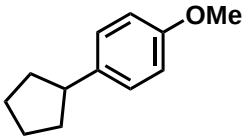

Colorless oil

$C_{12}H_{16}O$

176.26 g/mol

Yield 23.8 mg (0.14 mmol, 27%)

TLC R_f = 0.63 (SiO_2, *n*-pentane/ethyl acetate 19:1)

^{1}H-NMR (300 MHz, $CDCl_3$) δ 7.22 – 7.14 (m, 2H), 6.89 – 6.81 (m, 2H), 3.80 (s, 3H), 2.95 (tt, J = 9.6, 7.4 Hz, 1H), 2.14 – 1.97 (m, 2H), 1.87 – 1.49 (m, 6H).

^{13}C-NMR (75 MHz, $CDCl_3$) δ 157.8, 138.7, 128.1, 113.8, 55.4, 45.3, 34.9, 25.6.

GC-MS t_R = 7.74 min, (EI, 70 eV): m/z = 176 [M^+], 161, 147, 134, 121, 103, 91, 77, 65, 51.

Analytical data in accordance with literature data: F. González-Bobes, and G. C. Fu, *J. Am. Chem. Soc.* **2006**, *128*, 5360–5361.

1-Methyl-4-nonylbenzene

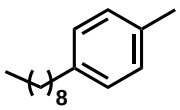

Colorless oil

$C_{16}H_{26}$

218.38 g/mol

Yield 94.0 mg (0.43 mmol, 86%)

TLC R_f = 0.55 (SiO_2, *n*-pentane)

^{1}H-NMR (300 MHz, $CDCl_3$) δ 7.13 – 7.04 (m, 4H), 2.56 (t, J = 7.9 Hz, 2H), 2.32 (s, 3H), 1.67 – 1.52 (m, 2H), 1.39 – 1.18 (m, 12H), 0.88 (t, J = 6.9 Hz, 3H).

^{13}C-NMR (75 MHz, $CDCl_3$) δ 140.0, 135.1, 129.0, 128.4, 35.7, 32.1, 31.8, 29.7, 29.7, 29.5, 22.8, 21.2, 14.3.

GC-MS t_R = 8.75 min, (EI, 70 eV): m/z = 218 [M^+], 161, 147, 131, 118, 105, 91, 77, 65, 55.

Analytical data in accordance with literature data: M. Moreno-Manas, A. Trius, *Bull. Chem. Soc. Jpn.* **1983**, *56*, 2154-2158.

1-Methoxy-4-nonylbenzene

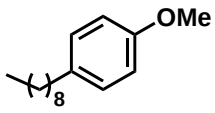

Colorless oil

$C_{16}H_{26}O$

234.38 g/mol

Yield 36.1 mg (0.16 mmol, 31%)

TLC R_f = 0.52 (SiO_2, *n*-pentane/ethyl acetate 19:1)

^{1}H-NMR (300 MHz, $CDCl_3$) δ 7.10 (dt, J = 8.7, 2.2 Hz, 2H), 6.82 (dt, J = 8.6, 2.1 Hz, 2H), 3.79 (s, 3H), 2.54 (t, J = 7.7 Hz, 2H), 1.56 (q, J = 7.2 Hz, 2H), 1.36 – 1.20 (m, 12H), 0.88 (t, J = 6.9 Hz, 3).

^{13}C-NMR (75 MHz, $CDCl_3$) δ 157.7, 135.2, 129.4, 113.8, 55.4, 35.2, 32.1, 31.9, 29.7, 29.7, 29.5, 29.4, 22.8, 14.3.

GC-MS t_R = 9.45 min, (EI, 70 eV): m/z = 234 [M^+], 147, 134, 121, 107, 91, 77, 65, 55.

Analytical data in accordance with literature data: M. Moreno-Manas, A. Trius, *Bull. Chem. Soc. Jpn.* **1983**, *56*, 2154-2158.

1-Methyl-2-nonylbenzene

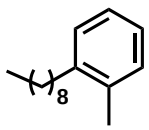

Colorless oil

$C_{16}H_{26}$

218.38 g/mol

Yield 80 mg (0.37 mmol, 73%)

TLC R_f = 0.57 (SiO_2, *n*-pentane)

^{1}H-NMR (300 MHz, $CDCl_3$) δ 7.19 – 7.02 (m, 4H), 2.58 (t, J = 8.1 Hz, 2H), 2.31 (s, 3H), 1.65 – 1.49 (m, 2H), 1.46 – 1.20 (m, 12H), 0.89 (t, J = 7.0 Hz, 3H).

^{13}C-NMR (75 MHz, $CDCl_3$) δ 141.3, 136.0, 130.2, 128.9, 126.0, 125.8, 33.5, 32.1, 30.5, 29.9, 29.7, 29.5, 22.8, 19.5, 14.3.

GC-MS t_R = 8.79 min, (EI, 70 eV): m/z = 218 [M^+], 161, 147, 133, 117, 105, 91, 79, 65, 57.

Analytical data in accordance with literature data: D. L. J. Clive, M. P. Pham, *J. Org. Chem.* **2009**, *74*, 1685–1690.

1-Benzyl-4-methylbenzene

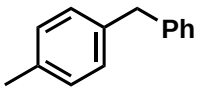

Colorless oil

$C_{14}H_{14}$

182.27 g/mol

Yield 95% (determined by GC-FID)

^{1}H-NMR (300 MHz, $CDCl_3$) δ 7.34 – 7.27 (m, 2H), 7.25 – 7.18 (m, 3H), 7.16 – 7.08 (m, 4H), 3.97 (s, 2H), 2.34 (s, 3H).

^{13}C-NMR (75 MHz, $CDCl_3$) δ 141.5, 138.2, 135.7, 129.3, 129.0, 128.9, 128.6, 126.1, 41.7, 21.2.

GC-MS t_R = 8.08 min, (EI, 70 eV): m/z = 182 [M^+], 167, 152, 139, 128, 115, 105, 91, 77, 65, 51.

Analytical data in accordance with literature data: M. Nambo, E. C. Keske, J. P. G. Rygus, J. C.-H. Yim, C. M. Crudden, *ACS Catalysis* **2017**, *7*, 1108-1112.

2-(*p*-Tolyl)naphthalene

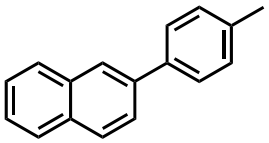

Colorless oil

$C_{17}H_{14}$

218.30 g/mol

Yield 8% (determined by GC-FID)

^{1}H-NMR (300 MHz, $CDCl_3$) δ 8.04 (d, J = 1.8 Hz, 1H), 7.95 – 7.83 (m, 3H), 7.76 (dd, J = 8.5, 1.8 Hz, 1H), 7.68 – 7.61 (m, 2H), 7.55 – 7.45 (m, 2H), 7.35 – 7.29 (m, 2H), 2.44 (s, 3H).

^{13}C-NMR (75 MHz, $CDCl_3$) δ 138.6, 138.3, 137.3, 133.8, 132.6, 129.7, 128.5, 128.3, 127.8, 127.4, 126.4, 125.9, 125.7, 125.6, 21.3.

GC-MS t_R = 10.58 min, (EI, 70 eV): m/z = 218 [M^+], 202, 189, 176, 165, 152, 139, 126, 109, 101, 91, 75, 63, 51.

Analytical data in accordance with literature data: M. Kuriyama, R. Shimazawa, R. Shirai, *Tetrahedron* **2007**, *63*, 9393–9400.

1-(But-3-en-1-yl)-4-methylbenzene

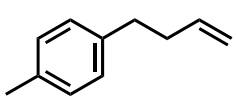

	Colorless oil
	$C_{11}H_{14}$
	146.23 g/mol
Yield	68% (determined by NMR)
^{1}H-NMR	(300 MHz, $CDCl_3$) δ 7.11 – 7.07 (m, 4H), 5.87 (ddt, J = 16.9, 10.2, 6.5 Hz, 1H), 5.05 (dq, J = 17.2, 1.7 Hz, 1H), 4.98 (ddt, J = 10.2, 2.2, 1.3 Hz, 1H), 2.68 (dd, J = 9.1, 6.6 Hz, 2H), 2.42 – 2.35 (m, 2H), 2.33 (s, 3H).
GC-MS	t_R = 5.74 min, (EI, 70 eV): m/z = 146 [M^+], 131, 115, 105, 91, 77, 65, 51.

Analytical data in accordance with literature data: Y.-L. Lai, J.-M. Huang, *Org. Lett.* **2017**, *19*, 2022–2025.

5.4.9 Cyclic Voltammetry

Cyclic voltammetry measurements (THF, 0.1 M [N(*n*-Bu)$_4$][PF_6], scan rate: 200 mVs^{-1}) were performed with a CH Instruments CHI 600E potentiostat using a Pt disc working electrode (1 mm), a Pt counter electrode, and a silver wire as pseudo-reference electrode. Ferrocene (FcH) was employed as internal standards. The experiments were conducted in a nitrogen-filled glovebox.

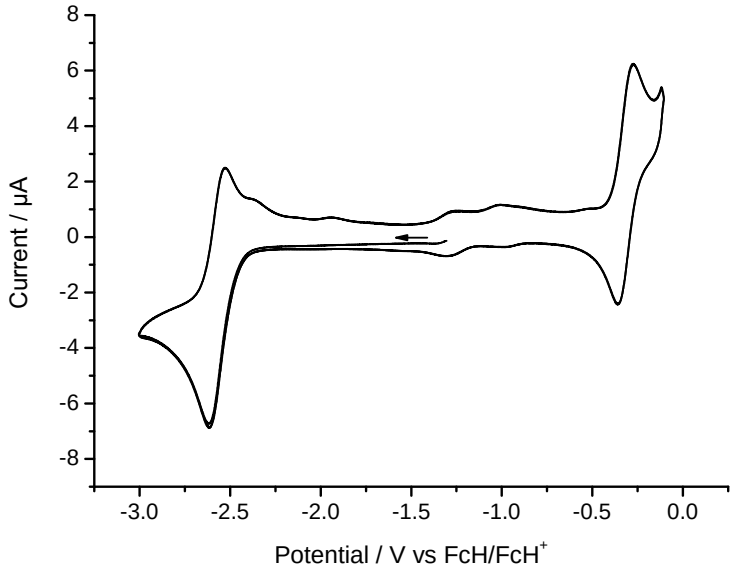

Figure 5.7: Cyclic voltammogram of **5a** measured in tetrahydrofuran/[N(*n*-Bu)$_4$][PF_6] at a scan rate of 200mVs^{-1}.

5.4.10 UV/Vis Experiments

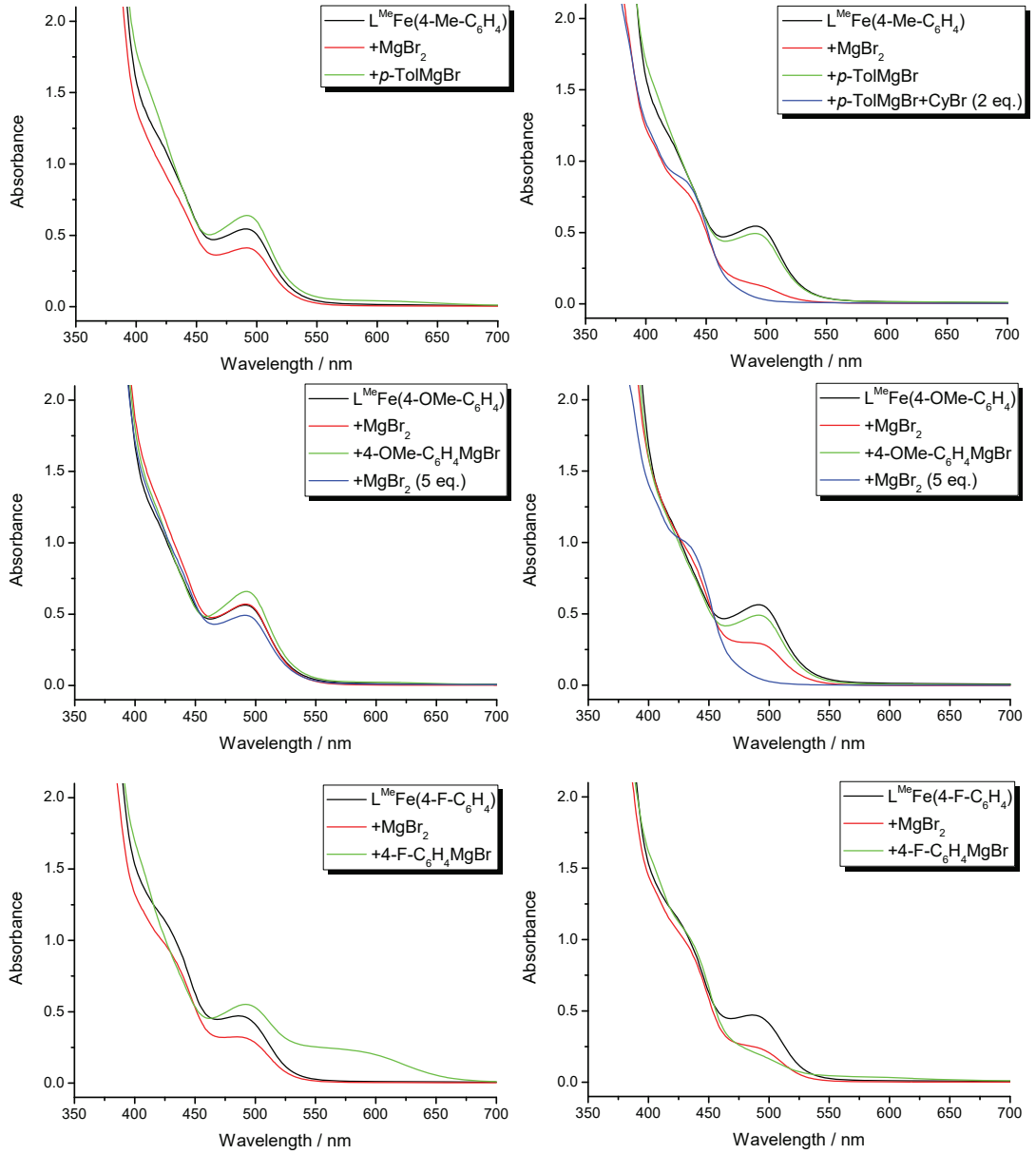

Figure 5.8: UV/Vis spectra: stoichiometric reactions of $L^{Me}Fe(4\text{-}X\text{-}C_6H_4)$ (**5a-c**) and cyclohexyl bromide in presence of different additives before the addition of cyclohexyl bromide (left side) and after three hours reaction time (right side).

5.4.11 NMR Reaction Analysis

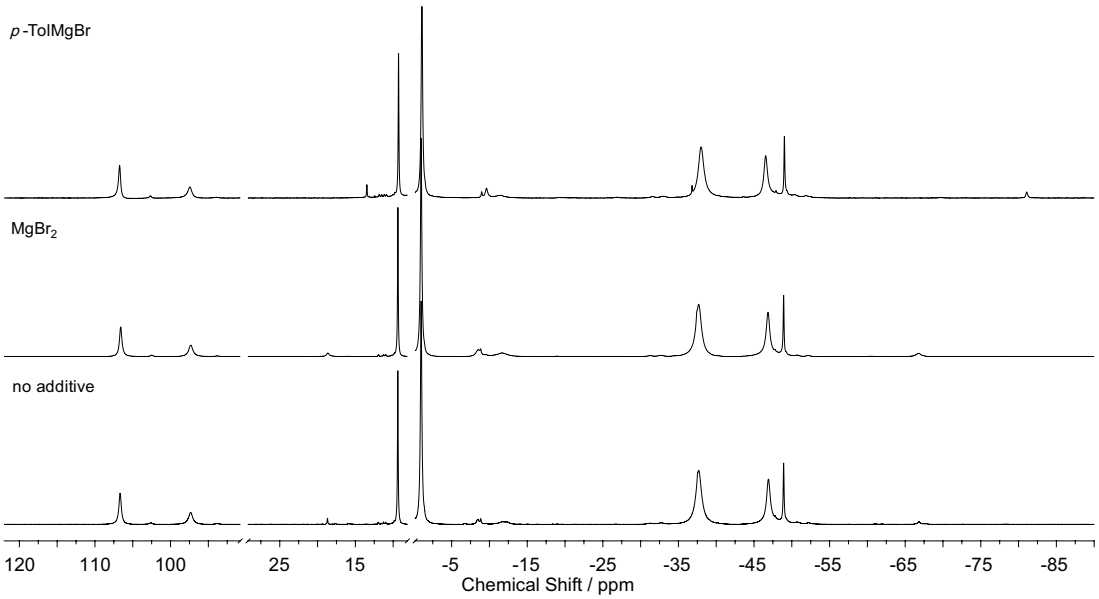

Figure 5.9: ^{1}H NMR spectra of $L^{Me}Fe(4\text{-Me-}C_6H_4)$ (**5a**) measured in THF-d_8 after addition of 1 equiv. $MgBr_2$ or *p*-TolMgBr.

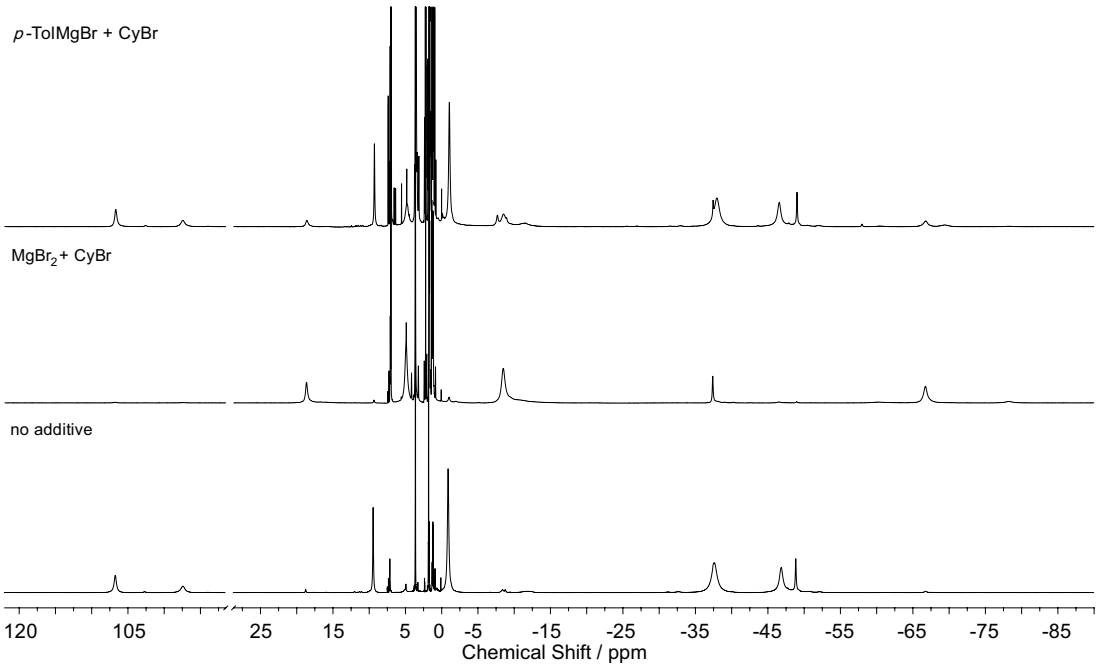

Figure 5.10: ^{1}H NMR spectra of $L^{Me}Fe(4\text{-Me-}C_6H_4)$ (**5a**) measured in THF-d_8 after addition of 1 equiv. $MgBr_2$ or *p*-TolMgBr and subsequent reaction with cyclohexyl bromide.

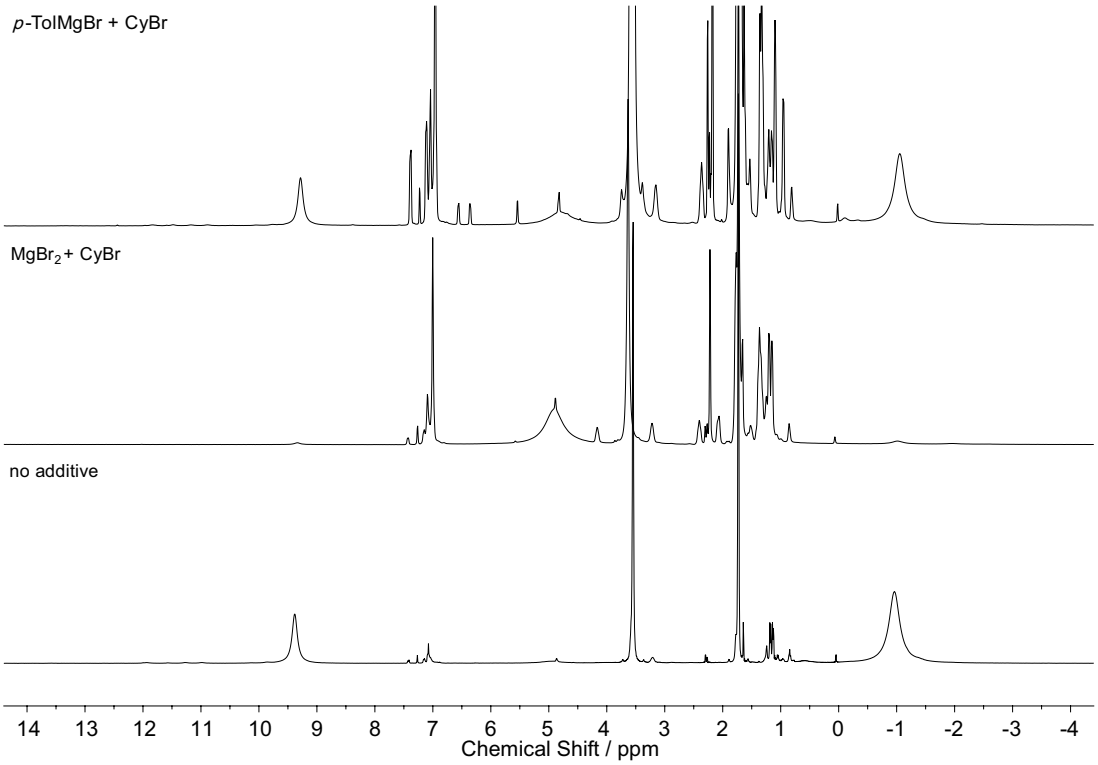

Figure 5.11: ^{1}H NMR spectra of $L^{Me}Fe(4\text{-}Me\text{-}C_6H_4)$ (**5a**) measured in THF-d_8 after addition of 1 equiv. $MgBr_2$ or *p*-TolMgBr and subsequent reaction with cyclohexyl bromide.

5.4.12 X-Ray Crystallography

Single crystals of **5a**, **5b**, and **5c** could be obtained by recrystallization from *n*-hexane at 15 °C. Data were collected with an Agilent Technologies SuperNova Atlas CCD diffractometer with microfocus Cu K_α radiation (= 1.54184 Å). The structures were solved by direct methods and refined by full-matrix least-squares procedures on F^2.[33] All non-hydrogen atoms were refined anisotropically, and a riding model was employed in the treatment of the hydrogen atom positions. The molecular structures are shown in Figures 5.3b.

Selected bond distances (Å), angles (°):

5a: C2–C3 1.4020(17), C2–N1 1.3309(19), C4–N1 1.4426(18), C16–Fe1 2.018(2), N1–Fe1 1.9830(12); C2–N1–C4 120.94(12), C2–N1–Fe1 123.66(10), C4–N1–Fe1 115.21(9), C16–Fe1–N1 132.71(4), N1–Fe1–N1A 94.41(7).

5b: C2–C3 1.408(4), C2–N1 1.328(4), C3–C4 1.390(4), C4–N2 1.334(4), C6–N1 1.444(4), C18–N2 1.444(3), C30–Fe1 2.004(3), C33–O1 1.378(4), C36–O1 1.411(4), N1–Fe1 1.979(2), N2–Fe1 1.978(2); C2–N1–C6 120.8(2), C2–N1–Fe1 123.22(17), C6–N1–Fe1 116.0(2), C4–N2–C18 121.8(20), C4–N2–Fe1 124.00(17), C18–N2–Fe1 113.9(20), C30–Fe1–N1 134.58(11), C30–Fe1–N2 130.87(10), C33–O1–C36 117.1(2), N1–Fe1–N2 94.55(9).

5c: C1–N1 1.4355(17), C13–C14 1.3998(16), C13–N1 1.3327(17), C16–Fe1 2.024(2), C19–F1 1.363(2), N1–Fe1 1.9681(12); C1–N1–C13 121.45(11), C1–N1–Fe1 112.11(8), C13–N1–Fe1 126.43(9), C16–Fe1–N1 133.58(3), N1–Fe1–N1A 92.84(7).

Table 5.23: Crystal data and structure refinement for compounds **5a**, **5b**, and **5c**.

Compound	**5a**	**5b**	**5c**
Empirical formula	$C_{36}H_{48}FeN_2$	$C_{36}H_{48}FeN_2$ O	$C_{35}H_{45}FFeN_2$
Formula weight	564.61	580.61	568.60
Temperature [K]	123(2)	123(2)	123.01(10)
Crystal system	orthorhombic	monoclinic	monoclinic
Space group	*P*nma	$P2_1/n$	$P2_1/m$
a [Å]	15.9333(5)	9.7285(6)	8.3090(1)
b [Å]	20.6504(5)	15.9498(10)	20.6288(4)
c [Å]	9.5703(3)	20.4915(9)	9.5163(2)
α [°]	90	90	90
β [°]	90	92.053(5)	104.745(2)

γ[°]	90	90	90
Volume [Å^3]	3148.91(16)	3177.6(3)	1577.42(5)
Z	4	4	2
ρcalc [g/cm^3]	1.191	1.214	1.197
μ [mm^{-1}]	4.016	4.018	4.059
F(000)	1216	1248	607
Crystal size [mm^3]	0.19 × 0.16 × 0.11	0.17 × 0.14 × 0.04	0.23 × 0.12 × 0.05
Radiation	CuK$_\alpha$ (λ = 1.54184)	CuK$_\alpha$ (λ = 1.54184)	CuK$_\alpha$ (λ = 1.54184)
Range for data collection [°]	4.28 < 2Θ < 73.63	3.51 < 2Θ < 73.63	4.29 < 2Θ < 73.67
Index ranges	-18 ≤ h ≤ 19 -25 ≤ k ≤ 17 -11 ≤ l ≤ 10	-11 ≤ h ≤ 11 -19 ≤ k ≤ 19 -16 ≤ l ≤ 25	-9 ≤ h ≤ 10 -23 ≤ k ≤ 25 -11 ≤ l ≤ 11
Reflections collected	9552	11215	10826
Independent reflections	3191 R_{int} = 0.0285	11215 R_{int} = —	3194 R_{int} = 0.0260
Data/restraints/ parameters	3191/0/211	11215/0/373	3194/0/211
Goodness-of-fit on F^2	1.039	0.820	1.063
Final R indexes [I ≥ 2σ(I)]	R_1 = 0.0327 wR_2 = 0.0777	R_1 = 0.0431 wR_2 = 0.0902	R_1 = 0.0310 wR_2 = 0.0815
Final R indexes [all data]	R_1 = 0.0391 wR_2 = 0.0820	R_1 = 0.0767 wR_2 = 0.0973	R_1 = 0.0331 wR_2 = 0.0839
Largest diff. peak/hole [eÅ^{-3}]	0.198/-0.197	0.496/-0.270	0.216/-0.363

5.4.13 Selected NMR-Spectra

Dipp$_2$nacnacFe(4-Me-C$_6$H$_4$) (5a)

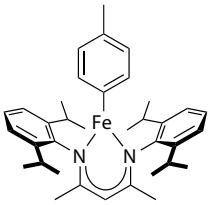

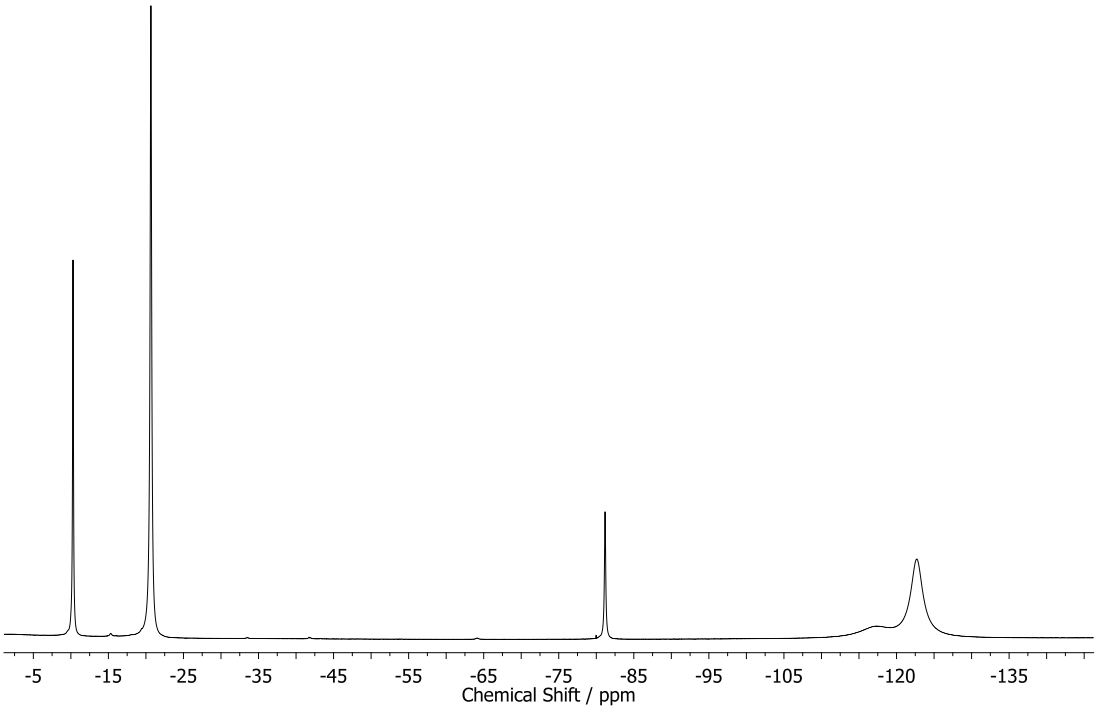

Dipp$_2$nacnacFe(4-MeO-C$_6$H$_4$) (5b)

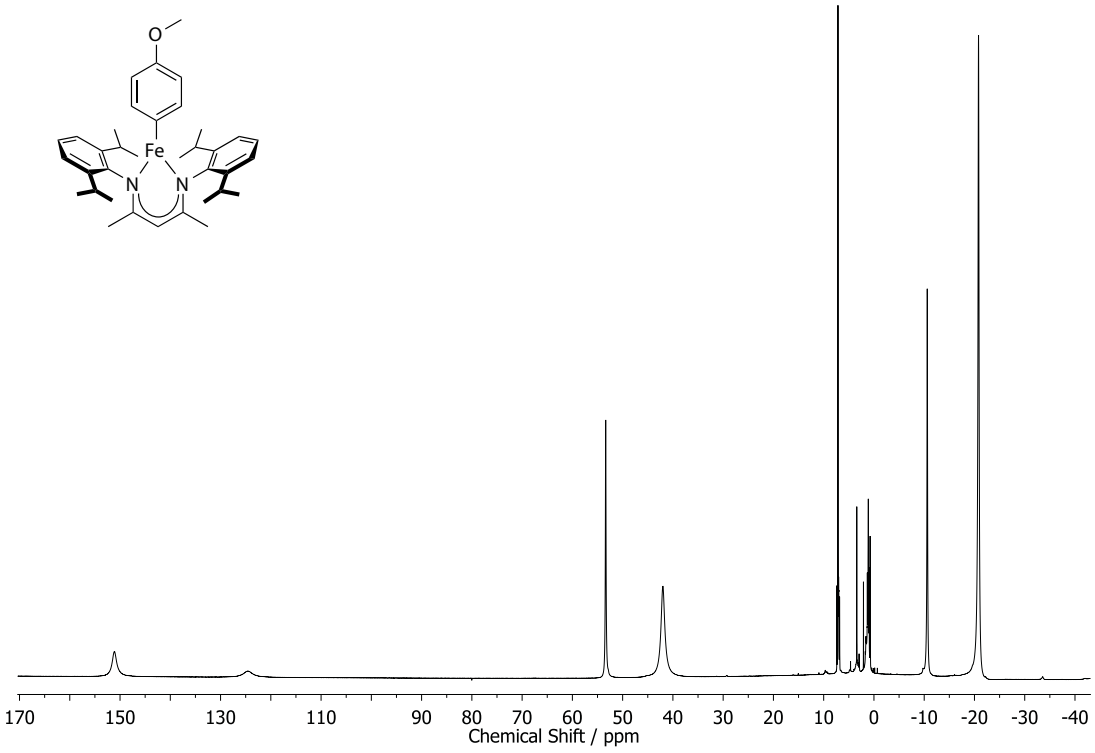

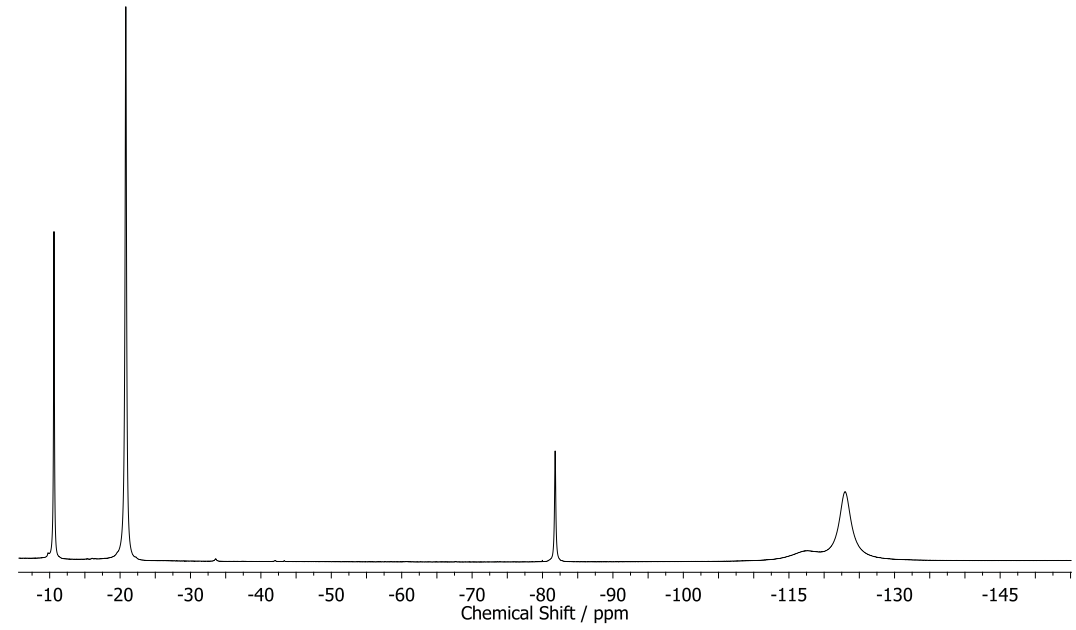

Dipp$_2$nacnacFe(4-F-C$_6$H$_4$) (5c)

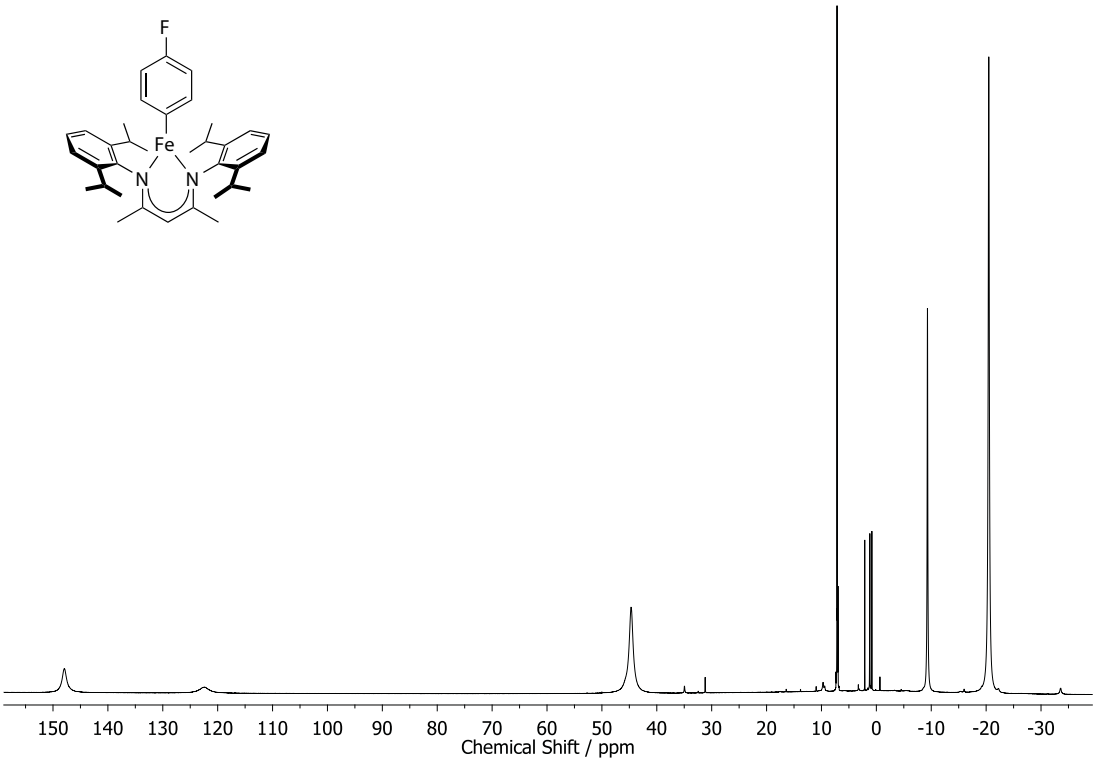

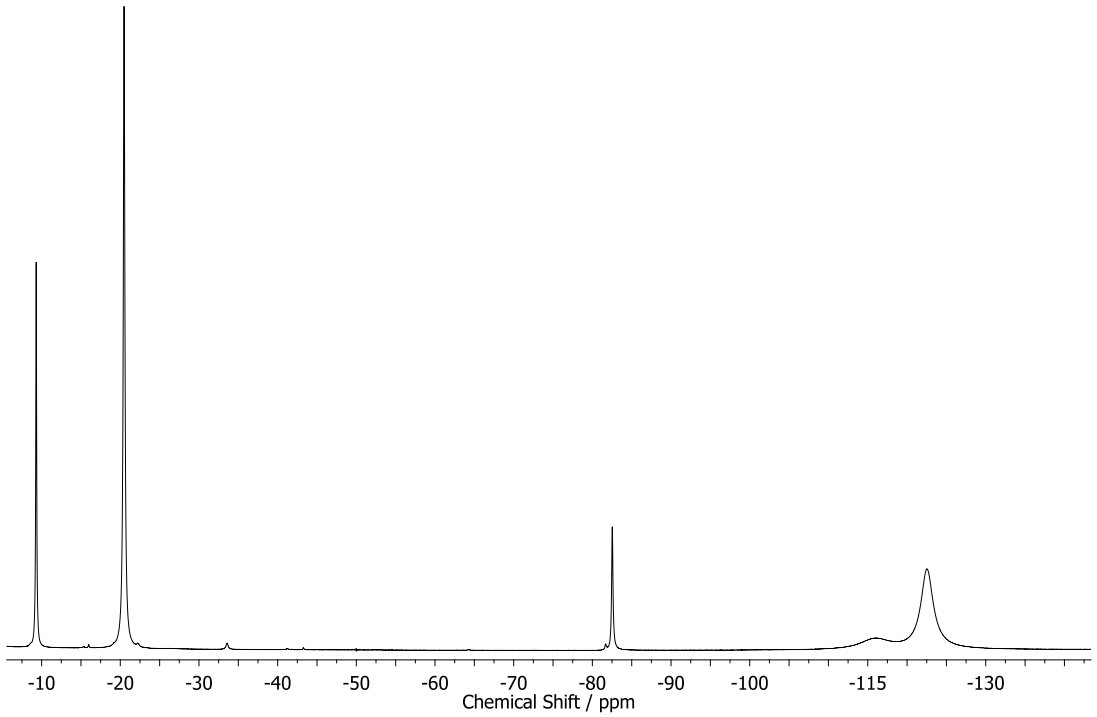

5.5 References

[1] (a) de Meijere, A., Bräse, S., Oestreich, M., Eds. *Metal-Catalyzed Cross-Coupling Reactions and More*; Wiley-VCH Verlag GmbH & Co. KGaA, **2014**; (b) Sherry, B. D.; Fürstner, A. The Promise and Challenge of Iron-Catalyzed Cross Coupling. *Acc. Chem. Res.* **2008**, *41*, 1500–1511.

[2] Czaplik, W. M.; Mayer, M.; Cvengroš, J.; von Wangelin, A. J. Coming of Age: Sustainable Iron-Catalyzed Cross-Coupling Reactions. *ChemSusChem* **2009**, *2*, 396–417.

[3] Piontek, A.; Bisz, E.; Szostak, M. Iron-Catalyzed Cross-Couplings in the Synthesis of Pharmaceuticals: In Pursuit of Sustainability. *Angew. Chem. Int. Ed.* **2018**, *57*, 11116–11128.

[4] (a) Nakamura, M.; Matsuo, K.; Ito, S.; Nakamura, E. Iron-Catalyzed Cross-Coupling of Primary and Secondary Alkyl Halides with Aryl Grignard Reagents. *J. Am. Chem. Soc.* **2004**, *126*, 3686–3687; (b) Martin, R.; Fürstner, A. Cross-Coupling of Alkyl Halides with Aryl Grignard Reagents Catalyzed by a Low-Valent Iron Complex. *Angew. Chem. Int. Ed.* **2004**, *43*, 3955–3957; (c) Bedford, R. B.; Bruce, D. W.; Frost, R. M.; Goodby, J. W.; Hird, M. Iron(iii) salen-type catalysts for the cross-coupling of aryl Grignards with alkyl halides bearing β-hydrogens. *Chem. Commun.* **2004**, 2822–2823; (d) Nagano, T.; Hayashi, T. Iron-Catalyzed Grignard Cross-Coupling with Alkyl Halides Possessing β-Hydrogens. *Org. Lett.* **2004**, *6*, 1297–1299; (e) Bedford, R. B.; Bruce, D. W.; Frost, R. M.; Hird, M. Simple iron-amine catalysts for the cross-coupling of aryl Grignards with alkyl halides bearing β-hydrogens. *Chem. Commun.* **2005**, 4161; (f) Bica, K.; Gaertner, P. An Iron-Containing Ionic Liquid as Recyclable Catalyst for Aryl Grignard Cross-Coupling of Alkyl Halides. *Org. Lett.* **2006**, *8*, 733–735; (g) Chowdhury, R. R.; Crane, A. K.; Fowler, C.; Kwong, P.; Kozak, C. M. Iron(iii) amine-bis(phenolate) complexes as catalysts for the coupling of alkyl halides with aryl Grignard reagents. *Chem. Commun.* **2008**, 94–96; (h) Czaplik, W.; Mayer, M.; Jacobi von Wangelin, A. Domino Iron Catalysis: Direct Aryl-Alkyl Cross-Coupling. *Angew. Chem. Int. Ed.* **2009**, *48*, 607–610; (i) Kawamura, S.; Ishizuka, K.; Takaya, H.; Nakamura, M. The first iron-catalysed aluminium-variant Negishi coupling: critical effect of co-existing salts on the dynamic equilibrium of arylaluminium species and their reactivity. *Chem. Commun.* **2010**, *46*, 6054; (j) Nakamura, E.; Yoshikai, N. Low-Valent Iron-Catalyzed C-C Bond Formation-Addition, Substitution, and C-H Bond Activation. *J. Org. Chem.* **2010**, *75*, 6061–6067; (k) Hatakeyama, T.; Hashimoto, T.; Kondo, Y.; Fujiwara, Y.; Seike, H.; Takaya, H.; Tamada, Y.; Ono, T.; Nakamura, M. Iron-Catalyzed Suzuki-Miyaura Coupling of Alkyl Halides. *J. Am. Chem. Soc.* **2010**, *132*, 10674–10676; (l) Qian, X.; Dawe, L. N.; Kozak, C. M. Catalytic alkylation of arylGrignard reagents by iron(iii) amine-bis(phenolate) complexes. *Dalton Trans.* **2011**, *40*, 933–943; (m) Hasan, K.; Dawe, L. N.; Kozak, C. M. Synthesis, Structure, and C-C Cross-

Coupling Activity of (Amine)bis(phenolato)iron(acac) Complexes. *Eur. J. Inorg. Chemi.* **2011**, *2011*, 4610–4621; (n) Xia, C.-L.; Xie, C.-F.; Wu, Y.-F.; Sun, H.-M.; Shen, Q.; Zhang, Y. Efficient cross-coupling of aryl Grignard reagents with alkyl halides by recyclable ionic iron(iii) complexes bearing a bis(phenol)-functionalized benzimidazolium cation. *Org. Biomol. Chem.* **2013**, *11*, 8135; (o) Bedford, R. B.; Brenner, P. B.; Carter, E.; Carvell, T. W.; Cogswell, P. M.; Gallagher, T.; Harvey, J. N.; Murphy, D. M.; Neeve, E. C.; Nunn, J.; Pye, D. R. Expedient Iron-Catalyzed Coupling of Alkyl, Benzyl and Allyl Halides with Arylboronic Esters. *Chem. Eur. J.* **2014**, *20*, 7935–7938; (p) Li, Z.; Sun, H.-M.; Shen, Q. Iron-mediated inter- and intramolecular reductive cross-coupling of unactivated alkyl chlorides with aryl bromides. *Org. Biomol. Chem.* **2016**, *14*, 3314–3321.

[5] Ghorai, S. K.; Jin, M.; Hatakeyama, T.; Nakamura, M. Cross-Coupling of Non-activated Chloroalkanes with Aryl Grignard Reagents in the Presence of Iron/N-Heterocyclic Carbene Catalysts. *Org. Lett.* **2012**, *14*, 1066–1069.

[6] Briel, O.; Cazin, C. S. J. In *N-Heterocyclic Carbenes in Transition Metal Catalysis and Organocatalysis*; Cazin, C. S., Ed.; Springer Netherlands, **2011**; Chapter *N*-Heterocyclic Carbene Complexes in Industrial Processes, pp. 315–324.

[7] (a) Hatakeyama, T.; Hashimoto, S.; Ishizuka, K.; Nakamura, M. Highly Selective Biaryl Cross-Coupling Reactions between Aryl Halides and Aryl Grignard Reagents: A New Catalyst Combination ofN-Heterocyclic Carbenes and Iron, Cobalt, and Nickel Fluorides. *J. Am. Chem. Soc.* **2009**, *131*, 11949–11963; (b) Guisán-Ceinos, M.; Tato, F.; Buñuel, E.; Calle, P.; Cárdenas, D. J. Fe-catalysed Kumada-type alkyl–alkyl cross-coupling. Evidence for the intermediacy of Fe(i) complexes. *Chem. Sci.* **2013**, *4*, 1098; (c) Przyojski, J. A.; Veggeberg, K. P.; Arman, H. D.; Tonzetich, Z. J. Mechanistic Studies of Catalytic Carbon–Carbon Cross-Coupling by Well-Defined Iron NHC Complexes. *ACS Catalysis* **2015**, *5*, 5938–5946; (d) Fleischauer, V. E.; III, S. B. M.; Neate, P. G. N.; Brennessel, W. W.; Neidig, M. L. NHC and nucleophile chelation effects on reactive iron(ii) species in alkyl–alkyl cross-coupling. *Chem. Sci.* **2018**, *9*, 1878–1891.

[8] (a) Fujita, M. Palladium(0)/LiCl Promoted Cross-Coupling Reaction of (4-Pyridyl)stannanes and Aromatic Bromides: Easy Access to Poly(4-pyridyl)-Substituted Aromatics. *Tetrahedron Lett.* **1995**, *36*, 5247–5250; (b) Li, B.-J.; Xu, L.; Wu, Z.-H.; Guan, B.-T.; Sun, C.-L.; Wang, B.-Q.; Shi, Z.-J. Cross-Coupling of Alkenyl/Aryl Carboxylates with Grignard Reagent via Fe-Catalyzed C-O Bond Activation. *J. Am. Chem. Soc.* **2009**, *131*, 14656–14657; (c) McCann, L. C.; Organ, M. G. On The Remarkably Different Role of Salt in the Cross-Coupling of Arylzincs From That Seen With Alkylzincs. *Angew. Chem. Int. Ed.* **2014**, *53*, 4386–4389; (d) Minami, H.; Saito, T.; Wang, C.; Uchiyama, M. Organoaluminum-Mediated Direct Cross-Coupling Reactions. *Angew. Chem. Int. Ed.* **2015**, *54*, 4665–4668.

[9] (a) Krasovskiy, A.; Knochel, P. A LiCl-Mediated Br/Mg Exchange Reaction for the Preparation of Functionalized Aryl- and Heteroarylmagnesium Compounds from Organic Bromides. *Angew. Chem. Int. Ed.* **2004**, *43*, 3333–3336; (b) Ren, H.; Krasovskiy, A.; Knochel, P. Stereoselective Preparation of Functionalized Acyclic Alkenylmagnesium Reagents Usingi-PrMgCl·LiCl. *Org. Lett.* **2004**, *6*, 4215–4217.

[10] (a) Bedford, R. B.; Brenner, P. B.; Carter, E.; Cogswell, P. M.; Haddow, M. F.; Harvey, J. N.; Murphy, D. M.; Nunn, J.; Woodall, C. H. TMEDA in Iron-Catalyzed Kumada Coupling: Amine Adduct versus Homoleptic "ate" Complex Formation. *Angew. Chem. Int. Ed.* **2014**, *53*, 1804–1808; (b) Bedford, R. B. How Low Does Iron Go? Chasing the Active Species in Fe-Catalyzed Cross-Coupling Reactions. *Accounts of Chemical Research* **2015**, *48*, 1485–1493.

[11] Bauer, G.; Wodrich, M. D.; Scopelliti, R.; Hu, X. Iron Pincer Complexes as Catalysts and Intermediates in Alkyl–Aryl Kumada Coupling Reactions. *Organometallics* **2015**, *34*, 289–298.

[12] Bedford, R. B.; Betham, M.; Bruce, D. W.; Davis, S. A.; Frost, R. M.; Hird, M. Iron nanoparticles in the coupling of alkyl halides with aryl Grignard reagents. *Chem. Commun.* **2006**, 1398.

[13] Welther, A.; Bauer, M.; Mayer, M.; Jacobi von Wangelin, A. Iron(0) Particles: Catalytic Hydrogenations and Spectroscopic Studies. *ChemCatChem* **2012**, *4*, 1088–1093.

[14] Jin, M.; Adak, L.; Nakamura, M. Iron-Catalyzed Enantioselective Cross-Coupling Reactions of α-Chloroesters with Aryl Grignard Reagents. *J. Am. Chem. Soc.* **2015**, *137*, 7128–7134.

[15] Miranda, P. O.; Carballo, R. M.; Martín, V. S.; Padrón, J. I. A New Catalytic Prins Cyclization Leading to Oxa- and Azacycles. *Org. Lett.* **2009**, *11*, 357–360.

[16] Sun, C.-L.; Krause, H.; FÃŒrstner, A. A Practical Procedure for Iron-Catalyzed Cross-Coupling Reactions of Sterically Hindered Aryl-Grignard Reagents with Primary Alkyl Halides. *Adv. Synth. Catal.* **2014**, *356*, 1281–1291.

[17] Fürstner, A.; Martin, R.; Krause, H.; Seidel, G.; Goddard, R.; Lehmann, C. W. Preparation, Structure, and Reactivity of Nonstabilized Organoiron Compounds. Implications for Iron-Catalyzed Cross Coupling Reactions. *J. Am. Chem. Soc.* **2008**, *130*, 8773–8787.

[18] (a) Gülak, S.; Stepanek, O.; Malberg, J.; Rad, B. R.; Kotora, M.; Wolf, R.; Jacobi von Wangelin, A. Highly chemoselective cobalt-catalyzed biaryl coupling reactions. *Chem. Sci.* **2013**, *4*, 776–784; (b) Hedström, A.; Izakian, Z.; Vreto, I.; Wallentin, C.-J.; Norrby, P.-O. On the Radical Nature of Iron-Catalyzed Cross-Coupling Reactions. *Chem. Eur. J.* **2015**, *21*, 5946–5953; (c) Heggen, B.; Thiel, W.

Theoretical investigation on the mechanism of iron catalyzed cross coupling reactions via ferrate intermediates. *J. Organomet. Chem.* **2016**, *804*, 42–47; (d) Parchomyk, T.; Koszinowski, K. Ate Complexes in Iron-Catalyzed Cross-Coupling Reactions. *Chem. Eur. J.* **2016**, *22*, 15609–15613.

[19] Gary S. Silverman, P. E. R. *Handbook of Grignard Reagents*; Marcel Dekker Inc, **1996**.

[20] Wu, W.; Teng, Q.; Chua, Y.-Y.; Huynh, H. V.; Duong, H. A. Iron-Catalyzed Cross-Coupling Reactions of Arylmagnesium Reagents with Aryl Chlorides and Tosylates: Influence of Ligand Structural Parameters and Identification of a General N-Heterocyclic Carbene Ligand. *Organometallics* **2017**, *36*, 2293–2297.

[21] (a) Luh, T.-Y.; kit Leung, M.; Wong, K.-T. Transition Metal-Catalyzed Activation of Aliphatic C-X Bonds in Carbon-Carbon Bond Formation. *Chem. Rev.* **2000**, *100*, 3187–3204; (b) Cárdenas, D. J. Advances in Functional-Group-Tolerant Metal-Catalyzed Alkyl–Alkyl Cross-Coupling Reactions. *Angew. Chem. Int. Ed.* **2003**, *42*, 384–387; (c) Hu, X.; Bauer, G.; Cheung, C. Cross-Coupling of Non-activated Primary and Secondary Alkyl Halides with Aryl Grignard Reagents Catalyzed by Chiral Iron Pincer Complexes. *Synthesis* **2015**, *47*, 1726–1732; (d) Przyojski, J. A.; Veggeberg, K. P.; Arman, H. D.; Tonzetich, Z. J. Mechanistic Studies of Catalytic Carbon–Carbon Cross-Coupling by Well-Defined Iron NHC Complexes. *ACS Catal.* **2015**, *5*, 5938–5946.

[22] Bedford, R. B.; Brenner, P. B.; Elorriaga, D.; Harvey, J. N.; Nunn, J. The influence of the ligand chelate effect on iron-amine-catalysed Kumada cross-coupling. *Dalton Trans.* **2016**, *45*, 15811–15817.

[23] (a) Bourget-Merle, L.; Lappert, M. F.; Severn, J. R. The Chemistry of β-Diketiminatometal Complexes. *Chem. Rev.* **2002**, *102*, 3031–3066; (b) Tsai, Y.-C. The chemistry of univalent metal β-diketiminates. *Coord. Chem. Rev.* **2012**, *256*, 722–758.

[24] (a) Dai, X.; Warren, T. H. Dioxygen activation by a neutral β-diketiminato copper(i) ethylene complex. *Chem. Commun.* **2001**, 1998–1999; (b) Smith, J. M.; Lachicotte, R. J.; Pittard, K. A.; Cundari, T. R.; Lukat-Rodgers, G.; Rodgers, K. R.; Holland, P. L. Stepwise Reduction of Dinitrogen Bond Order by a Low-Coordinate Iron Complex. *J. Am. Chem. Soc.* **2001**, *123*, 9222–9223; (c) Smith, J. M.; Sadique, A. R.; Cundari, T. R.; Rodgers, K. R.; Lukat-Rodgers, G.; Lachicotte, R. J.; Flaschenriem, C. J.; Vela, J.; Holland, P. L. Studies of Low-Coordinate Iron Dinitrogen Complexes. *J. Am. Chem. Soc.* **2006**, *128*, 756–769; (d) Stoian, S. A.; Vela, J.; Smith, J. M.; Sadique, A. R.; Holland, P. L.; Münck, E.; Bominaar, E. L. Mössbauer and Computational Study of an N_2-Bridged Diiron Diketiminate Complex: Parallel Alignment of the Iron Spins by Direct Antiferromagnetic Exchange with Activated Dinitrogen. *J. Am. Chem. Soc.* **2006**, *128*, 10181–10192; (e) Pfirrmann, S.; Limberg, C.; Herwig, C.; Stößer, R.; Ziemer, B. A Dinuclear Nickel(I) Dinitrogen Complex and its Reduction in Single-Electron Steps.

Angew. Chem. Int. Ed. **2009**, *48*, 3357–3361; (f) Spitzer, F.; Graßl, C.; Balázs, G.; Zolnhofer, E. M.; Meyer, K.; Scheer, M. Influence of the nacnac Ligand in Iron(I)-Mediated P_4 Transformations. *Angew. Chem. Int. Ed.* **2016**, *55*, 4340–4344.

[25] (a) Lee, D.-H.; Taher, A.; Hossain, S.; Jin, M.-J. An Efficient and General Method for the Heck and Buchwald–Hartwig Coupling Reactions of Aryl Chlorides. *Org. Lett.* **2011**, *13*, 5540–5543; (b) Lee, D.-H.; Jin, M.-J. An Extremely Active and General Catalyst for Suzuki Coupling Reaction of Unreactive Aryl Chlorides. *Org. Lett.* **2011**, *13*, 252–255; (c) Lee, D.-H.; Kwon, Y.-J.; Jin, M.-J. Highly Active Palladium Catalyst for the Sonogashira Coupling Reaction of Unreactive Aryl Chlorides. *Adv. Synth. Catal.* **2011**, *353*, 3090–3094; (d) Lee, D.-H.; Qian, Y.; Park, J.-H.; Lee, J.-S.; Shim, S.-E.; Jin, M.-J. A Highly Active and General Catalyst for the Stille Coupling Reaction of Unreactive Aryl, Heteroaryl, and Vinyl Chlorides under Mild Conditions. *Adv. Synth. Catal.* **2013**, *355*, 1729–1735.

[26] Yu, Y.; Brennessel, W. W.; Holland, P. L. Borane B-C Bond Cleavage by a Low-Coordinate Iron Hydride Complex and N-N Bond Cleavage by the Hydridoborate Product. *Organometallics* **2007**, *26*, 3217–3226.

[27] After two recrystallizations, **5b** was still contaminated with 2-3% of 4,4′-dimethoxy-1,1′-biphenyl (via NMR and GC-FID analysis).

[28] Holland *et al.* assigned the ^{1}H NMR resonances of dipp$_2$nacnacFe(C_6H_5) at 126 ppm to H-4/C_6H_5 and at 28 ppm to the ligand backbone-CH. For our recorded NMR spectra of **5a-c**, the opposite assignment is more likely, as for all three complexes a resonance with an integral of 1H is observed at 123-125 ppm.

[29] (a) Andres, H.; Bominaar, E. L.; Smith, J. M.; Eckert, N. A.; Holland, P. L.; Münck, E. Planar Three-Coordinate High-Spin Fe^{II}Complexes with Large Orbital Angular Momentum: Mössbauer, Electron Paramagnetic Resonance, and Electronic Structure Studies. *J. Am. Chem. Soc.* **2002**, *124*, 3012–3025; (b) Lin, P.-H.; Smythe, N. C.; Gorelsky, S. I.; Maguire, S.; Henson, N. J.; Korobkov, I.; Scott, B. L.; Gordon, J. C.; Baker, R. T.; Murugesu, M. Importance of Out-of-State Spin–Orbit Coupling for Slow Magnetic Relaxation in Mononuclear Fe^{II}Complexes. *J. Am. Chem. Soc.* **2011**, *133*, 15806–15809; (c) Sulway, S. A.; Collison, D.; McDouall, J. J. W.; Tuna, F.; Layfield, R. A. Iron(II) Cage Complexes of N-Heterocyclic Amide and Bis(trimethylsilyl)amide Ligands: Synthesis, Structure, and Magnetic Properties. *Inorg. Chem.* **2011**, *50*, 2521–2526.

[30] Full characterization of L^{Me}FeBr(THF): Z. J. Tonzetich, F. Héroguel, L. H. Do, S. J. Lippard, *Inorg. Chem.* **2011**, *50*, 1570-1579.

[31] Kovacic, P.; Brace, N. O. In *Inorganic Syntheses*; Rochow, E. G., Ed.; John Wiley & Sons, Inc., **1960**; Vol. 6; pp. 172–173.

[32] Stender, M.; Wright, R. J.; Eichler, B. E.; Prust, J.; Olmstead, M. M.; Roesky, H. W.; Power, P. P. The synthesis and structure of lithium derivatives of the sterically encumbered β-diketiminate ligand [{(2,6-$Pr^i_2H_3C_6$)N(CH_3)C}$_2$CH]$^-$, and a

modified synthesis of the aminoimine precursor. *J. Chem. Soc., Dalton Trans.* **2001**, 3465–3469.

[33] Sheldrick, G. M. A short history of SHELX. *Acta Crystallogr. Sect. A* **2008**, *64*, 112–122.

Transition Metal-Free Reductive Silylation of (Het)Aryl Bromides

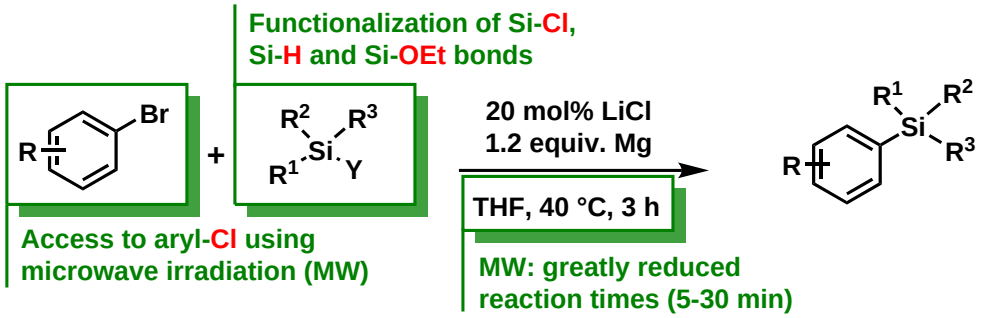

Abstract: A facile reductive silylation of (het)aryl bromides with chlorosilanes in the presence of magnesium as reductant was developed. Silanes and siloxanes exhibited similar reactivity. With this method, a total of over 25 tri- and tetraorganosilanes were synthesized. The reaction was then extended to more challenging substrates (aryl chlorides, triorganosilyl ethers) by the use of microwave heating, leading to short reaction times. The reaction constitutes an operationally simple method for the synthesis of tetraorganosilanes and an alternative to the conventional lithiation method.

6.1 Introduction

Organosilanes constitute important synthetic building blocks in polymer and materials synthesis, in the derivatization of organic molecules for analytical purposes (GC, MS), and as protective groups in the masking of chemical functionalities (mostly ethers).[1,2] Since the discovery of the Hiyama coupling reaction, silane-accelerated C-C-bond forming reactions became a vast research area.[3] The introduction of silicon atoms into organic molecules exerts various stereo-electronic effects due to the significantly lower electronegativity of silicon compared with carbon or hydrogen, the larger van der Waals radius vs. carbon, the high energies of Si-O and Si-F bonds, and the stabilization of positive charge in α-position (α-effect).[1] The preparation of Si-heteratom linkages is part of the standard repertoire of organic chemists. Numerous protection group strategies have been employed in the context of complex organic synthesis, mostly through base-mediated substitution of a heteroatom-bonded proton with a triorganosilyl group.[4] While hydrosilylations of olefins and alkynes constitute an especially versatile method for the construction of Si-C bonds,[5] arylsilanes cannot be prepared by this method.

Several protocols exist for the transition-metal catalyzed silylation reaction.[6] In many cases, Grignard reagents are employed in the presence of transition metal salts (e.g. nickel,[7] copper,[8] silver,[9] yttrium[10]). Most recently, Vulovic *et al*. reported on the acceleration of silane substitutions by use of a palladium complex.[11]

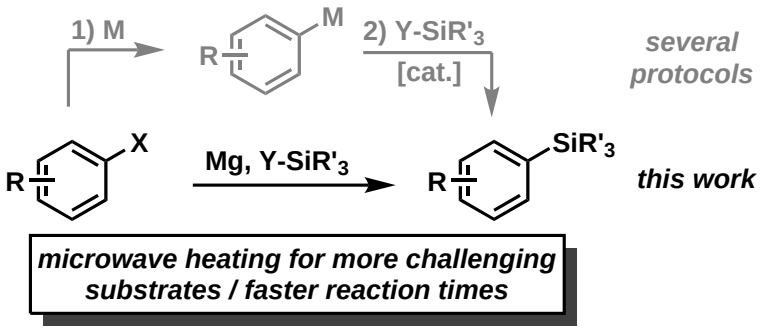

Scheme 6.1: Sequential metalation/cross-coupling vs. direct reductive coupling.

However, the preparation of arylmagnesium halides by metal-halogen exchange or transmetalation is not trivial in terms of practicality, reproducibility, safety, and scalability.[12] An attractive alternative to sequential metalation/cross-coupling methods are reductive processes between two electrophilic reagents.[13] This approach requires the presence of a suitable reductant, avoids the preformation and handling of hazardous organometallic reagents and, hence, contributes to a safer reaction processing. We investigated such synthetic strategy toward the preparation of arylsilanes starting from readily available aryl bromides and chlorosilanes. The low propensity of chlorosilanes to undergo insertion of magnesium is a key criterion for high cross-coupling selectivity (Scheme 6.1).[14]

6.2 Results and Discussion

We chose the reaction between 4-anisyl bromide (ArBr) and chloro(dimethyl)phenylsilane (DMPSCl) as model system. Initial experiments already indicated the viability of our synthetic plan (Table 6.1). Similar yields of the desired arylsilane were obtained under reductive coupling conditions (addition of Mg) and cross-coupling conditions (preformation of ArMgBr), respectively (entries 1, 2). An increase in temperature and concentration of LiCl generally led to a higher yield.[1] The optimized set of conditions involved treatment of the aryl bromide (1.2 equiv.) and DMPSCl with 1.2 equiv. Mg ribbons in THF at 40 °C for 3 h. The beneficial effect of LiCl in magnesiation reactions has already been extensively studied and appears to comprise the formation of reactive magnesiate species, the cleaning of Mg surface, and the increase of the ionic strength of the reagents solution.[15]

Table 6.1: Selected optimization experiments for the silylation of 4-bromoanisole.

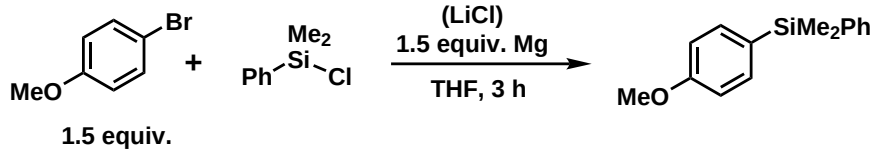

Entry	Conditions	Yield [%] [a]
1	20 °C	65 (88)
2	pre-formed 4-$MeOC_6H_4MgBr$, 20 °C	68 (84)
3	99.998% Mg, 20 °C	68 (91)
4	20% LiCl, 20 °C	79 (96)
5	100% LiCl, 20 °C	96 (99)
6	40 °C	81 (99)
7	20% LiCl, 40 °C	98 (99)
8	**20% LiCl, 40 °C, 1.2 equiv. Mg/DMPS-Cl**	**97 (100)**
9	20% LiCl, 40 °C, 1.1 equiv. Mg/DMPS-Cl	85 (100)

[a] GC yields vs. internal reference; in parentheses: yields after 20 h.

[1] For a comprehensive overview on the effect of temperature, reaction time and LiCl concentration see subsection 6.4.3 on p. 244.

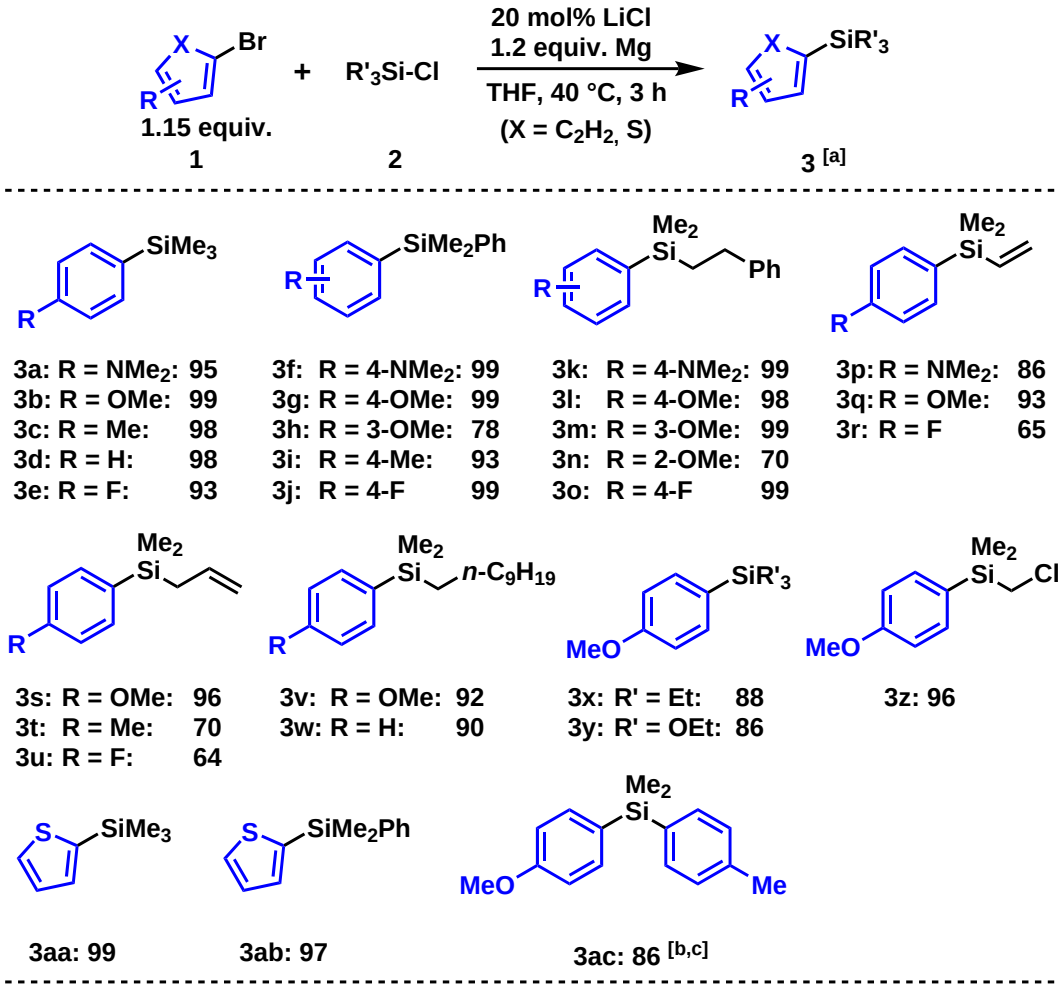

[a] isolated yields obtained after aqueous work-up and SiO_2 flash chromatography; [b] from dichlorodimethylsilane, Me_2SiCl_2; [c] sequential addition of 4-anisyl bromide and 4-tolyl bromide.

Scheme 6.2: Substrate scope of the general procedure for the reductive coupling between (hetero)aryl bromides and chlorosilanes.

The optimized reaction condition were used to produce a range of functionalized arylsilanes. Scheme 6.2 illustrates the substrate scope of the developed general procedure for the reductive coupling between (hetero)aryl bromides and chlorosilanes. Using electron-rich aryl bromides generally afforded the desired arylsilanes in excellent yields. Moderate to good reaction yields are in some cases seen for aryl bromides bearing a fluorine moiety as well as for *ortho*-substituted aryl bromides. The reaction allowed the synthesis of alkyl, aryl, chloromethyl, vinyl and allyl substituted arylsilanes. The latter three products provide ample opportunities for further functionalization at the silyl side chain by substitution or addition reactions. A diarylsilane was prepared by sequential addition of 4-anisyl bromide and 4-tolyl bromide to the reaction. Silylations of 2-bromothiophene also showed quantitative conver-

sion. Functional heteroarenes of this type are key intermediates in the synthesis of oligomeric materials for photonic and electronic applications.[16]

Hydrosilanes showed similar reactivity under standard conditions. While chlorodiphenylsilane was susceptible to selective chloride substitution, employment of diphenylsilane afforded the same product upon hydride displacement (Scheme 6.3a). Trisubstituted silanes, however, only showed poor results compared to the respective chlorosilanes which indicates a change in mechanism.

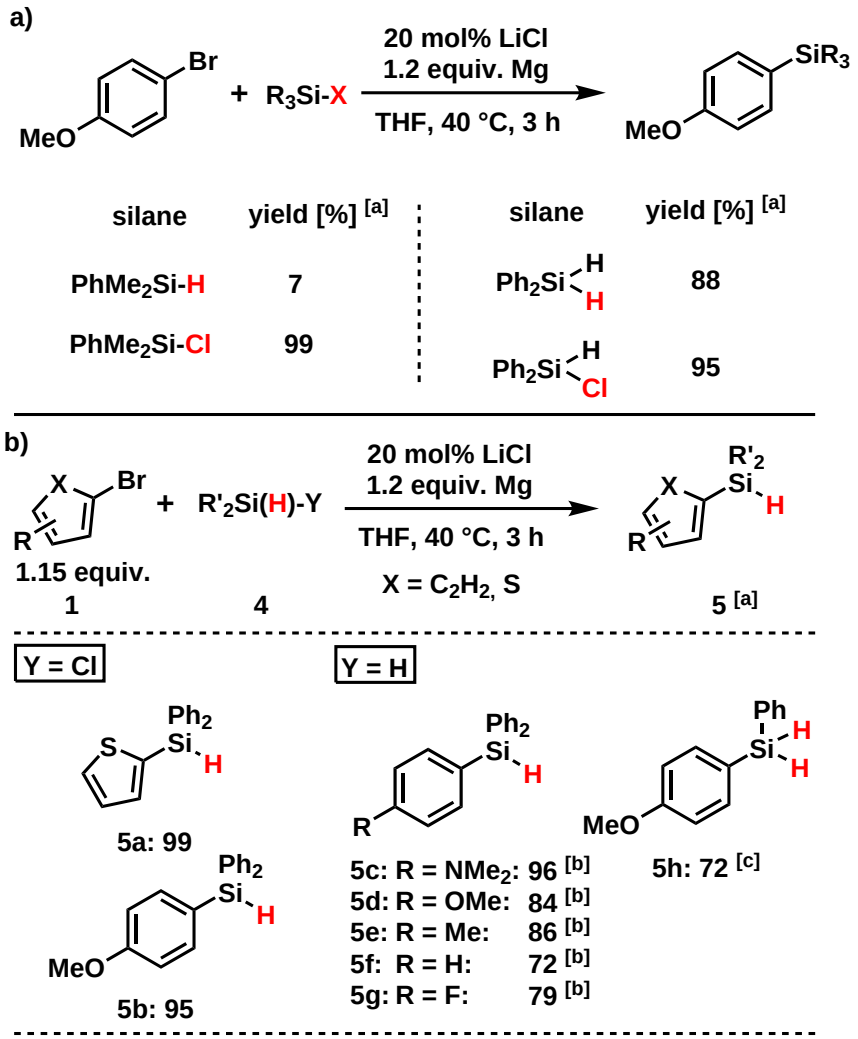

[a] yields were determined via GC-FID analysis vs. internal reference; [b] yields were determined via NMR analysis vs. internal reference; [c] 9% of diarylated product was obtained as side-product (Ar_2PhSiH).

Scheme 6.3: a) Comparison of the reaction yield for the silylation of 4-bromoanisol using mono- and dihydrosilanes as well as mono-chlorosilanes; b) Reaction scope for the synthesis of hydrosilane products.

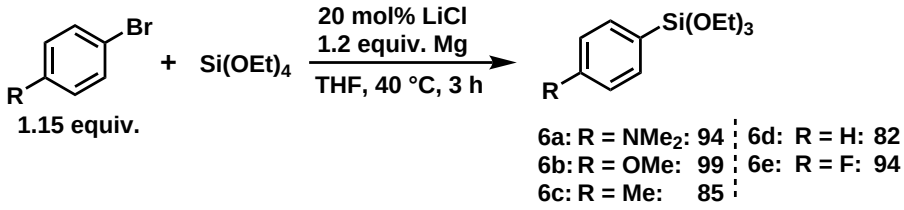

Scheme 6.4: Reductive silyl coupling using tetraethyl orthosilicate $Si(OEt)_4$. Yield was determined using NMR analysis with *n*-pentadecane as internal standard.

Using silanes and chlorohydrosilanes, it was possible to synthesize several di- and trisubstituted hydrosilanes in good to excellent yields (Scheme 6.3b). Since products **5a**-**5g** are trisubstituted silanes and barely undergo hydride displacement, no diarylated by-products were detected. In the reaction of phenylsilane and 4-bromoanisole a ratio of the mono- and difunctionalized coupling products was obtained (9:1). Tetraethyl orthosilicate $Si(OEt)_4$, also proved to be a competent silylation reagent (Scheme 6.4) and provided clean conversion without side-product formation. Electron withdrawing and -donating substituents again didn't impact the reaction significantly. Thus, this is an easy and cheap way to synthesize aryl triethoxysilanes e.g. as competent substrates for the Hiyama cross-coupling reaction.

Using the standard oil bath conditions (OB), more demanding substrates such as silyl ethers and aryl chlorides only show poor conversions (see Table 6.3, entries 1, 4, 6). Dielectric microwave heating (MW) seems to be a promising method to not only achieve these challenging coupling reactions but also to drastically reduce overall reaction times (entry 3; 5 min @ 120 °C vs 3 h @ 40 °C). In contrast to $Si(OEt)_4$ which is a well known precurser for the synthesis of aryltrialkoxysilanes,[17] only few literature reports exist that show isolated examples of triorganosilyl ethers used in silyl coupling reactions.[18] In our case, the high reaction temperature and pressure provided by the microwave enabled increased product formation in the reaction of ethoxydimethyl(phenyl)silane and 4-bromoanisole (entry 1). As discussed above, trisubstituted silanes only showed low reactivity even under harsh reaction conditions (entry 2). Aryl chlorides provide a compelling alternative to the corresponding bromides and iodides due to their smaller molecular mass and generally lower cost. However, they have seen only little attention in the synthesis of organosilanes owing to the strong C-Cl bond requiring harsch reaction conditions (e.g. highly reactive reagents,[19] long reation times and/or toxic solvents[20]), special equipment (e.g. electrochemical reductive silylation),[21] or the use of an expensive noble metal catalyst.[22] Surprisingly, the *m*-substituted chloroanisole exhibited higher yields than its bromo derivative using MW-irradiation, whereas the reaction completely stops under the conventional heating method (Table 6.3, entries 5/6).

Recently, Landais *et al*. published the synthesis of chiral silylium ions containing a binaphthalene backbone.[23] In our studies the synthesis of similar silanes **5i**, **5j** was possible in moderate to excellent yields after only 15 min reaction time (Scheme

Table 6.3: Silyl coupling of aryl bromides and chlorides under oil bath (OB; THF, 40 °C, 3 h) and microwave conditions (MW).

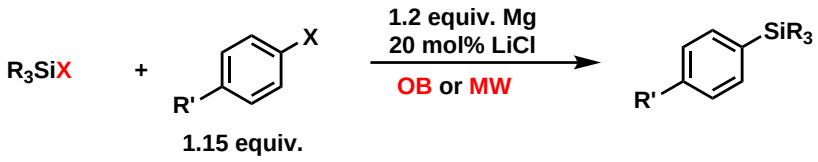

entry	silane	Ar-X	yield [a]
1	$PhMe_2SiOEt$		OB: 5% MW, 180 °C, 30 min: 86%
2	$PhMe_2SiH$	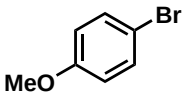	OB: 7% MW, 180 °C, 30 min: 8%
3	$PhMe_2SiCl$		OB: 99% MW, 120 °C, 5 min: 99%
4	$PhMe_2SiCl$	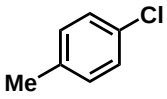	OB: 0% MW, 160 °C, 30 min: 85%
5	$PhMe_2SiCl$	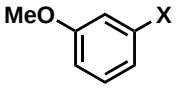	X = Br: OB: 78% MW, 120 °C, 15 min: 68%
6			X = Cl: OB: 0% MW, 140 °C, 30 min: 93%

[a] Yields were determined using GC-FID analysis vs. internal reference.

6.5a). The sterically less demanding 1-bromo-2-(methoxymethyl)benzene furnished complete conversion to the silane **5k**.

We optimized the reaction conditions using MW-irradiation in silylation reactions of 4-tolyl bromide and chloride at multiple reaction temperatures and times. In the case of the aryl bromide, complete conversion is expected after 5 min at 120 °C whereas the aryl chloride only shows trace amounts of product under the same conditions. In the same timeframe, the aryl chloride requires a reaction temperature of 180 °C to reach full conversion.[2] This opens up the possibility to selectively activate aryl halide bonds at certain temperatures. To utilize these properties, a reaction procedure was devised for the unsymmetrical double coupling of dichlorodimethylsilane with an aryl bromide and chloride in one pot. Contrary to the standard literature procedure in which both organometal compounds have to be made separately and added in sequence, the MW method allows reaction control by setting up a temperature profile

[2] A graphical representation of the optimization data is given in subsection 6.4.3 on p. 245.

(see Scheme 6.5b). Using this method, it was possible to synthesize **3ad** in 54% yield in a fast and operationally simple way.

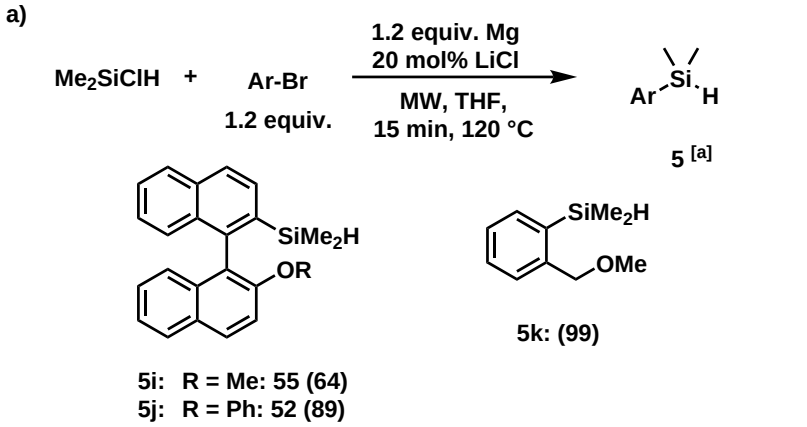

[a] isolated yields obtained after aqueous work-up and SiO_2 flash chromatography. The values in parentheses indicate the GC-FID yield after the reaction.

Scheme 6.5: a) Microwave-mediated reductive silylation of sterically hindered arly bromides; b) Unsymmetrical diarylcoupling of dichlorodimethylsilane in one pot using MW-irradiation.

6.3 Conclusion

In summary, we developed a simple and straightforward method for the synthesis of functionalized arylsilanes. The procedure can be carried out in one pot without the use of a transition metal catalyst under mild reaction conditions. Microwave-irradiation expands the scope of the reaction towards the use of aryl chlorides as well as silyl ethers in a quick, easy and reproducable way. Moreover, the advanced temperature control awarded by the MW enabled the selective, unsymmetrical diarylation of dichlorosilanes without the use of further reaction steps. The resultant arylsilanes constitute versatile building blocks that engage in electrophilic aromatic substitutions, polymerizations and cross-couling reactions. Selective silylarene hydrogenation, on the other hand, opens the way for the synthesis of novel saturated silyl compounds.[24]

6.4 Experimental Section

6.4.1 General Information

Analytical Thin-Layer Chromatography: Thin layer chromatography was performed using aluminium plates with silica gel and fluorescent indicator (Merck, 60F254). TLC plates were visualized by exposure to ultraviolet light and/or by immersion in a staining solution of molybdatophosphoric acid in ethanol or in a solution of potassium permanganate in water.

Column Chromatography: Flash column chromatography with silica gel 60 from KMF (40-63μm). As solvents mixtures of petrolether/ethyl acetate or *n*-pentane/ ethyl acetate were used.

Gas Chromatography with FID: HP6890 GC-System with injector 7683B, carrier gas: hydrogen GC-FID was used for all optimization experiments; quantification with *n*-pentadecane as internal standard and analytically pure samples.

Gas Chromatography with Mass-Selective Detector: Agilent 6890N Network GC-System, mass detector 5975 MS. Column: HP-5MS (30 m x 0.25 mm x 0.25 μm, 5% phenylmethylsiloxane), carrier gas: hydrogen. Standard heating procedure: 50 °C (2 min), 25 °C/min -> 300 °C (5 min).

NMR Spectroscopy: ^{1}H and ^{13}C nuclear magnetic resonance spectra were recorded on a Bruker Avance 300 (300 MHz). ^{1}H-NMR: The following abbreviations are used to indicate multiplicities: s, singlet; d, doublet; t, triplet; q, quartet; m, multiplet. ^{13}C-CPD-NMR (Composite Pulse Decoupling): d (doublet) was used to indicate a C-F fluorine coupling. The carbon signals were assigned as: Q, quaternary carbon; CH_{Ar}, aromatic CH; -CH=, α-vinyl carbon; $=CH_2$, α-vinyl carbon, CH_2, aliphatic CH_2 group; CH_3, methyl group; OCH_3, methoxy group; Ar-CH_3, benzylic CH_3; NCH_3, N-methyl group; $SiCH_3$, silylmethyl group; $SiCH_2$, silylmethylene group.

IR Spectroscopy: ATR technique on a Thermo Nicolet 380 FT-IR. Intensities: s = strong, m = medium, w = weak.

High Resolution Mass Spectrometry (HRMS): Mass spectra were recorded on a Finnigan MAT 900s (EI).

Melting Point: Melting points were determined on a Büchi apparatus according to Dr. Tottoli and are uncorrected.

Chemicals: All chemicals were purchased from commercial suppliers and used without further purification unless otherwise noted. THF was distilled over sodium and benzophenone under an argon atmosphere. $CDCl_3$ (0.03 % TMS, 0.01 % H_2O) from Eurisotop was stored over 4 Å molecular sieves. LiCl (> 99%) from Aldrich were stored and handled in a glove box. All Arylbromides and Silicon compounds were used without further purification. Magnesium (99.0 % and 99.998%) were purchased from Aldrich and stored in a glovebox.

6.4.2 General Procedures

General Procedure 1 (for Monochloro Silicon Compounds):

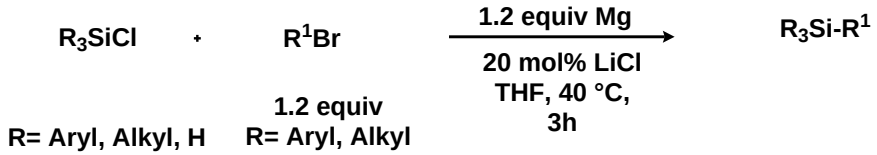

8 mg (20 mol%, 0.2 mmol) LiCl and 29mg (120 mol%, 1.2 mmol) Magnesium turnings were loaded into a 10 ml-flask under an atmosphere of argon and treated with 4 ml dry THF. The reaction mixture was put in a water bath at 40 °C and treated with 1.2 mmol of the organobromine followed by 1 mmol of the silyl chloride. The mixture was then stirred at 40 °C for 3 h. Then, saturated aqueous ammonium chloride was added, and the mixture extracted with ethyl acetate. The combined organic phases were dried (Na_2SO_4) and concentrated in vacuo. Silica gel column chromatography afforded the pure silicon compounds.

General Procedure 2 (Use of Dichloro Silicon Compounds):

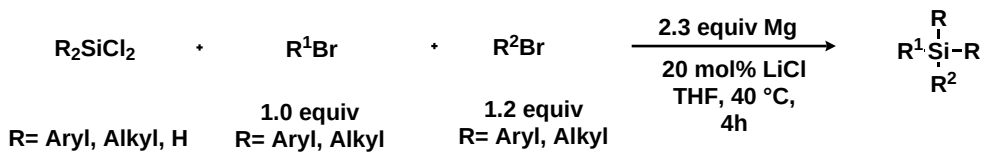

8 mg (20 mol%, 0.2 mmol) LiCl and 55 mg (230 mol%, 2.3 mmol) Magnesium turnings were loaded into a 10 ml-flask under an atmosphere of argon and treated with 4 ml dry THF. The reaction mixture was put in a water bath at 40 °C and treated with 1.0 mmol of the first organobromine followed by 1 mmol of the silyl chloride. After 1 h at 40 °C 1.2 mmol of the second organobromine was added. The mixture was then stirred at 40 °C for additional 3 h. Then, saturated aqueous ammonium chloride was added, and the mixture extracted with ethyl acetate. The combined organic phases were dried (Na_2SO_4) and concentrated in vacuo. Silica gel column chromatography afforded the pure silicon compounds.

General Procedure 3 (Use of Silanes and Alkoxysilanes):

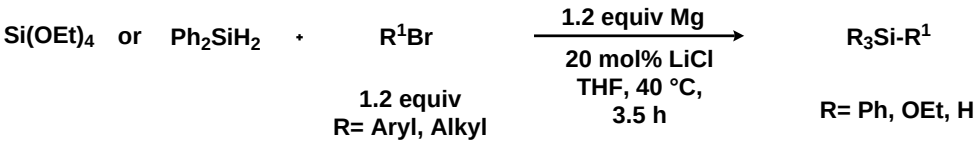

8 mg (20 mol%, 0.2 mmol) LiCl and 29mg (120 mol%, 1.2 mmol) Magnesium turnings were loaded into a 10 ml-flask under an atmosphere of argon and treated with 4 ml dry THF. The reaction mixture was put in a water bath at 40°C and treated with 1.2 mmol of the organobromine followed by 1 mmol of diphenyl silane or tetraethyl orthosilicate. The mixture was then stirred at 40°C for 3.5 h. Then, saturated aqueous ammonium chloride was added, and the mixture extracted with ethyl acetate. The combined organic phases were dried (Na_2SO_4) and concentrated in vacuo. Silica gel column chromatography afforded the pure silicon compounds.

General Procedure 4 (Microwave Irradiation):

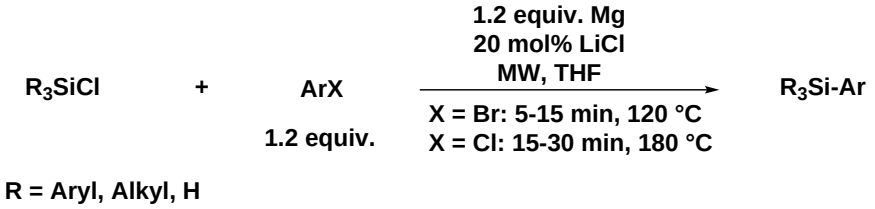

In an ovendried vial, magnesium powder (6 mg, 0.26 mmol, 1.2 equiv.) was suspended in a solution of LiCl (5 mg, 0.044 mmol, 20 mol%) in dry THF (2 ml), then the aryl bromide or chloride and the silyl chloride were added. The mixture was heated by MW irradiation for 5-15 minutes at 120°C or 15-30 minutes at 180 °C respectively. The endpoint of the reaction was visible via video monitoring when almost all magnesium was consumed. The reaction mixture was then quenched by addition of a saturated solution of NH_4Cl (2 ml). The aqueous phase was extracted three times with ethyl acetate (4 ml each) and combined organic layers were dried over Na_2SO_4. Conversion was determined using GC.

6.4.3 Reaction Optimization

Optimization of Standard Oil Bath Conditions

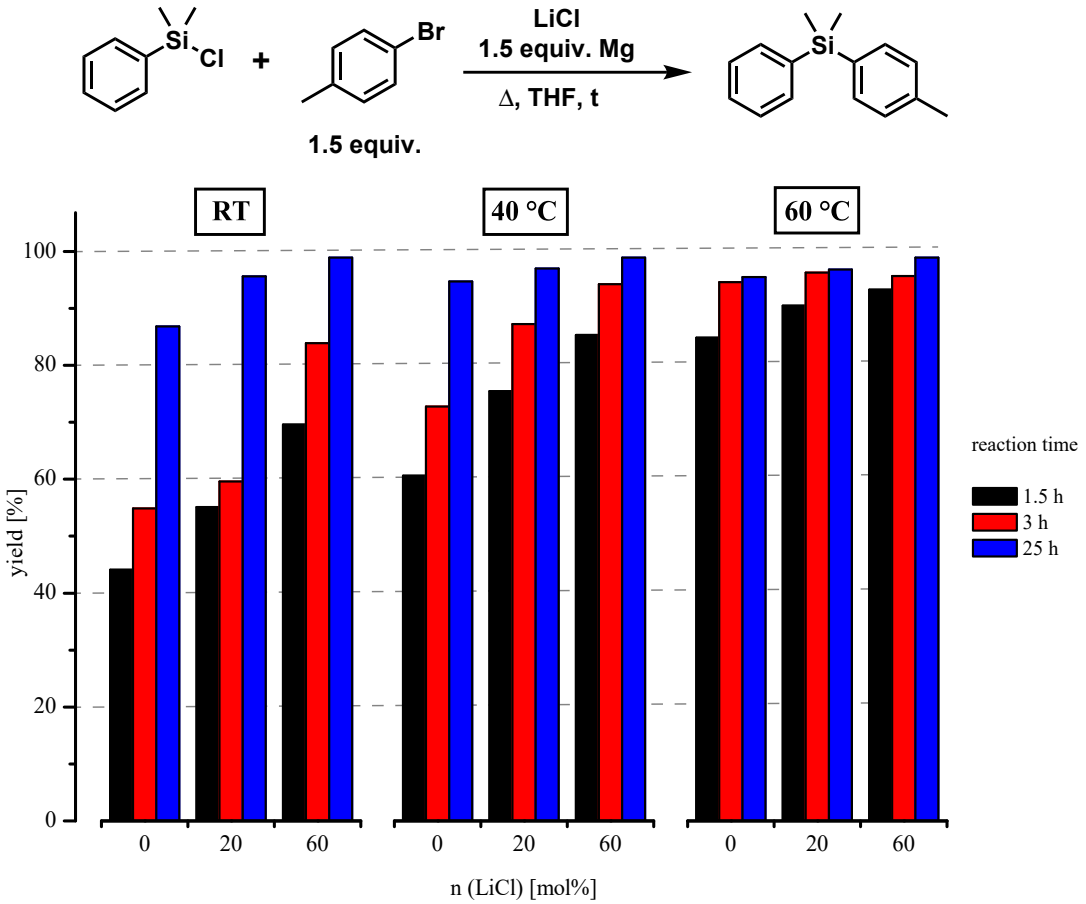

Figure 6.1: Optimization of standard oil bath conditions. Various temperatures, reaction times and quantities of lithium chloride in the reaction of DMPS-Cl with 4-bromotoluene.

The reactions were performed according to general procedure 1 and analyzed via GC-FID.

Optimization of Microwave-Mediated Silyl Coupling

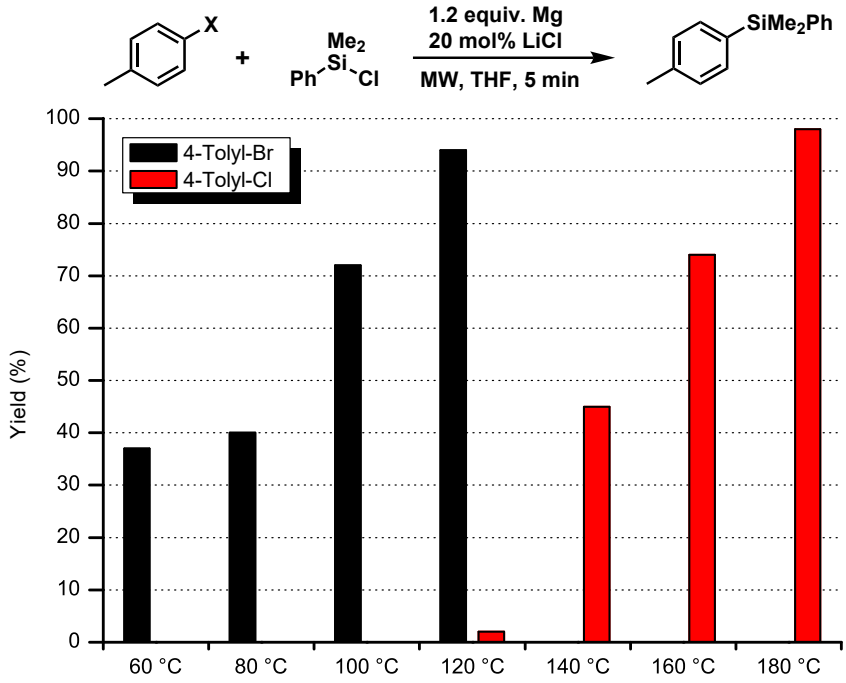

Figure 6.2: Reaction optimization in coupling of a chlorosilane and an aryl chloride using MW-irradiation.

Figure 6.2 shows the reaction yields for a coupling reaction between a chlorosilane and 4-tolyl-chloride under different reaction conditions using MW-irradiation. Independent of reaction times, the C-Cl bond could not be activated at 120 °C, whereas total conversion was achieved only at 180 °C and extended reaction times. At the same time bromoarenes can be converted efficiently at 120 °C which opens up the possibility to selectively activate aryl halide bonds at certain temperatures.

6.4.4 Synthesis of Starting Materials

General Synthetic Scheme

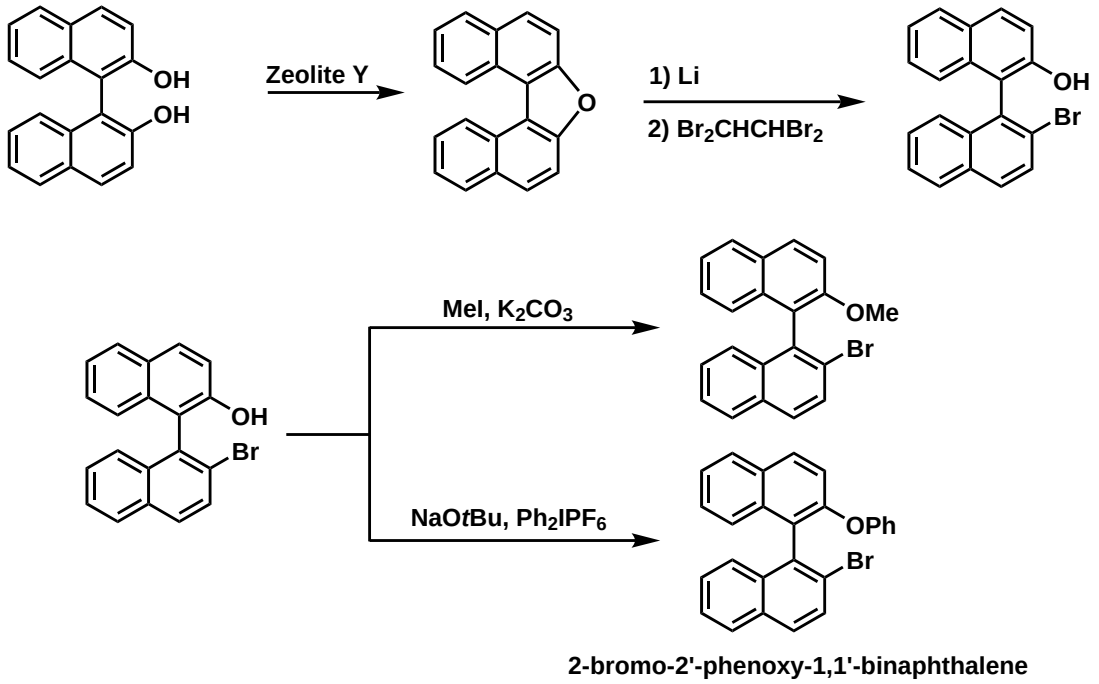

Figure 6.3: Reaction optimization in coupling of a chlorosilane and an aryl chloride using MW-irradiation.

Binaphtofuran

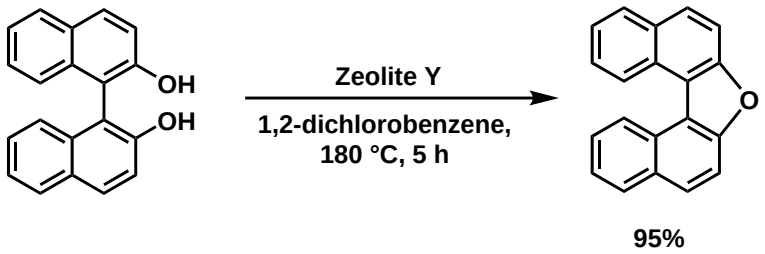

The target compound was synthesized according to following literature report: I. A. Shuklov, N. V. Dubrovina, H. Jiao, A. Spannenberg, A. Börner, *Eur. J. Org. Chem.* **2010**, 1669–1680.

In a 250 ml flask equipped with a magnetic stirrer, zeolite (7 g) was heated in a sand bath at 400 °C under vacuum for 16 h. After cooling to room temperature, *rac*-BINOL

(12g, 41.91 mmol) and freshly distilled 1,2- dichlorobenzene (70 ml) were added. The colorless suspension was then stirred for 5 h at 180 °C slowly turning blue. After cooling to room temperature, it was filtered on celite and the solvent removed under vacuum to yield a pale red solid which was used in further step without purification (10.77 g, 37.45 mmol, 95 %).

^{1}H NMR (300 MHz, $CDCl_3$): δ 9.17 (d, J = 8.5 Hz, 2H), 8.08 (d, J = 8.1 Hz, 2H), 7.97 (d, J = 8.9 Hz, 2H), 7.85 (d, J = 8.9 Hz, 2H), 7.76 (ddd, J = 8.4, 6.9, 1.3 Hz, 2H), 7.66 – 7.54 (m, 2H); **GC-MS:** t_R = 13.34 min, m/z = 268 [M^+]; **TLC:** R_f = 0.67 (hexanes/5% Et_2O).

2′-Bromo-1,1′-binaphthyl-2-ol

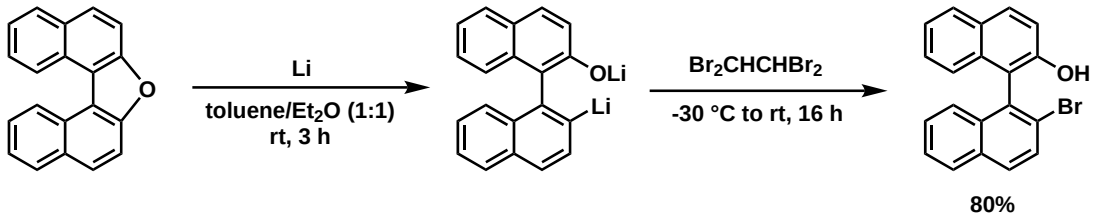

The target compound was synthesized according to following literature report: X. Xie, L. Ding, G. Ni, Z. Zhang, J. Gao, *Chin. J. Chem.* **2010**, *28*, 1630–1634.

In a dry 250 ml two necked flask equipped with a magnetic stirrer was added lithium wire (0.69 g, 10.0 mmol) in several portions to a clear solution of binaphthofuran (2.68 g, 10.0 mmol) in dry toluene (35 ml) and dry diethyl ether (35 ml). The suspension turned deep red and was stirred at room temperature for 3 h. The solution was canulated into a dry 250 ml two neck flask equipped with a magnetic stirrer. It was then cooled to -30 °C and 1,1,2,2-tetrabromoethane (1.75 ml, 15.0 mmol) was added dropwise (15 min). The solution was stirred for 2 h at -30 °C and then at room temperature overnight. The endpoint of the reaction was determined with TLC (pentane/5% ethyl acetate). The reaction mixture was acidified with 2 M HCl (20 ml), the organic layer was separated and the aqueous layer extracted three times with Et_2O (20 ml). Combined organic layers were dried over Na_2SO_4, filtered and solvent concentrated under vacuum. The crude product was purified by flash chromatography on silica gel (pentane/7% ethyl acetate) afforded the desired product as a pale yellow solid (2.8 g, 8.0 mmol, 80 %).

^{1}H NMR (300 MHz, $CDCl_3$): δ 8.00 – 7.83 (m, 5H), 7.53 (ddd, J = 8.1, 6.7, 1.3 Hz, 1H), 7.39 – 7.30 (m, 3H), 7.30 – 7.22 (m, 2H), 6.97 (dd, J = 8.3, 0.6 Hz, 1H), 4.73 (brs, 1H); **GC-MS:** t_R = 12.99 min, m/z = 348 [M^+]; **TLC:** R_f = 0.36 (*n*-pentane/7% EtOAc).

2-Bromo-2′-methoxy-1,1′-binaphthalene

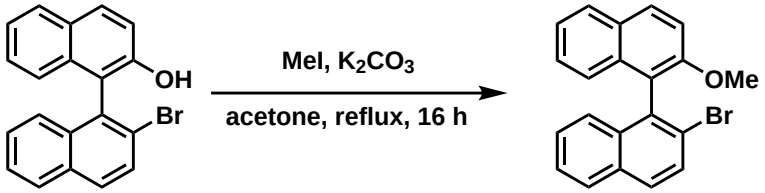

85%

The target compound was synthesized according to following literature report: F. Ma, X. Xie, L. Zhang, Z. Peng, L. Ding, L. Fu, Z. Zhang, *J. Org. Chem.* **2012**, *77*, 5279–5285.

In a dry 25 ml flask equipped with a magnetic stirrer and a condenser was added 2′-bromo-1,1′-binaphthyl-2-ol (1.22 g, 3.5 mmol) in acetone (7 ml). K_2CO_3 (1.45 g, 10.5 mmol) and iodomethane (0.65 ml, 10.5 mmol) were added and the suspension was refluxed for 16 h. After cooling to room temperature, the suspension was filtered and washed with acetone. The filtrate was concentrated under vacuum to afford the desired product as a white solid (1.09 g, 3.0 mmol, 85%).

^{1}H NMR (300 MHz, DMSO-d_6): δ 8.15 (d, J = 9.1 Hz, 1H), 8.10 – 7.95 (m, 3H), 7.87 (d, J = 8.8 Hz, 1H), 7.66 (d, J = 9.1 Hz, 1H), 7.53 (dd, J = 11.0, 4.0 Hz, 1H), 7.42 – 7.21 (m, 3H), 6.99 (d, J = 8.4 Hz, 1H), 6.79 (d, J = 7.9 Hz, 1H), 3.76 (s, 3H); **GC-MS:** t_R = 12.85 min, m/z = 364 [M^+].

2-Bromo-2′-phenoxy-1,1′-binaphthalene

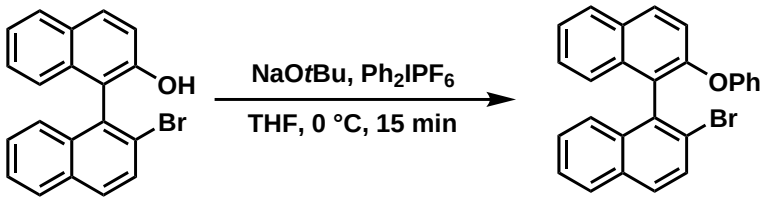

99%

The target compound was synthesized according to following literature report: P. Ducos,V.Liautard, F. Robert, Y. Landais, *Chem. Eur.J.* **2015**, *21*, 11573–11578.

In a dry 25 ml flask equipped with a magnetic stirrer was added 2′-bromo-1,1′-binaphthyl-2-ol (0.70 g, 2.0 mmol) in dry THF (3 ml). The solution was cooled to 0 °C, then sodium *tert*-butoxide (211 mg, 2.2 mmol) was added and the resulting mixture

stirred for 15 min. Diphenyliodonium hexafluorophosphate (1.02 g, 2.4 mmol) was added in one portion and after 5 min. at 0 °C, the orange reaction mixture was heated to 40 °C for 4 h. The endpoint of the reaction was determined with GC-MS analysis. After cooling to room temperature, H_2O (10 ml) was added, the aqueous layer was separated and the organic layer was extracted twice with EtOAc. Combined organic layers were dried over Na_2SO_4, filtered and concentrated under vacuum. Purification by flash chromatography on silica gel (pentane/3% ethyl acetate) afforded the desired product as a white solid (0.85 g, 2.0 mmol, 99%).

^{1}H NMR (300 MHz, $CDCl_3$): δ 8.00 – 7.84 (m, 3H), 7.83 – 7.72 (m, 2H), 7.52 – 7.39 (m, 2H), 7.36 – 7.27 (m, 4H), 7.24 – 7.16 (m, 2H), 7.13 (d, J = 7.8 Hz, 1H), 7.04 – 6.89 (m, 3H); **GC-MS:** t_R = 15.51 min, m/z = 426 [M^+]; **TLC:** R_f = 0.32 (*n*-pentane/2% EtOAc).

Dimethyl(ethoxy)phenylsilane.

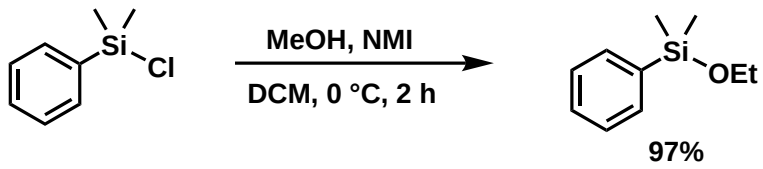

The target compound was synthesized according to following literature report: P. Bohn, A. Deyine, R. Azzouz, L. Bailly, C. Fiol-Petit, L. Bischoff , C. Fruit, F. Marsais, P. Vera, *Nucl. Med. Biol.* **2009**, *36*, 895–905.

To a solution of chloro(dimethyl)phenylsilane (1.7 g, 10.0 mmol) in dichloromethane at 0 °C was slowly added a mixture of ethanol (1.2 ml, 20 mmol, 2 equiv.) and *N*-methylimidazole (880 μL, 11.0 mmol, 1.1 equiv.). The resulting mixture was stirred for 2 h at 0 °C. The precipitated *N*-methylimidazolium chloride was removed by filtration. The filtrate was concentrated in vacuo to yield the target compound as a colorless oil (1.75 g , 9.7 mmol, 97%) .

^{1}H NMR (300 MHz, $CDCl_3$): δ 7.65-7.51 (m, 2H), 7.42-7.31 (m, 3H), 3.75-3.62 (m, 2H), 1.28-1.15 (m, 3H), 0.45-0.26 (m, 6H); **GC-MS:** t_R = 6.34 min, m/z = 180 [M^+].

6.4.5 Isolated Coupling Products

4-(Trimethylsilyl)-*N*,*N*-dimethylaniline (3a)

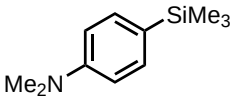

	Pale yellow oil
	$C_{11}H_{19}NSi$
	193.13 g/mol
Yield	95%
TLC	R_f = 0.39 (SiO_2, *n*-pentane/ethyl acetate (19:1))
^{1}H-NMR	(300 MHz, $CDCl_3$) δ 7.37-7.30 (m; 2H), 7.23-7.13 (m; 2H), 2.88 (s; 6H), 0.16 (s; 9H).
^{13}C-NMR	(75 MHz, $CDCl_3$) δ 151.1 (Q), 134.5 (CH_{Ar}), 129.2 (Q), 112.2 (CH_{Ar}), 40.4 (NCH_3) , -0.72 ($SiCH_3$).
GC-MS	t_R = 6.16 min, (EI, 70 eV): m/z = 193 [M^+], 178, 162, 148, 134, 119, 105, 87, 73, 59.

Analytical data were in full agreement with K. Aikawa, Y. Hioki, K. Mikami, *Chem. Asian J.* **2010**, 2346-2350.

(4-Methoxyphenyl)trimethylsilane (3b)

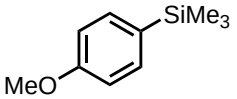

	Colorless oil
	$C_{10}H_{16}OSi$
	180.10 g/mol
Yield	100%
TLC	R_f = 0.54 (SiO_2, *n*-pentane/ethyl acetate (19:1))
^{1}H-NMR	(300 MHz, $CDCl_3$) δ 7,49-7.42 (m; 2H), 6.95-6.89 (m; 2H), 3.82 (s; 3H), 0.25 (s; 9H).
^{13}C-NMR	(75 MHz, $CDCl_3$) δ 160.4 (Q), 134.9 (CH_{Ar}), 131.5 (Q), 113.6 (CH_{Ar}), 55.2 (OCH_3), -0.79 ($SiCH_3$).
GC-MS	t_R = 6.39 min, (EI, 70 eV): m/z = 180 [M^+], 165, 135, 107, 77, 59.

Analytical data were in full agreement with L. T. Ball, G. C. Lloyd-Jones, C. A. Russell, *Chem. Eur. J.* **2012**, *18*, 2931-2937.

Trimethyl(*p*-tolyl)silane (3c)

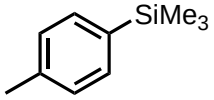

	Colorless oil
	$C_{10}H_{16}Si$
	164.10 g/mol
Yield	98%
TLC	R_f = 0.58 (SiO_2, *n*-pentane)
^{1}H-NMR	(300 MHz, $CDCl_3$) δ 7.44 (d; 7.9 Hz; 2H), 7.19 (d; 7.5 Hz; 2H), 2.36 (s; 3H), 0.26 (s; 9H).
^{13}C-NMR	(75 MHz, $CDCl_3$) δ 138.8 (Q), 137.0 (Q), 133.5 (CH_{Ar}), 128.7 (CH_{Ar}), 21.6 (Ar-CH_3), -1.09 ($SiCH_3$).
GC-MS	t_R = 6.16 min, (EI, 70 eV): m/z = 164 [M^+], 149, 133, 121, 105, 91, 77, 65, 53.

Analytical data were in full agreement with L. T. Ball, G. C. Lloyd-Jones, C. A. Russell *Chem. Eur. J.* **2012**, *18*, 2931-2937.

Trimethyl(phenyl)silane (3d)

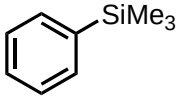

	Colorless oil
	$C_9H_{14}Si$
	150.09 g/mol
Yield	95%
TLC	R_f = 0.50 (SiO_2, *n*-pentane)
^{1}H-NMR	(300 MHz, $CDCl_3$) δ 7.59-7.50 (m; 2H), 7.40-7.30 (m; 2H), 0.26 (s; 9H).
^{13}C-NMR	(75 MHz, $CDCl_3$) δ 140.6 (Q), 133.4 (CH_{Ar}), 128.9 (CH_{Ar}), 127.9 (CH_{Ar}), -1.00 ($SiCH_3$).
GC-MS	t_R = 4.61 min, (EI, 70 eV): m/z = 150 [M^+], 135, 119, 105, 91, 77, 65, 53.

Analytical data were in full agreement with H. Inubushi , H. Kondo , A. Lesbani , M. Miyachi , Y. Yamanoi, H. Nishihara, *Chem. Commun.* **2013**, *49*, 134-136.

(4-Fluorophenyl)trimethylsilane (3e)

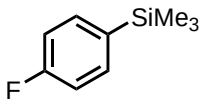

Colorless oil

$C_9H_{13}FSi$

168.08 g/mol

Yield 93%

TLC R_f = 0.52 (SiO_2, *n*-pentane)

^{1}H-NMR (300 MHz, $CDCl_3$) δ 7.49 (dd; 6.27/8.56 Hz; 2H), 7.05 (dd; 8.65/9.35 Hz; 2H), 0.26 (s; 9H).

^{13}C-NMR (75 MHz, $CDCl_3$) δ 166.7 (d; 247.4 Hz; Q), 136.0 (d; 3.8 Hz; Q), 135.3 (d; 7.3 Hz; CH_{Ar}), 115.0 (d; 19.5 Hz; CH_{Ar}), -0.11 ($SiCH_3$).

GC-MS t_R = 4.67 min, (EI, 70 eV): m/z = 168 [M^+], 153, 137, 123, 109, 91, 77, 65, 53.

Analytical data were in full agreement with C. Heiss, E. Marzi, F. Mongin, M. Schlosser, *Eur. J. Org. Chem.* **2007**, 669-675.

4-(Dimethyl(phenyl)silyl)-*N*,*N*-dimethylaniline (3f)

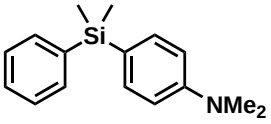

Pale yellow oil

$C_{16}H_{21}NSi$

255.14 g/mol

Yield 100%

TLC R_f = 0.42 (SiO_2, *n*-pentane/ethyl acetate (19:1))

^{1}H-NMR (300 MHz, $CDCl_3$) δ 7.56-7.50 (m; 2H), 7.43-7.38 (m; 2H), 7.37-7.31 (m; 3H), 6.82-6.68 (m; 2H), 2.97 (s; 6H), 0.51 (s; 6H).

^{13}C-NMR (75 MHz, $CDCl_3$) δ 151.2 (Q), 139.5 (Q), 135.4 (CH_{AR}), 134.3 (CH_{AR}), 128.9 (CH_{AR}), 127.8 (CH_{AR}), 123.1 (Q), 40.3 (NH_3), -2.0 ($SiCH_3$).

GC-MS t_R = 10.16 min, (EI, 70 eV): m/z = 255 [M^+], 240, 224, 210, 197, 178, 165, 148, 134, 120, 105, 91, 78, 64, 51.

HRMS (EI, 70 eV, m/z): 255.1438, calcd: 255.1443.

FT-IR (ATR film) $1/\lambda$ [cm^{-1}] = 3070 (w), 2957 (w), 1252 (m), 1117 (s), 1048 (s), 827 (s), 783 (s), 696 (s), 469 (m).

(4-Methoxyphenyl)dimethyl(phenyl)silane (3g)

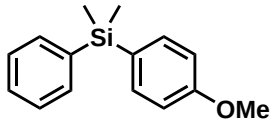

	Colorless oil
	$C_{15}H_{18}OSi$
	242.11 g/mol
Yield	99%
TLC	R_f 0.51 (SiO_2, *n*-pentane/ethyl acetate (19:1))
^{1}H-NMR	(300 MHz, $CDCl_3$) δ 7.55-7.49 (m; 2H), 7.48-7.30 (m; 2H), 7.38-7.33 (m; 3H), 6.95-6.89 (m; 2H), 3.82 (s; 3H), 0.53 (s; 6H).
^{13}C-NMR	(75 MHz, $CDCl_3$) δ 160.6 (Q), 138.8 (Q), 135.8 (CH_{AR}), 134.3 (CH_{AR}), 129.1 (CH_{AR}), 129.1 (Q), 127.9 (CH_{AR}), 113.7 (CH_{AR}), 55.2 (OCH_3), -2.1 ($SiCH_3$).
GC-MS	t_R = 9.29 min, (EI, 70 eV): m/z = 242 [M^+], 227, 212, 197, 184, 169, 152, 135, 121, 105, 91, 77, 68, 59, 50.

Analytical data were in full agreement with Y. Yamanoi, *J. Org. Chem.* **2005**, *70*, 9607-9609.

(3-Methoxyphenyl)dimethyl(phenyl)silane (3h)

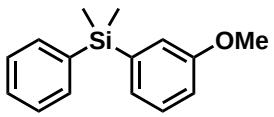

	Colorless oil
	$C_{15}H_{18}OSi$
	242.11 g/mol
Yield	71%
TLC	R_f 0.52 (SiO_2, *n*-pentane/ethyl acetate (19:1))
^{1}H-NMR	(300 MHz, $CDCl_3$) δ 7.56-7.48 (m; 2H), 7.39-7.27 (m; 4H), 7.14-7.03 (m; 2H), 6.94-6.87 (m; 1H), 3.80 (s; 3H), 0.55 (s; 6H).
^{13}C-NMR	(75 MHz, $CDCl_3$) δ 159.6 (Q), 140.4 (Q), 138.6 (Q), 134.7 (CH_{AR}), 129.6 (CH_{AR}), 129.5 (CH_{AR}), 128.3 (CH_{AR}), 126.9 (CH_{AR}), 120.2 (CH_{AR}), 114.5 (CH_{AR}), 55.1 (OCH_3), -2.8 ($SiCH_3$).
GC-MS	t_R = 9.10 min, (EI, 70 eV): m/z = 242 [M^+], 227, 211, 197, 181, 165, 152, 135, 119, 105, 91, 77, 59.

HRMS	(EI, 70 eV, m/z): 242.1127, calcd: 242.1127.
FT-IR	(ATR film) $1/\lambda$ [cm^{-1}] = 3003 (w), 2955 (w), 2832 (w), 1569 (m), 1406 (m), 1227 (s), 1109 (m), 1046 (m), 828 (m), 803 (s), 770 (s), 697 (s).

Dimethyl(4-methylphenyl)phenylsilane (3i)

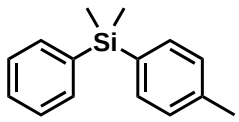

	Colorless oil
	$C_{15}H_{18}Si$
	226.12 g/mol
Yield	93%
TLC	R_f = 0.25 (SiO_2, *n*-pentane)
^{1}H-NMR	(300 MHz, $CDCl_3$) δ 7.55-7.49 (m; 2H), 7.45-7.40 (m; 2H), 7.38-7.32 (m; 3H), 7.21-7.15 (m; 2H), 2.35 (s; 3H), 0.54 (s; 6H).
^{13}C-NMR	(75 MHz, $CDCl_3$) δ 139.1 (Q), 138.6 (Q), 134.7 (Q), 134.4 (CH_{AR}), 134.3 (CH_{AR}), 129.2 (CH_{Ar}), 128.8 (CH_{AR}), 127.9 (CH_{AR}), 21.6 (Ar-CH_3), -2.2 ($SiCH_3$).
GC-MS	t_R = 8.58 min, (EI, 70 eV): m/z = 226 [M^+], 211, 195, 181, 165, 149, 135, 119, 105, 91, 77, 65, 51.

Analytical data were in full agreement with K. Murakami, K. Hirano, H. Yorimitsu, K. Oshima, *Angew. Chem. Int. Ed.* **2008**, *47*, 5833-5835.

(4-Flourophenyl)dimethyl(phenyl)silane (3j)

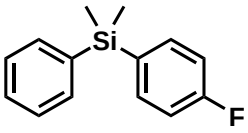

	Colorless oil
	$C_{14}H_{15}FSi$
	230.09 g/mol
Yield	87%
TLC	R_f = 0.62 (SiO_2, *n*-pentane/ethyl acetate (19:1))
^{1}H-NMR	(300 MHz, $CDCl_3$) δ 7.53-7.45 (m; 4H), 7.40-7.32 (m; 3H), 7.09-7.01 (m; 2H), 0.55 (s; 6H).
^{13}C-NMR	(75 MHz, $CDCl_3$) δ 163.9 (d; 248.07 Hz; Q), 138.1 (Q), 136.2 (d; 7.36 Hz; CH_{AR}), 134.3 (CH_{AR}), 133.9 (d; 3.3 Hz; Q), 129.4 (CH_{AR}), 128.0 (CH_{AR}), 115.1 (d; 19.70 Hz; CH_{AR}), -2.2 ($SiCH_3$).

GC-MS	t_R = 8.03 min, (EI, 70 eV): m/z = 230 [M^+], 215, 199, 183, 174, 165, 152, 135, 123, 105, 91, 77, 63, 51.

Analytical data were in full agreement with K. Murakami, K. Hirano, H. Yorimitsu, K. Oshima, *Angew. Chem. Int. Ed.* **2008**, *47*, 5833-5835.

4-(Dimethyl(phenethyl)silyl)-N,N-dimethylaniline (3k)

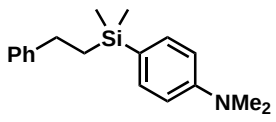

	Pale yellow oil
	$C_{18}H_{25}NSi$
	283.18 g/mol
Yield	100%
TLC	R_f = 0.48 (SiO_2, *n*-pentane/ethyl acetate (19:1))
^{1}H-NMR	(300 MHz, $CDCl_3$) δ 7.49-7.42 (m; 2H), 7.35-7.15 (m; 5H), 6.80 (d; 8.0 Hz, 2H); 2.98 (s; 6H), 2.68-2.60 (m; 2H), 1.14-1.05 (m; 2H), 0.29 (s; 6H).
^{13}C-NMR	(75 MHz, $CDCl_3$) δ 151.1 (Q), 145.5 (Q), 134.8 (CH_{Ar}), 128.4 (CH_{Ar}), 127.9 (CH_{Ar}), 125.5 (CH_{Ar}), 124.1 (Q), 40.4 (NH_3), 30.2 (Ar-CH_2), 18.2 ($SiCH_2$), -2.0 ($SiCH_3$).
GC-MS	t_R = 10.95 min, (EI, 70 eV): m/z = 283 [M^+], 224, 197, 178, 147, 121, 91, 65.
HRMS	(EI, 70 eV, m/z): 283.1758, calcd: 283.1756.
FT-IR	(ATR film) $1/\lambda$ [cm^{-1}] = 3026 (w), 2954 (w), 2925 (w), 1495 (w), 1252 (s), 1049 (s), 836 (s), 777 (s), 696 (s).

(4-Methoxyphenyl)dimethyl(phenethyl)silane (3l)

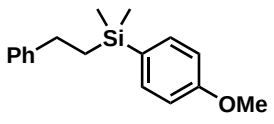

	Pale yellow oil
	$C_{17}H_{22}OSi$
	270.14 g/mol
Yield	98%
TLC	R_f = 0.42 (SiO_2, *n*-pentane/ethyl acetate (99:1))

^{1}H-NMR	(300 MHz, $CDCl_3$) δ 7.46 (d; 8.62 Hz; 2H), 7.30-7.15 (m; 5H), 6.92 (d; 8.62 Hz; 2H), 3.81 (s; 3H), 2.70-2.60 (m; 2H), 1.15-1.02 (m; 2H), -0.26 (s; 6H).
^{13}C-NMR	(75 MHz, $CDCl_3$) δ 160.5 (Q), 145.2 (Q), 135.2 (CH_{AR}), 130.0 (Q), 128.4 (CH_{AR}), 127.9 (CH_{AR}), 125.6 (CH_{AR}), 113.7 (CH_{AR}), 55.2 (OCH_3), 30.1 ($SiCH_2$), 18.1 (Ar-CH_2), -2.8 ($SiCH_3$).
GC-MS	t_R = 10.21 min, (EI, 70 eV): m/z = 270 [M^+], 255, 238, 227, 165, 151, 135, 121, 105, 91, 77, 59.
HRMS	(EI, 70 eV, m/z): 270.1442, calcd: 270.1440.
FT-IR	(ATR film) $1/\lambda$ [cm^{-1}] = 3024 (w), 2951 (w), 2914 (w), 1593 (s), 1502 (s), 1276 (s), 1244 (s), 1181 (m), 1110 (s), 785 (s), 768 (s), 696 (s).

(3-Methoxyphenyl)dimethyl(phenethyl)silane (3m)

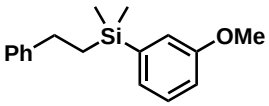

	Pale yellow oil
	$C_{17}H_{22}OSi$
	270.14 g/mol
Yield	99%
TLC	R_f = 0.59 (SiO_2, *n*-pentane/ethyl acetate (19:1))
^{1}H-NMR	(300 MHz, $CDCl_3$) δ 7.32-7.11 (m; 6H), 7.08 (dt; 1.00/7.18 Hz; 1H), 7.04 (dd; 0.56/2.72 Hz; 1H), 3.80 (s; 3H), 2.65-2.57 (m; 2H), 1.13-1.05 (m; 2H), 0.26 (s; 6H).
^{13}C-NMR	(75 MHz, $CDCl_3$) δ 159.6 (Q), 145.5 (Q), 141.3 (Q), 129.5 (CH_{Ar}), 128.7 (CH_{Ar}), 128.2 (CH_{Ar}), 126.3 (CH_{Ar}), 126.0 (CH_{Ar}), 119.7 (CH_{Ar}), 114.3 (CH_{Ar}), 55.1 (OCH_3), 29.8 (Ar-CH_2), 17.4 ($SiCH_2$), -3.5 ($SiCH_3$).
GC-MS	t_R = 10.04 min, (EI, 70 eV): m/z = 270 [M^+], 255, 238, 227, 165, 151, 135, 121, 105, 91, 77, 59.
HRMS	(EI, 70 eV, m/z): 270.1438, calcd: 270.1440

(2-Methoxyphenyl)dimethyl(phenethyl)silane (3n)

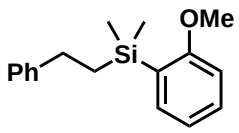

	Pale yellow oil
	$C_{17}H_{22}OSi$
	270.14 g/mol
Yield	67%
TLC	R_f = 0.57 (SiO_2, *n*-pentane/ethyl acetate (19:1))
^{1}H-NMR	(300 MHz, $CDCl_3$) δ 7.41-7.23 (m; 4H), 7.21-7.11 (m; 3H), 7.00-6.90 (m; 1H), 6.86-6.82 (m; 1H); 3.81 (s; 3H), 2.66-2.58 (m; 2H), 1.21-1.14 (m; 2H), 0.29 (s; 6H).
^{13}C-NMR	(75 MHz, $CDCl_3$) δ 164.5 (Q), 145.7 (Q), 135.4 (CH_{Ar}), 131.0 (CH_{Ar}), 128.3 (CH_{Ar}), 127.9 (CH_{Ar}), 126.7 (Q), 125.5 (CH_{Ar}), 120.6 (CH_{Ar}), 109.6 (CH_{Ar}), 55.1 (OCH_3), 30.3 (Ar-CH_2), 17.7 ($SiCH_2$), -2.6 ($SiCH_3$).
GC-MS	t_R = 9.83 min, (EI, 70 eV): m/z = 270 [M^+], 255, 238, 195, 165, 151, 135, 121, 105, 91, 77, 59.
HRMS	(EI, 70 eV, m/z): 270.1424, calcd: 270.1440

(4-Flourophenyl)dimethyl(phenethyl)silane (3o)

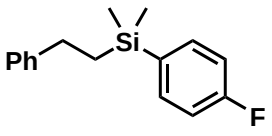

	Colorless oil
	$C_{16}H_{19}FSi$
	258.12 g/mol
Yield	100%
TLC	R_f = 0.68 (SiO_2, *n*-pentane/ethyl acetate (19:1))
^{1}H-NMR	(300 MHz, $CDCl_3$) δ 7.53-7.46 (m; 2H), 7.30-7.23 (m; 2H), 7.20-7.12 (m; 3H), 7.11-7.02 (m; 2H); 2.67-2.58 (m; 2H), 1.16-1.07 (m; 2H), 0.29 (s; 6H).
^{13}C-NMR	(75 MHz, $CDCl_3$) δ 163.8 (d; 247.77; Q), 144.9 (Q), 135.6 (d; 7,32 Hz; CH_{Ar}), 134.6 (d; 3,6 Hz; Q), 128.5 (CH_{Ar}), 127.9 (CH_{Ar}), 125.7 (CH_{Ar}), 115.1 (d; 19.52 Hz; CH_{Ar}), 30.0 ($SiCH_2$), 17.9(Ar-CH_2), -2.85 ($SiCH_3$).
GC-MS	t_R = 9.07 min, (EI, 70 eV): m/z = 258 [M^+], 243, 215, 153, 139, 123, 105, 91, 77, 65, 51.
HRMS	(EI, 70 eV, m/z): 258.1241, calcd: 258.1240.

(4-Dimethylaminophenyl)dimethyl(vinyl)silane (3p)

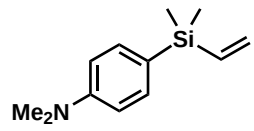

Colorless oil

$C_{12}H_{19}NSi$

205.38 g/mol

Yield	86%
^{1}H-NMR	(400 MHz, $CDCl_3$) δ 7.42 (d, J = 8.6 Hz, 2H), 6.77 (d, J = 8.1 Hz, 2H), 6.30 (dd, J = 20.3, 14.6 Hz, 1H), 6.03 (dd, J = 14.6, 3.9 Hz, 1H), 5.74 (dd, J = 20.2, 3.9 Hz, 1H), 2.98 (s, 6H), 0.33 (s, 6H).
^{13}C-NMR	(101 MHz, $CDCl_3$) δ 151.12 (C_{Ar}-N), 139.07 (=CH_2), 135.07 (C_{Ar}-H), 132.24 (C_{Ar}-Si), 112.21 (Si-CH), 40.46 (N-CH_3), -2.51 (Si-CH_3)
GC-MS	t_R = 8.10 min, (EI, 70 eV): m/z = 205 [M^+], 190, 178, 164, 147, 134, 120, 105, 91, 81, 77, 59, 53.
HRMS	(EI, 70 eV, m/z): 205.12812, calcd: 205.12813.
FT-IR	(ATR film) $1/\lambda$ [cm^{-1}] = 2956 (m), 2803 (w), 1595 (s), 1513 (m), 1353 (m), 1111 (s).

(4-Methoxyphenyl)dimethyl(vinyl)silane (3q)

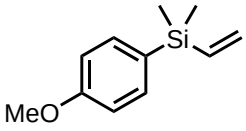

Colorless oil

$C_{11}H_{16}OSi$

192.10 g/mol

Yield	93%
TLC	R_f = 0.68 (SiO_2, hexanes/ethyl acetate (95 :5))
^{1}H-NMR	(300 MHz, $CDCl_3$) δ 7.51-7.42 (m; 2H), 6.96-6.89 (m; 2H), 6.29 (dd; 20.1/14.6 Hz; 1H), 6.05 (dd; 14.6/3.9 Hz; 1H), 5.74 (dd; 20.1/3.9 Hz; 1H), 3.84 (s; 3H), 0.34 (s; 6H).
^{13}C-NMR	(75 MHz, $CDCl_3$) δ 160.5 (C_{Ar}-O), 138.5 (=CH_2), 135.4 (C_{Ar}-H), 132.7 (CH=), 129.3 (C_{Ar}-Si), 113.7 (CH_{Ar}), 55.2 (OCH_3), -2.6 ($SiCH_3$).
GC-MS	t_R = 6.16 min, (EI, 70 eV): m/z = 192 [M^+], 177, 165, 151, 135, 121, 107, 91, 77, 67, 59, 51.

Analytical data were in full agreement with L. H. Luehning, M. Rosien, S. Doye, *Synlett* **2017**, *28*, 2489-2494.

(4-Fluorophenyl)dimethyl(p-tolyl)silane (3r)

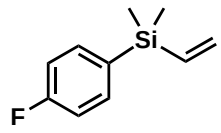

Colorless oil

$C_{10}H_{13}FSi$

180.30 g/mol

Yield	64%
^{1}H-NMR	(400 MHz, $CDCl_3$) δ 7.49 (tt, J = 6.3, 2.2 Hz, 2H), 7.10 – 7.00 (m, 2H), 6.27 (dd, J = 20.2, 14.6 Hz, 1H), 6.06 (dd, J = 14.6, 3.8 Hz, 1H), 5.74 (dd, J = 20.2, 3.8 Hz, 1H), 0.34 (s, 6H).
^{13}C-NMR	(101 MHz, $CDCl_3$) δ 163.85 (d, J = 247.89 Hz, C_{Ar}-F), 137.90 (=CH2), 135.87 (d, J = 7.36 Hz, C_{Ar}-H), 133.96 (d, J = 3.79, C_{Ar}-Si), 133.18 (CH=), 115.06 (d, J = 19.55, C_{Ar}-H), -2.66 (Si-CH_3).
GC-MS	t_R = 5.50 min, (EI, 70 eV): m/z = 180 [M^+], 165, 153, 139, 123, 109, 91, 77, 63, 53.
HRMS	(EI, 70 eV, m/z): 180.07622, calcd: 180.07651.
FT-IR	(ATR film) $1/\lambda$ [cm^{-1}] = 3053 (w), 2959 (m), 2855 (w), 1588 (s), 1498 (m), 1230 (m), 1103 (m).

Allyl(4-methoxyphenyl)dimethylsilane (3s)

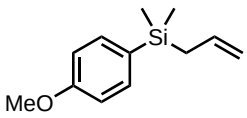

Pale yellow oil

$C_{12}H_{18}OSi$

206.11 g/mol

Yield	96%
TLC	R_f = 0.60 (SiO_2, hexanes/ethyl acetate (95:5))
^{1}H-NMR	(300 MHz, $CDCl_3$) δ 7.48-7.45 (m; 2H), 7.00-6.92 (m; 2H), 5.91-5.73 (m; 1H), 4.90-4.80 (m; 2H), 3.84 (s; 3H), 1.77 (dt; 8.1/1.22 Hz; 2H), 0.30 (s; 6H).
^{13}C-NMR	(75 MHz, $CDCl_3$) δ 160.5 (Q), 135.2 (CH_{Ar}), 134.9 (-CH=), 129.5 (Q), 113.6 (CH_{Ar}), 113.4 (=CH_2), 55.1 (OCH_3), 24.1 ($SiCH_2$), -3.2 ($SiCH_3$).
GC-MS	t_R = 7.47 min, (EI, 70 eV): m/z = 206 [M^+], 191, 165, 151, 135, 122, 107, 91, 77, 67, 51.

Analytical data were in full agreement with F. X. Woolard, J. Paetsch, J. A. Ellman, *J. Org. Chem.* **1997**, 6102-6103.

Allyl(4-methylphenyl)dimethylsilane (3t)

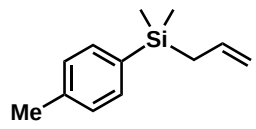

Colorless oil

$C_{12}H_{18}Si$

190.36 g/mol

Yield	81%
^{1}H-NMR	(400 MHz, $CDCl_3$) δ 7.42 (d, J = 7.8 Hz, 2H), 7.19 (d, J = 7.9 Hz, 1H), 5.78 (ddt, J = 17.0, 10.2, 8.1 Hz, 1H), 4.90 – 4.82 (m, 2H), 2.35 (s, 3H), 1.75 (d, J = 8.1 Hz, 1H), 0.27 (s, 6H).
^{13}C-NMR	(75 MHz, $CDCl_3$) δ 139.00 (Q), 135.14 (C_{Ar}-Si), 134.91 (=CH), 133.81 (C_{Ar}-H), 128.73 (C_{Ar}-H), 113.40 (=CH_2), 23.94 (Si-CH_2), 21.60 (CH_3), -3.25 (Si-CH_3).
GC-MS	t_R = 6.79 min, (EI, 70 eV): m/z = 190 [M^+], 175, 159, 149, 135, 121, 105, 91, 77, 67, 59, 53.
HRMS	(EI, 70 eV, m/z): 190.11703, calcd: 190.11723.
FT-IR	(ATR film) $1/\lambda$ [cm^{-1}] = 3071 (w), 2959 (m), 2922 (w), 1633 (s), 1495 (m), 1248 (m).

Allyl(4-methoxyphenyl)dimethylsilane (3u)

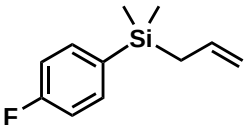

Colorless oil

$C_{11}H_{15}FSi$

194.32 g/mol

Yield	64%
^{1}H-NMR	(300 MHz, $CDCl_3$) δ 7.48 (dd, J = 8.4, 6.2 Hz, 2H), 7.05 (dd, J = 9.3, 8.6 Hz, 2H), 5.86 – 5.68 (m, 1H), 4.91 – 4.80 (m, 2H), 1.74 (dt, J = 8.2, 1.2 Hz, 2H), 0.28 (s, 6H).
^{13}C-NMR	(75 MHz, $CDCl_3$) δ 163.70 (d, J = 247.94, C_{Ar}-F), 135.51 (d, J = 7.34, C_{Ar}-H), 134.38 (=CH_2), 134.05 (d, J = 3.94, C_{Ar}-Si), 114.89 (d, J = 19.57, C_{Ar}-H), 113.58 (CH=), 23.75 (CH_2), -3.35 (Si-CH_3).
GC-MS	t_R = 6.18 min, (EI, 70 eV): m/z = 194 [M^+], 179, 163, 153, 139, 123, 109, 91, 77, 63, 53.
HRMS	(EI, 70 eV, m/z): 194.09184, calcd: 194.09216.

Decyl(4-methoxyphenyl)dimethylsilane (3v)

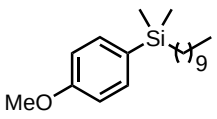

	Colorless oil
	$C_{19}H_{34}OSi$
	306.24 g/mol
Yield	80%
TLC	R_f = 0.40 (SiO_2, *n*-pentane/DCM (95:5))
^{1}H-NMR	(300 MHz, $CDCl_3$) δ 7.50-7.40 (m; 2H), 6.98-6.88 (m; 2H), 3.82 (s; 3H), 1.40-1.20 (m; 16H), 0.89 (t; 6.7 Hz; 3H), 0.80-0.65 (m; 2H), 0.24 (s; 6H).
^{13}C-NMR	(75 MHz, $CDCl_3$) δ 160.3 (Q), 135.1 (CH_{Ar}), 130.7 (Q), 113.6 (CH_{Ar}), 55.1 (OCH_3), 33.8 (CH_2), 32.1 (CH_2), 29.8 (CH_2), 29.8 (CH_2), 29.5 (CH_2), 29.5 (CH_2), 24.1 (CH_2), 22.9 (CH_2), 16.1 (CH_2), 14.3 (CH_2), -2.7 ($SiCH_3$).
GC-MS	t_R = 10.46 min, (EI, 70 eV): m/z = 306 [M^+], 291, 274, 261, 245, 215, 198, 183, 165, 151, 139, 127, 108, 89, 73, 59.
HRMS	(EI, 70 eV, m/z): 306.2373, calcd: 306.2379.

Decyl(dimethyl)phenylsilane (3w)

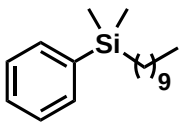

	Colorless oil
	$C_{18}H_{32}Si$
	276.23 g/mol
Yield	86%
TLC	R_f = 0.54 (SiO_2, *n*-pentane)
^{1}H-NMR	(300 MHz, $CDCl_3$) δ 7.54-7.48 (m; 2H), 7.38-7.32 (m; 3H), 1.38-1.18 (m; 16H), 0.88 (t; 6.75 Hz; 3H), 0.78-0.69 (m; 2H), 0.25 (s; 6H).
^{13}C-NMR	(75 MHz, $CDCl_3$) δ 140.3 (Q), 134.1 (CH_{AR}), 129.2 (CH_{AR}), 128.1 (CH_{AR}), 33.5 (CH_2), 31.8 (CH_2), 29.5 (CH_2), 29.5 (CH_2), 29.2 (CH_2), 29.2 (CH_2), 23.7 (CH_2), 22.5 (CH_2), 15.5 (CH_2), 13.9 (CH_3), -3.4 ($SiCH_3$).
GC-MS	t_R = 9.48 min, (EI, 70 eV): m/z = 276 [M^+], 261, 198, 170, 135, 121, 105, 91, 73, 55.

HRMS	(EI, 70 eV, m/z): 276.2270, calcd: 276.2273.
FT-IR	(ATR film) $1/\lambda$ [cm^{-1}] = 2921 (m), 2852 (m), 1247 (m), 1112 (s), 833 (s), 811 (s), 725 (m), 698 (s).

Triethyl(4-methoxyphenyl)silane (3x)

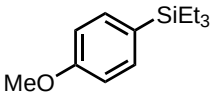

	Pale yellow oil
	$C_{13}H_{22}OSi$
	222.14 g/mol
Yield	88%
TLC	R_f = 0.74 (SiO_2, hexanes/ethyl acetate (95 :5))
^{1}H-NMR	(300 MHz, $CDCl_3$) δ 7.49-7.40 (m; 2H), 7.00-6.90 (m; 2H), 3.84 (s; 3H), 1.04-0.93 (m; 9H), 0.85-0.73 (m; 6H).
^{13}C-NMR	(75 MHz, $CDCl_3$) δ 160.3 (Q), 135.7 (CH_{Ar}), 128.3 (Q), 113.6 (CH_{Ar}), 55.1 (OCH_3), 7.56 ($SiCH_2$), 3.63 (CH_3).
GC-MS	t_R = 6.16 min, (EI, 70 eV): m/z = 222 [M^+], 193, 165, 151, 137, 121, 107, 91, 77, 67, 59.

Analytical data were in full agreement with Y. Yamanoi, H. Nishihara, *J. Org. Chem.* **2008**, 6671-6678.

Triethoxy(4-methoxyphenyl)silane (3y)

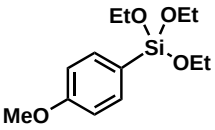

	Colorless oil
	$C_{13}H_{22}O_4Si$
	270.13 g/mol
Yield	86%
TLC	R_f = 0.24 (SiO_2, hexanes/ethyl acetate (95 :5))
^{1}H-NMR	(300 MHz, $CDCl_3$) δ 7.65-7.55 (m; 2H), 6.96-6.89 (m; 2H), 3.92-3.79 (m; 9H), 1.24 (t; 7.0 Hz; 6H).
^{13}C-NMR	(75 MHz, $CDCl_3$) δ 161.5 (Q), 136.6 (CH_{Ar}), 121.9 (Q), 113.7 (CH_{Ar}), 58.8 (OCH_2), 55.1 (OCH_3), 18.4 (CH_3).
GC-MS	t_R = 6.16 min, (EI, 70 eV): m/z = 270 [M^+], 255, 241, 225, 211, 197, 181, 169, 147, 135, 119, 108, 91, 79, 63, 51.

Analytical data were in full agreement with M. Murata, H. Yamasaki, T. Ueta, M. Nagata, M. Ishikura, S. Watanabe, Y. Masuda, *Terahedron*, **2007**, *63*, 4087-4094.

(Chloromethyl)(4-methoxyphenyl)dimethylsilane (3z)

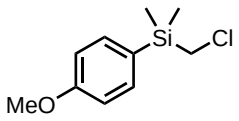

Colorless oil

$C_{10}H_{15}ClOSi$

214.06 g/mol

Yield 96%

TLC R_f = 0.58 (SiO_2, hexanes/ethyl acetate (95 :5))

^{1}H-NMR (300 MHz, $CDCl_3$) δ 7.53-7.45 (m; 2H), 6.98-6.91 (m; 2H), 3.83 (m; 3H), 2.93 (s; 2H), 0.40 (2; 6H).

^{13}C-NMR (75 MHz, $CDCl_3$) δ 161.0 (Q), 135.6 (CH_{Ar}), 127.0 (Q), 113.9 (CH_{Ar}), 58.2 (OCH_3), 30.9 ($SiCH_2$), -4.3 ($SiCH_3$).

GC-MS t_R = 6.16 min, (EI, 70 eV): m/z = 214 [M^+], 199, 188, 180, 165, 150, 135, 121, 105, 91, 77, 63, 53.

Analytical data were in full agreement with C. B. Ankianiec, G. B. Young, *Polyhedron*, **2007**, *14*, 249-265.

Trimethyl(thiophen-2-yl)silane (3aa)

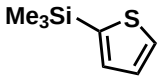

Colorless oil

$C_7H_{12}SSi$

156.04 g/mol

Yield 99%

TLC R_f = 0.58 (SiO_2, *n*-pentane)

^{1}H-NMR (300 MHz, $CDCl_3$) δ 7.62 (dd; 4.6/0.9 Hz; 1H), 7.30 (dd; 3.3/0.9 Hz; 1H), 7.22 (dd; 4.6/3.3 Hz; 1H), 0.36 (s; 9H).

^{13}C-NMR (75 MHz, $CDCl_3$) δ 140.2 (Q), 134.1 (CH_{Ar}), 130.5 (CH_{Ar}), 128.2 (CH_{Ar}), 0.2 ($SiCH_3$).

GC-MS t_R = 4.46 min, (EI, 70 eV): m/z = 156 [M^+], 141, 127, 115, 105, 91, 83, 75, 65, 53.

Analytical data were in full agreement with O. V. Borshchev, S. A. Ponomarenko, A. Kleymyuk, Y. N. Luponosov, N. M. Surin, A. M. Muzafarov, *Russ. Chem. Bull.* **2010**, *4*, 797-805.

Dimethyl(phenyl)(thiophen-2-yl)silane (3ab)

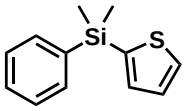

	Colorless oil
	$C_{12}H_{14}SSi$
	218.06 g/mol
Yield	97%
TLC	R_f = 0.26 (SiO_2, *n*-pentane)
^{1}H-NMR	(300 MHz, $CDCl_3$) δ 7.70-7.60 (m; 2H), 7.48-7.42 (m; 3H), 7.37 (dd; 3.3/0.9 Hz; 1H), 7.28 (dd; 4.6/3.3 Hz; 1H), 0.69 (s; 6H).
^{13}C-NMR	(75 MHz, $CDCl_3$) δ 138.0 (Q), 137.8 (Q), 135.5 (CH_{Ar}), 134.0 (CH_{Ar}), 131.3 (CH_{Ar}), 129.5 (CH_{Ar}), 128.3 (CH_{Ar}), 128.0 (CH_{Ar}), -1.1 ($SiCH_3$).
GC-MS	t_R = 8.04 min, (EI, 70 eV): m/z = 218 [M^+], 203, 177, 160, 150, 141, 128, 115, 105, 91, 75, 65, 51.

Analytical data were in full agreement with S.-S. Hu, W. P. Weber, *J. Organomet. Chem.* **1989**, *369*, 155-163.

(4-Methoxyphenyl)dimethyl(*p*-tolyl)silane (3ac)

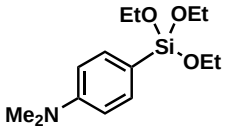

	Colorless oil
	$C_{16}H_{20}OSi$
	256.13 g/mol
Yield	85%
TLC	R_f = 0.45 (SiO_2, hexanes/ethyl acetate (95 :5))
^{1}H-NMR	(300 MHz, $CDCl_3$) δ 7.50-7.40 (m; 4H), 7.20 (d; 8.0 Hz; 2H), 6.93 (d; 8.3 Hz; 2H), 3.83 (s; 3H), 2.37 (s; 3H), 0.53 (s; 6H).
^{13}C-NMR	(75 MHz, $CDCl_3$) δ 160.5 (Q), 139.0 (Q), 135.8 (CH_{Ar}), 135.1 (Q), 134.3 (CH_{Ar}), 129.4 (Q), 128.8 (CH_{Ar}), 113.7 (CH_{Ar}), 55.2 (OCH_3), 26.6 (Ar-CH_3), -2.0 ($SiCH_3$).
GC-MS	t_R = 9.73 min, (EI, 70 eV): m/z = 256 [M^+], 241, 225, 211, 198, 183, 165, 149, 135, 119, 105, 91, 77, 59.

Analytical data were in full agreement with K. Murakami, K. Hirano, H. Yorimitsu, K. Oshima, *Angew. Chem. Int. Ed.* **2008**, *47*, 5833-5835.

Diphenyl(thiophen-2-yl)silane (5a)

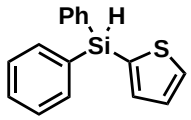

	Colorless oil
	$C_{16}H_{14}SSi$
	266.06 g/mol
Yield	99%
TLC	R_f = 0.53 (SiO_2, hexanes/ethyl acetate (95 :5))
^{1}H-NMR	(300 MHz, $CDCl_3$) δ 7.85-7.69 (m; 5H), 7.61-7.42 (m; 7H), 7.33 (dd; 4.6/3.4 Hz; 1H), 5.74 (s; 1H).
^{13}C-NMR	(75 MHz, $CDCl_3$) δ 138.0 (CH_{Ar}), 135.7 (CH_{Ar}), 133.2 (Q), 132.8 (CH_{Ar}), 131.9 (Q), 130.2 (CH_{Ar}), 128.6 (CH_{Ar}), 128.2 (CH_{Ar}).
GC-MS	t_R = 6.16 min, (EI, 70 eV): m/z = 266 [M^+], 233, 220, 207, 188, 167, 155, 138, 128, 115, 105, 91, 78, 63, 51.

Analytical data were in full agreement with Y. Yamanoi, T. Taira, J. Sato, I. Nakamula, H. Nishihira, *Org. Lett.* **2007**, *9*, 4543-4546.

(4-Methoxyphenyl)diphenylsilane (5b)

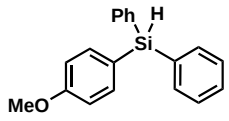

	Colorless oil
	$C_{19}H_{18}OSi$
	290.11 g/mol
Yield	95%
TLC	R_f = 0.34 (SiO_2, hexanes/ethyl acetate (95 :5))
^{1}H-NMR	(300 MHz, $CDCl_3$) δ 7.64-7.57 (m; 4H), 7.57-7.51 (m; 2H), 7.49-7.35 (m; 6H), 7.00-6.93 (m; 2H), 5.49 (s; 1H), 3.84 (s; 3H).
^{13}C-NMR	(75 MHz, $CDCl_3$) δ 161.1 (Q), 137.5 (CH_{Ar}), 135.9 (CH_{Ar}), 133.9 (Q), 129.9 (CH_{Ar}), 128.2 (CH_{Ar}), 124.0 (Q), 114.0 (CH_{Ar}), 55.2 (OCH_3).
GC-MS	t_R = 6.16 min, (EI, 70 eV): m/z = 290 [M^+], 275, 257, 245, 230, 213, 197, 213, 197, 181, 167, 152, 136, 117, 105, 91, 78, 59.

Analytical data were in full agreement with Y. Yamanoi, T. Taira, J. Sato, I. Nakamula, H. Nishihira, *Org. Lett.* **2007**, *9*, 4543-4546.

4-(Diphenylsilyl)-*N*,*N*-dimethylaniline (5c)

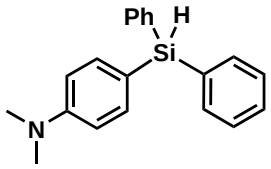

Colorless oil

$C_{20}H_{21}NSi$

303.48 g/mol

Yield 96%

^{1}H-NMR (400 MHz, $CDCl_3$) δ 7.62 – 7.56 (m, 4H), 7.47 – 7.32 (m, 8H), 6.76 (d, J = 7.9 Hz, 2H), 5.44 (s, 1H), 2.98 (s, 6H).

GC-MS t_R = 12.27 min, (EI, 70 eV): m/z = 303 [M^+], 286, 259, 226, 210, 197, 181, 155, 120, 105, 91, 78, 63.

Analytical data were in full agreement with Q.-A. Chen, H. F. T. Klare, M. Oestreich, *J. Am. Chem. Soc.*, **2016**, *138*, 7868–7871.

(4-Methoxyphenyl)diphenylsilane (5d)

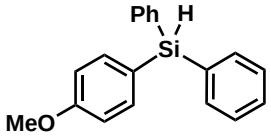

Colorless oil

$C_{19}H_{18}OSi$

290.44 g/mol

Yield 84%

^{1}H-NMR (400 MHz, $CDCl_3$) δ 7.61 – 7.54 (m, 4H), 7.51 (d, J = 8.5 Hz, 2H), 7.46 – 7.32 (m, 6H), 6.94 (d, J = 8.5 Hz, 2H), 5.46 (s, 1H), 3.82 (s, 3H).

^{13}C-NMR (101 MHz, $CDCl_3$) δ 161.21 (Q), 137.48 (CH_{Ar}), 135.90 (CH_{Ar}), 133.94 (Q), 129.86 (CH_{Ar}), 128.15 (CH_{Ar}), 124.10 (Q), 114.03 (CH_{Ar}), 55.20 (CH_3).

GC-MS t_R = 11.47 min, (EI, 70 eV): m/z = 290 [M^+], 275, 257, 245, 230, 213, 197, 181, 167, 152, 136, 105, 78, 59.

Analytical data were in full agreement with Y. Yamanoi, T. Taira, J. Sato, I. Nakamula, H. Nishihara, *Org. Lett.*, **2007**, *9*, 4543–4546.

Diphenyl(4-tolyl)silane (5e)

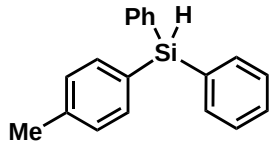

	Colorless oil
	$C_{19}H_{18}Si$
	274.44 g/mol
Yield	86%
^{1}H-NMR	(400 MHz, $CDCl_3$) δ 7.60 (dd, J = 7.9, 1.6 Hz, 4H), 7.50 (d, J = 7.9 Hz, 2H), 7.46 – 7.35 (m, 6H), 7.25 – 7.20 (m, 2H), 5.49 (s, 1H), 2.39 (s, 3H).
^{13}C-NMR	(101 MHz, $CDCl_3$) δ 139.65 (Q), 135.68 (CH_{Ar}), 135.61 (CH_{Ar}), 135.51 (Q), 129.55 (CH_{Ar}), 129.42 (Q), 128.74 (CH_{Ar}), 127.95 (CH_{Ar}), 127.84 (CH_{Ar}), 21.40 (CH_3).
GC-MS	t_R = 10.88 min, (EI, 70 eV): m/z = 274 [M^+], 196, 181, 165, 155, 143, 129, 119, 105, 91, 78, 63, 51.

Analytical data were in full agreement with Y. Yamanoi, T. Taira, J. Sato, I. Nakamula, H. Nishihara, *Org. Lett.*, **2007**, *9*, 4543–4546.

Triphenylsilane (5f)

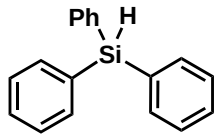

	Colorless oil
	$C_{18}H_{16}Si$
	260.41 g/mol
Yield	72%
^{1}H-NMR	(400 MHz, $CDCl_3$) δ 7.63 – 7.58 (m, 6H), 7.47 – 7.35 (m, 9H), 5.50 (s, 1H).
^{13}C-NMR	(101 MHz, $CDCl_3$) δ 135.85 (CH_{Ar}), 133.38 (Q), 129.85 (CH_{Ar}), 128.09 (CH_{Ar}).
GC-MS	t_R = 10.46 min, (EI, 70 eV): m/z = 260 [M^+], 229, 182, 155, 129, 105, 78, 63, 51.

Analytical data were in full agreement with Y. Yamanoi, T. Taira, J. Sato, I. Nakamula, H. Nishihara, *Org. Lett.*, **2007**, *9*, 4543–4546.

(4-Fluorophenyl)diphenylsilane(5g)

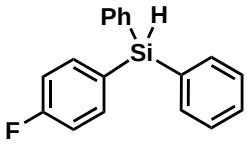

Colorless oil

$C_{18}H_{15}FSi$

278.40 g/mol

Yield 79%

^{1}H-NMR (400 MHz, $CDCl_3$) δ 7.64 – 7.56 (m, 2H), 7.58 – 7.53 (m, 2H), 7.47 – 7.32 (m, 6H), 7.12 – 7.03 (m, 1H), 4.93 (s, 1H).

^{13}C-NMR (101 MHz, $CDCl_3$) δ 137.83 (d, J = 7.67 Hz), 135.75, 135.70, 134.47, 134.34, 133.11, 131.52, 129.97, 129.90, 128.14, 115.36 (d, J = 19.83 Hz).

GC-MS t_R = 10.37 min, (EI, 70 eV): m/z = 277 $[M\text{-}H]^+$, 225, 214, 200, 181, 172, 152, 123, 105, 96, 78, 63, 51.

Analytical data were in full agreement with Y. Yamanoi, T. Taira, J. Sato, I. Nakamula, H. Nishihara, *Org. Lett.*, **2007**, *9*, 4543–4546.

4-Methoxyphenyl(phenyl)silane (5h)

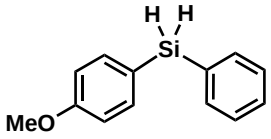

Colorless oil

$C_{13}H_{14}OSi$

214.34 g/mol

Yield 82%

^{1}H-NMR (400 MHz, $CDCl_3$) δ 7.62 (dd, J = 7.8, 1.7 Hz, 2H), 7.59 – 7.52 (m, 2H), 7.41 (ddd, J = 12.3, 7.5, 5.8 Hz, 3H), 6.99 – 6.93 (m, 2H), 4.94 (s, 2H), 3.84 (s, 3H).

^{13}C-NMR (101 MHz, $CDCl_3$) δ 161.28 (C_{Ar}-O), 137.36 (CH_{Ar}), 135.73 (CH_{Ar}), 132.20 (C_{Ar}-Si), 129.91 (CH_{Ar}), 128.22 (CH_{Ar}), 122.16 (C_{Ar}-Si), 114.12 (CH_{Ar}), 55.19 (CH_3).

GC-MS t_R = 9.01 min, (EI, 70 eV): m/z = 214 $[M^+]$, 199, 183, 169, 152, 136, 121, 105, 91, 65, 59, 51.

Analytical data were in full agreement with J. F. Dunne, S. R. Neal, J. Engelkemier, A. Ellern, A. D. Sadow, *J. Am. Chem. Soc.*, **2011**, *133*, 16782–16785.

Bis(4-methoxyphenyl)(phenyl)silane (5h')

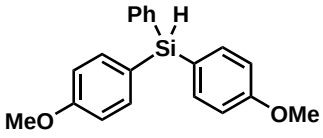

Colorless oil

$C_{20}H_{20}O_2Si$

320.46 g/mol

Yield 13%

^{1}H-NMR (300 MHz, $CDCl_3$) δ 7.59 – 7.53 (m, 2H), 7.52 – 7.46 (m, 4H), 7.41 – 7.34 (m, 3H), 6.99 – 6.86 (m, 4H), 5.43 (s, 1H), 3.82 (s, 6H).

^{13}C-NMR (75 MHz, $CDCl_3$) δ 161.10 (C_{Ar}-O), 137.41 (CH_{Ar}), 135.83 (CH_{Ar}), 129.76 (C_{Ar}-Si), 128.11 (CH_{Ar}), 124.54 (C_{Ar}-Si), 113.97 (CH_{Ar}), 55.20 (CH_3).

GC-MS t_R = 12.39 min, (EI, 70 eV): m/z = 320 [M^+], 305, 287, 275, 260, 243, 227, 212, 197, 181, 167, 152, 135, 115, 105, 92, 78, 65, 59, 51.

Analytical data were in full agreement with P. B. Garland, P. J. Serafinowski, *Org. Biomol. Chem.*, **2009**,*7*, 451-459.

(2'-Methoxy-[1,1'-binaphthalen]-2-yl)dimethylsilane (5i)

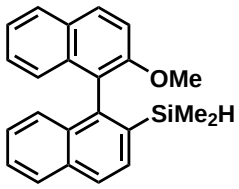

Pale yellow crystals

$C_{23}H_{22}OSi$

342.51 g/mol

Yield 55%

TLC R_f = 0.58 (SiO_2, *n*-pentane)

^{1}H-NMR (400 MHz, $CDCl_3$) δ 8.01 (d, *J* = 9.2 Hz, 1H), 7.95 (d, *J* = 8.2 Hz, 1H), 7.91 (d, *J* = 8.2 Hz, 1H), 7.87 (d, *J* = 8.1 Hz, 1H), 7.81 (d, *J* = 8.2 Hz, 1H), 7.48 – 7.45 (m, 1H), 7.43 (d, *J* = 9.1 Hz, 1H), 7.31 (ddd, *J* = 8.1, 6.7, 1.2 Hz, 1H), 7.25 – 7.22 (m, 2H), 7.19 (ddd, *J* = 8.2, 6.7, 1.3 Hz, 1H), 6.96 (dd, *J* = 8.6, 1.0 Hz, 1H), 3.90 (hept, *J* = 3.8 Hz, 1H), 3.77 (s, 4H), 0.09 (d, *J* = 3.8 Hz, 4H), 0.11 (d, *J* = 3.8 Hz, 4H).

^{13}C-NMR (101 MHz, $CDCl_3$) δ 154.89, 135.74, 134.82, 134.17, 131.13, 129.80, 128.83, 128.11, 127.86, 126.88, 126.49, 126.34, 126.33, 126.09, 125.77, 123.61, 123.11, 113.15, 56.22, 3.32, 3.36.

GC-MS	t_R = 12.23 min, (EI, 70 eV): m/z = 342 [M^+], 327, 311, 295, 283, 265, 252, 237, 222, 207, 187, 166, 154, 140, 125, 112, 99, 89, 75, 59.
HRMS	(EI, 70 eV, m/z): 342.14254, calcd: 342.14344.
FT-IR	(ATR film) $1/\lambda$ [cm^{-1}] = 3049, 2922, 2855, 2106, 1592, 1506, 1461, 1334, 1245, 887, 809, 746.

Dimethyl(2′-phenoxy-[1,1′-binaphthalen]-2-yl)silane (5j)

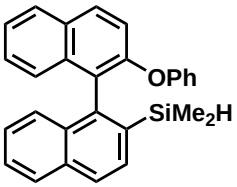

White powder

$C_{28}H_{24}OSi$

404.58 g/mol

Yield	89%
TLC	R_f = 0.45 (SiO_2, *n*-pentane)
^{1}H-NMR	(400 MHz, $CDCl_3$) δ 8.01 – 7.91 (m, 4H), 7.85 (d, J = 8.2 Hz, 1H), 7.54 – 7.42 (m, 3H), 7.35 – 7.29 (m, 3H), 7.25 (dd, J = 8.6, 7.3 Hz, 2H), 7.19 (dd, J = 8.5, 1.1 Hz, 1H), 7.03 (td, J = 7.3, 1.1 Hz, 1H), 6.96 (d, J = 8.0 Hz, 2H), 4.08 (hept, J = 3.8 Hz, 1H), 0.12 (d, J = 3.8 Hz, 3H), 0.09 (d, J = 3.8 Hz, 3H).
^{13}C-NMR	(101 MHz, $CDCl_3$) δ 157.02, 152.80, 140.71, 136.19, 135.06, 134.07, 132.82, 130.80, 130.07, 129.57, 129.53, 128.09 , 128.00, 127.14, 126.67, 126.51, 126.38, 126.28, 126.04, 124.72, 123.20, 119.55, 118.60, 118.24, 2.98, 3.18.
GC-MS	t_R = 14.22 min, (EI, 70 eV): m/z = 404 [M^+], 387, 370, 346, 327, 311, 295, 279, 266, 252, 239, 224, 207, 191, 167, 151, 128, 115, 77, 63, 51.
HRMS	(EI, 70 eV, m/z): 404.15847, calcd: 404.15909.
FT-IR	(ATR film) $1/\lambda$ [cm^{-1}] = 3042, 2956, 2117, 1737, 1588, 1487, 1230, 887, 746, 686.

(2-(Methoxymethyl)phenyl)dimethylsilane (5k)

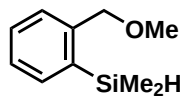

	Pale yellow oil
	$C_{10}H_{16}OSi$
	180.32 g/mol
Yield	100%
TLC	R_f = 0.23 (SiO_2, *n*-pentane)
^{1}H-NMR	(400 MHz, $CDCl_3$) δ 7.57 (dd, J = 7.1, 1.1 Hz, 1H), 7.38-7.34 (m, 1H), 7.36 (dd, J = 5.6 Hz, 1.1 Hz, 1H), 7.30 (ddd, J = 7.2, 5.4, 3.3 Hz, 1H), 4.55 (s, 2H), 4.51 (hept, J = 3.8 Hz, 1H), 0.37 (d, J = 3.7 Hz, 6H).
^{13}C-NMR	(101 MHz, $CDCl_3$) δ 143.79, 136.86, 135.16, 129.44, 128.18, 127.28, 75.02, 57.94, 2.83.
GC-MS	t_R = 6.46 min, (EI, 70 eV): m/z = 179 $[M-H]^+$, 165, 149, 135, 121, 105, 91, 77, 59.
HRMS	(EI, 70 eV, m/z): 179.08912 $[M-H^+]$, calcd: 179.08867.
FT-IR	(ATR film) $1/\lambda$ [cm^{-1}] = 3056, 2956, 2926, 2822, 2121, 1439, 1379, 1249, 1096, 880, 835, 749.

***N,N*-Dimethyl-4-(triethoxysilyl)aniline (6a)**

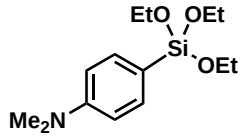

	Colorless oil
	$C_{14}H_{25}NO_3Si$
	283.44 g/mol
Yield	94%
^{1}H-NMR	(400 MHz, $CDCl_3$) δ 7.54 (dd, J = 8.9, 2.4 Hz, 2H), 6.73 (d, J = 8.1 Hz, 2H), 3.86 (q, J = 7.0 Hz, 6H), 2.98 (s, 6H), 1.24 (t, J = 7.0 Hz, 9H).
^{13}C-NMR	(101 MHz, $CDCl_3$) δ 151.87 (C_{Ar}-N), 136.20 (CH_{Ar}), 111.76 (CH_{Ar}), 58.64 (OEt), 40.20 (NMe_2), 18.39 (OEt).
GC-MS	t_R = 9.21 min, (EI, 70 eV): m/z = 283 $[M^+]$, 268, 254, 238, 224, 210, 194, 180, 166, 147, 135, 121, 103, 91, 79, 63, 51.

Analytical data were in full agreement with M. Murata, K. Suzuki, S. Watanabe, and Y. Masuda, *J. Org. Chem.*, **1997**, *62*, 8569–8571.

4-(Triethoxysilyl)anisole(6b)

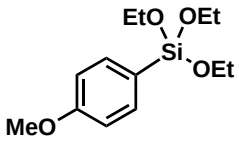

	Colorless oil
	$C_{13}H_{22}O_4Si$
	270.13 g/mol
Yield	100%
TLC	R_f = 0.24 (SiO_2, hexanes/ethyl acetate (95 :5))
^{1}H-NMR	(300 MHz, $CDCl_3$) δ 7.65-7.55 (m; 2H), 6.96-6.89 (m; 2H), 3.92-3.79 (m; 9H), 1.24 (t; 7.0 Hz; 6H).
^{13}C-NMR	(75 MHz, $CDCl_3$) δ 161.5 (Q), 136.6 (CH_{Ar}), 121.9 (Q), 113.7 (CH_{Ar}), 58.8 (OCH_2), 55.1 (OCH_3), 18.4 (CH_3).
GC-MS	t_R = 8.31 min, (EI, 70 eV): m/z = 270 [M^+], 255, 241, 225, 211, 197, 181, 169, 147, 135, 119, 108, 91, 79, 63, 51.

Analytical data were in full agreement with M. Murata, K. Suzuki, S. Watanabe, and Y. Masuda, *J. Org. Chem.*, **1997**, *62*, 8569–8571.

4-(Triethoxysilyl)toluene (6c)

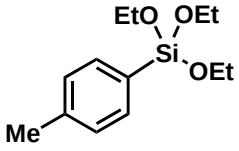

	Colorless oil
	$C_{13}H_{22}O_3Si$
	254.40 g/mol
Yield	85%
^{1}H-NMR	(400 MHz, $CDCl_3$) δ 7.56 (t, J = 7.6 Hz, 2H), 7.19 (t, J = 7.2 Hz, 2H), 3.86 (q, J = 7.0 Hz, 6H), 2.36 (s, 3H), 1.24 (t, J = 7.0 Hz, 9H).
^{13}C-NMR	(101 MHz, $CDCl_3$) δ 140.47 (Q), 140.17 (Q), 135.01 (CH_{Ar}), 128.82 (CH_{Ar}), 58.81 (OEt), 21.77 (CH_3), 18.38 (OEt).
GC-MS	t_R = 7.56 min, (EI, 70 eV): m/z = 254 [M^+], 239, 225, 209, 195, 181, 162, 147, 135, 119, 105, 91, 79, 65, 51.

Analytical data were in full agreement with M. Murata, K. Suzuki, S. Watanabe, and Y. Masuda, *J. Org. Chem.*, **1997**, *62*, 8569–8571.

Triethoxyphenylsilane(6d)

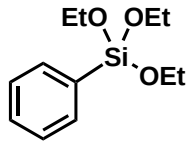

Colorless oil

$C_{12}H_{20}O_3Si$

240.37 g/mol

Yield 82%

^{1}H-NMR (400 MHz, $CDCl_3$) δ 7.72 – 7.63 (m, 2H), 7.46 – 7.32 (m, 3H), 3.88 (q, J = 7.0 Hz, 6H), 1.40 – 1.01 (m, 9H).

GC-MS t_R = 7.03 min, (EI, 70 eV): m/z = 240 [M^+], 225, 211, 195, 181, 162, 147, 139, 119, 105, 91, 77, 63, 51.

Analytical data were in full agreement with M. Murata, K. Suzuki, S. Watanabe, and Y. Masuda, *J. Org. Chem.*, **1997**, *62*, 8569–8571.

4-Methoxyphenyl(phenyl)silane (6e)

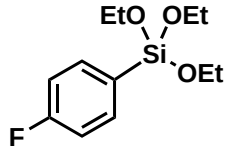

Colorless oil

$C_{12}H_{19}FO_3Si$

258.36 g/mol

Yield 71%

^{1}H-NMR (400 MHz, $CDCl_3$) δ 7.71 – 7.59 (m, 2H), 7.11 – 7.03 (m, 3H), 3.91 – 3.81 (m, 6H), 1.25 (t, J = 7.3 Hz, 9H).

GC-MS t_R = 6.96 min, (EI, 70 eV): m/z = 258 [M^+], 243, 229, 213, 199, 181, 169, 157, 147, 141, 119, 109, 96, 77, 63, 51.

Analytical data were in full agreement with J. Yu, J. Liu, G. Shi, C. Shao, Y. Zhang, *Angew. Chem., Int. Ed.*, *2015*, **54**, 4079-4082.

6.5 References

[1] Calas, R. Thirty years in organosilicon chemistry. *J. Organomet. Chem.* **1980**, *200*, 11–36.

[2] Sun, D.; Ren, Z.; Bryce, M. R.; Yan, S. Arylsilanes and siloxanes as optoelectronic materials for organic light-emitting diodes (OLEDs). *J. Mater. Chem. C* **2015**, *3*, 9496–9508.

[3] (a) Hirabayashi, K.; Mori, A.; Kawashima, J.; Suguro, M.; Nishihara, Y.; Hiyama, T. Palladium-Catalyzed Cross-Coupling of Silanols, Silanediols, and Silanetriols Promoted by Silver(I) Oxide. *J. Org. Chem.* **2000**, *65*, 5342–5349; (b) Brenzovich, W. E.; Brazeau, J.-F.; Toste, F. D. Gold-Catalyzed Oxidative Coupling Reactions with Aryltrimethylsilanes. *Org. Lett.* **2010**, *12*, 4728–4731; (c) Bi, L.; Georg, G. I. Direct Hiyama Cross-Coupling of Enaminones With Triethoxy(aryl)silanes and Dimethylphenylsilanol. *Org. Lett.* **2011**, *13*, 5413–5415; (d) Nakao, Y.; Hiyama, T. Silicon-Based Cross-Coupling Reactions Through Intramolecular Activation. *J. Synth. Org. Chem Jpn.* **2011**, *69*, 1221–1230; (e) Tang, S.; Takeda, M.; Nakao, Y.; Hiyama, T. Nickel-catalysed cross-coupling reaction of aryl(trialkyl)silanes with aryl chlorides and tosylates. *Chem. Commun.* **2011**, *47*, 307–309; (f) Ball, L. T.; Lloyd-Jones, G. C.; Russell, C. A. Gold-Catalysed Oxyarylation of Styrenes and Mono- andgem-Disubstituted Olefins Facilitated by an Iodine(III) Oxidant. *Chem. Eur. J.* **2012**, *18*, 2931–2937.

[4] Lalonde, M.; Chan, T. H. Use of Organosilicon Reagents as Protective Groups in Organic Synthesis. *Synthesis* **1985**, *1985*, 817–845.

[5] (a) Speier, J. L. Homogeneous Catalysis and of and Hydrosilation by Transition and Metals. *Adv. Organomet. Chem.* **1979**, *17*, 407–447; (b) Bart, S. C.; Lobkovsky, E.; Chirik, P. J. Preparation and Molecular and Electronic Structures of Iron(0) Dinitrogen and Silane Complexes and Their Application to Catalytic Hydrogenation and Hydrosilation. *J. Am. Chem. Soc.* **2004**, *126*, 13794–13807; (c) Berkefeld, A.; Piers, W. E.; Parvez, M. Tandem Frustrated Lewis Pair/Tris(pentafluorophenyl)borane-Catalyzed Deoxygenative Hydrosilylation of Carbon Dioxide. *J. Am. Chem. Soc.* **2010**, *132*, 10660–10661; (d) Gribble, M. W.; Pirnot, M. T.; Bandar, J. S.; Liu, R. Y.; Buchwald, S. L. Asymmetric Copper Hydride-Catalyzed Markovnikov Hydrosilylation of Vinylarenes and Vinyl Heterocycles. *J. Am. Chem. Soc.* **2017**, *139*, 2192–2195.

[6] (a) Yamanoi, Y. Palladium-Catalyzed Silylations of Hydrosilanes with Aryl Halides Using Bulky Alkyl Phosphine. *J. Org. Chem.* **2005**, *70*, 9607–9609; (b) Yamanoi, Y.; Taira, T.; ichi Sato, J.; Nakamula, I.; Nishihara, H. Efficient Preparation of Monohydrosilanes Using Palladium-Catalyzed Si-C Bond Formation. *Org. Lett.* **2007**, *9*, 4543–4546; (c) McNeill, E.; Barder, T. E.; Buchwald, S. L. Palladium-Catalyzed Silylation of Aryl Chlorides with Hexamethyldisilane.

Org. Lett. **2007**, *9*, 3785–3788; (d) Inubushi, H.; Kondo, H.; Lesbani, A.; Miyachi, M.; Yamanoi, Y.; Nishihara, H. Direct synthesis of alkylsilanes by platinum-catalyzed coupling of hydrosilanes and iodoalkanes. *Chem. Commun.* **2013**, *49*, 134–136; (e) Minami, Y.; Shimizu, K.; Tsuruoka, C.; Komiyama, T.; Hiyama, T. Synthesis of HOMSi Reagents by Pd/Cu-Catalyzed Silylation of Bromoarenes with Disilanes. *Chem. Lett.* **2014**, *43*, 201–203; (f) Yamamoto, Y.; Matsubara, H.; Murakami, K.; Yorimitsu, H.; Osuka, A. Activator-Free Palladium-Catalyzed Silylation of Aryl Chlorides with Silylsilatranes. *Chem. Asian J.* **2014**, *10*, 219–224; (g) Zarate, C.; Martin, R. A Mild Ni/Cu-Catalyzed Silylation via C–O Cleavage. *J. Am. Chem. Soc.* **2014**, *136*, 2236–2239; (h) Cinderella, A. P.; Vulovic, B.; Watson, D. A. Palladium-Catalyzed Cross-Coupling of Silyl Electrophiles with Alkylzinc Halides: A Silyl-Negishi Reaction. *J. Am. Chem. Soc.* **2017**, *139*, 7741–7744; (i) Zarate, C.; Nakajima, M.; Martin, R. A Mild and Ligand-Free Ni-Catalyzed Silylation via C–OMe Cleavage. *J. Am. Chem. Soc.* **2017**, *139*, 1191–1197.

[7] Corriu, R.; Massé, J.; Meunier, B. Activation catalytique des réactifs de grignard par des complexes du nickel en série organosiliciée. *J. Organomet. Chem.* **1973**, *55*, 73–84.

[8] Morita, E.; Murakami, K.; Iwasaki, M.; Hirano, K.; Yorimitsu, H.; Oshima, K. Copper-Catalyzed Arylation of Chlorosilanes with Grignard Reagents. *Bull. Chem. Soc. Jpn.* **2009**, *82*, 1012–1014.

[9] Murakami, K.; Hirano, K.; Yorimitsu, H.; Oshima, K. Silver-Catalyzed Transmetalation between Chlorosilanes and Aryl and Alkenyl Grignard Reagents for the Synthesis of Tetraorganosilanes. *Angew. Chem. Int. Ed.* **2008**, *47*, 5833–5835.

[10] Hirone, N.; Sanjiki, H.; Tanaka, R.; Hata, T.; Urabe, H. Acceleration of the Substitution of Silanes with Grignard Reagents by Using either LiCl or YCl_3/MeLi. *Angew. Chem. Int. Ed.* **2010**, *49*, 7762–7764.

[11] Vulovic, B.; Cinderella, A. P.; Watson, D. A. Palladium-Catalyzed Cross-Coupling of Monochlorosilanes and Grignard Reagents. *ACS Catalysis* **2017**, *7*, 8113–8117.

[12] (a) Rakita, P. E. *Kirk-Othmer Encyclopedia of Chemical Technology*; American Cancer Society, **2005**; (b) Kadam, A.; Nguyen, M.; Kopach, M.; Richardson, P.; Gallou, F.; Wan, Z.-K.; Zhang, W. Comparative performance evaluation and systematic screening of solvents in a range of Grignard reactions. *Green Chem.* **2013**, *15*, 1880.

[13] Knappke, C. E. I.; Grupe, S.; Gärtner, D.; Corpet, M.; Gosmini, C.; Jacobi von Wangelin, A. Reductive Cross-Coupling Reactions between Two Electrophiles. *Chem. Eur. J.* **2014**, *20*, 6828–6842.

[14] (a) Rösch, L.; Erb, W.; Müller, H. NOTIZEN: Hinweise auf die Existenz von Trimethylsilylmagnesiumverbindungen. *Z. Naturforsch. B* **1976**, *31*; (b) Goddard, R.; Krüger, C.; Ramadan, N. A.; Ritter, A. Silicon Analogues of Grignard

Compounds: Synthesis and Structure of Amine-Stabilized Trimethylsilylmagnesium Halides. *Angew. Chem. Int. Ed.* **1995**, *34*, 1030–1032; (c) Gaderbauer, W.; Zirngast, M.; Baumgartner, J.; Marschner, C.; Tilley, T. D. Synthesis of Polysilanylmagnesium Compounds. *Organometallics* **2006**, *25*, 2599–2606.

[15] (a) Hevia, E.; Mulvey, R. E. Split Personality of Lithium Chloride: Recent Salt Effects in Organometallic Recipes. *Angew. Chem. Int. Ed.* **2011**, *50*, 6448–6450; (b) Schnegelsberg, C.; Bachmann, S.; Kolter, M.; Auth, T.; John, M.; Stalke, D.; Koszinowski, K. Association and Dissociation of Grignard Reagents RMgCl and Their Turbo Variant RMgCl·LiCl. *Chem. Eur. J.* **2016**, *22*, 7752–7762.

[16] (a) Simmons-Potter, K.; Jamison, G. M.; Potter, B. G.; Thomes, W. J.; Phifer, C. C. Polysilane-Based Thin Films with High Photosensitivity. *MRS Proceedings* **2002**, *726*; (b) Fang, L.; Li, Y.; Wang, R.; Xu, C.; Li, S. Synthesis and photophysical properties of poly(aryleneethynylene)s bearing dialkylsilyl side substituents. *Eur. Polym. J.* **2009**, *45*, 1092–1097; (c) Jessop, I. A.; Tundidor-Camba, A.; Terraza, C. A.; González-Henríquez, C. M.; Tagle, L. H. Synthesis and thermal, optical and morphological characterization of oligomeric polyamides based on thiophene and alkyl/phenyl-silane moieties. Study of the electrospun deposition process. *J. Appl. Polym. Sci.* **2016**, *133*.

[17] (a) Klokov, B. A. Continuous organomagnesium synthesis of phenylethoxysilanes from a mixture of phenyltriethoxysilane with phenyltrichlorosilane. *Main Group Met. Chem.* **1999**, *22*, 1–4; (b) Manoso, A. S.; Ahn, C.; Soheili, A.; Handy, C. J.; Correia, R.; Seganish, W. M.; DeShong, P. Improved Synthesis of Aryltrialkoxysilanes via Treatment of Aryl Grignard or Lithium Reagents with Tetraalkyl Orthosilicates. *J. Org. Chem.* **2004**, *69*, 8305–8314; (c) Lee, A. S.-Y.; Chang, Y.-T.; Chu, S.-F.; Tsao, K.-W. A facile and efficient synthesis of aryltriethoxysilanes via sonochemical Barbier-type reaction. *Tetrahedron Lett.* **2006**, *47*, 7085–7087.

[18] (a) Terunuma, D.; Senda, K.; Sanazawa, M.; Nohira, H. The Configurations of Benzylmethyl (*o*- or *p*-tolyl)silylmethylamine and the Stereochemistry of the Reactions of Benzylmethylmethoxyphenylsilane with Some Organometallic Agents. *Bull. Chem. Soc. Jpn.* **1982**, *55*, 924–927; (b) Tacke, R.; Kropfgans, M.; Tafel, A.; Wiesenberger, F.; Sheldrick, W. S.; Mutschler, E.; Egerer, H.; Rettenmayr, N.; Gross, J.; Waelbroeck, M.; Lambrecht, G. (Hydroxymethyl)diphenyl(piperidinoalkyl)silane des Typs $(HOCH_2)(C_6H_5)_2Si(CH_2)_nNC_5H_{10}$ (n = 2,3) und deren Methoiodide: Synthese, Struktur und antimuscarinische Eigenschaften. *Z. Naturforsch. B* **1994**, *49b*, 898–910; (c) Park, S.; Lee, D. Gold-Catalyzed Intramolecular Allylation of Silyl Alkynes Induced by Silane Alcoholysis. *J. Am. Chem. Soc.* **2006**, *128*, 10664–10665; (d) Volchkov, I.; Park, S.; Lee, D. Ring Strain-Promoted Allylic Transposition of Cyclic Silyl Ethers. *Org. Lett.* **2011**, *13*, 3530–3533; (e) Ortega, R.; Sanchez-Quesada, J.; Lorenz, C.; Dolega, G.; Karawajczyk, A.; Sanz, M.; Showell, G.;

Giordanetto, F. Design and synthesis of 1,1-disubstituted-1-silacycloalkane-based compound libraries. *Bioorganic Med. Chem.* **2015**, *23*, 2716–2720.

[19] (a) Polis, A. Ueber aromatische Siliciumverbindungen. *Ber. Dtsch. Chem. Ges.* **1885**, *18*, 1540–1544; (b) Freiser, H.; Eagle, M. V.; Speier, J. Electric Moments and Structures of Organosilicon Compounds. II. The Aromatic Carbon-Silicon Bond. *J. Am. Chem. Soc.* **1953**, *75*, 2821–2824; (c) van den Ancker, T. R.; Hodgson, M. J. Arene catalysed sodium reactions. *J. Chem. Soc., Perkin Trans. 1* **1999**, 2869–2870; (d) van den Ancker, T. R.; Love, C. J. Polymer supported naphthalene-catalysed sodium reactions. *Org. Biomol. Chem.* **2007**, *5*, 3520.

[20] (a) Effenberger, F. Darstellung von Aryl- und Heteroaryltrimethylsilanen durch „in-situ"-Grignard-Synthese. *Liebigs Annalen der Chemie* **1979**, *1979*, 842–857; (b) Postigo, A.; Rossi, R. A. A Novel Type of Nucleophilic Substitution Reactions on Nonactivated Aromatic Compounds and Benzene Itself with Trimethylsiliconide Anions. *Org. Lett.* **2001**, *3*, 1197–1200.

[21] (a) Bordeau, M.; Biran, C.; Pons, P.; Leger-Lambert, M. P.; Dunogues, J. The electrochemical reductive trimethylsilylation of aryl chlorides: a good route to aryltrimethylsilanes and a novel route to tris(trimethylsilyl)cyclohexadienes. *J. Org. Chem.* **1992**, *57*, 4705–4711; (b) Grogger, C.; Loidl, B.; Stueger, H.; Kammel, T.; Pachaly, B. Electrochemical Synthesis of Functional Organosilanes II: Direct Electrochemical Formation of Si-C Bonds. *J. Electrochem. Soc.* **2013**, *160*, G88–G92.

[22] (a) Matsumoto, H.; Nagashima, S.; Yoshihiro, K.; Nagai, Y. Silicon—carbon bond formation by the reaction of disilanes with halobenzenes in the presence of tetrakis(triphenylphosphine)palladium(0). *J. Organomet. Chem.* **1975**, *85*, C1–C3; (b) Matsumoto, H.; Yoshihiro, K.; Nagashima, S.; Watanabe, H.; Nagai, Y. Conversion of disilanes to functional monosilanes. *Journal of Organometallic Chemistry* **1977**, *128*, 409–413; (c) Iwasawa, T.; Komano, T.; Tajima, A.; Tokunaga, M.; Obora, Y.; Fujihara, T.; Tsuji, Y. Phosphines Having a 2,3,4,5-Tetraphenylphenyl Moiety: Effective Ligands in Palladium-Catalyzed Transformations of Aryl Chlorides. *Organometallics* **2006**, *25*, 4665–4669.

[23] Ducos, P.; Liautard, V.; Robert, F.; Landais, Y. Chiral Memory in Silylium Ions. *Chem. Eur. J.* **2015**, *21*, 11573–11578.

[24] Wiesenfeldt, M. P.; Knecht, T.; Schlepphorst, C.; Glorius, F. Silylarene Hydrogenation: A Strategic Approach that Enables Direct Access to Versatile Silylated Saturated Carbo- and Heterocycles. *Angew. Chem. Int. Ed.* **2018**, *57*, 8297–8300.

Chapter 7

Appendix

7.1 List of Figures

7.2 List of Schemes

7.3 List of Tables

7.4 Acknowledgements

Zunächst möchte ich mich ganz herzlich bei meinem Doktorvater Prof. Dr. Axel Jacobi von Wangelin für die herausragende Betreuung während meiner Promotion sowie meiner Masterarbeitszeit bedanken. Er war nicht nur eine endlose Quelle für fachliches Wissen, seine Sichtweise hat mich auch in anderen Gebieten ungemäß bereichert. Seine faire und gelassene aber geistig fordernde Art hat das angenehme Klima innerhalb der Gruppe sowohl in der Universität als auch in extracurricularen Aktivitäten geprägt. Für die Übernahme des Zweitgutachtens und den wetvollen Disskussionen innerhalb der Gruppenseminare möchte ich mich bei Jun.-Prof. Dr. Ivana Fleischer bedanken. Weiterhin gilt mein Dank Prof. Dr. Frank-Michael Matysik für die Übernahme des Amtes als Drittprüfer. Als letztes Mitglied der Prüfungskommision möchte ich mich bei Apl. Prof. Dr. Rainer Müller bedanken, der sich bereitgestellt hat den Prüfungsvorsitz zu übernehmen.

Ein überaus großer Dank gilt natürlich all meinen Arbeitkollegen am Arbeitskreis Jacobi. Samet Gülak, der mich durch mein Forschungspraktikum begleitet hat. Die tolle Zeit unter seiner Anleitung war der Hauptgrund, dass ich mich am Ende für die Arbeitsgruppe entschieden habe. Dr. Dominik Gärtner, der mir lange Zeit als Labornachbar geblieben ist und welchen ich nach kurzer Zeit schon ins Herz geschlossen hatte. Dr. Michal Majek für die unzähligen und ungemein bereichernden Unterhaltungen und Geschichten, die den Arbeitsalltag sowie jeden gemeinsamen UM-gefüllten Abende erhellt haben. Dr. Tim Gieshoff, Dr. Josef Schachtner und Dr. Matteo Villa, die den Arbeitstag nicht nur durch ihre Kicker-Fähigkeiten bereichert haben und die immer da waren, wenn man ihre Hilfe benötigte. Dr. Raul Perez-Ruiz und Dr. Uttam Chakraborty, deren Gegenwart die Arbeitspausen ungemein bereichert haben. Sebastian Sandl, der Dominiks Rolle als Labornachbar hervorragend besetzt und immer für gute Stimmung gesorgt hat. Josef Bernauer, Patrick Bayer, Bernhard Gregori und Michael Neumeier für die unvergesslichen Bier-Abende und Singstar-Abenteuer, die es mehr als wert waren, erst in der Nacht die Uni wieder zu verlassen. Dr. Dieter Schaarschmidt, dessen Expertise mich in einigen Unterhaltungen sehr bereichert hat. Ganz herzlich möchte ich mich auch bei Michaela Lutz bedanken, die als Frau-für-alles einen unermesslichen Wert in der Gruppe eingenommen hat.

Ich möchte mich ebenfalls bei der Arbeitsgruppe Gschwind bedanken für die unterhaltsamen Küchen-Aufenthalte. Insbesondere möchte ich mich bei Dr. Julian Greindl und Florian Hastreiter bedanken, die als angemessene Gegner in unseren Kicker-Tournieren gedient haben. Dr. Andreas Seegerer als fähiger Boulder-Partner und Verena Streitferdt, Philipp Nitschke und Kerstin Rothermel für die gemeinsamen Abende sowie Dult- und Volksfest-Besuche. Desweiteren möchte ich mich noch bei den Mitarbeitern der Arbeitsgruppen Wolf, Fleischer und Garcia bedanken für die gemeinsamen Weihnachts- und Doktorfeiern. Insbesondere gilt mein Dank Philipp Büschelberger - einen besseren Kooperationspartner hätte man sich nicht wünschen können.

Weiterhin gilt mein Dank Tobias Burger, dessen Freundschaft über das gesamte Studium hinweg einen unermesslichen Wert hat und der mir immer mit Rat und Tat zur Seite stand. Andreas Meyer, Claudia De Giorgi und Samuel Tragl für die vielzähligen gemeinsamen Abende und die tolle gemeinsame Studiumszeit.

Meiner Freundin, Nele Berg, danke ich von ganzem Herzen dafür, wie sehr sie mir im letzte Jehr meiner Promotion geholfen hat, für alle wunderschönen vergangenen sowie zukünftigen Momente. Ein besonderer Dank geht an meine Mutter Sabine Reyes-Rodriguez, die mich über die vielen Jahre durch alle Hochs und Tiefs hindurch unterstützt hat und die immer an meiner Seite war. Vielen Dank auch an meinen Bruder Jerome Reyes-Rodriguez, der immer für mich da war, wenn ich jemanden zum Reden oder eine Ablenkung brauchte. Ein großer Dank geht natürlich auch an alle weiteren Familienmitglieder, die durchwegs verständnisvoll waren und bei denen ich mich immer geborgen fühle.

7.5 Eidesstattliche Erklärung

(1) Ich erkläre hiermit an Eides statt, dass ich die vorliegende Arbeit ohne unzulässige Hilfe Dritter und ohne Benutzung anderer als der angegebenen Hilfsmittel angefertigt habe; die aus anderen Quellen direkt oder indirekt übernommenen Daten und Konzepte sind unter Angabe des Literaturzitats gekennzeichnet.

(2) Alle Personen, die mir bei der Auswahl und Auswertung des folgenden Materials in der jeweils beschriebenen Weise unentgeltlich geholfen haben, sind am Ende des ersten Kapitels aufgeführt.

(3) Weitere Personen waren an der inhaltlich-materiellen Herstellung der vorliegenden Arbeit nicht beteiligt. Insbesondere habe ich hierfür nicht die entgeltliche Hilfe eines Promotionsberaters oder anderer Personen in Anspruch genommen. Niemand hat von mir weder unmittelbar noch mittelbar geldwerte Leistungen für Arbeiten erhalten, die im Zusammenhang mit dem Inhalt der vorgelegten Dissertation stehen.

(4) Die Arbeit wurde bisher weder im In- noch im Ausland in gleicher oder ähnlicher Form einer anderen Prüfungsbehörde vorgelegt.

Efrain Reyes-Rodriguez
19.12.2018